

# Non-equilibrium properties of superconducting structures in the presence of spin-dependent fields



Universidad del País Vasco/Euskal Herriko Unibertsitatea UPV/EHU  
Departamento de Física/Fisika saila

**Alberto Hijano Mendizabal**

Supervised by Dr. F. Sebastián Bergeret Sbarbaro  
and Prof. José María Pitarke de la Torre

January 2024



# Agradecimientos

*I am a brother to dragons,  
and a companion to owls.*

— Job 30:29

Primeramente quisiera agradecer a Sebas haber dirigido mi doctorado, desde la primera vez que me uní al grupo de física mesoscópica en aquellas prácticas de verano ha sido un placer haber trabajado bajo tu supervisión. Soy consciente de que todas las correcciones han servido para perfeccionar esta Tesis. Txemari ere eskerrak eman nahi dizkiot, pena bat da kolaboratzeko aukerarik izan ez izana. Me gustaría agradecer también a Stefan toda la ayuda que me ha brindado, sobre todo en las primeras etapas del doctorado. Nos vemos en unos meses en Jyväskylä. Gracias también a Tim por las conversaciones que hemos tenido, es un placer trabajar con gente como tú, estoy seguro de que te espera un futuro brillante. No me puedo olvidar del resto de miembros del grupo de física mesoscópica; Vitaly and Yao, your comments are always very insightful; Jon, Anastasiia, Xianpeng, Cristina y Mikel os tengo presentes aunque no haya tenido la ocasión de interactuar mucho con vosotros durante el doctorado.

A continuación, tengo que agradecer a mi familia todo el apoyo que me han ofrecido. Gracias aita y ama por haber estimulado mi curiosidad por la ciencia desde pequeño, recuerdo entre otras la serie de *Cosmos* que me enseñó sobre el Big Bang y la estructura del ADN. Gracias aita por el trabajo que te tomaste para enseñarme todo lo que sabes, no habría llegado tan lejos sin tu ayuda. Gracias ama por estar siempre ahí. Gracias Guille por el apoyo, eres una persona excepcional, estoy muy orgulloso de ti.

Eskerrik asko Dario for your support, y gracias Eusebio y Diego por las discusiones que hemos tenido. Por supuesto, Celia y Max ha sido un placer colaborar con vosotros. I would also like to thank Francesco and Alessandro for welcoming me to Pisa, I am very proud of the work we did there. Tero and Pauli, my stay in Finland was amazing, I am looking forward to going back. Sakineh, I remember fondly our discussions, I am confident that our paths will cross again. Jason and Hisa it was a pleasure collaborating with you.

Ahora os toca a *los magias*. Martín e Iker, mis compañeros de despacho, gracias por esos momentos tan divertidos. Miriam, siempre con una sonrisa, se te echa de menos por el CFM. Bruno, a ver si volvemos a echar unas partidas. Álvaro, gracias por organizar esas comidas increíbles en la sociedad. María, mucho ánimo con el doctorado. No me olvido de todos con los que he coincidido en la cafetería del CFM todos estos años: Djordje, sigue mejorando tu español; Victor, you always brought the best courses; Rubén *el Bueno*, jarraitu horrela; Diego tus conversaciones fueron muy interesantes, Adam, Zuzanna, Alba, Ane, Joseph, Anish, Shah, Alexey, Ion, Joseba *el Bueno* y Rodrigo.

Y por supuesto al resto de la gente del CFM, DIPC y Nanogune con la que he tenido el placer de coincidir, ya sea en las comidas de los viernes, en el pintxo-pote o en alguna casa rural. Carlos,

recordaré tus charlas intelectuales; Josu, nos queda pendiente un fútbolín; Carmen, el alma del grupo; Cris, Mikel *Ttiritt*, Jon *Laser*, Auguste, Txemikel, Jonathan, Antton, Miguel, Adrián, Nikos, Mikel, Xabi, Mireia, Asier, Roberto, Jorge *JOT*, Joseba *el malo*, Quimey, Isaac, Jorge, Jason, Ángel, Divya, Stefano, Raúl, Unai, Isa, David, Sara, Xabier, Paula, David, Daniel, Jaakko, Stefan, Eli, Matteo, Marina, Julen, Diana y Tamara.

Perdón si me he olvidado de alguien, si estás leyendo esto seguramente también seas alguien que ha marcado mi etapa predoctoral. Escribiendo esto me he dado cuenta de la cantidad de personas que he conocido durante estos años. Por último, me gustaría agradecer a todas las personas que invierten su tiempo en la ciencia, ya sea ayudando a organizar conferencias, realizando labores de divulgación, realizando revisión por pares, etc.

Muchas gracias a todos,  
Alberto

# Resumen

Múltiples trabajos teóricos y experimentales resaltan la versatilidad de las estructuras híbridas superconductoras. Ofrecen aplicaciones en diversos ámbitos, tales como la espintrónica, la termoelectricidad y los sensores. La mayoría de estas aplicaciones se basan en las propiedades de no-equilibrio de los superconductores, *i.e.*, propiedades que surgen fuera del equilibrio termodinámico. En esta tesis abordamos las propiedades de no-equilibrio de los superconductores en presencia de campos dependientes del espín, es decir, campos que interactúan con el espín de las cuasipartículas, tales como los campos de Zeeman y el acoplamiento espín-órbita. Específicamente, investigamos el transporte de carga, termoeléctrico y espintrónico en varios dispositivos híbridos superconductores y de espín.

Los efectos termoeléctricos son un tema de investigación popular debido a su potencial para convertir calor en trabajo. Un factor fundamental que permite la termoelectricidad en conductores electrónicos es la ruptura de la simetría entre portadores de carga con energía positiva (electrones) y energía negativa (huecos). Esta asimetría de la densidad de estados se logra aplicando un campo de desdoblamiento de espín. En consecuencia, el acoplamiento de un superconductor con un sistema polarizado en espín se postula como un enfoque prometedor para inducir efectos termoeléctricos. Se han propuesto detectores termoeléctricos en ámbitos como la astrofísica para la detección del fondo cósmico de microondas, y para la detección de radiación de terahercios utilizada, por ejemplo, en imágenes de seguridad. Destacablemente, el detector termoeléctrico superconductor utiliza directamente la radiación absorbida para generar la señal de medición deseada, sin necesidad de una fuente de energía externa.

La utilidad del transporte de carga y calor abarca diversas aplicaciones, incluyendo termometría a baja temperatura, el desarrollo de termómetros de electrones altamente sensibles y la realización de convertidores de temperatura-frecuencia. Notablemente, el transporte de calor tiene el potencial de generar corrientes de espín gigantes debido a la presencia de pares de Cooper con un estado triplete de espín. Además, las estructuras híbridas superconductoras con campos dependientes del espín ofrecen una plataforma para crear válvulas de espín y calor altamente eficientes. Estas estructuras híbridas también facilitan la refrigeración a escala nanométrica, y más recientemente, la implementación de una batería de fase cuántica. Otra aplicación basada en la electrónica superconductora incluye los diodos superconductores. En los superconductores habituales, la simetría electrón-hueco da como resultado un transporte de carga recíproco. Esta simetría se rompe en superconductores con desdoblamiento de espín y filtrado de espín, resultando en una ruptura de la reciprocidad. La eficacia de estas aplicaciones se basa en superconductores caracterizados por una densidad de estados desdoblada en espín bien definida y un gap de energía robusto.

Otro ingrediente clave en las estructuras superconductoras híbridas es el acoplamiento espín-órbita (SOC, por sus siglas en inglés). A diferencia de los campos de Zeeman, el SOC induce una interacción de espín dependiente del momento. El acoplamiento de los grados de libertad orbital y de espín es esencial en la espintrónica. Por ejemplo, el efecto Hall de espín implica la generación de una corriente de espín transversal en respuesta a una corriente de carga. En superconductores, el efecto Hall de espín acopla la corriente de espín tanto a la corriente de cuasipartículas como a la corriente (de equilibrio) superconductora. La superconductividad topológica puede surgir en

dispositivos híbridos que involucran superconductores convencionales y semiconductores con fuerte acoplamiento espín-órbita. La manifestación más llamativa de la superconductividad topológica son los modos cero de Majorana, cuya existencia se ha predicho en los extremos de los nanohilos con espín-órbita. Este tipo de plataformas híbridas superconductor-semiconductor se han propuesto en esquemas de computación cuántica topológica.

El estudio de la interacción entre la superconductividad y los campos dependientes del espín en sistemas híbridos se ha establecido como un campo de investigación prolífico y activo en las últimas décadas. El propósito de esta Tesis de doctorado es estudiar teóricamente las propiedades de no-equilibrio de estructuras superconductoras sujetas a diferentes tipos de campos dependientes del espín. Los campos dependientes del espín pueden clasificarse como términos de SOC que rompen la simetría de inversión, y términos magnéticos (tipo Zeeman) que rompen la simetría de inversión temporal. Las estructuras híbridas reales muestran un desorden no controlable que debe modelarse adecuadamente. Una posibilidad es implementar desorden en los modelos microscópicos, por ejemplo, a través de modelos de *tight-binding*. Este enfoque es computacionalmente muy costoso. Otro enfoque posible basado en el método de la función de Green (GF, por sus siglas en inglés) es reducir las ecuaciones microscópicas a ecuaciones cinéticas. En este método, las interfaces entre los diferentes materiales se describen mediante condiciones de frontera. Además, los materiales estudiados son sistemas prácticamente metálicos donde la energía de Fermi es mucho mayor que las otras escalas de energía en el sistema, por lo que se puede utilizar la aproximación cuasiclásica para simplificar las ecuaciones.

Para la Tesis se han seleccionado cuatro publicaciones derivadas de la investigación llevada a cabo durante mi doctorado. Dichas publicaciones se recopilan como Capítulos en esta tesis. En la introducción, se presenta la teoría pertinente a los superconductores, que son el ingrediente central que conforma las estructuras híbridas estudiadas. Se introduce el método de la función de Green cuasiclásica, que es la principal herramienta teórica utilizada para analizar las estructuras híbridas y se derivan las ecuaciones para la función de Green cuasiclásica. Este Capítulo tiene dos objetivos: en primer lugar, sirve como base teórica para los sistemas estudiados en los Capítulos posteriores. En segundo lugar, pretende servir como una guía para familiarizarse con el formalismo GF cuasiclásico. En la introducción se incluye la derivación de las ecuaciones cuasiclásicas de Eilenberger y Usadel, y se delimitan las condiciones de frontera y los observables relevantes necesarios para estudiar fenómenos de no-equilibrio dependientes del tiempo. Posteriormente, presentamos una explicación más detallada de los modelos y métodos utilizados para estudiar cada uno de los cuatro sistemas abordados en esta Tesis: 1) un superconductor en proximidad con un aislante ferromagnético con una pared de dominio, 2) una unión de Josephson anómala acoplada a un dispositivo interferómetro de Andreev, 3) una unión túnel superconductora asimétrica irradiada por microondas y 4) un superconductor bidimensional con un campo magnético o con SOC bajo un campo eléctrico dinámico. A su vez, presentamos los principales resultados que conforman la espina dorsal de esta tesis.

Primero, investigamos la densidad de estados de las cuasipartículas y las correlaciones tripletes en un superconductor alrededor de una pared de dominio y estudiamos cómo se manifiestan las correlaciones tripletes en una medición de corriente de túnel. Un superconductor (S) crecido sobre un aislante ferromagnético (FI, por sus siglas en inglés) muestra una densidad de estados desdoblada en espín debido al efecto de proximidad. Esta división del espín permite que las correlaciones de estado singlete del condensado convivan con correlaciones de estado triplete. La interacción ferromagnética puede describirse mediante un campo de canje interfacial en la interfaz FI/S que induce correlaciones triplete en el superconductor. Si la capa superconductora es delgada en comparación con la longitud de coherencia, se puede suponer que el desdoblamiento de espín es constante a lo largo del grosor de la muestra. Esta suposición está justificada, incluso en una situación de multidominio, si el tamaño de dominio característico de FI es mucho más grande que la longitud de coherencia superconductora. Sin embargo, la no homogeneidad de la interacción de canje es relevante cuando el tamaño del

dominio es del orden de la longitud de coherencia, o si el superconductor se encuentra en las proximidades de una pared de dominio aguda, como se muestra en la Fig. 2.1. El efecto de las paredes de dominio en magnetos y aislantes ferromagnéticos sobre superconductores adyacentes ha sido estudiado tanto teóricamente como experimentalmente. Un trabajo reciente proporcionó evidencia experimental de que el EuS, un aislante ferromagnético, está formado por múltiples dominios con un tamaño del orden de la longitud de coherencia de una capa de Al (superconductora) adjunta. Los autores de este último trabajo utilizaron un modelo teórico que asumía dominios antiparalelos de diferentes tamaños para explicar las mediciones espectroscópicas.

En esta publicación, generalizamos esta configuración para considerar un FI/S difusivo donde el FI está formado por dos dominios magnéticos con una magnetización arbitraria, como se muestra en la Fig. 2.2. Casi todos los trabajos experimentales en sistemas FI/S se centran en estudiar su espectro de cuasipartículas, pero hay un aspecto clave que no se cubre a menudo en estos trabajos: un campo de canje interfacial lleva a la conversión de correlaciones superconductoras singletes a tripletes. Además, en bicapas FI/S donde el FI tiene una magnetización no colineal, las correlaciones tripletes con diferentes proyecciones de espín pueden coexistir con las correlaciones singletes. En esta publicación, estudiamos las propiedades de equilibrio de una bicapa FI/S con una pared de dominio aguda que separa dos dominios magnéticos con magnetizaciones arbitrarias. Proporcionamos expresiones analíticas para la densidad de estados en diferentes casos límite. Además, estudiamos la evolución espacial de las correlaciones triplete cerca de la pared de dominio y proponemos un método para detectarlas cubriendo el superconductor con una capa ferromagnética y realizando espectroscopia túnel sobre ella.

En el segundo trabajo, calculamos las propiedades (estáticas) de no-equilibrio de superconductores con campos dependientes del espín. Específicamente, exploramos el efecto Josephson anómalo en un interferómetro de Andreev. Si se colocan dos superconductores en proximidad, puede fluir una supercorriente entre ellos además de la corriente usual de cuasipartículas. Esta corriente depende de la fase relativa entre los dos superconductores. Tales uniones se conocen como uniones Josephson, nombradas en honor a Brian Josephson, quien predijo la relación entre la supercorriente y el voltaje a través de la unión en 1962. El efecto Josephson de corriente continua establece que la supercorriente que fluye entre dos superconductores con una diferencia de fase  $\varphi$  es  $I_J \propto \sin \varphi$ .

La relación corriente-fase adquiere una forma más general en sistemas donde la simetría de inversión espacial y temporal están rotas:  $I_S \propto I_c \sin(\varphi + \varphi_0)$ . Tales uniones se conocen como uniones- $\varphi_0$ , y el efecto correspondiente como el efecto Josephson anómalo (AJE, por sus siglas en inglés). En general, esta relación corriente-fase puede descomponerse en una corriente usual proporcional a  $\sin \varphi$ , y una corriente anómala proporcional a  $\cos \varphi$ . La corriente anómala solo puede ser distinta de cero si las simetrías de inversión espacial y temporal están rotas simultáneamente, lo que conduce a una supercorriente finita incluso con una diferencia de fase nula entre los superconductores.

Los sistemas híbridos superconductores con campos dependientes del espín ofrecen una plataforma para obtener el efecto AJE. En esta publicación, consideramos dos realizaciones de una unión Josephson anómala: una unión Josephson con acoplamiento espín-órbita de tipo Rashba [Fig. 2.4(a)] y estructuras ferromagnéticas multicapa [Fig. 2.4(b)]. En el primer ejemplo, un campo de Zeeman y el acoplamiento espín-órbita proporcionan la ruptura de simetría temporal y de inversión, respectivamente, lo que conduce al desplazamiento de fase anómala. En el segundo ejemplo, una magnetización no coplanar combinada con interfaces de filtrado de espín proporciona las rupturas de simetría requeridas.

Por lo tanto, el efecto AJE refleja la interacción entre los campos dependientes del espín y la superconductividad. Esta interacción es la base de varios efectos y aplicaciones que están atrayendo el interés de una gran comunidad, como la superconductividad topológica y no convencional, la espintrónica superconductora, y los nuevos elementos electrónicos superconductores. Las propuestas

más conocidas para el AJE involucran estructuras superconductoras en presencia de interacción espín-órbita, algunas de las cuales han sido probadas con éxito en experimentos. Otros estudios teóricos han propuesto numerosas realizaciones alternativas del AJE: uniones S/F/S con una textura de magnetización no homogénea, uniones de superconductores no convencionales y entre cables superconductores topológicamente no triviales. La relación corriente-fase anómala también se puede obtener bajo una situación de no-equilibrio en estructuras multiterminales. Las uniones- $\varphi_0$  podrían ser un componente clave para la electrónica cuántica, ya que pueden proporcionar una diferencia de fase estable a circuitos cuánticos, y por lo tanto podrían ser particularmente útiles en electrónica y espintrónica superconductora coherente en fase.

En esta publicación, analizamos el efecto  $\varphi_0$  en un dispositivo conocido como interferómetro de Andreev. Un interferómetro de Andreev consta de una unión Josephson acoplada a un conductor mesoscópico, como se esquematiza en la Fig. 2.5. Las correlaciones superconductoras se inducen en el conductor normal debido al efecto de proximidad. Dichas correlaciones dependen de la diferencia de fase de la unión Josephson, por lo que la resistencia del lazo conductor se vuelve sensible a  $\varphi$ . En otras palabras, una simple medición de resistencia realizada en el conductor podría potencialmente revelar la relación corriente-fase a lo largo de la unión Josephson adyacente. Una ventaja importante de esta geometría es que permite un desacoplamiento entre el lazo superconductor con la unión- $\varphi_0$  y el circuito normal donde se realiza la medición de resistencia, de modo que el ruido asociado con el proceso de medición no perturba la unión- $\varphi_0$ . La interferometría de Andreev estuvo particularmente activa durante los años 90, se propusieron teóricamente varios tipos de interferómetros de Andreev que han sido implementados experimentalmente. Los interferómetros de Andreev se han utilizado para estudiar las oscilaciones de la magnetorresistencia, el transporte eléctrico, el poder termoeléctrico y el transporte térmico en estructuras S/N. En esta publicación, investigamos cómo se modifica la relación corriente-fase en el conductor mesoscópico debido al efecto  $\varphi_0$ . Con este propósito, resolvemos la ecuación de Usadel en los bucles superconductor y normal, y calculamos la supercorriente y la corriente de cuasipartícula que fluyen a través de ellos, respectivamente.

En el tercer trabajo, investigamos las capacidades termoeléctricas y de enfriamiento promediadas en el tiempo en uniones túnel superconductoras asimétricas. La termoelectricidad consiste en la generación de energía eléctrica debido a una diferencia de temperatura. El efecto Seebeck, que describe la fuerza electromotriz desarrollada entre dos puntos a diferentes temperaturas, fue descubierto de manera independiente por A. Volta en 1794 y por T. J. Seebeck en 1821. Los portadores de carga en el material tienen una mayor energía cinética a temperaturas más altas, por lo que los gradientes de temperatura en el material causan la difusión de los portadores de carga desde las regiones calientes hacia las frías. En la mayoría de los materiales, a temperatura ambiente, la diferencia de potencial generada es proporcional a la diferencia de temperatura  $V \propto \Delta T$ , esta relación lineal permite, por ejemplo, calibrar fácilmente dispositivos eléctricos como termopares para construir sensores de temperatura.

En el estado normal, dentro del régimen lineal, la termoelectricidad escala linealmente con la temperatura de operación, por lo que la sensibilidad de los sensores termoeléctricos disminuye drásticamente a bajas temperaturas. Este problema se solventa en materiales superconductores, ya que a estas temperaturas la termoelectricidad es muy fuerte debido a la no linealidad del efecto en los superconductores. Se ha registrado experimentalmente que los efectos termoeléctricos en las uniones superconductoras son órdenes de magnitud más grandes de lo esperado en metales no superconductores a la misma temperatura de operación. Los efectos termoeléctricos en las uniones superconductoras se han estudiado tanto teórica como experimentalmente en los últimos 10 años: los sistemas superconductores híbridos con simetría explícitamente rota entre partículas y huecos muestran termoelectricidad unipolar. La simetría entre partículas y huecos alrededor de la superficie de Fermi de los superconductores de tipo Bardeen-Cooper-Schrieffer puede romperse, por ejemplo, en estructuras híbridas S/F. El efecto de proximidad magnética en una bicapa delgada S/FI causa



un desdoblamiento de espín casi homogéneo en la densidad de estados. Si el transporte electrónico está polarizado en espín, por ejemplo, mediante un filtro de espín de tunelización, la contribución a la densidad de estados (DoS, por sus siglas en inglés) de una componente del espín predomina sobre la otra, lo que lleva a una ruptura efectiva de la simetría entre partículas y huecos.

Se han propuesto varias aplicaciones basadas en las propiedades termoeléctricas únicas de las uniones S/I/S' y FI/S/I/F: detectores de radiación termoeléctrica ultrasensibles que se pueden utilizar en diversas aplicaciones que van desde observaciones astrofísicas hasta imágenes de seguridad y caracterización de materiales, osciladores de alta frecuencia controlados por flujo alimentados con un gradiente térmico y generadores controlados galvánicamente desconectados de circuitos externos.

Recientemente, se ha demostrado teóricamente y experimentalmente que las uniones de túnel superconductoras, donde el acoplamiento Josephson está adecuadamente suprimido, desarrollan un gran efecto termoeléctrico si el electrodo con el gap más grande tiene una temperatura más alta. A diferencia de los sistemas con efecto de proximidad magnética, en estas uniones superconductoras la simetría electrón-hueco se rompe por la combinación de un gradiente térmico suficientemente fuerte y una DoS que disminuye monótonamente, lo que induce una polarización de voltaje espontánea. La termoelectricidad resultante es bipolar y fuertemente no lineal.

En esta publicación, estudiamos el efecto termoeléctrico en uniones Josephson asimétricas bajo la tunelización asistida por fotones (PAT, por sus siglas en inglés). El PAT ha sido estudiado extensamente en el régimen disipativo. Sin embargo, la influencia del PAT en la termoelectricidad bipolar recientemente descubierta no ha sido explorada todavía. Además, estudiamos las propiedades de enfriamiento de la unión. Al aplicar un voltaje externo, para condiciones de temperatura específicas, es posible extraer calor y reducir la temperatura electrónica del superconductor con el gap más bajo.

Finalmente, estudiamos el efecto Hall de carga y espín dinámicos en superconductores difusivos. El efecto Hall fue descubierto por E. Hall en el siglo XIX. La inyección de una corriente eléctrica en un conductor con un campo magnético perpendicular produce una corriente de carga transversal. En conductores de tamaño finito (abiertos), la carga transportada por la corriente transversal se acumula en los lados del conductor, generando un voltaje Hall. El efecto Hall puede incorporarse directamente en el modelo de Drude de conducción electrónica incluyendo la fuerza de Lorentz debido al campo magnético. El efecto Hall de corriente alterna describe la corriente de carga transversal bajo un campo eléctrico variable, en metales normales difusivos la conductividad Hall es proporcional a la conductividad longitudinal y al campo magnético aplicado. En el estado superconductor las corrientes longitudinal y Hall se vuelven dependientes de la frecuencia, presentando contribuciones de corriente en fase y fuera de fase. Además, las conductividades longitudinal y Hall tienen diferente dependencia en frecuencia, por lo que ya no son proporcionales.

El componente en fase de la respuesta longitudinal describe transiciones electrónicas en el superconductor y presenta un gap superconductor a bajas temperaturas. La respuesta fuera de fase surge debido a la supercorriente. A pesar de algunos intentos a lo largo de los años basados en modelos fenomenológicos de dos fluidos y la teoría de Bardeen-Cooper-Schrieffer, no ha habido una extensión microscópica del modelo de Drude para la respuesta Hall dinámica en superconductores en el régimen difusivo. El formalismo cuasiclásico permite un tratamiento sencillo del efecto Hall dinámico en superconductores. En esta publicación, extendemos la teoría de Mattis-Bardeen para la respuesta dinámica de superconductores para incluir la respuesta Hall. Además, estudiamos el efecto Hall de espín dinámico en superconductores. En presencia de la interacción espín-órbita, una corriente de carga en un conductor genera una corriente de espín transversal, y viceversa. Hay dos mecanismos principales para el efecto Hall de espín: en el mecanismo *intrínseco* surge debido a la ruptura de la simetría de inversión ya sea debido a la red cristalina (acoplamiento espín-órbita de Dresselhaus) o la estructura de la muestra (acoplamiento espín-órbita de Rashba), y el mecanismo *extrínseco* resulta de una dispersión por impurezas dependiente del espín.



# Table of Contents

<b>Resumen</b>	<b>v</b>
<b>Table of Contents</b>	<b>xi</b>
<b>List of Figures</b>	<b>xiii</b>
<b>Nomenclature</b>	<b>xv</b>
<b>1 Introduction</b>	<b>1</b>
1.1 Theory of superconductivity . . . . .	3
1.2 Green's function method . . . . .	5
1.2.1 Gor'kov equations . . . . .	6
1.2.2 The Matsubara formalism . . . . .	9
1.3 Method of quasiclassical Green's functions . . . . .	10
1.3.1 Normalization condition . . . . .	11
1.3.2 Observables . . . . .	12
1.3.3 Self-consistency of the order parameter . . . . .	13
1.4 Diffusive limit: the Usadel equation . . . . .	13
1.4.1 Example: homogeneous BCS superconductor . . . . .	14
1.4.2 Observables . . . . .	15
1.4.3 Self-consistency of the order parameter . . . . .	16
1.4.4 Quasiclassical equations in systems with SOC . . . . .	17
1.5 Boundary conditions . . . . .	18
1.5.1 Interface with a ferromagnetic insulator . . . . .	18
1.5.2 Interface between conducting materials . . . . .	19
1.5.3 Unconventional superconductors . . . . .	19
1.6 Summary . . . . .	20
<b>2 Models, methods, and results</b>	<b>21</b>
2.1 Quasiparticle density of states and triplet correlations in S/FI structures across a sharp domain wall . . . . .	21
2.1.1 Model and methods . . . . .	22
2.1.2 Summary of the results . . . . .	25
2.2 Anomalous Andreev interferometer: Study of an anomalous Josephson junction coupled to a normal wire . . . . .	26
2.2.1 Model and methods . . . . .	29
2.2.2 Summary of the results . . . . .	31
2.3 Microwave-Assisted Thermoelectricity in S-I-S' Tunnel Junctions . . . . .	32
2.3.1 Model and methods . . . . .	33
2.3.2 Summary of the results . . . . .	37

---

2.4	Dynamical Hall responses of disordered superconductors . . . . .	37
2.4.1	Model and methods . . . . .	38
2.4.2	Summary of the results . . . . .	41
<b>3</b>	<b>Summary</b>	<b>43</b>
<b>4</b>	<b>Quasiparticle density of states and triplet correlations in superconductor/ferromagnetic-insulator structures across a sharp domain wall</b>	<b>45</b>
<b>5</b>	<b>Anomalous Andreev interferometer: Study of an anomalous Josephson junction coupled to a normal wire</b>	<b>57</b>
<b>6</b>	<b>Microwave-Assisted Thermoelectricity in S-I-S' Tunnel Junctions</b>	<b>67</b>
<b>7</b>	<b>Dynamical Hall responses of disordered superconductors</b>	<b>77</b>
	<b>Full list of publications</b>	<b>89</b>
	<b>References</b>	<b>91</b>

# List of Figures

1.1	(a) Diagram illustrating the electron-electron interaction via the emission/absorption of a phonon. (b) In the BCS theory, the attractive electron-electron interaction only occurs in a small energy shell around the Fermi surface. The thickness of the shell is of the order of Debye energy. . . . .	4
1.2	Schwinger-Keldysh contour, the direction of the arrows indicates the ordering of times along the forward ( $C_+$ ) and backward ( $C_-$ ) branches. The branches have been shifted vertically for clarity. . . . .	5
1.3	Energy integrating contours in real time $C_+^{(r)}$ (retarded) and $C_-^{(r)}$ (advanced), and their equivalent contours $C_+^{(i)}$ and $C_-^{(i)}$ , encircling the poles of the distribution function. The integral can be replaced by a sum over the Matsubara frequencies $\omega_n$ (dots on the imaginary axis). . . . .	13
1.4	Density of states for a homogeneous superconductor. The dashed curve corresponds to an ideal BCS superconductor ( $\Gamma \rightarrow 0^+$ ), and the solid curve to a real superconductor with a finite inelastic scattering rate ( $\Gamma = 0.02\Delta$ ). . . . .	15
2.1	Top view of a ferromagnetic insulator with a sharp domain wall. The FI has two domains with arbitrary in-plane magnetisation direction with a relative orientation angle $\alpha$ . . . . .	21
2.2	Schematic view of the S/FI structure under consideration. The ferromagnetic insulator has two domains with arbitrary in-plane magnetisation direction. The magnetisations of the two domains lie on the $xy$ -plane, and they form an angle $\alpha$ . . . . .	22
2.3	Proposed geometry to detect the triplet correlations. An F layer is placed on top of an S layer; if the F layer is thick enough, only the triplet correlations perpendicular to the magnetisation of the F layer will propagate along the ferromagnet. The long-range triplet correlations manifest as a zero-energy peak on the local DoS, probed through tunnel differential conductance measurements with a normal metal electrode (N). . . . .	25
2.4	(a) S/F/S structure. Here, F is a wire with Rashba spin-orbit coupling, and a spin-splitting field $\mathbf{h}$ . (b) S/FI/F/FI/S structure. FI layers act as spin-filtering barriers with polarizations $\mathbf{P}_{r/l}$ , and they induce spin-splitting fields $\mathbf{h}_{r/l}$ in adjacent S layers. F is a ferromagnet with an exchange field $\mathbf{h}$ . . . . .	27
2.5	Schematic structure of the Andreev interferometer. An anomalous Josephson junction is coupled to a mesoscopic conductor. . . . .	28
2.6	Simple circuit scheme of the photon-assisted bipolar thermoelectricity. The two superconductors have a different gap $\Delta_1 > \Delta_2$ and are subject to a temperature difference $T_1 > T_2$ . The S-I-S' junction is powered by a DC and an AC voltage source. . . . .	32
2.7	Non-linear thermoelectricity (red) and cooling (blue) regions for a superconductor with $T_{c,1} = 2T_{c,2}$ . The dashed line delimits the equal temperature contour $T_1 = T_2$ . The solid horizontal line shows the temperature $T_2 = T_{c,2}$ above which $S_2$ becomes a normal metal. . . . .	35

- 
- 2.8 Tunnelling quasiparticle current for (a) S/N junction at  $T_1 = T_2 = 0$ , (b) S/S junction at  $T_1 = T_2 = 0$ , (c) S/S junction at  $T_1 > T_2$ , and (d) S/S' junction with  $\Delta_{0,1} > \Delta_{0,2}$  at  $T_1 > T_2$ . . . . . 36
- 2.9 (a) Proposed setup for the measurement of the Hall effect. Materials subjected to a magnetic field show circular birefringence, *i.e.* left and right polarized light waves propagate with different velocities. The Kerr rotation angle is related to the longitudinal and transversal conductivities of the material. (b) Proposed setup for the detection of the inverse spin Hall effect in a superconductor using a lateral spin valve. Suppose a charge current  $I_Q$  is injected from the ferromagnet (F) to the normal metal (N). In that case, the non-equilibrium spin accumulation generated at the interface generates a pure spin current  $I_S$  to the right of F. The superconductor absorbs the spin current owing to its strong SOC, generating a charge current  $I'_Q$  due to the inverse spin Hall effect. . . . . 40

# Nomenclature

## Abbreviations

AC	Alternating current
AJE	Anomalous Josephson effect
BCS	Bardeen-Cooper-Schrieffer
DC	Direct current
DoS	Density of states
F	Ferromagnet
FI	Ferromagnetic insulator
GF	Green's function
I	Insulator
JJ	Josephson junction
N	Normal metal
PAT	Photon-assisted tunnelling
S	Superconductor
SOC	Spin-orbit coupling

## List of Symbols

<b><math>A</math></b>	Magnetic vector potential
$\check{A}^\mu$	Generalised four-potential
$a$	Voltage amplitude
$\alpha$	Rashba spin-orbit coupling strength
<b><math>B</math></b>	Magnetic field
COP	Coefficient of performance
$D$	Diffusion constant
$\Delta$	Superconducting order parameter
$\check{\Delta}$	Pair potential
$\Delta_0$	Superconducting order parameter at $T = 0$ and $h = 0$

---

$E^{j\nu}$	Generalised electric field
$e$	Electron charge
$\varepsilon$	Excitation energy
$\varepsilon_F$	Fermi energy
$\eta$	Thermoelectric efficiency
$\tilde{F}^{\mu\nu}$	Generalised field strength tensor
$\hat{f}$	Anomalous Green's function in spin space
$\Phi$	Magnetic flux
$\Phi_0$	Flux quantum
$\varphi$	Scalar potential or superconducting phase
$\varphi_0$	Anomalous phase
$\tilde{G}$	Exact Green's function in Nambu-spin space or Keldysh-Nambu-spin space
$G_T$	Tunnelling conductance
$\hat{g}$	Normal Green's function in spin space
$\check{g}$	Quasiclassical Green's function in Nambu-spin or Keldysh-Nambu-spin space
$\Gamma$	Inelastic scattering factor
$\mathbf{h}$	Zeeman/exchange field
$\check{h}$	Distribution function
$\check{\mathcal{H}}$	Hamiltonian
$I_c$	Critical current
$I_J$	Josephson current
$I_S$	Supercurrent
$I_{qp}$	Quasiparticle current
$\check{\mathbf{J}}$	Matrix current
$\mathbf{j}$	Current density
$j^{i\mu}$	Charge-spin current density
$\varkappa$	Spin-swapping coefficient
$\ell$	Transport mean free path
$m$	Electron mass
$\mu_{ch}$	Chemical potential
$N(\varepsilon)$	Density of states
$N_0$	Density of states in the normal state
$\hat{\mathbf{n}}$	Unit vector along the Fermi momentum



---

$\Omega_D$	Debye frequency
$\omega$	Angular frequency
$\omega_c$	Cyclotron frequency
$\omega_n$	Matsubara frequency
$\omega_p$	Plasma frequency
$P$	Barrier polarization
$\dot{Q}$	Heat current
$R$	Resistance
$R_{\square}$	Interface resistance per unit area
$\check{\Sigma}, \check{\Sigma}_s$	Self-energy
$\sigma^{i\mu,j\nu}$	Generalised conductivity tensor
$\sigma_j, j = 1, 2, 3$	Pauli matrices in spin space
$\sigma_N$	Drude conductivity
$T$	Wick-time ordering operation
$T$	Temperature
$T_c$	Critical temperature
$T_{c0} = \Delta_0/1.76$	Field free critical temperature
$\tau$	Transport mean free time or imaginary time
$\tau_j, j = 1, 2, 3$	Pauli matrices in Nambu space
$\tau_{SO}$	Spin-orbit relaxation time
$\theta$	Spin Hall angle
$\theta_F, \theta_K$	Faraday and Kerr rotation angles
$V$	Voltage
$V_p$	Matching peak
$v_F$	Fermi velocity
$\dot{W}$	Power
$\xi_{\varepsilon}$	Normal state coherence length
$\xi_F$	Magnetic length
$\xi_{\mathbf{k}}$	Free-particle energy measured from the Fermi level
$\xi_s, \xi_0$	Superconducting coherence lengths



# Chapter 1

## Introduction

*If God had consulted me before  
embarking on the Creation,  
I would have suggested something simpler.*

— Alfonso X the Wise, on the Ptolemaic model

Extensive theoretical and experimental works highlight the versatility of hybrid superconducting structures. They find applications in diverse domains such as spintronics, thermoelectricity, and sensors [1–4]. Most of these applications are based on the non-equilibrium properties of superconductors, i.e., properties that arise out of thermodynamic equilibrium. In this thesis we study the non-equilibrium properties of superconductors in the presence of spin-dependent fields, that is, fields that interact with the spin of quasiparticles, such as Zeeman fields and spin-orbit coupling. Specifically, we study the charge, thermoelectric and spintronic transport in several superconducting hybrid devices.

Thermoelectric effects are a popular research topic, due to their potential to convert heat into work. A fundamental factor enabling thermoelectricity in electronic conductors is the breaking of the symmetry between positive-energy (electrons) and negative-energy (holes) charge carriers. This asymmetry of the density of states (DoS) is achieved by applying a spin-splitting field. Consequently, coupling superconductors with a spin-polarized system emerges as a promising approach for inducing thermoelectric effects [2, 3, 5–8]. Thermoelectric detectors [9] have been proposed in astrophysics for the detection of the cosmic microwave background [10], and terahertz-radiation sensing used, for example, in security imaging [11]. Remarkably, the superconducting thermoelectric detector directly uses the absorbed radiation to generate the desired measurement signal, without the need for an external energy source.

The utility of charge and thermoelectric transport extends to various applications, including low-temperature thermometry, the development of highly sensitive electron thermometers, and the realization of temperature-to-frequency converters [12]. Notably, heat transport has the potential to generate giant spin currents due to the presence of spin-triplet Cooper pairs [5, 13, 14]. Furthermore, superconducting hybrid structures featuring spin-dependent fields offer a platform for creating highly efficient spin and heat valves [15–18]. These hybrid structures also facilitate cooling in the nanoscale [19, 20], and more recently, the implementation of a quantum phase battery [21]. Other applications based on superconducting electronics are the superconducting diodes [22]. In usual superconductors, the electron-hole symmetry results in reciprocal charge transport. This symmetry is broken in spin-split superconductor with spin filtering, allowing for non-reciprocity. Notably, the efficacy of these applications relies on superconductors characterized by a well-defined spin-split DoS and a distinct energy gap.

Another key ingredient in hybrid superconducting structures is spin-orbit coupling (SOC). Unlike Zeeman fields, the SOC induces a momentum-dependent spin interaction. The coupling

of the orbital and spin degrees of freedom is a key ingredient in spintronics. For instance, the spin Hall effect involves the generation of a transverse spin current in response to a charge current. In superconductors, the spin Hall effect couples the spin current to both the quasiparticle current and the (equilibrium) supercurrent [23–27]. Topological superconductivity can emerge in hybrid devices involving conventional superconductors and semiconductors with strong spin-orbit coupling [28]. The most appealing manifestation of topological superconductivity is the Majorana zero modes that are predicted to exist at the ends of the proximitised nanowires. This kind of superconductor–semiconductor hybrid platforms have been proposed for topological quantum computing schemes [29].

The exploration of the interaction between superconductivity and spin-dependent fields in hybrid systems has emerged as a prolific and vibrant field of research over the past decades. The purpose of this PhD thesis is to theoretically study the non-equilibrium properties of superconducting structures subjected to different types of spin-dependent fields. Spin-dependent fields can be classified as SOC terms that break the inversion symmetry, and magnetic (Zeeman-like) terms that break the time-reversal symmetry. Real hybrid structures show non-controllable disorder that needs to be appropriately modelled. One possibility is to implement disorder into the microscopic models, for example through tight-binding models. This approach is computationally very expensive. Another possible approach, based on the Green’s function (GF) method, is to reduce the microscopic equations to kinetic-like equations. In this approach, interfaces between different materials are described by boundary conditions. On top of this, the studied materials are practically metallic systems where the Fermi energy is much larger than the other energy scales in the system, so one may use the quasiclassical approximation to simplify the equations.

This thesis is organised according to the following structure. In Chap. 1, we introduce the systems to be studied in the Thesis and outline the formalism used to study them. We devote Sec. 1.1 to the theory of superconductors that conform the hybrid structures studied in the Thesis. In Sec. 1.2 we define the GF method, which is the main theoretical tool used in this Thesis, and introduce the Gor’kov equation for a superconductor. The Gor’kov equation contains much information that is irrelevant for the transport properties of the studied systems. Therefore, in Secs. 1.3 and 1.4, we get rid of the rapid oscillations on the Fermi wavelength scale and introduce the quasiclassical approximation. We derive the kinetic (Eilenberger) equation for the quasiclassical GF. In the diffusive limit, the impurity concentration is so high that a material can be taken to be isotropic. In this case, the Eilenberger equation reduces to the Usadel equation. All the systems studied in this Thesis are described by the Usadel equation, we use different extensions to account for different types of spin-dependent fields. In Sec. 1.5 we theoretically describe the hybrid interfaces between different types of materials, and introduce the corresponding boundary conditions.

In Chap. 2, we present a more in-depth explanation of the models and methods used to study each of the four systems covered in this Thesis. In addition, we summarize the main results that conform the backbone of this Thesis. We exhibit our main conclusions in Chap. 3. Selected publications derived from the work done during this doctorate are compiled as Chapters 4–7. In Chap. 4, we study the singlet and triplet correlations in the vicinity of a sharp domain wall and explain how they manifest in the local density of states (DoS). Next, in Chap. 5, we study the anomalous Josephson effect in an Andreev interferometer device. In Chap. 6, we investigate the interplay of photon-assisted tunnelling and bipolar thermoelectric generation in asymmetric superconducting tunnel junctions. Finally, in Chap. 7, we present a unified description of dynamical charge and spin transport in diffusive superconductors.

## 1.1 Theory of superconductivity

Many metals undergo a phase transition into a superconducting state at sufficiently low temperatures. This state of matter is characterised by perfect, zero-resistance, conductivity. This means that the current flows through a superconductor without any energy dissipation. H. Kamerlingh Onnes discovered superconductivity in 1911 when he studied the low-temperature resistivity of mercury [30]. This discovery was followed by the report of superconductivity in other metals. The temperature at which a metal transitions from the normal state to the superconducting state is referred to as the critical temperature  $T_c$ ; in conventional superconductors the critical temperature typically lies in the 1-10 K range. Georg Bednorz and K. Alex Müller discovered superconductivity in ceramic materials in 1986 [31]. This kind of superconductors are known as high-temperature superconductors, with a critical temperature above 77 K, which is the boiling point of liquid nitrogen.

Another characteristic property of superconductors is the Meissner-Ochsenfeld effect: the expulsion of magnetic fields of a bulk superconductor [32]. If a superconductor is subjected to a constant magnetic field, the magnetic field will only penetrate into the superconductor over a penetration depth of the order of  $10^{-8}$  m. The perfect diamagnetism of superconductors enables them to be used for magnetic levitation.

The Barden-Cooper-Schrieffer (BCS) theory [33] was the first theory to explain superconductivity microscopically in 1957. In the ground state of a free electron gas, the electrons fill all one-electron states below the Fermi energy  $\varepsilon_F$ . However, this ground state becomes unstable in the presence of an attractive interaction between the electrons, regardless of the interaction strength. Cooper showed in 1956 that a weak attraction between electrons can bind electron pairs into bound states [34]. This result is a consequence of the Fermi statistics and the existence of the background Fermi-sea. Since the formation of pairs is energetically favourable, the interaction rebuilds the ground state of the system. This ground state is accompanied by an energy gap in the excitation spectrum, equal to the energy of formation of a bound pair.

In conventional superconductors, the physical mechanism that leads to an attractive interaction between electrons in a crystal is the electron-phonon interaction. This interaction usually occurs for energies close to  $\varepsilon_F$ , and vanishes for energy transfers larger than a cutoff value, see Fig. 1.1. This phonon-mediated interaction leads to an exchange of momentum between the electrons and the vibrating crystal lattice. This pairing mechanism was first proposed by Fröhlich in 1950 [35]. Independently, the isotope effect, *i.e.*, the proportionality  $T_c \propto M^{-1/2}$  of the critical temperature for isotopes of the same element, where  $M$  is the mass of the given isotope, was discovered the same year [36, 37]. This clear dependence of superconductivity on the mass of the ions confirmed the electron-phonon interaction hypothesis. The phonon interaction is effective when the exchange of energy is smaller than the characteristic Debye energy  $\Omega_D$ . The electrons also experience Coulomb repulsive forces; in general, the problem of treating both interactions into account is very complicated, so superconductivity is typically described by a simple model where electrons have a quadratic dispersion law, and the electrons that lie near the Fermi surface suffer an effective attractive interaction. The so-called pairing Hamiltonian or BCS Hamiltonian is given by

$$H = \sum_{\mathbf{k}, \sigma} \xi_{\mathbf{k}} c_{\mathbf{k}, \sigma}^{\dagger} c_{\mathbf{k}, \sigma} + \sum_{\mathbf{k}, \mathbf{k}'} V_{\mathbf{k}, \mathbf{k}'} c_{\mathbf{k}, \uparrow}^{\dagger} c_{-\mathbf{k}, \downarrow}^{\dagger} c_{-\mathbf{k}', \downarrow} c_{\mathbf{k}', \uparrow}, \quad (1.1)$$

where  $c_{\mathbf{k}, \sigma}^{\dagger}$  and  $c_{\mathbf{k}, \sigma}$  are the creation and annihilation operators for state with momentum  $\mathbf{k}$  and spin  $\sigma$ , respectively. The BCS Hamiltonian (1.1) assumes that electrons group into pairs with opposite momenta and spin.

For an s-wave superconductor, the interaction  $V_{\mathbf{k}, \mathbf{k}'}$  is an isotropic attraction which is constant

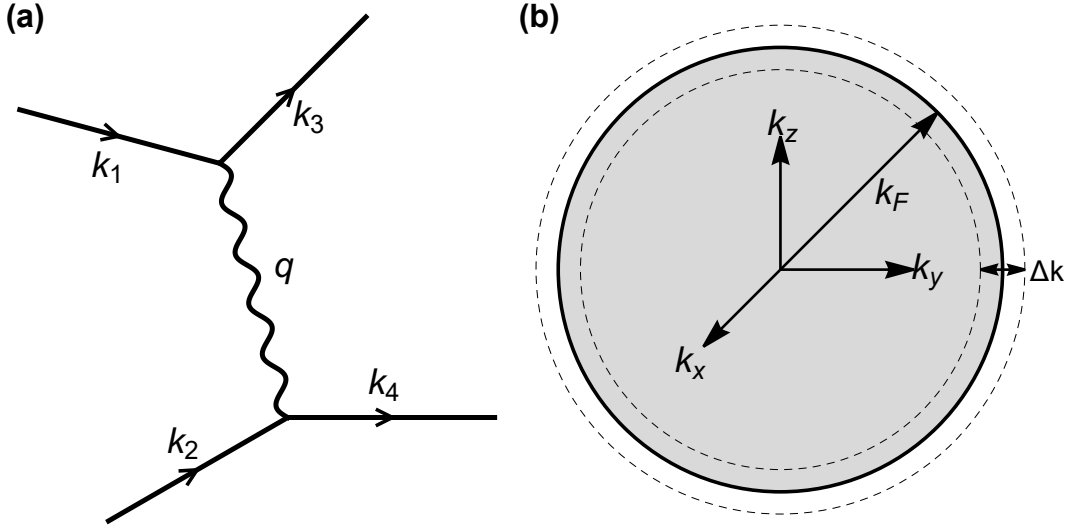


Figure 1.1: (a) Diagram illustrating the electron-electron interaction via the emission/absorption of a phonon. (b) In the BCS theory, the attractive electron-electron interaction only occurs in a small energy shell around the Fermi surface. The thickness of the shell is of the order of Debye energy.

in an energy band around the Fermi energy:

$$V_{\mathbf{k},\mathbf{k}'} = \begin{cases} -V, & \text{if } \xi_{\mathbf{k}}, \xi_{\mathbf{k}'} \leq \Omega_D, \\ 0, & \text{otherwise} \end{cases}, \quad (1.2)$$

where  $\xi_{\mathbf{k}} = k^2/(2m) - \varepsilon_F$  is the free-particle energy measured from the Fermi level,  $V > 0$  and  $VL^3N_0 \ll 1$ , with  $N_0$  the normal state DoS at the Fermi level and  $L^3$  the volume of the crystal. If  $V$  is strong enough to overcome the repulsive Coulomb interaction between electrons, superconductivity may arise.

The BCS interaction takes place at zero momentum, so it involves infinite-range interaction between pairs. This long-range aspect makes the BCS model suitable for treating the interaction as a mean-field. The mean-field pair potential is given by

$$\Delta = -V \int \frac{d\mathbf{k}}{(2\pi/L)^3} \langle c_{-\mathbf{k},\downarrow} c_{\mathbf{k},\uparrow} \rangle. \quad (1.3)$$

$\Delta$  is known as the order parameter, whose magnitude  $|\Delta|$  sets the size of the gap in the excitation spectrum.

In the thermodynamic limit, we may expand the BCS interaction in powers of the fluctuations of  $-Vc_{-\mathbf{k},\downarrow}c_{\mathbf{k},\uparrow}$  and keep the leading order to write the BCS mean-field Hamiltonian [38]:

$$H = \sum_{\mathbf{k},\sigma} \xi_{\mathbf{k}} c_{\mathbf{k},\sigma}^\dagger c_{\mathbf{k},\sigma} + \sum_{\mathbf{k}} \left( \Delta^* c_{-\mathbf{k},\downarrow} c_{\mathbf{k},\uparrow} + c_{\mathbf{k},\uparrow}^\dagger c_{-\mathbf{k},\downarrow}^\dagger \Delta \right) + V|\Delta|^2. \quad (1.4)$$

The last term in the Hamiltonian may be absorbed into the chemical potential.  $\Delta$  needs to be determined self-consistently by minimizing the free energy

$$\Delta = \frac{\Omega_D}{\sinh [2/(VL^3N_0)]} \approx 2\Omega_D e^{-2/(VL^3N_0)}. \quad (1.5)$$

The last approximation is valid in the weak-coupling limit  $VL^3N_0 \ll 1$ .

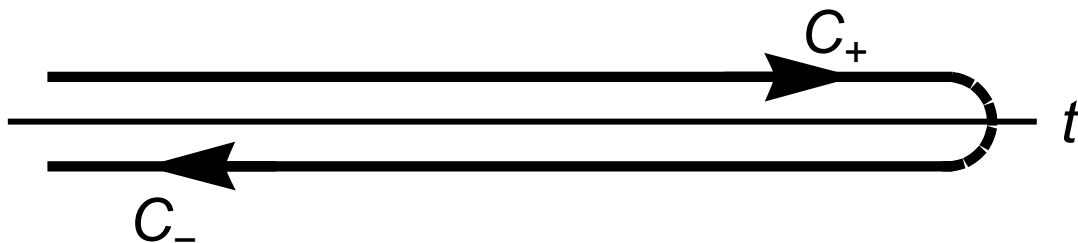


Figure 1.2: Schwinger-Keldysh contour, the direction of the arrows indicates the ordering of times along the forward ( $C_+$ ) and backward ( $C_-$ ) branches. The branches have been shifted vertically for clarity.

The  $\Delta^* c_{-\mathbf{k},\downarrow} c_{\mathbf{k},\uparrow}$  term in the mean-field Hamiltonian describes the conversion of two particles into a condensate pair. Alternatively,  $c_{-\mathbf{k},\downarrow}$  may be interpreted as the creation of a hole with momentum  $\mathbf{k}$  and spin  $\uparrow$ . This process where an electron scatters into a condensate pair and a hole is known as Andreev reflection.

In the absence of disorder, the BCS mean-field Hamiltonian (1.4) can be diagonalised by taking a linear combination of creation and annihilation operators (Bogoliubov transformation)

$$\begin{aligned} c_{\mathbf{k},\uparrow} &= u_{\mathbf{k}}^* \gamma_{\mathbf{k},0} + v_{\mathbf{k}} \gamma_{\mathbf{k},1}^\dagger \\ c_{-\mathbf{k},\downarrow}^\dagger &= -v_{\mathbf{k}}^* \gamma_{\mathbf{k},0} + u_{\mathbf{k}} \gamma_{\mathbf{k},1}^\dagger, \end{aligned} \quad (1.6)$$

where  $\gamma^\dagger$  and  $\gamma$  are the new Fermi operators, and  $|u_{\mathbf{k}}|^2 + |v_{\mathbf{k}}|^2 = 1$ .

Choosing appropriate values for  $u_{\mathbf{k}}$  and  $v_{\mathbf{k}}$ , one obtains the Bogoliubov-de-Gennes Hamiltonian

$$H = \sum_{\mathbf{k}} (\xi_{\mathbf{k}} - E_{\mathbf{k}}) + \sum_{\mathbf{k}} E_{\mathbf{k}} (\gamma_{\mathbf{k},0}^\dagger \gamma_{\mathbf{k},0} + \gamma_{\mathbf{k},1}^\dagger \gamma_{\mathbf{k},1}). \quad (1.7)$$

The first term is a constant that gives the energy of the BCS ground state. The second term gives the energy increase  $E_{\mathbf{k}} = \sqrt{\xi_{\mathbf{k}}^2 + |\Delta|^2}$  due to the creation of excitations, the so-called Bogoliubons [39–41].

Hamiltonian (1.7) shows that the minimum excitation energy for the ground state is  $|\Delta|$ , implying the existence of a gap [42]. The superconducting gap is related to the critical temperature  $T_{c0}$  by [43]

$$|\Delta| = \frac{\pi}{e^\gamma} T_{c0} \approx 1.764 T_{c0}, \quad (1.8)$$

where  $\gamma \approx 0.577$  is the Euler–Mascheroni constant.

The Bogoliubov-de-Gennes equations are convenient to obtain results in clean superconductors. However, real materials show impurities which need to be treated appropriately to describe the materials realistically. In the following section, we introduce the Green's function method first introduced by Gor'kov, which allows to treat different scattering processes, hybrid structures and time-dependent phenomena conveniently.

## 1.2 Green's function method

The theoretical tool used in this Thesis to study superconductivity is the Green's function (GF) method. It is a very useful method in the microscopic theory of many-fermion systems. For instance,

the microscopic properties of the system can be extracted from the GF. Gor'kov [44] and Migdal [45] developed this method for the case of superconducting systems.

The time-ordered one-particle GF for a many-fermion system is defined as

$$G(r, r') = -i\langle T\Psi(r)\Psi^\dagger(r') \rangle, \quad (1.9)$$

where  $\Psi^\dagger(r)$  and  $\Psi(r)$  are the quantum field operators in the Heisenberg representation  $\Psi(r) = e^{iHt}\Psi(\mathbf{r})e^{-iHt}$ , respectively,  $\langle \dots \rangle$  denotes the thermodynamic average, and  $T$  represents Wick-time ordering operation for fermions. The physical interpretation of the GF is the propagation of disturbances in which a single particle is added and removed from the many-particle equilibrium system. For instance, for positive time ( $t > t'$ ), Eq. (1.9) describes the propagation of a disturbance of a particle added at  $r'$  and removed at  $r$ , returning the system to the equilibrium state. For negative time ( $t < t'$ ), the disturbance is produced by the removal of a particle at  $r$  and added at point  $r'$ , describing the propagation of holes.

In the following, we introduce the Keldysh GF technique [46], which allows us to describe many-body systems outside equilibrium. We assume that the system is at thermal equilibrium at  $t = -\infty$ . The Keldysh contour consists of a forward and backward branch running from  $t = -\infty$  to  $t = \infty$  and back, as shown in Fig. 1.2. The GFs are defined on this Keldysh contour, depending on whether they are defined on the forward or backward paths they reduce to different analytic functions. These functions are grouped into a  $2 \times 2$  matrix in the so-called Keldysh space (forward/backward branch space). However, only three of the terms are linearly independent, so it is convenient to linear transform the GF into a triangular matrix representation [47]

$$\check{G} = \begin{pmatrix} G^R & G^K \\ 0 & G^A \end{pmatrix}, \quad (1.10)$$

where the  $\check{\cdot}$  accent denotes a matrix in Keldysh space. This triangular matrix structure is very convenient for calculations. The components of the matrix GF are the retarded, advanced and Keldysh GFs  $G^{R/A/K}$ ,

$$G^R(r, r') = -i\theta(t - t')[\langle \Psi(r)\Psi^\dagger(r') \rangle + \langle \Psi^\dagger(r')\Psi(r) \rangle] \quad (1.11a)$$

$$G^A(r, r') = i\theta(t' - t)[\langle \Psi(r)\Psi^\dagger(r') \rangle + \langle \Psi^\dagger(r')\Psi(r) \rangle] \quad (1.11b)$$

$$G^K(r, r') = i[\langle \Psi^\dagger(r')\Psi(r) \rangle - \langle \Psi(r)\Psi^\dagger(r') \rangle]. \quad (1.11c)$$

The retarded and advanced GFs determine the equilibrium properties of the system, such as the density of states (DoS). In contrast, the Keldysh GF  $G^K$  determines the transport (non-equilibrium) properties of the system, such as the charge, heat and spin currents.

### 1.2.1 Gor'kov equations

In the following, we extend the GFs defined in the previous section to account for the superconducting pair potential introduced in Eq. (1.4). The GF in Nambu space, which combines the particle and hole spaces [48], is given by

$$\check{G}(r, r') = -i\langle T\hat{\Psi}(r)\hat{\Psi}^\dagger(r') \rangle = \begin{pmatrix} G(r, r') & F(r, r') \\ F^\dagger(r, r') & G^\dagger(r, r') \end{pmatrix}, \quad (1.12)$$

where  $G(r, r') = -i\langle T\Psi_\uparrow(r)\Psi_\uparrow^\dagger(r') \rangle$  is the normal component of the GF, and  $F(r, r') = -i\langle T\Psi_\uparrow(r)\Psi_\downarrow^\dagger(r') \rangle$  is the anomalous component of the GF, which describes the superconducting correlations.  $\hat{\Psi}^\dagger = (\Psi_\uparrow^\dagger, \Psi_\downarrow)$  is a pseudo-spinor; since the annihilation of an electron is equivalent



to the creation of a hole,  $\hat{\Psi}^\dagger$  contains two creation operators, one for a spin up electron and one for a hole with spin down. In order to account for spin-dependent fields, one should include the creation/annihilation operators for spin down/up in  $\hat{\Psi}^\dagger = (\Psi_\uparrow^\dagger, \Psi_\downarrow^\dagger, -\Psi_\downarrow, \Psi_\uparrow)$ , so that  $G(r, r')$  and  $F(r, r')$  become  $2 \times 2$  matrices in spin space (usually denoted by a hat accent  $\hat{G}$ )

$$\check{G}(r, r') = \begin{pmatrix} \hat{G}(r, r') & \hat{F}(r, r') \\ \hat{F}^\dagger(r, r') & \hat{G}^\dagger(r, r') \end{pmatrix}. \quad (1.13)$$

Here, the  $\check{\cdot}$  accent denotes a  $4 \times 4$  matrix in Nambu-spin space and the  $\hat{\cdot}$  accent a  $2 \times 2$  matrix in spin space.

It is possible to define the retarded/advance/Keldysh GFs as in Eq. (1.11) in Nambu-spin space, so the equivalent of Eq. (1.10) including all degrees of freedom is

$$\check{G} = \begin{pmatrix} \check{G}^R & \check{G}^K \\ 0 & \check{G}^A \end{pmatrix}, \quad (1.14)$$

where  $\check{G}$  is a  $8 \times 8$  matrix in Keldysh-Nambu-spin space.

The Green's functions may be calculated using the diagram technique. If the particles making up the system are subject to a weak interaction, we may write a perturbation series with respect to the interaction:

$$\check{\mathcal{H}} = \check{\mathcal{H}}_0 + \check{V}_s, \quad (1.15)$$

where  $\check{V}_s$  is an arbitrary scattering potential.  $\check{V}_s$  may describe the electron-electron interactions, for example, but in this Thesis we only consider scattering by random elastic and magnetic potentials.  $\check{\mathcal{H}}_0$  is the BCS Hamiltonian in Keldysh-Nambu-spin space

$$\check{\mathcal{H}}_0(r) = \frac{1}{2m}(-i\nabla_{\mathbf{r}} + e\mathbf{A}(r)\tau_3)^2 - \mu_{\text{ch}} - e\varphi(r) + \mathbf{h}(r) \cdot \boldsymbol{\sigma}\tau_3 - i\check{\Delta}(r), \quad (1.16)$$

obtained from Eq. (1.4) as

$$H = \int d\mathbf{r} \hat{\Psi}^\dagger(\mathbf{r}) \check{\mathcal{H}}_0(\mathbf{r}) \hat{\Psi}(\mathbf{r}). \quad (1.17)$$

Hamiltonian (1.16) has been generalised to contain Zeeman fields  $\mathbf{h}$ , electromagnetic potentials  $\varphi$  and  $\mathbf{A}$ , and a spatially dependent superconducting order parameter  $\check{\Delta} = \begin{pmatrix} 0 & \Delta \\ \Delta^* & 0 \end{pmatrix}$ .

The pair potential is related to the anomalous GF through the self-consistency equation

$$\check{\Delta}(r) = -i\frac{\lambda}{2}\check{F}(r, r), \quad (1.18)$$

where  $\lambda$  is the strength of the attractive electron-electron interaction, related to the  $V$  introduced in Eq. (1.2).

In most cases, it is not enough to consider the first few diagrams in the perturbation series. Instead, one should sum an infinite series of terms containing the ‘‘principal diagrams’’, that are of the same order of magnitude. The addition of the terms can graphically be represented as a summation of diagrams. This means that a diagram represents the sum of infinite terms, each of which might also represent a summation.

Formally, the diagrams consist of lines (Green's functions) and vertex operators, which are joined through coordinate integration. The diagrams may be split into blocks, made up of unperturbed Green's functions  $\check{G}_0$  and elementary vertices. Any part of a diagram which can be joined to the rest of the diagram by  $\check{G}_0$  lines is called a self-energy part [49]. If the self-energy part cannot be split into different parts by removing a single  $\check{G}_0$ -line, it is called an irreducible self-energy part.

All the terms in a diagram begin with a  $\check{G}_0$ -line, followed by an irreducible self-energy part  $\check{\Sigma}$ . If these two terms are removed from the parts of the diagrams, the resulting diagram begins with a  $\check{G}_0$ -line plus an arbitrary sum of self-energy parts, *i.e.* the exact  $\check{G}$ -line. This identity is described by the Dyson equation

$$\check{G} = \check{G}_0 - i\check{G}_0 \circ \check{\Sigma} \circ \check{G}, \quad (1.19)$$

or equivalently,

$$(\check{G}_0^{-1} + i\check{\Sigma}) \circ \check{G} = \delta(r - r'), \quad (1.20)$$

where  $\circ$  denotes convolution, *i.e.*, integration over intermediate variables.

In a superconductor, the GF (1.14) is determined by the generalised Dyson equation for the BCS model, also known as the Gor'kov equation [50]. The matrix operator  $\check{G}_0^{-1}$  is given by

$$\check{G}_0^{-1}(r, r') = \left( i\tau_3 \frac{\partial}{\partial t} - \check{\mathcal{H}}_0(r) \right) \delta(r - r'), \quad (1.21)$$

and  $\check{\Sigma}$  is the self-energy term which generates collision integrals for the different scattering processes of the kinetic transport theory, including processes such as scattering with impurities, magnetic impurities and electron-phonon interaction described by the  $\check{V}_s$  potential. For instance, for a random scattering potential  $\check{V}_s$  is given by

$$\check{V}_s(\mathbf{r}) = \sum_{i=1}^{N_{\text{imp}}} v(\mathbf{r} - \mathbf{R}_i), \quad (1.22)$$

where  $N_{\text{imp}}$  is the number of impurity scatterers and  $\mathbf{R}_i$  are the positions of scatterers that follow a constant distribution function. In this case, the exact GF takes the form

$$\begin{aligned} \check{G} = & \check{G}_0 + \sum_i \check{G}_0 \circ v(r - R_i) \delta(r - r') \circ \check{G}_0 \\ & + \sum_{i,j} \check{G}_0 \circ v(r - R_i) \delta(r - r') \circ \check{G}_0 \circ v(r - R_j) \delta(r - r') \circ \check{G}_0 + \dots \end{aligned} \quad (1.23)$$

Since we are dealing with a random potential, we are not interested in the exact solution. The physical characteristics of the system are determined by impurity averaging, *i.e.*, an average over the ensemble of all possible impurity configurations. This allows us to replace the sums with integrations over impurity positions  $\sum_i \rightarrow n_{\text{imp}} \int d\mathbf{r}_i$ , with  $n_{\text{imp}} = N_{\text{imp}}/L^3$  the impurity density.

Equation (1.23) may be written as a Dyson equation (1.19), where the self-energy term in the momentum representation is given by

$$\check{\Sigma}(\mathbf{p}) = in_{\text{imp}} \int \frac{d\mathbf{p}_1}{(2\pi)^3} |v(\mathbf{p} - \mathbf{p}_1)|^2 \check{G}(\mathbf{p}_1). \quad (1.24)$$

We assume that the Born approximation is valid, which implies that the scattering potential is small compared to the characteristic atomic potential, which is of the order of the Fermi energy. In the Born approximation only the momenta close to the Fermi surface are relevant, so the scattering potential depends only on the angle  $\theta$  between  $\mathbf{p}$  and  $\mathbf{p}_1$ . For isotropic scattering by impurities  $v(\theta) = v$ , the self-energy is independent of momentum direction, and it may be written as

$$\check{\Sigma} = \frac{i}{\pi N(0)\tau} \int \frac{d\mathbf{p}_1}{(2\pi)^3} \check{G}(\mathbf{p}_1), \quad (1.25)$$

where  $N(0)$  is the DoS at the Fermi level, and  $\tau$  is the mean scattering time

$$\tau^{-1} = \pi N(0) |v|^2 n_{\text{imp}}. \quad (1.26)$$

Finally, inserting Eq. (1.21) into Eq. (1.20) we obtain the Gor'kov equation for a superconductor

$$\boxed{\left( i\tau_3 \frac{\partial}{\partial t} \delta(r - r'') - \check{\mathcal{H}}_0(r) \delta(r - r'') + i\check{\Sigma}(r, r'') \right) \circ \check{G}(r'', r') = \delta(r - r')}. \quad (1.27)$$

## 1.2.2 The Matsubara formalism

The Matsubara technique was developed to describe many-body systems in equilibrium at finite temperature [51]. If the system is on thermal equilibrium, then there is no need to compute the Keldysh GF; instead, one may use the Matsubara GF, which is related to the retarded/advanced GFs, effectively reducing the matrix dimension of the GF (1.14). The key idea behind this formalism is the relation between the time evolution of a quantum system, given by the unitary operator  $e^{-iHt}$ , and the Boltzmann weighting factor at a given temperature. In thermal equilibrium, the eigenvalues of physical observables do not depend on real-time. The expectation values of the observables are calculated in the grand canonical ensemble by taking traces of the operators multiplied by the weighting factor  $e^{-H/T}$ . Comparing both exponents, we find that temperature can be treated as an imaginary time  $1/T \equiv \tau = it$ .

The imaginary-time Green's function (also known as Matsubara Green's function) for fermions is defined as in Eq. (1.12) via analytical continuation for imaginary time  $0 < |\tau| < 1/T$  [49], where  $\tau = \tau' - \tau''$  is the imaginary-time difference

$$\check{G}(\tau' - \tau'', \mathbf{r}, \mathbf{r}') = -\langle \mathbb{T}_\tau \hat{\Psi}(\tau', \mathbf{r}) \hat{\Psi}^\dagger(\tau'', \mathbf{r}') \rangle. \quad (1.28)$$

The expressions of the GF at negative and positive imaginary times are related through the relation

$$\check{G}(\tau < 0) = -\check{G}(\tau + 1/T), \quad (1.29)$$

where the expression of the GF for the r.h.s. of Eq. (1.29) corresponds to the positive imaginary-time one.

Since the time  $\tau$  is defined within a finite range, we can expand the GF in a Fourier series

$$\check{G}(\tau) = T \sum_n e^{-i\omega_n \tau} \check{G}(\omega_n), \quad (1.30)$$

where the frequencies  $\omega_n = n\pi T$ ,  $n \in \mathbb{Z}$ , are discrete. These frequencies are called the Matsubara frequencies. The Fourier coefficients are given by

$$\check{G}(\omega_n) = \frac{1}{2} \int_{-1/T}^{1/T} d\tau e^{i\omega_n \tau} \check{G}(\tau) = \frac{1}{2} (1 - e^{-i\omega_n/T}) \int_0^{1/T} d\tau e^{i\omega_n \tau} \check{G}(\tau). \quad (1.31)$$

As shown by Eq. (1.31), the Fourier coefficients for fermions are nonzero only for odd  $n$ . For this reason, the Matsubara frequencies are usually labelled as  $\omega_n = 2\pi T(n + 1/2)$ ,  $n \in \mathbb{Z}$ , with

$$\check{G}(\omega_n) = \int_0^{1/T} d\tau e^{i\omega_n \tau} \check{G}(\tau). \quad (1.32)$$

The Matsubara GF is related to the (real-time) retarded  $\check{G}^R(\varepsilon)$  and advanced  $\check{G}^A(\varepsilon)$  GFs<sup>1</sup> through the relations

$$\begin{aligned} \check{G}(\omega_n) &= \check{G}^R(i\omega_n), \quad \omega_n > 0 \\ \check{G}(\omega_n) &= \check{G}^A(i\omega_n), \quad \omega_n < 0. \end{aligned} \quad (1.33)$$

The Fourier transformed GF  $\check{G}^R(\varepsilon)$  is an analytical function of  $\varepsilon$  in the upper half-plane of complex  $\varepsilon$ . Similarly, the advanced GF  $\check{G}^A(\varepsilon)$  is an analytical function of  $\varepsilon$  in the lower half-plane.

The Gor'kov equation (1.27) may be written in the Matsubara representation as

$$\boxed{(i\omega_n \tau_3 \delta(\mathbf{r} - \mathbf{r}'') - \check{\mathcal{H}}_0(\mathbf{r}) \delta(\mathbf{r} - \mathbf{r}'') + i\check{\Sigma}(\mathbf{r}, \mathbf{r}'')) \circ \check{G}(\mathbf{r}'', \mathbf{r}') = \delta(\mathbf{r} - \mathbf{r}').} \quad (1.34)$$

This equation is equivalent to Eq. (1.27) in the thermal equilibrium. In the following sections we derive the method of quasiclassical Green's functions in the time domain, but one may use the Matsubara formalism to derive the quasiclassical equations provided that the equilibrium condition is satisfied.

<sup>1</sup>See Eq. (1.43) for the definition of the real-time Fourier transformed GFs.

### 1.3 Method of quasiclassical Green's functions

All presently known superconductors have the Fermi energy considerably larger than the order parameter  $\Delta$ . This condition is especially well satisfied for conventional, low-temperature superconductors where the ratio  $\varepsilon_F/\Delta$  can be as high as  $10^3$ . In this case, the Fermi momentum is much larger than the inverse coherent length  $\xi_0^{-1} \sim \Delta/v_F$ . When all relevant energies involved are smaller than the Fermi energy, it is convenient to work in the quasiclassical approximation. The quasiclassical method makes the basis for the modern microscopic theory of nonstationary phenomena in superconductors [47]. Its main advantage is that it can coherently incorporate various relaxation mechanisms. For example, it can describe the interaction with impurities in superconducting alloys.

Subtracting the Gor'kov equation (1.27) and its conjugate

$$\left( i\tau_3 \frac{\partial}{\partial t} \delta(r - r'') - \check{\mathcal{H}}_0(r) \delta(r - r'') + i\check{\Sigma}(r, r'') \right) \circ \check{G}(r'', r') = \delta(r - r'), \quad (1.35a)$$

$$\check{G}(r, r'') \circ \left( -i\tau_3 \frac{\partial}{\partial t'} \delta(r'' - r') - \check{\mathcal{H}}_0(r') \delta(r'' - r') + i\check{\Sigma}(r'', r') \right) = \delta(r - r'), \quad (1.35b)$$

we obtain a commutator equation:

$$\left\{ i\tau_3 \frac{\partial}{\partial t} \delta(r - r') \circ \check{G}(r, r') \right\} + [-\check{\mathcal{H}}_0(r) \delta(r - r') + i\check{\Sigma}(r, r') \circ \check{G}(r, r')] = 0, \quad (1.36)$$

where the (anti)commutator  $[A \circ B] = A \circ B - B \circ A$  implies convolution<sup>2</sup>. Equation (1.36) is an inhomogeneous equation, so it has a broader set of solutions than the Gor'kov equation, specifically for any solution  $\check{G}_0$ ,  $c\check{G}_0$  with  $c \in \mathbb{C}$  will also be a solution of (1.36). Therefore, Eq. (1.36) must be supplemented with an inhomogeneous condition, which is introduced in Sec. 1.3.1 for the quasiclassical approximation.

In the following, we work in the centre-of-mass/relative spatial coordinates  $\mathbf{r} = (\mathbf{r}' + \mathbf{r}'')/2$  and  $\boldsymbol{\rho} = \mathbf{r}' - \mathbf{r}''$ , and introduce the Wigner transform in the spatial coordinates

$$\check{G}(\mathbf{r}, \mathbf{p}) = \int d\boldsymbol{\rho} e^{-i\mathbf{p}\cdot\boldsymbol{\rho}} \check{G}(\mathbf{r}, \boldsymbol{\rho}), \quad (1.37)$$

which separates the fast oscillating modes from the low modes. In this representation, the spatial convolutions become Moyal products [52], which are expressed as [53]

$$(A \circ B)(\mathbf{r}, \mathbf{p}) = e^{\frac{i}{2}(\partial_{\mathbf{r}}^A \partial_{\mathbf{p}}^B - \partial_{\mathbf{p}}^A \partial_{\mathbf{r}}^B)} A(\mathbf{r}, \mathbf{p}) B(\mathbf{r}, \mathbf{p}). \quad (1.38)$$

In the systems considered, the involved fields change slowly in the centre-of-mass coordinate  $\mathbf{r}$  with respect to the Fermi wavelength. For instance, in superconducting systems the changes of the order-parameter happen over the superconducting coherence length  $\xi_0$ . The derivatives can be approximated as  $\partial_{\mathbf{r}} \partial_{\mathbf{p}} \rightarrow 1/(\xi_0 p_F) \ll 1$ , so we may neglect short-range oscillations and expand Eq. (1.38) to leading order. Thus, the spatial convolutions are replaced with products of the Wigner transforms. In the quasiclassical approximation, the characteristic energies of the system are small compared to  $\varepsilon_F$ , so the electrons occupy a small region in momentum space around the Fermi surface. The GF contains fast oscillations in the  $|\boldsymbol{\rho}|$  coordinate, this produces a pronounced peak of the GF at  $|\mathbf{p}| = p_F$  in the momentum representation [54]. Therefore, the GF depends weakly on the magnitude of momentum. We remove this momentum magnitude dependence by defining the quasiclassical GF [55]

$$\check{g}(\mathbf{r}, \hat{\mathbf{n}}) \equiv \frac{i}{\pi} \int d\xi_p \check{G}(\mathbf{r}, \xi_p, \hat{\mathbf{n}}), \quad (1.39)$$

<sup>2</sup>Notice the additional minus sign in the time derivative term of Eq. (1.35b).

where  $\xi_p = p^2/(2m) - \mu_{\text{ch}}$ ,  $\hat{\mathbf{n}}$  is the unit vector along the Fermi momentum, and the integration takes the contribution from the poles close to the Fermi surface into account.

In Eq. (1.36), only  $\tilde{G}(\mathbf{r}, \mathbf{p})$  has a sharp dependence on  $p_F$ , so the equation can be integrated with respect to  $\xi_p$  to obtain the quasiclassical equation (Eilenberger equation of motion) for  $\check{g}$ . Expanding the commutator equation (1.36) to linear order on the (spatial) gradients, we obtain the Eilenberger equation [56]

$$\boxed{iv_F \hat{\mathbf{n}} \cdot \nabla \check{g} + \left\{ i\tau_3 \frac{\partial}{\partial t} \delta(t-t') \circ \check{g} \right\} + \left[ (-\mathbf{h} \cdot \boldsymbol{\sigma} \tau_3 + i\check{\Delta}) \delta(t-t') + i\check{\Sigma}_s + \frac{i}{2\tau} \langle \check{g} \rangle_{\hat{\mathbf{n}}} \circ \check{g} \right]} = 0, \quad (1.40)$$

where  $v_F$  is the Fermi velocity, and  $\langle \dots \rangle_{\hat{\mathbf{n}}}$  denotes average over the Fermi surface. The first (kinetic-like) term in Eq. (1.40) arises from the kinetic energy term in the Hamiltonian (1.16). The last term in the commutator is the self-energy term accounting for elastic impurity scattering within the Born approximation (1.25). Rewriting the momentum integral as  $\frac{d\mathbf{p}}{(2\pi)^3} \rightarrow \pi^2 N(0) \frac{d\Omega}{4\pi} \frac{d\xi_p}{2\pi^2}$  and applying the definition for the quasiclassical GF (1.39), we directly obtain that the self-energy term accounting for elastic impurity scattering is  $\check{\Sigma} = \langle \check{g} \rangle_{\hat{\mathbf{n}}} / (2\tau)$ . The  $\check{\Sigma}_s$  term in Eq. (1.40) accounts for all other self-energy terms, describing processes such as orbital depairing, spin-flip or spin-orbit relaxation.

The Eilenberger equation (1.40) is much simpler than the Gor'kov equation (1.20). The former gets rid of the rapid oscillations on the Fermi wavelength scale, which are irrelevant for transport equations in most systems.

### 1.3.1 Normalization condition

As anticipated in Sec. 1.2.1, the Eilenberger equation needs to be supplemented with a normalization condition that fixes the value of  $\check{g}$ . Multiplying Eq. (1.40) with  $\check{g}$  from the left/right, adding both equations, and applying that  $\check{g}$  is traceless, it follows that  $\check{g} \circ \check{g} = c\delta(t-t')$  [57].

Direct calculation of the Gorkov equation (1.35) for a bulk superconductor in equilibrium, we obtain that the proportionality constant is equal to  $c = 1$ , so the normalization condition reads:

$$\boxed{\check{g} \circ \check{g} = \delta(t-t')} . \quad (1.41)$$

The Keldysh GF can then be parametrised as [see Eq. (1.14)]

$$\boxed{\check{g}^K = \check{g}^R \circ \check{h} - \check{h} \circ \check{g}^A}, \quad (1.42)$$

where  $\check{h}$  is known as the distribution function.

In many systems it is convenient to Wigner transform the GF in the relative time coordinate  $\tau = t' - t$ <sup>3</sup> into the energy domain,

$$\check{g}(t, \varepsilon) = \int d\tau e^{i\varepsilon\tau} \check{g}(t, \tau). \quad (1.43)$$

This transformation is particularly useful in systems with time translational symmetry, where the GF does not depend on the centre-of-mass coordinate  $t = (t' + t'')/2$ . For the retarded (advanced) GF one should add the convergence factor  $\Gamma \rightarrow 0^+$  to the energy  $\varepsilon + (-)i\Gamma$  that guarantees that  $\check{g}^R = 0$  ( $\check{g}^A = 0$ ) for  $\tau < 0$  ( $\tau > 0$ ) [see Eq. (1.11)]. A finite  $\Gamma$  may also describe inelastic scattering effects present in real materials (assuming that they are frequency independent) [58]. In time translationally invariant systems, the normalization condition reduces to

$$\check{g}(\varepsilon)^2 = 1 \quad (1.44)$$

<sup>3</sup>Not to be confused with the imaginary time  $\tau$  defined in Sec. 1.2.2.

in the energy representation, and the Keldysh GF is given by  $\check{g}^K(\varepsilon) = \check{g}^R(\varepsilon)\check{h}(\varepsilon) - \check{h}(\varepsilon)\check{g}^A(\varepsilon)$ . In thermal equilibrium, the distribution function is given by the Fermi-Dirac distribution:

$$\check{h}_{\text{eq}}(\varepsilon) = \tanh \frac{\varepsilon}{2T}. \quad (1.45)$$

The retarded/advanced GFs are usually parametrised to account for the normalization condition. In systems without spin-dependent interactions, one may use the  $\theta$ -parametrisation

$$\check{g}^{R/A} = \cos \theta \tau_3 + \sin \theta \tau_1, \quad (1.46)$$

which transforms the quasiclassical equations into trigonometric differential equations. The generalised  $\theta$ -parametrisation [59] allows to describe systems with arbitrary magnetisation, such as the domain wall considered in Sec. 2.1

$$\check{g}^{R/A} = (\cos \theta V_0 - \sin \theta \mathbf{V} \cdot \boldsymbol{\sigma}) \tau_3 + (\sin \theta V_0 + \cos \theta \mathbf{V} \cdot \boldsymbol{\sigma}) \tau_1, \quad (1.47)$$

where  $V_0$  and  $\mathbf{V}$  are related to the singlet and triplet correlations<sup>4</sup>, respectively, and satisfy the condition

$$V_0^2 + \mathbf{V}^2 = 1. \quad (1.48)$$

In systems with a homogeneous Zeeman field  $\mathbf{h}$ ,  $\mathbf{V}$  becomes parallel to  $\mathbf{h}$ .

The generalised  $\theta$ -parametrisation is useful to obtain analytical results, but it is troublesome for numerical calculations due to the multivaluedness of the  $\theta$  parameter. This issue is especially significant when the thickness of the system is longer than the superconducting coherence length. The Riccati parametrisation [60] solves this issue by considering parameters that are bounded

$$\check{g}^{R/A} = \begin{pmatrix} (1 + \hat{\gamma}\hat{\gamma})^{-1} & 0 \\ 0 & (1 + \hat{\gamma}\hat{\gamma})^{-1} \end{pmatrix} \begin{pmatrix} (1 - \hat{\gamma}\hat{\gamma}) & 2\hat{\gamma} \\ 2\hat{\gamma} & -(1 - \hat{\gamma}\hat{\gamma}) \end{pmatrix}. \quad (1.49)$$

In addition, the Riccati parametrisation allows describing systems with phase-dependent order parameters such as Josephson junctions.

### 1.3.2 Observables

Knowledge of the quasiclassical GF provides all observables of the system. For instance, the spectral properties of the system are provided by the retarded and advanced GFs

$$\begin{aligned} N(t, \mathbf{r}, \varepsilon) &= \frac{N_0}{8} \text{Tr} \langle \tau_3 (\check{g}^R(t, \mathbf{r}, \varepsilon, \hat{\mathbf{n}}) - \check{g}^A(t, \mathbf{r}, \varepsilon, \hat{\mathbf{n}})) \rangle_{\hat{\mathbf{n}}} \\ &= \frac{N_0}{4} \text{Re} \{ \text{Tr} \langle \tau_3 \check{g}^R(t, \mathbf{r}, \varepsilon, \hat{\mathbf{n}}) \rangle_{\hat{\mathbf{n}}} \}, \end{aligned} \quad (1.50)$$

while the out-of-equilibrium properties such as the local charge, spin and energy currents are provided by the Keldysh GF. Specifically, the charge current is given by

$$\mathbf{j}(t, \mathbf{r}) = -\frac{eN_0}{4} \int d\varepsilon \text{Tr} \langle v_F \hat{\mathbf{n}} \tau_3 \check{g}^K(t, \mathbf{r}, \varepsilon, \hat{\mathbf{n}}) \rangle_{\hat{\mathbf{n}}}. \quad (1.51)$$

Here,  $N_0$  is the DoS in the normal state at the Fermi level. If the system is in thermal equilibrium, the energy integrals can conveniently be computed in the Matsubara representation

$$\mathbf{j}(t, \mathbf{r}) = -i2\pi T \frac{eN_0}{4} \sum_{\omega_n} \text{Tr} \langle v_F \hat{\mathbf{n}} \tau_3 \check{g}(t, \mathbf{r}, \omega_n, \hat{\mathbf{n}}) \rangle_{\hat{\mathbf{n}}}. \quad (1.52)$$

---

<sup>4</sup>see Sec. 2.1 for additional information.

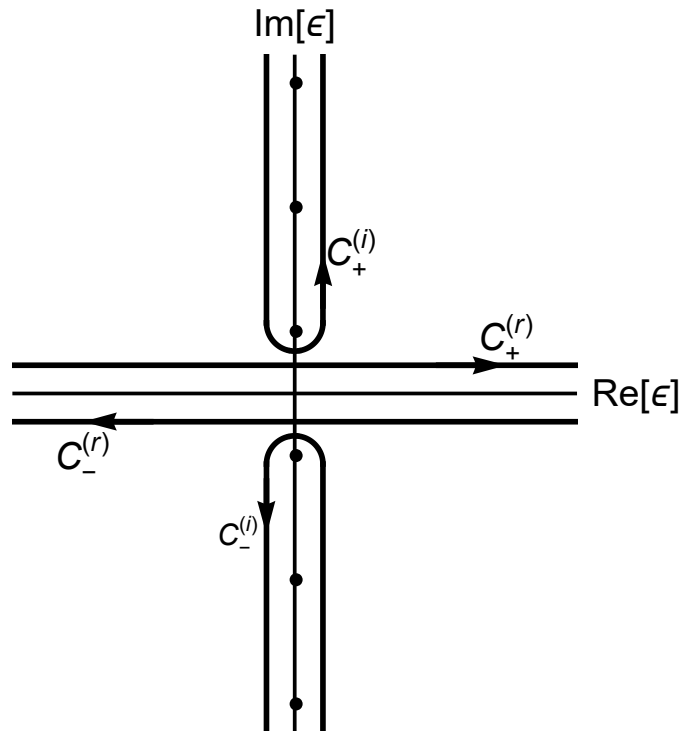


Figure 1.3: Energy integrating contours in real time  $C_+^{(r)}$  (retarded) and  $C_-^{(r)}$  (advanced), and their equivalent contours  $C_+^{(i)}$  and  $C_-^{(i)}$ , encircling the poles of the distribution function. The integral can be replaced by a sum over the Matsubara frequencies  $\omega_n$  (dots on the imaginary axis).

The energy integral contours of the retarded  $C_+^{(r)}$  and advanced  $C_-^{(r)}$  GFs may be shifted to the imaginary frequency axis, as shown in Fig. 1.3. The poles of the integrand in Eq. (1.51) are given by the equilibrium distribution function (1.45). The poles are precisely the Matsubara frequencies, which are located along the imaginary energy axis, and thus are encircled by the  $C_+^{(i)}$  and  $C_-^{(i)}$  paths. Using the residue theorem, the integrals may be replaced with sums over the Matsubara frequencies as shown by Eq. (1.52).

### 1.3.3 Self-consistency of the order parameter

The order parameter needs to be computed self-consistently from the anomalous GF as given by Eq. (1.18). In the Matsubara representation, this condition is given by

$$\check{\Delta}(t, \mathbf{r}) = \lambda N_0 \pi T \sum_{\omega_n}^{\Omega_D} \langle \check{f}(t, \mathbf{r}, \omega_n, \hat{\mathbf{n}}) \rangle_{\hat{\mathbf{n}}}, \quad (1.53)$$

where  $\check{f}$  is the anomalous part of the Matsubara GF. The summation over Matsubara frequencies is divergent, so an effective cutoff must be introduced. As explained in Sec. 1.1, the electron-electron interaction in superconductors is mediated by phonons, so the Debye frequency  $\Omega_D$  is an appropriate cutoff.

## 1.4 Diffusive limit: the Usadel equation

The Eilenberger equation can be simplified considerably in the diffusive limit, that is, when the impurity scattering rate is much larger than the critical temperature  $\tau^{-1} \gg T_c$ . This condition

is equivalent to the assumption that the mean free path  $\ell$  is small compared to the other lengths involved in the problem, except for the Fermi wavelength  $\lambda_F$ .

A strong scattering by impurities produces averaging over momentum directions. Therefore, in the first approximation, the GFs do not depend on the momentum direction. The first-order correction is linear in  $\mathbf{v}_F$ , so the GF can be written as

$$\check{g} \approx \check{g}_0 + \hat{\mathbf{n}} \cdot \delta\check{g}, \quad (1.54)$$

where  $\check{g}_0$  is  $\hat{\mathbf{n}}$ -independent and  $|\delta\check{g}| \ll \check{g}_0$ . Averaging Eq. (1.40) over the momentum direction we arrive at

$$i\frac{v_F}{3}\nabla \cdot \delta\check{g} + \left\{ i\tau_3 \frac{\partial}{\partial t} \delta(t-t') \circ \check{g}_0 \right\} + [(-\mathbf{h} \cdot \boldsymbol{\sigma}\tau_3 + i\check{\Delta})\delta(t-t') + i\check{\Sigma}_s \circ \check{g}_0] = 0, \quad (1.55)$$

while averaging Eq. (1.40) after multiplication by  $\hat{\mathbf{n}}$  yields

$$iv_F\nabla\check{g}_0 + \left\{ i\tau_3 \frac{\partial}{\partial t} \delta(t-t') \circ \delta\check{g} \right\} + [(-\mathbf{h} \cdot \boldsymbol{\sigma}\tau_3 + i\check{\Delta})\delta(t-t') + i\check{\Sigma}_s \circ \delta\check{g}] + \frac{i}{2\tau}(\check{g}_0 \circ \delta\check{g} - \delta\check{g} \circ \check{g}_0) = 0. \quad (1.56)$$

In the diffusive limit  $\tau^{-1} \gg \partial\check{g}/\partial t, h, \Delta$ , so the (anti)commutator in equation Eq. (1.56) can be neglected. Multiplying this equation by  $\check{g}_0$ , and using the normalization condition (1.41) for  $\check{g}_0$  and  $\delta\check{g}$ , we obtain the following relation:

$$\delta\check{g} = -\ell\check{g}_0 \circ \nabla\check{g}_0, \quad (1.57)$$

where  $\ell = v_F\tau$  is the mean free path. As explained in Sec. 1.3, the GF changes over a characteristic coherence length  $\xi_0$ , so its spatial derivatives are of the order of  $\nabla \sim \xi_0^{-1}$ . In the diffusive limit, the mean free path is much shorter than the coherence length  $\ell/\xi_0 \ll 1$ , so the approximation (1.54) is justified. The  $\delta\check{g}$  term is identified with the current matrix

$$\check{\mathbf{J}} = \check{g} \circ \nabla\check{g}. \quad (1.58)$$

Here and below we omit the subscript for the isotropic GF  $\check{g}_0$ .

Using relation (1.57) in Eq. (1.55), we obtain the Usadel equation [61]

$$D\nabla \cdot (\check{g} \circ \nabla\check{g}) - \left\{ \tau_3 \frac{\partial}{\partial t} \delta(t-t') \circ \check{g} \right\} - [(i\mathbf{h} \cdot \boldsymbol{\sigma}\tau_3 + \check{\Delta})\delta(t-t') + \check{\Sigma}_s \circ \check{g}] = 0, \quad (1.59)$$

where  $D = v_F\ell/3$  is the diffusion constant. Essentially, for equal times  $t = t'$ , the Eilenberger and Usadel quasiclassical equations correspond to the conservation of the current matrix.

In the energy domain, the Usadel equation reads

$$D\nabla \cdot (\check{g}\nabla\check{g}) + [i\varepsilon\tau_3 - i\mathbf{h} \cdot \boldsymbol{\sigma}\tau_3 - \check{\Delta} - \check{\Sigma}_s, \check{g}] = 0, \quad (1.60)$$

while the Matsubara representation is obtained by replacing  $\varepsilon \pm i\Gamma \rightarrow i\omega_n$  on the retarded/advanced part of Eq. (1.60).

### 1.4.1 Example: homogeneous BCS superconductor

In the following, we consider a simple example: a bulk BCS superconductor with no spin-dependent fields. In this case, the spatial derivatives vanish, so the Usadel equation for the retarded GF reads

$$[i(\varepsilon + i\Gamma)\tau_3 - \check{\Delta}, \check{g}^R] = 0, \quad (1.61)$$



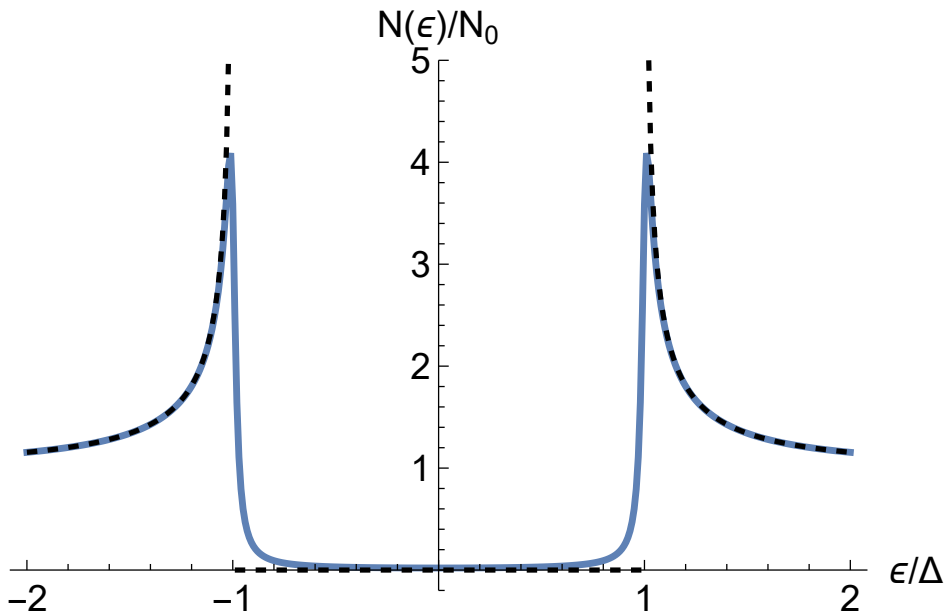


Figure 1.4: Density of states for a homogeneous superconductor. The dashed curve corresponds to an ideal BCS superconductor ( $\Gamma \rightarrow 0^+$ ), and the solid curve to a real superconductor with a finite inelastic scattering rate ( $\Gamma = 0.02\Delta$ ).

where  $\check{\Delta} = \Delta\tau_1$ . The Green's function is a linear combination of Pauli matrices in Nambu space (not including the unit matrix), so it must be proportional to the l.h.s. of the commutator. Taking the normalization condition (1.44) into account, the GF of a bulk superconductor is given by

$$\check{g}^R(\varepsilon) = \frac{-i(\varepsilon + i\Gamma)\tau_3 + \Delta\tau_1}{\sqrt{\Delta^2 - (\varepsilon + i\Gamma)^2}}. \quad (1.62)$$

There is still some freedom on the branch on the square root that needs to be taken in Eq. (1.62). The GF needs to provide logical values for the observable quantities of the system. For instance, the DoS needs to be positive for all energies. This property is satisfied by the principal branch of the square root in Eq. (1.62).

Equation (1.62) can easily be generalised for a superconductor in a homogeneous Zeeman field  $\mathbf{h}$ :

$$\check{g}^R(\varepsilon) = \frac{-i(\varepsilon + i\Gamma - \mathbf{h} \cdot \boldsymbol{\sigma})\tau_3 + \Delta\tau_1}{\sqrt{\Delta^2 - (\varepsilon + i\Gamma - \mathbf{h} \cdot \boldsymbol{\sigma})^2}}. \quad (1.63)$$

Using the principal branch of the square root for each spin direction we obtain a positive DoS for each spin species.

## 1.4.2 Observables

Observable quantities of the system are easily computed in the diffusive limit. For instance, the DoS is given by

$$N(t, \mathbf{r}, \varepsilon) = \frac{N_0}{8} \text{Tr} \tau_3 (\check{g}^R(t, \mathbf{r}, \varepsilon) - \check{g}^A(t, \mathbf{r}, \varepsilon)) = \frac{N_0}{4} \text{Re} \left\{ \text{Tr} \tau_3 \check{g}^R(t, \mathbf{r}, \varepsilon) \right\}. \quad (1.64)$$

For example, the DoS for a bulk superconductor considered in Sec. 1.4.1 is [see Eq. (1.62)]

$$N(\varepsilon) = N_0 \text{Re} \left\{ \frac{-i(\varepsilon + i\Gamma)}{\sqrt{\Delta^2 - (\varepsilon + i\Gamma)^2}} \right\}. \quad (1.65)$$

Ideally, the BCS theory predicts a divergent DoS at  $\varepsilon = \pm\Delta$ , but this sharp behaviour is smoothed by inelastic scattering processes, described by a finite Dynes parameter  $\Gamma$  [58], as shown in Fig. 1.4. In the normal state, the superconducting gap vanishes  $\Delta = 0$ , so the DoS becomes constant  $N(\varepsilon) = N_0$  (at energies small compared to the Fermi energy).

Plugging Eq. (1.57) into Eq. (1.51), one directly obtains the charge current in terms of the matrix current (1.58)

$$\boxed{\mathbf{j}(t, \mathbf{r}) = -\frac{\pi\sigma_N}{8e} \text{Tr} \tau_3 \check{\mathbf{J}}(t, t, \mathbf{r})^K} . \quad (1.66)$$

In time translation-invariant systems, the current can easily be computed in the energy domain as

$$\mathbf{j}(\mathbf{r}) = -\frac{\sigma_N}{16e} \int d\varepsilon \text{Tr} \tau_3 \check{\mathbf{J}}(\mathbf{r}, \varepsilon)^K , \quad (1.67)$$

or, if the system is in thermal equilibrium, in the Matsubara representation:

$$\mathbf{j}(\mathbf{r}) = -i2\pi T \frac{\sigma_N}{16e} \sum_{\omega_n} \text{Tr} \tau_3 \check{\mathbf{J}}(\mathbf{r}, \omega_n)^K , \quad (1.68)$$

where  $\sigma_N$  is the Drude conductivity. The spin and heat currents can similarly be defined in terms of the current matrix as

$$\mathbf{j}_s^i(\mathbf{r}) = \frac{\sigma_N}{32e^2} \int d\varepsilon \text{Tr} \sigma_i \check{\mathbf{J}}(\mathbf{r}, \varepsilon)^K , \quad (1.69)$$

and

$$\mathbf{j}_Q(\mathbf{r}) = \frac{\sigma_N}{16e^2} \int d\varepsilon \varepsilon \text{Tr} \check{\mathbf{J}}(\mathbf{r}, \varepsilon)^K , \quad (1.70)$$

respectively.

### 1.4.3 Self-consistency of the order parameter

The self-consistency equation for the order parameter in the diffusive limit is directly obtained from Eq. (1.53)

$$\check{\Delta}(t, \mathbf{r}) = \lambda N_0 \pi T \sum_{\omega_n}^{\Omega_D} \check{f}(t, \mathbf{r}, \omega_n) . \quad (1.71)$$

The value of the BCS coupling constant  $\lambda$  is generally not an easily accessible quantity. The order parameter becomes 0 at the BCS critical temperature  $T_{c0}$ , which is a temperature that can easily be extracted experimentally by measuring the resistance drop in the metal. Close to the critical temperature, we can expand the anomalous part of the GF (1.62) to the lowest order in  $\Delta$ ,  $\check{f}(\omega_n) \approx \frac{\check{\Delta}}{\omega_n}$ . In this case, the summation over Matsubara frequencies can be calculated analytically. Inserting the value of  $\check{f}$  in Eq. (1.71), we may write the value of  $\lambda$  in terms of the critical temperature. The self-consistency equation can then be rewritten as

$$\boxed{\check{\Delta} \ln \frac{T}{T_{c0}} = \pi T \sum_{\omega_n} \left( \check{f}(\omega_n) - \frac{\check{\Delta}}{\omega_n} \right) ,} \quad (1.72)$$

where it is no longer necessary to cutoff the summation due to the summand converging fast enough at high frequencies.

### 1.4.4 Quasiclassical equations in systems with SOC

In this subsection, we present the Usadel equation (1.59) in the presence of spin-orbit coupling (SOC) fields. The derivation of the equation is beyond the goal of this Thesis, so references are provided for completeness. SOC is an essential ingredient of mesoscopic physics, leading to effects such as weak antilocalization, the spin Hall effect and the anomalous Josephson effect.

There are two types of spin-orbit coupling: the *intrinsic* SOC arises in systems with broken inversion symmetry. Rashba and Dresselhaus SOC's belong to this type of SOC; in the former, the inversion symmetry is broken by the sample structure, while in the latter it is broken due to the lattice. The *extrinsic* SOC appears on systems with spin-dependent scattering. In the following, we first present the Usadel equation for a system with intrinsic linear-in-momentum SOC. Next, we show the Usadel equations for extrinsic SOC.

Linear-in-momentum spin-orbit coupling can be treated as an effective SU(2) potential [62]. The Hamiltonian (1.16) for a system with linear SOC can be generalised as

$$\check{\mathcal{H}}_0 = \frac{(\mathbf{p} - \check{\mathbf{A}})^2}{2m} - \mu_{\text{ch}} + V_{\text{imp}} + \tau_3 \check{A}^0 - i\check{\Delta}. \quad (1.73)$$

$V_{\text{imp}}$  is a random impurity potential that consists of the usual elastic scattering and the spin-orbit interaction [63–65].  $\check{A}^\mu$  is the generalized four-potential containing both U(1), and SU(2) components [66–68] given by

$$\check{A}^0 = -e\varphi\tau_3 + \frac{1}{2}A^{0j}\sigma_j \quad (1.74a)$$

$$\check{A}^i = -eA^i\tau_3 + \frac{1}{2}A^{ij}\sigma_j. \quad (1.74b)$$

$\varphi$  and  $\mathbf{A}$  are the usual U(1) scalar and vector electromagnetic potentials, while  $A^{0j}$  and  $A^{ij}$  are SU(2) potentials describing the Zeeman or exchange field<sup>5</sup> and the linear-in-momentum SOC, respectively [69]. Here and below sum over repeated indices is assumed.

As in conventional electrodynamics, we can define the field strength associated with  $\check{A}$ :

$$\check{F}^{\mu\nu} = \partial^\mu \check{A}^\nu - \partial^\nu \check{A}^\mu - i[\check{A}^\mu, \check{A}^\nu]. \quad (1.75)$$

The last commutator appears because of the fact that the SU(2) components are non-abelian. Here and below Greek indices range  $\mu = 0, 1, 2, 3$ .

The SU(2) covariant version of the Usadel equation is obtained from a generalization of the nonlinear  $\sigma$ -model for diffusive superconductors. The Usadel equation is the saddle point equation of the nonlinear  $\sigma$ -model in the presence of SOC. The covariant version of the Usadel equation [65, 70] allows describing the Hall and intrinsic spin Hall effects. For intrinsic SOC, the Usadel equation reads [66–68]

$$D\check{\nabla}_i \check{J}^i - \{\tau_3 \partial_t \delta(t-t') \circ \check{g}\} - [(i\check{A}^0 \tau_3 + \check{\Delta}) \delta(t-t') \circ \check{g}] = 0, \quad (1.76)$$

where  $\check{\nabla}_i \check{X} = \partial_i \check{X} - i/[\check{A}^i \circ \check{X}]$  is the covariant derivative, and  $\check{J}^i$  is the matrix current given by

$$\check{J}^i = \check{g} \circ \check{\nabla}_i \check{g} + \frac{\tau}{4m} (\{\check{F}^{ij} \delta(t-t') + \check{g} \circ \check{F}^{ij} \check{g} \circ \check{\nabla}_j \check{g}\} - i\check{\nabla}_j (\check{g} \circ [\check{\nabla}_i \check{g} \circ \check{\nabla}_j \check{g}])) \quad (1.77)$$

for intrinsic SOC [70].

<sup>5</sup>Note that the Zeeman field  $\mathbf{h}$  in Eq. (1.16) is now replaced by the  $\frac{1}{2}A^{0j}$  term, where the  $\frac{1}{2}$  factor is the ‘‘spin charge’’.

In systems where the SOC is introduced by impurities (extrinsic SOC), the Usadel equation is given by [65]

$$D(\nabla_i \check{J}^i + \check{\mathcal{T}}) - \{\tau_3 \partial_t \delta(t-t') \circ \check{g}\} - \left[ (i\check{A}^0 \tau_3 + \check{\Delta}) \delta(t-t') + \frac{\sigma_i \check{g} \sigma_i}{8\tau_{\text{SO}}} \circ \check{g} \right] = 0, \quad (1.78)$$

where  $\tau_{\text{SO}} = 9\tau/(8\lambda^4 p_F^4)$  is the spin-orbit relaxation time,  $\lambda$  describes the SOC strength, and  $\check{\mathcal{T}}$  is an extrinsic SOC correction due to an effective torque originating from the spin Hall and the spin swapping effects [63, 64]

$$\check{\mathcal{T}} = i\epsilon_{ijk} \frac{\varkappa}{4} [\check{\nabla}_i \check{g} \circ \check{\nabla}_j \check{g} \circ \sigma_k \delta(t-t')] + \epsilon_{ijk} \frac{\theta}{4} [\sigma_k \delta(t-t') \circ \check{g} \circ \check{\nabla}_i \check{g} \circ \check{\nabla}_j \check{g}]. \quad (1.79)$$

The current matrix is given by [65]

$$\check{J}^i = \check{g} \circ \check{\nabla}_i \check{g} - i\epsilon_{ijk} \frac{\varkappa}{4} [\check{g} \circ \check{\nabla}_j \check{g} \circ \sigma_k \delta(t-t') + \check{g} \circ \sigma_k \check{g}] - \epsilon_{ijk} \frac{\theta}{4} \{\check{\nabla}_j \check{g} \circ \sigma_k \delta(t-t') + \check{g} \circ \sigma_k \check{g}\}. \quad (1.80)$$

Here,  $\varkappa = 2p_F^2 \lambda^2 / 3$  and  $\theta = 2p_F \lambda^2 / \ell$  are spin-swapping and spin Hall coefficients [71], respectively, with  $\epsilon_{ijk}$  the Levi-Civita symbol, and  $\ell$  the mean free path. The first term in Eqs. (1.77) and (1.80) is the standard diffusive current, while the second term is the leading contribution from spin-charge coupling describing the Hall effect.

## 1.5 Boundary conditions

The Usadel equation needs to be supplemented with boundary conditions that describe hybrid interfaces between different materials. For example, at interfaces with vacuum or an insulator, the spectral current should vanish. This translates in the language of GFs into a vanishing current matrix (1.58) at the boundary ( $x = 0$ )

$$\check{J}(x=0) = \check{g} \circ \partial_x \check{g}|_{x=0} = 0. \quad (1.81)$$

In the following, we provide different boundary conditions that describe the interface of superconductors with other materials typically used in mesoscopic physics.

### 1.5.1 Interface with a ferromagnetic insulator

A superconducting layer grown on top of a ferromagnetic insulator shows a spin-splitting of the superconducting density of states, which is the basis for many applications in spintronics, thermoelectricity, and sensors [1–4]. The ferromagnetic interaction is described by an interfacial exchange field at the FI/S interface that induces triplet correlations in the superconductor.

The quasiclassical and isotropic approximations break down close to interfaces, so the boundary conditions for the quasiclassical GF cannot be derived within the quasiclassical theory. The boundary conditions for superconductors involving spin-active interfaces were derived in Refs. [72, 73]. These boundary conditions are valid as soon as the quasiclassical isotropic approximation can be performed. The interfacial exchange field  $\mathbf{h}_{\text{int}}$  is introduced as an effective boundary condition at the FI/S interface [74–76]. Assuming that the exchange interaction occurs over an effective layer of small thickness  $a \ll \xi_0$ , the boundary condition is obtained by integrating the Usadel equation (1.60) around the interface [74, 77, 78]

$$\check{g} \circ \partial_x \check{g}|_{x=0} = \frac{1}{D} [ia\mathbf{h}_{\text{int}} \cdot \boldsymbol{\sigma} \tau_3 \delta(t-t') \circ \check{g}] \Big|_{x=0}. \quad (1.82)$$

### 1.5.2 Interface between conducting materials

The current needs to be conserved at the interface between two conducting materials. If the interface transparency between the two conducting layers is low enough, the current flowing through the interface is given by the Kupriyanov-Lukichev boundary condition [79],

$$\sigma_L \check{g}_L \circ \partial_x \check{g}_L|_{x=0} = \sigma_R \check{g}_R \circ \partial_x \check{g}_R|_{x=0} = \frac{1}{2R_\square} [\check{g}_L \circ \check{g}_R]|_{x=0}, \quad (1.83)$$

where  $R_\square$  is the interface resistance per unit area, and  $\sigma_{L/R}$  are the conductivities of the left and right materials. In the clean interface resistance limit  $R_\square \rightarrow 0$ ,  $\check{g}_L$  and  $\check{g}_R$  need to commute so that the current becomes finite. Therefore, for clean interfaces, the last equality in Eq. (1.83) is replaced by the  $\check{g}_L(0) = \check{g}_R(0)$  condition.

In the tunnelling limit  $R_\square \rightarrow \infty$ , the two materials are not corrected by the proximity effect, so the left and right GFs are given by their bulk value. In this limit, one may use the boundary condition (1.83) to conveniently compute the current along the junction (1.66)

$$I(t) = -\frac{\pi}{16eR} \text{Tr} \tau_3 [\check{g}_L(t, t') \circ \check{g}_R(t', t)]^K. \quad (1.84)$$

In a junction with a constant voltage bias, the quasiparticle contribution to the current is given by the tunnelling current

$$I_{\text{qp}} = \frac{1}{eR} \int d\varepsilon \frac{N_L(\varepsilon)}{N_0} \frac{N_R(\varepsilon - V)}{N_0} (f(\varepsilon) - f(\varepsilon - V)), \quad (1.85)$$

where  $f(\varepsilon)$  is the Fermi-Dirac distribution function.

The Kupriyanov-Lukichev boundary conditions can be generalised for spin-filtering barriers. The generalized Kupriyanov-Lukichev boundary condition [74, 80] reads

$$\sigma_L \check{g}_L \circ \partial_x \check{g}_L|_{x=0} = \sigma_R \check{g}_R \circ \partial_x \check{g}_R|_{x=0} = \frac{1}{2R_\square} [\check{\Gamma} \check{g}_L \check{\Gamma}^\dagger \circ \check{g}_R]|_{x=0}, \quad (1.86)$$

where  $\check{\Gamma} = t + u \hat{\mathbf{m}} \cdot \boldsymbol{\sigma} \tau_3$  is the spin-polarized tunnelling matrix, with  $t = \sqrt{(1 + \sqrt{1 - P^2})}/2$ ,  $u = \sqrt{(1 - \sqrt{1 - P^2})}/2$ , and  $P$  being the spin-filter efficiency of the barrier.

The Nazarov boundary condition [81] generalises the Kupriyanov-Lukichev boundary condition to high transparency junctions:

$$\sigma_L \check{g}_L \circ \partial_x \check{g}_L|_{x=0} = \sigma_R \check{g}_R \circ \partial_x \check{g}_R|_{x=0} = \frac{1}{2R_\square} \frac{4[\check{g}_L \circ \check{g}_R]}{4 - 2\tilde{T} + \tilde{T}\{\check{g}_L \circ \check{g}_R\}} \Big|_{x=0}, \quad (1.87)$$

where  $\tilde{T}$  is the dimensionless interface transparency.

### 1.5.3 Unconventional superconductors

The Nazarov boundary condition assumes that the GF is isotropic, so it does not adequately model unconventional superconductor junctions. This kind of interfaces are described by the Tanaka-Nazarov boundary conditions [82, 83], which are an extension to unconventional superconductor junctions of the Nazarov boundary conditions. The odd-parity correlations in the superconductor induce odd-frequency even-parity correlations in adjacent material.

Here we show a form of the Tanaka-Nazarov boundary conditions suitable for mixed s+p-wave superconductors [84]

$$\boxed{\check{g} \circ \partial_x \check{g}|_{x=0} = \frac{1}{2\sigma R_\square} \langle \check{S}(\varphi) \rangle}, \quad (1.88)$$

where the angular averaging  $\langle \cdot \rangle$  is taken over all modes that pass through the interface,  $\varphi$  is the injection angle with respect to the direction normal to the interface,  $\sigma$  is the conductivity of the non-superconducting material in the absence of a proximity effect, and

$$\check{S}(\varphi) = \check{T}((1 + T_1^2)\delta(t - t') + T_1(\check{C} \circ \check{g} + \check{g} \circ \check{C}))^{-1} \circ (\check{C} \circ \check{g} - \check{g} \circ \check{C}), \quad (1.89)$$

$$\check{C} = \check{H}_+^{-1} \circ (1 - \check{H}_-), \quad (1.90)$$

$$\check{H}_+ = \frac{1}{2}(\check{g}_S(\varphi) + \check{g}_S(\pi - \varphi)), \quad (1.91)$$

$$\check{H}_- = \frac{1}{2}(\check{g}_S(\varphi) - \check{g}_S(\pi - \varphi)). \quad (1.92)$$

Here,  $\check{g}_S$  is the bulk superconductor GF,  $T_1 = \check{T}/(2 - \check{T} + 2\sqrt{1 - \check{T}})$ , and the interface transparency  $\check{T}$  is given by

$$\check{T}(\varphi) = \frac{\cos^2 \varphi}{\cos^2 \varphi + z^2}, \quad (1.93)$$

where  $z$  is the BTK parameter [85], characterizing the strength of the barrier. It is assumed that the Fermi surface mismatch is negligible, that is, that the magnitude of the Fermi momentum is of similar magnitude in both layers.

## 1.6 Summary

In this chapter, we laid out the theoretical formalism to analyse the non-equilibrium properties of superconducting structures subjected to spin-dependent fields. Essentially, within quasiclassical Green's function formalism, systems are described by a quasiclassical equation of motion, which in the diffusive limit is the Usadel equation (1.59). Solving the Usadel equation, together with the boundary conditions which describe the hybrid interfaces between different materials, we obtain the quasiclassical GF of the system, from which the spectral and transport properties of the material may be extracted.

In the following chapter, we introduce different superconducting systems with Zeeman fields or different kinds of spin-orbit coupling. We apply the formulas derived in this chapter to analyse the charge, heat and spin transport properties of the systems.

# Chapter 2

## Models, methods, and results

*HIC SVNT LEONES*

— Latin inscription on  
uncharted territory

In this chapter, we introduce the models and methods used to study the systems covered in this Thesis. We also provide a summary of the main results obtained. In Sec. 2.1, we study the DoS and triplet correlations in a superconductor across a domain wall and how the triplet correlations manifest in a tunnelling current measurement. This section serves as an introductory chapter to get acquainted with the GF formalism and understand the physical information contained in each component of the GF. Next, in Sec. 2.2, we propose a way to detect the anomalous Josephson effect in an Andreev interferometer device. In this section, we explain how to extract the non-equilibrium properties of different systems with spin-dependent fields. Then, in Sec. 2.3, we study the microwave-assisted thermoelectricity in asymmetric superconducting tunnel junctions. Finally, in Sec. 2.4, we study the longitudinal and transverse (Hall) charge and spin currents in a 2D superconductor under a microwave field, and compare the results to the corresponding normal-state behaviour. The former two systems involve static fields that do not change in time, while the latter two systems are subjected to dynamical electric or spin-fields. A detailed analysis of each of the four systems is shown in the publications included in Chaps. 4-7. This chapter works as an introduction to the publications included in the Thesis, so it is recommended to read each publication directly after or alongside its corresponding section in this chapter to follow the thread of the discussion.

### 2.1 Quasiparticle density of states and triplet correlations in superconductor/ferromagnetic-insulator structures across a sharp domain wall

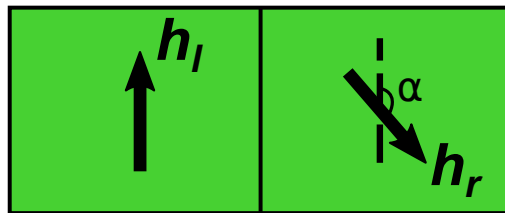


Figure 2.1: Top view of a ferromagnetic insulator with a sharp domain wall. The FI has two domains with arbitrary in-plane magnetisation direction with a relative orientation angle  $\alpha$ .

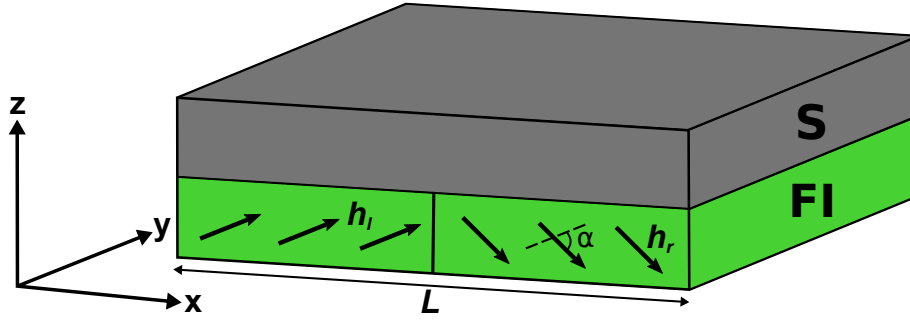


Figure 2.2: Schematic view of the S/FI structure under consideration. The ferromagnetic insulator has two domains with arbitrary in-plane magnetisation direction. The magnetisations of the two domains lie on the  $xy$ -plane, and they form an angle  $\alpha$ .

A superconductor (S) grown on top of a ferromagnetic insulator (FI) shows a spin split density of states due to the proximity effect [86–89]. This spin splitting causes the singlet-state correlations of the condensate to become odd-in-frequency triplet correlations. The ferromagnetic interaction may be described by an interfacial exchange field at the FI/S interface that induces triplet correlations in the superconductor. If the superconducting layer is thin compared to the coherence length, the spin-splitting can be assumed to be constant along the thickness of the sample. Most works additionally assume a homogeneous spin-splitting field along the length of the S layer [78, 90–92]. This assumption is justified, even in a multidomain situation, if the characteristic domain size of the FI is much larger than the superconducting coherence length  $\xi_0$ . However, the non-homogeneity of the exchange interaction is relevant when the domain size is of the order of the coherence length, or if the superconductor is grown in the vicinity of a sharp domain wall, as sketched in Fig. 2.1. The effect of domain walls in magnetic and insulating ferromagnets on adjacent superconductors has been studied both theoretically [93–97] and experimentally [89, 98]. Specifically, Ref. [99] studied the influence of domain-wall dynamics on superconductivity, and Ref. [89] provided experimental evidence that EuS, a ferromagnetic insulator, consists of multiple domains with a size of the order of the coherence length of the (superconducting) Al layer attached to it. The authors of the latter work used a theoretical model that assumed alternating up/down domains of different sizes to explain the spectroscopic measurements.

In this section, we generalise this configuration to consider a diffusive FI/S bilayer where the FI consists of two magnetic domains with an arbitrary magnetisation, as shown in Fig. 2.2. Almost all experimental works on FI/S systems focus on studying its quasiparticle spectrum, but there is a key aspect that is not often covered in these works: an interfacial exchange field leads to the conversion of singlet superconducting correlations to triplet ones [76, 100–102]. Moreover, in FI/S bilayers where the FI has a non-collinear magnetisation, triplet correlations with different spin-projections may coexist with the singlet correlations. In the following, we study the equilibrium properties of an FI/S bilayer with a sharp domain wall separating two magnetic domains with arbitrary magnetisations. We provide analytical expressions for the DoS in different limiting cases. Additionally, we study the spatial evolution of the triplet correlations near a domain wall and propose a method to detect them by covering the superconductor with a ferromagnetic (F) layer and performing tunnelling spectroscopy over it.

### 2.1.1 Model and methods

In order to study the spectral properties of the FI/S bilayer we use the quasiclassical GF technique in the diffusive limit, as introduced in Sec. 1.4. The Usadel equation for this system



reads

$$D\partial_x(\check{g}\partial_x\check{g}) + [i\varepsilon\tau_3 - i\mathbf{h} \cdot \boldsymbol{\sigma}\tau_3 - \check{\Delta}, \check{g}] = 0, \quad (2.1)$$

where  $D$  is the diffusion constant,  $\varepsilon$  is the energy,  $\mathbf{h}$  is the effective exchange field stemming from the interface, and  $\check{\Delta} = \Delta\tau_1$  is the order parameter. In Eq. (2.1) we are assuming that the thickness of the S layer is smaller than the coherence length  $\xi_0 = \sqrt{D/\Delta}$ , so that we can integrate the Usadel equation over the thickness of the superconductor to reduce the dimensionality of the problem and assume a homogeneous exchange field over the thickness of the S layer.

Since we are interested in the spectral properties of the system, it is only necessary to solve the retarded part of the equation. We are dealing with superconductivity and spin-dependent fields, so the GF  $\check{g}$  is a  $4 \times 4$  matrix in Nambu-spin space. The general structure of  $\check{g}$  is:

$$\check{g} = \hat{g}\tau_3 + \hat{f}\tau_1, \quad (2.2)$$

where  $\hat{g}$  and  $\hat{f}$  are the normal and anomalous GFs in spin-space, and  $\sigma_i$  ( $\tau_i$ ),  $i = 1, 2, 3$  are the Pauli matrices in the spin (Nambu) space. The normal (diagonal) part of the GF describes the quasiparticle spectral properties of the system. For instance, the local DoS is related to the GF through the expression [see Eq. (1.64)]

$$\frac{N(\varepsilon)}{N_0} = \frac{1}{2} \text{Re}\{\text{Tr} \hat{g}(\varepsilon)\}. \quad (2.3)$$

Within our model, pair correlations are described by the anomalous component  $\hat{f}$ . In Eq. (2.2) we only consider a  $\tau_1$  off-diagonal component, whereas superconducting systems with a phase difference, such as Josephson junctions, also show a finite  $\tau_2$  component. The anomalous GF has the following spin structure:

$$\hat{f} = f_0 + \mathbf{f} \cdot \boldsymbol{\sigma}, \quad (2.4)$$

where  $f_0$  describes the singlet and  $f_j$ ,  $j = 1, 2, 3$  the triplet correlations. Because we consider the strict diffusive limit, all components of  $\hat{f}$  are isotropic in momentum (s-wave symmetry). From the Fermi statistics for Fermion pairs, it follows that  $f_0$  is an even function of frequency, whereas  $f_j$  are odd [100, 103–105]. The following association between the different components of the condensate and the spin state of electron pairs can be made [106]

$$(\uparrow\downarrow - \downarrow\uparrow) \leftrightarrow 2f_0 \quad (2.5)$$

$$-(\uparrow\uparrow - \downarrow\downarrow) \leftrightarrow 2f_1 \quad (2.6)$$

$$(\uparrow\uparrow + \downarrow\downarrow) \leftrightarrow 2if_2 \quad (2.7)$$

$$(\uparrow\downarrow + \downarrow\uparrow) \leftrightarrow 2f_3. \quad (2.8)$$

In other words, each triplet component of the condensate is associated with maximally entangled states. In a conventional BCS superconductor, only the singlet component  $f_0$  is finite. Triplet components arise in the presence of spin-fields such as the exchange field introduced by the FI, as can be seen by exploring Eq. (2.1).

We parametrise the GF in the generalised  $\theta$ -parametrisation [59] given by Eqs. (1.47-1.48). Comparing the different components of the GF with Eq. (2.4), we see that  $V_0$  and  $\mathbf{V}$  describe the singlet and triplet correlations, respectively. If  $\mathbf{h}$  is homogeneous, then  $\mathbf{V}$  is parallel to the exchange field, but in general,  $\mathbf{V}$  is a spatially dependent quantity that needs not be parallel to the local exchange field. In the  $\theta$ -parametrisation, the Usadel equation reduces to the following set of equations

$$D\nabla^2\theta + 2i\varepsilon \sin\theta V_0 - 2i \cos\theta \mathbf{h} \cdot \mathbf{V} + 2\Delta \cos\theta V_0 = 0 \quad (2.9a)$$

$$D(V_0\nabla^2\mathbf{V} - \mathbf{V}\nabla^2V_0) + 2i\varepsilon \cos\theta \mathbf{V} - 2i \sin\theta \mathbf{h}V_0 - 2\Delta \sin\theta \mathbf{V} = 0. \quad (2.9b)$$

Equation (2.9) forms a set of 4 second-order differential equations for  $\theta$  and  $\mathbf{V}$  ( $V_0$  is related to  $\mathbf{V}$  through relation (1.48)). These equations are the Euler-Lagrange equations corresponding to the following Lagrangian:

$$\mathcal{L} = \frac{D}{2} \sum_{\mu} (\nabla V_{\mu})^2 + \frac{D}{2} (\nabla \theta)^2 + 2i\varepsilon \cos \theta V_0 + 2i \sin \theta \mathbf{h} \cdot \mathbf{V} - 2\Delta \sin \theta V_0, \quad (2.10)$$

with  $\mu = 0, 1, 2, 3$ . This Lagrangian coincides with the form of the non-linear  $\sigma$ -model from which the Usadel equation can also be derived [107, 108].

The above equations (2.9) are valid for arbitrary magnetic textures. In the following, we focus on the situation of two semi-infinite magnetic domains with constant magnetisation. The domains are separated by a sharp domain wall at  $x = 0$  with a length much smaller than the superconducting coherence length. We assume that one of the domains ( $x < 0$ ) is polarized along the  $y$  axis, whereas the magnetisation of the other domain ( $x > 0$ ) forms an angle  $\alpha$  with the  $y$  axis, see Fig. 2.2. The Usadel equation needs to be supplemented with boundary conditions that describe the boundaries of the system. Since we are considering an infinite superconductor, at distances much larger than the coherence length ( $|x| \gg \xi_0$ ) the GF should take its bulk form.

On each domain, the Lagrangian (2.10) does not depend explicitly on the position  $\mathbf{r}$ , so the corresponding Hamiltonian is an integral of motion in each domain. The conserved quantity is namely given by

$$\mathcal{E} = \frac{D}{2} \sum_{\mu} (\nabla V_{\mu})^2 + \frac{D}{2} (\nabla \theta)^2 - 2i\varepsilon \cos \theta V_0 - 2i \sin \theta \mathbf{h} \cdot \mathbf{V} + 2\Delta \sin \theta V_0. \quad (2.11)$$

The values of  $\mathcal{E}$  can be easily obtained far away from the domain wall, where the GF is given by the bulk solution and therefore is constant in space:

$$\mathcal{E} = -2i\varepsilon \cos \bar{\theta} \bar{V}_0 - 2i \sin \bar{\theta} \mathbf{h} \cdot \bar{\mathbf{V}} + 2\Delta \sin \bar{\theta} \bar{V}_0, \quad (2.12)$$

where the bulk values  $\bar{\theta}$  and  $\bar{\mathbf{V}}$  of the GF are given by the inverse relations of Eq. (1.47)

$$\tan \theta = \frac{f_0}{g_0} \quad (2.13a)$$

$$\mathbf{V} = -\frac{\mathbf{g}}{\sin \theta} \quad (2.13b)$$

$$V_0 = \frac{g_0}{\cos \theta}, \quad (2.13c)$$

and the bulk GF is given by [see Eq. (1.63)]

$$\hat{g} = \frac{-i(\varepsilon - \mathbf{h} \cdot \boldsymbol{\sigma})}{\sqrt{\Delta^2 - (\varepsilon - \mathbf{h} \cdot \boldsymbol{\sigma})^2}} \quad (2.14a)$$

$$\hat{f} = \frac{\Delta}{\sqrt{\Delta^2 - (\varepsilon - \mathbf{h} \cdot \boldsymbol{\sigma})^2}}. \quad (2.14b)$$

with  $\hat{g} = g_0 + \mathbf{g} \cdot \boldsymbol{\sigma}$ ,  $\hat{f} = f_0 + \mathbf{f} \cdot \boldsymbol{\sigma}$ .

If the magnetisation in both domains is collinear, the problem can be greatly simplified. Firstly, only the component of the vector  $\mathbf{V}$  parallel to the magnetisation is non-zero. Without any loss of generality, we assume that the magnetisations lie in the  $z$  axis, such that  $V_1 = V_2 = 0$ . In this case, Eq. (2.9) reads:

$$D\theta'' + 2i\varepsilon \sin \theta \cos \theta_3 - 2ih \cos \theta \sin \theta_3 + 2\Delta \cos \theta \cos \theta_3 = 0 \quad (2.15a)$$

$$D\theta_3'' + 2i\varepsilon \cos \theta \sin \theta_3 - 2ih \sin \theta \cos \theta_3 - 2\Delta \sin \theta \sin \theta_3 = 0, \quad (2.15b)$$

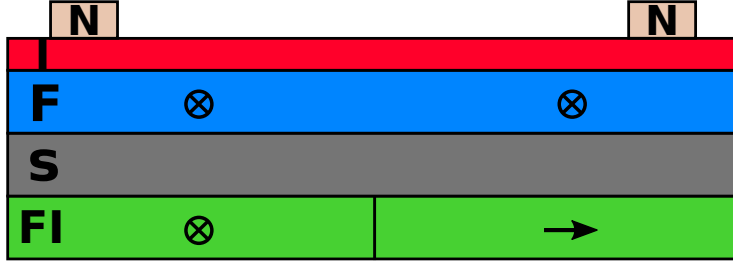


Figure 2.3: Proposed geometry to detect the triplet correlations. An F layer is placed on top of an S layer; if the F layer is thick enough, only the triplet correlations perpendicular to the magnetisation of the F layer will propagate along the ferromagnet. The long-range triplet correlations manifest as a zero-energy peak on the local DoS, probed through tunnel differential conductance measurements with a normal metal electrode (N).

where  $V_3 = \sin \theta_3$ . One can combine these equations to obtain two decoupled equations for each spin component:

$$D\theta_{\pm}'' + 2i\varepsilon \sin \theta_{\pm} \mp 2ih \sin \theta_{\pm} + 2\Delta \cos \theta_{\pm} = 0, \quad (2.16)$$

where  $\theta_{\pm} = \theta \pm \theta_3$  respectively describe the spin up and down components of the GF.

Since the problem is decoupled in spin space, one can derive the equations in (2.16) from two independent Lagrangians:

$$\mathcal{L}_{\pm} = \frac{D}{2} \theta_{\pm}'^2 + 2i\varepsilon \cos \theta_{\pm} \mp 2ih \cos \theta_{\pm} - 2\Delta \sin \theta_{\pm}. \quad (2.17)$$

Because  $\mathcal{L}_{\pm}$  do not depend explicitly on  $x$ , the following quantities are conserved in each domain:

$$\mathcal{E}_{\pm} = \frac{D}{2} \theta_{\pm}'^2 - 2i\varepsilon \cos \theta_{\pm} \pm 2ih \cos \theta_{\pm} + 2\Delta \sin \theta_{\pm}. \quad (2.18)$$

These expressions can be evaluated at the bulk where the spatial derivative vanishes and the GF is given by the bulk solution [see Eq. (2.14)].  $\cos \theta_{\pm}$  and  $\sin \theta_{\pm}$  are given by the spin components  $\hat{g}$  and  $\hat{f}$  respectively, where the  $\pm$  sign corresponds to the up/down spin index

$$\mathcal{E}_{\pm} = 2\sqrt{\Delta^2 - (\varepsilon \mp h)^2} = \frac{2\Delta}{\sin \bar{\theta}_{\pm}}. \quad (2.19)$$

Here,  $\bar{\theta}_{\pm}$  are the values of  $\theta_{\pm}$  at the bulk. Substituting equation (2.19) into (2.18) and applying trigonometric identities, in Chap. 4 we obtain an analytical solution to the Usadel equation when the two domains are collinear. In the general case where the domains have an arbitrary orientation, the Usadel equation (2.9) needs to be solved numerically.

## 2.1.2 Summary of the results

Here we summarise the main results obtained in the publication of Chap. 4. In this work, we study the quasiparticle DoS and the triplet correlation in an S/FI bilayer in the presence of a domain wall separating two magnetic domains. All the studied properties are extracted from the GF of the system, which is obtained by solving Eq. (2.1).

First, we focus on the quasiparticle spectrum and analyze how the density of states of the superconductor is affected by the magnetic configuration. In the particular case where the two domains are semi-infinite and collinear, using the analytical method derived in Sec. 2.1.1, it is possible to write two integrals of motion (2.19) that allow for an analytical solution of the Usadel equation. With the help of this solution, we determine the local DoS of the superconductor for

different values of the exchange field. If the domains have equal magnetisation strength and are antiparallel, or if one of the domains has a negligibly small exchange field, the splitting of the DoS peaks does not decrease smoothly as one would expect in a system where the exchange field is suppressed gradually over a length much larger than  $\xi_0$ . Instead, the DoS exhibits a “shark-fin” shape at the domain wall, as we show in Figs. 2 and 3 of Chap. 4. This behaviour was already predicted in Ref. [89].

We have also studied FI layers with non-collinear magnetisation direction. In this case, the system does not have enough integrals of motion to reduce the number of coupled equations, so we need to solve Eq. (2.9) numerically. We show that near the domain wall, the spin-splitting is quite robust with respect to the relative angle  $\alpha$  between the magnetisations (Fig. 4 of Chap. 4), but the heights of the coherent peaks are significantly affected by it. All these predictions can be verified by local tunnel spectroscopy experiments, which will reveal information about the local magnetic configuration of the FI.

Secondly, we have analysed how the triplet correlations induced by the FI in the S affect the spectral properties of the S layer [see Fig. 5 of Chap. 4]. In Fig. 2.3 we propose a FI/S/F junction to detect the triplet correlations in the superconductor. The singlet and triplet correlation parallel to the local magnetisation of the F layer are short-range correlations that decay over the magnetic length  $\xi_F = \sqrt{D/(2h_F)}$ , while the triplet correlations perpendicular to the local magnetisation are long-range triplet superconducting correlations that decay over the length  $\xi_\varepsilon = \sqrt{D/(2\varepsilon)}$ . By choosing an appropriate thickness  $t$  of the F layer  $\xi_F \ll t \ll \xi_\varepsilon$ , the DoS of F at the tunnelling barrier will only be corrected by the long-range triplet component. This situation can be realized by using F layers with a strong exchange field, such as Co or Fe. The presence of the triplet component manifests itself as a zero-bias maximum in the tunnelling differential conductance, as shown in Figs. 6 and 7 of Chap. 4. The proposed setup can then be used as a source of spin-triplet pairs, whose entanglement can be proved in experiments using quantum dots as pair splitters [109].

In this section, we showed how the quasiclassical GF formalism may be used to study the spectral properties of a superconductor with an exchange field. In the following, we study the equilibrium Josephson current and the non-equilibrium quasiparticle current in a Josephson junction coupled to an Andreev interferometer in the presence of different types of spin-dependent fields.

## 2.2 Anomalous Andreev interferometer: Study of an anomalous Josephson junction coupled to a normal wire

If two superconductors are placed in proximity, a supercurrent may flow between them in addition to the usual quasiparticle current. This current depends on the relative phase between the two superconductors. Such junctions are known as Josephson junctions (JJ), named after Brian Josephson, who predicted the relation between the supercurrent and the voltage across the junction in 1962 [110, 111]. The DC Josephson effect establishes that the supercurrent flowing between two superconductors with a phase difference  $\varphi$  is

$$I_J = I_c \sin \varphi , \quad (2.20)$$

where  $I_c$  is the critical current of the junction. A constant phase difference may be applied to the junction, for instance, by applying a magnetic flux  $\Phi$  to the closed circuit. The Josephson phase is related to  $\Phi$  through the relation  $\varphi = 2\pi\Phi/\Phi_0$ , where  $\Phi_0 = h/(2e)$  is the flux quantum. In such junctions, the phase-difference of the ground state is  $\varphi = 0$ .

In a system where time-reversal symmetry is broken, such as superconductor/ferromagnet/superconductor (S/F/S) structures, it was shown that the

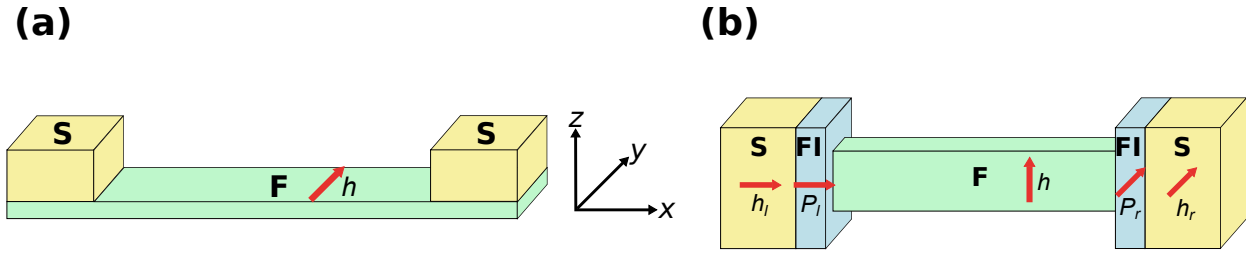


Figure 2.4: (a) S/F/S structure. Here, F is a wire with Rashba spin-orbit coupling, and a spin-splitting field  $\mathbf{h}$ . (b) S/FI/F/FI/S structure. FI layers act as spin-filtering barriers with polarizations  $\mathbf{P}_{r/l}$ , and they induce spin-splitting fields  $\mathbf{h}_{r/l}$  in adjacent S layers. F is a ferromagnet with an exchange field  $\mathbf{h}$ .

current-phase relation can acquire a phase-shift of  $\pi$ ,

$$I_J = I_c \sin(\varphi + \pi). \quad (2.21)$$

The ground state Josephson phase is  $\varphi = \pi$  [112], since the free energy of the junction is  $F \propto \cos \varphi$ , so such junctions are called  $\pi$ -junctions [113–116]. A more general current-phase relation is possible in systems with broken time-reversal and inversion symmetries [117]

$$I_S = I_c \sin(\varphi + \varphi_0) = I_0^S \sin \varphi + I_{\text{an}}^S \cos \varphi. \quad (2.22)$$

Such JJs are known as  $\varphi_0$ -junctions by analogy. This effect is referred to as the anomalous Josephson effect (AJE). In general, the current-phase relation of a JJ given by Eq. (2.22) can be decomposed into the usual current  $I_0^S$ , proportional to  $\sin \varphi$ , and an anomalous current  $I_{\text{an}}^S$ , proportional to  $\cos \varphi$ .  $I_{\text{an}}^S$  may only be non-zero if time-reversal and inversion symmetries are simultaneously broken, leading to a finite supercurrent even at zero phase difference between the superconductors.

Hybrid superconducting systems with spin-dependent fields offer a platform to obtain the AJE. In this section, we consider two realisations of an anomalous Josephson junction: a Josephson junction with Rashba spin-orbit coupling (SOC) [Fig. 2.4(a)] and a multilayer ferromagnetic structure [Fig. 2.4(b)]. In both cases the anomalous phase is related to the existence of a Lifshitz invariant in the free energy [118–120]. In the first example, such invariant stems from an interplay between a Zeeman field and the SOC, whereas in the second example, it stems from non-coplanar magnetisations of magnetic layers. In the first example, a Zeeman field and the spin-orbit coupling provide time-reversal and inversion symmetry breaking, respectively, which leads to the anomalous phase shift [67, 117]. In the second example, a non-coplanar magnetisation combined with spin-filtering interfaces provides the required symmetry breakings [121–128].

Therefore, the AJE reflects the interplay between spin-dependent fields and superconductivity. This interaction is the basis of several effects and applications that are attracting the interest of a large community, such as topological [129–131] and unconventional [100, 105] superconductivity, superconducting spintronics [132], and novel superconducting electronic elements [133]. The most well-known proposals for AJE involve superconducting structures in the presence of spin-orbit interaction [67, 117, 134–140], some of which have been successfully tested in experiment [21, 141–143]. Other theoretical studies have proposed numerous alternative realizations of AJE: in S/F/S junctions with a nonhomogeneous magnetisation texture [121–128], junctions of unconventional superconductors [144–147], and between topologically nontrivial superconducting leads [148]. An anomalous current-phase relation can also be obtained under a non-equilibrium situation in multiterminal structures [149–151].  $\varphi_0$ -junctions could prove to be a key component for quantum electronics, as they can provide a stable phase bias to quantum circuits, and could

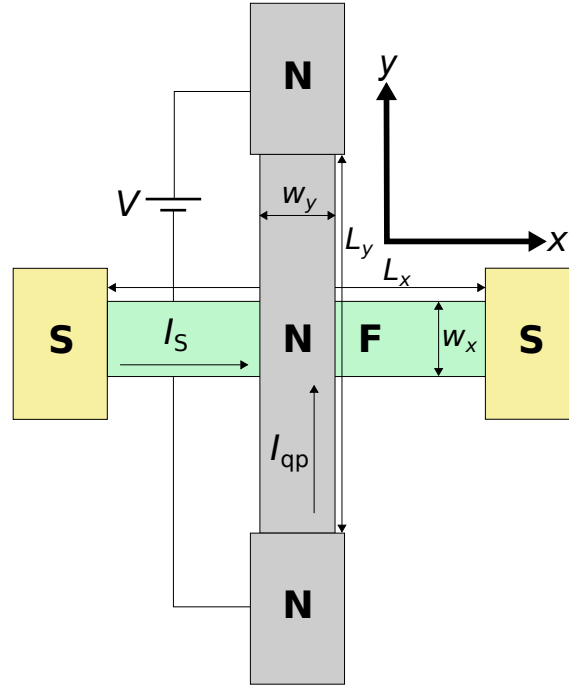


Figure 2.5: Schematic structure of the Andreev interferometer. An anomalous Josephson junction is coupled to a mesoscopic conductor.

therefore be particularly useful in phase-coherent superconducting electronics and spintronics [21, 132].

In this section, we analyse the  $\varphi_0$  effect in a device known as Andreev interferometer [152–155]. An Andreev interferometer consists of a Josephson junction coupled to a mesoscopic conductor, as sketched in Fig. 2.5. The superconducting correlations are induced in the normal conductor due to the proximity effect. Said correlations depend on the phase difference of the Josephson junction, so the conductance of the conducting loop becomes sensitive to  $\varphi$ . In other words, a simple resistance measurement performed on the conductor may potentially reveal the current-phase relation along the adjacent Josephson junction. An important advantage of this geometry is that it allows for a decoupling between the superconducting loop with the  $\varphi_0$ -junction and the normal wire where the conductance measurement is done, such that the noise associated with the measurement process does not perturb the  $\varphi_0$  junction. Andreev interferometry was particularly active during the 90s: several types of Andreev interferometers were theoretically proposed [156–159] and experimentally realized [160, 161]. Andreev interferometers have been used to study the magnetoresistance oscillations [162], electric transport [154, 163–168], and thermopower and thermal transport [169–172] in S/N structures.

In the following, we investigate how the  $\varphi_0$ -effect modifies the current-phase relationship in the mesoscopic conductor. For this purpose, we solve the Usadel equation in the superconducting and normal loops, and compute the supercurrent and quasiparticle currents flowing through them, respectively. In the case of the Josephson junction with SOC, we use the generalisation of the Usadel equation introduced in Sec. 1.4.4. To simplify the calculations, we assume that the S/F transmission coefficient is small, so that the proximity effect in the F wire is weak. In this case, the Usadel equation can be linearized in the superconducting order parameter  $\Delta$ .

## 2.2.1 Model and methods

### Josephson junction with Rashba SOC

We first study a Josephson junction consisting of a S/F/S structure, where the F wire has Rashba spin-orbit coupling, as shown in Fig. 2.4(a). We assume that the coupling between the F wire and the S reservoirs is weak, for example, due to a low S/F transmission coefficient, so that the superconducting reservoirs are not corrected by the F wire, while the F wire is weakly proximitised by the two superconductors. The GFs of the right and left superconductors are given by

$$\check{\mathcal{G}}_{0,r/l} = \frac{-i\varepsilon}{\sqrt{\Delta^2 - \varepsilon^2}}\tau_3 + \frac{\Delta}{\sqrt{\Delta^2 - \varepsilon^2}} \begin{pmatrix} 0 & e^{\eta_{r/l}i\varphi/2} \\ e^{-\eta_{r/l}i\varphi/2} & 0 \end{pmatrix}, \quad (2.23)$$

where  $\eta_{r/l} = \pm 1$  for the right and left superconductors, and  $\varphi$  is the phase difference of the Josephson junction.

The Green's function of a bulk normal metal or a ferromagnet has no anomalous component, so it is diagonal in Nambu space  $\check{g}^R = \tau_3$ . The superconducting correlations correct the anomalous (off-diagonal) part GF so that it has the following structure in Nambu-spin space:

$$\check{f}^R = \begin{pmatrix} 0 & \hat{f}(\varepsilon) \\ \hat{f}(-\varepsilon) & 0 \end{pmatrix}, \quad (2.24)$$

where  $\check{f}$  is linear in  $\Delta$ . The anomalous components of the GF are related through time reversal transformation as  $\hat{f} = \mathcal{T}\hat{f}\mathcal{T}^{-1}$ , where  $\mathcal{T} = i\sigma_2\mathcal{K}$  is the time-reversal transformation, with  $\mathcal{K}$  being the complex conjugate operation. Moreover, we can relate  $\check{f}^A$  to  $\check{f}^R$  as

$$\check{f}^A(\varepsilon, \mathbf{h}, \alpha) = \check{f}^R(-\varepsilon, -\mathbf{h}, -\alpha). \quad (2.25)$$

For the considered configuration [Fig. 2.4(a)], the anomalous Josephson current is only affected by the component of the exchange field perpendicular to the current direction  $x$ , so we consider a field oriented along the  $y$  direction  $\mathbf{h} = h\hat{\mathbf{u}}_y$  in order to maximize the  $\varphi_0$  effect [67].

In the diffusive limit, the GFs are obtained as a solution of the Usadel equation. The SOC can be included as a background SU(2) field as explained in Sec. 1.4.4 [62, 66, 68]. Superconducting correlations are described by the condensate GF (2.24),  $\hat{f}$ , which is a  $2 \times 2$  matrix in spin space that consists of a singlet component  $f_0$ , and in general, three triplet components,  $f_j\sigma_j$ , where  $j = 1, 2, 3$  and  $\sigma_j$  are the three Pauli matrices. For the situation under consideration, transport in  $x$ -direction and  $h$ -field in  $y$ -direction, only the condensate components  $f_0$  and  $f_2$  are finite and satisfy:

$$\pm\partial_{xx}^2 f_0^{R/A} + i\kappa_\varepsilon^2 f_0^{R/A} - i\kappa_F^2 f_2^{R/A} - \kappa_\alpha \partial_x f_2^{R/A} = 0 \quad (2.26a)$$

$$\pm\partial_{xx}^2 f_2^{R/A} + i\kappa_\varepsilon^2 f_2^{R/A} - i\kappa_F^2 f_0^{R/A} - \kappa_\alpha \partial_x f_0^{R/A} = 0 \quad (2.26b)$$

where  $\kappa_\varepsilon^2 = 2\varepsilon/D$ ,  $\kappa_F^2 = 2h/D$  and  $\kappa_\alpha = 4\alpha^3\tau/m$ . Here,  $\varepsilon$  is the energy,  $D$  is the diffusion constant,  $h$  is the exchange field, and  $\alpha$  is the Rashba coupling constant. The upper and lower sign correspond to the retarded and advanced condensate GFs  $\hat{f}^{R/A}$  respectively. In the following, we omit the superscript to simplify the notation. Moreover, to simplify the calculation, in Eq. (2.26) we have neglected the renormalization of the exchange field by the SOC, and the relaxation of the triplet component due to SOC [21].

The Usadel equation (2.26) is supplemented by boundary conditions describing the interfaces between different materials. The S/F junctions are described by the generalized Kuprianov-Lukichev conditions (1.83). Linearizing the boundary conditions we obtain

$$\pm\partial_n f_{0,r/l} + \eta_{r/l}\kappa_\alpha f_{2,r/l} = \mp \frac{1}{\gamma} \mathcal{F}_0 e^{i\eta_{r/l}\varphi/2} \quad (2.27a)$$

$$\partial_n f_{2,r/l} = 0. \quad (2.27b)$$

Here,  $\mathcal{F}_0 = \Delta/\sqrt{\Delta^2 - \varepsilon^2}$  is the anomalous part of the GF of the superconducting electrode, Eq. (2.23),  $\partial_n$  is the normal derivative at the surface, and  $\gamma = \sigma_F R_\square$  is the parameter describing the barrier strength, where  $R_\square$  is the normal-state tunnelling resistance per unit area, and  $\sigma_F$  is the conductivity of the ferromagnet.

Solving the equation system formed by Eqs. (2.26) and (2.27), we obtain the GF in the F wire. Having found the condensate function, we proceed to calculate the Josephson current in the F wire in the Matsubara domain using Eq. (1.68). The only contribution to the current will be the supercurrent mediated by the superconducting correlations induced in the F wire:

$$I_S = \frac{\pi\sigma_F T}{e} \sum_{\omega_n} \text{Im} (f_0^* (\partial_x f_0 - \kappa_\alpha f_2) - f_2^* \partial_x f_2) . \quad (2.28)$$

The Matsubara GF is obtained by analytic continuation of  $\check{f}$  to the complex plane  $\varepsilon \rightarrow i\omega_n$ . We can use the boundary conditions (2.27) to simplify the previous equation:

$$I_S = \frac{2\pi T}{e R_\square} \sum_{\omega_n > 0} \text{Im} f_0^* (L_x/2) \mathcal{F}_0 e^{i\varphi/2} . \quad (2.29)$$

### S/FI/F/FI/S junction

Another configuration to obtain a  $\varphi_0$ -junction is a S/FI/F/FI/S junction with non-coplanar magnetisations [Fig. 2.4(b)]. This configuration has not yet been realized experimentally, but it has theoretically been predicted to show AJE [121–128]. In these structures, the role of the FI layers is two-fold: firstly, they induce an exchange field  $\mathbf{h}_{r/l}$  in the adjacent S layer, and secondly, they act as spin-polarized tunnelling barriers with a polarization  $\mathbf{P}_{r/l}$ . The linearized Usadel equation in the F layer reads

$$\pm \partial_{xx}^2 \hat{f} + i\kappa_\varepsilon^2 \hat{f} - i\frac{\kappa_F^2}{2} \{\sigma_3, \hat{f}\} = 0 , \quad (2.30)$$

where  $\{.,.\}$  is an anticommutator. We have assumed, without loss of generality, that the exchange field in the F-wire points along the  $z$ -direction.

The S/F junctions with spin-filtering barriers are described by the generalized Kuprianov-Lukichev boundary condition [74, 80], introduced in Eq. (1.86). The exchange fields  $\mathbf{h}_{r/l}$  induced via the magnetic proximity effect in the S-electrodes point in the same direction as the polarization vectors  $\mathbf{P}_{r/l}$ . The linearized boundary conditions read

$$\pm \gamma \partial_n \hat{f}_{r/l} = \frac{1}{2} [\hat{\mathcal{G}}_{r/l} \mathbf{P}_{r/l} \cdot \boldsymbol{\sigma}, \hat{f}_{r/l}] + \frac{1}{2} \{\hat{\mathcal{G}}_{r/l}, \hat{f}_{r/l}\} \mp \sqrt{1 - P_{r/l}^2} \hat{\mathcal{F}}_{r/l} e^{i\eta_{r/l}\varphi/2} . \quad (2.31)$$

Here,  $\hat{\mathcal{G}}_{r/l}$  and  $\hat{\mathcal{F}}_{r/l}$  are the normal and anomalous GFs of the spin-split superconducting electrode, respectively. In the weak exchange field limit, they are given by

$$\hat{\mathcal{G}}_{r/l} = \mathcal{G}_0 - \mathbf{h}_{r/l} \cdot \boldsymbol{\sigma} \frac{d\mathcal{G}_0}{d\varepsilon} \quad (2.32a)$$

$$\hat{\mathcal{F}}_{r/l} = \mathcal{F}_0 - \mathbf{h}_{r/l} \cdot \boldsymbol{\sigma} \frac{d\mathcal{F}_0}{d\varepsilon} , \quad (2.32b)$$

where  $\mathcal{G}_0 = -i\varepsilon/\sqrt{\Delta^2 - \varepsilon^2}$  and  $\mathcal{F}_0 = \Delta/\sqrt{\Delta^2 - \varepsilon^2}$  are the singlet bulk superconductor GFs (2.23).

Following a similar procedure as for the S/F/S junction with Rashba SOC, we solve the Usadel equation (2.30) together with the boundary condition (2.31) to find the condensate function. Linearising Eq. (1.68), we obtain the supercurrent along the ferromagnetic wire

$$I_S = \pi\sigma_F \frac{T}{e} \sum_{\omega_n} \text{Im} \{ f_0^* \partial_x f_0 - \mathbf{f}^* \cdot \partial_x \mathbf{f} \} , \quad (2.33)$$



where  $\hat{f}(\omega_n) = f_0 + \mathbf{f} \cdot \boldsymbol{\sigma}$  is decomposed into the scalar singlet amplitude  $f_0$ , and the vector of triplet states  $\mathbf{f}$ .

### Normal wire

The condensate function in the  $y$  (normal) wire [see Fig. 2.5],  $\hat{f}_y$ , is induced by the proximity effect with the  $x$  wire. To find  $\hat{f}_y$ , we start from the Kuprianov-Lukichev condition (1.83) describing the interface between the two wires, and the Usadel equation in the normal wire. Provided that the widths of the wires  $w_{x,y}$  are much smaller than the superconducting coherence length, we can integrate the Usadel equation over the cross-section of the wire. If the interface resistance is much larger than the resistance of the wires,  $R_B \gg L_{x,y}/\sigma_{F,N}$ , we find the equation determining  $\hat{f}_y$ :

$$\pm \partial_{yy}^2 \hat{f}_y + i \kappa'_\varepsilon{}^2 \hat{f}_y = -\frac{w_x}{\gamma_0^2} \hat{f}(0) \delta(y). \quad (2.34)$$

Here,  $\gamma_0^2 = R_B \sigma_N w_y$  and  $\kappa'_\varepsilon{}^2 = 2\varepsilon/D_y$ , where  $R_B$  is the resistance per unit area between the interface of the  $x$  and  $y$  wires, and  $\sigma_N$  is the normal-state conductance of the  $y$  wire. The Dirac delta term describes the proximity effect, and is a source term. The contact of the  $y$  wire with the normal reservoirs is assumed to be ideal so that the condensate functions vanish at the ends of the wire  $\hat{f}_y(\pm L_y/2) = 0$ . Due to our assumption of a large  $R_B$  we can neglect the inverse proximity effect on the Josephson junction.

Unlike the Josephson junction, the normal circuit is subjected to a voltage bias  $V$ , so it is out-of-equilibrium. In this case, we may not use the equilibrium Matsubara formalism, so we compute the current using Eq. (1.67). The current along the N wire is mediated by quasi-particles, so it is a dissipative current. The quasi-particle current component is given by the normal part of the GFs  $\hat{g}$ , which to the lowest order is corrected as  $\hat{g}^{R/A} = \pm(1 - \hat{f}^{R/A}{}^2/2)$ . To leading order in the proximity effect, the phase-dependent correction to the current through the  $y$ -wire is given by [173–175]

$$\delta I_{\text{qp}} = \frac{-\sigma_N}{16eL_y} \int d\varepsilon F_T(\varepsilon, V/2) \langle \text{Tr}(\check{f}_y^R - \check{f}_y^A)^2 \rangle. \quad (2.35)$$

Here  $\langle \dots \rangle = 1/L_y \int_{-L_y/2}^{L_y/2} dy (\dots)$  denotes average over the length,  $\check{f}^{R/A}$  is the  $4 \times 4$  matrix GF in Nambu-spin space, and  $F_T$  is the transversal distribution function  $F_T(\varepsilon, V) = \frac{1}{2} [\tanh \frac{\varepsilon+eV}{2T} - \tanh \frac{\varepsilon-eV}{2T}]$  at the normal electrodes. Solving the boundary value problem, Eqs. (2.26) and (2.27) for the S/F/S junction with Rashba, or Eqs. (2.30) and (2.31) for the S/FI/F/FI/S junction, we first calculate the  $\hat{f}$  for the  $x$ -wire, and then  $\hat{f}_y$  for the  $y$ -wire from Eq. (2.34). Using Eq. (2.35) we then obtain the usual and anomalous quasiparticle currents.

### 2.2.2 Summary of the results

In the following, we summarise the main results obtained in this section. A full discussion of the analysed systems and the results can be found in Chap. 5. In this work, we have studied the anomalous Josephson effect in two different realisations of a Josephson junction coupled to a mesoscopic conductor. Both an S/F/S junction with Rashba SOC and an S/FI/F/FI/S junction with non-coplanar magnetisation break the required symmetries to show an anomalous component of the Josephson current. We establish how the anomalous phase shift  $\varphi_0$  manifests on the quasi-particle transport through the Andreev interferometer shown in Fig. 2.5.

Our main result is that the current-phase relation of the dissipative (quasi-particle) current through the normal arm of the interferometer, computed from (2.35), also shows an anomalous current component:

$$\delta I_{\text{qp}}(\varphi) = I_c^{\text{qp}} \cos(\varphi + \varphi_0^{\text{qp}}) = I_0^{\text{qp}} \cos \varphi + I_{\text{an}}^{\text{qp}} \sin \varphi. \quad (2.36)$$

Here,  $I_0^{\text{qp}}$  is the quasi-particle current in a conventional Andreev interferometer, which is proportional to  $\cos\varphi$ . The term proportional to  $\sin\varphi$  is the anomalous current component  $I_{\text{an}}^{\text{qp}}$ , which only arises if time-reversal and inversion symmetries are broken in the Josephson junction.

Therefore, the quasi-particle current also exhibits an anomalous phase shift  $\varphi_0^{\text{qp}}$ . In general, the phase shifts in the currents  $\varphi_0$  and  $\varphi_0^{\text{qp}}$  are not equal, but they have a similar magnitude and can be directly related to each other (see Fig. 2 of Chap. 5). Moreover, we have found that, to the lowest order in the fields, the usual and anomalous quasi-particle currents have the same dependence on the spin-dependent fields as the corresponding Josephson current components. Namely, up to the leading order terms in the exchange field and Rashba SOC, for the S/F/S configuration the usual contribution to the quasiparticle current  $I_0^{\text{qp}}$  is independent of the fields, and the anomalous contribution takes the following form:

$$I_{\text{an}}^{\text{qp}} \propto h\kappa_\alpha . \quad (2.37)$$

For the FI/S/F/S/FI configuration, the usual and anomalous quasiparticle currents are proportional to

$$I_0^{\text{qp}} \propto \mathbf{h}_{l\perp} \cdot \mathbf{h}_{r\perp} \quad (2.38a)$$

$$I_{\text{an}}^{\text{qp}} \propto \mathbf{n}_h \cdot (\mathbf{n}_l \times \mathbf{n}_r) , \quad (2.38b)$$

where  $\mathbf{h}_{r/l\perp}$  are the components of  $\mathbf{h}_{r/l}$  perpendicular to  $\mathbf{h}$ , and  $\mathbf{n}_h$  and  $\mathbf{n}_{r/l}$  are the unit vectors along the exchange field and polarization directions.

## 2.3 Microwave-Assisted Thermoelectricity in S-I-S' Tunnel Junctions

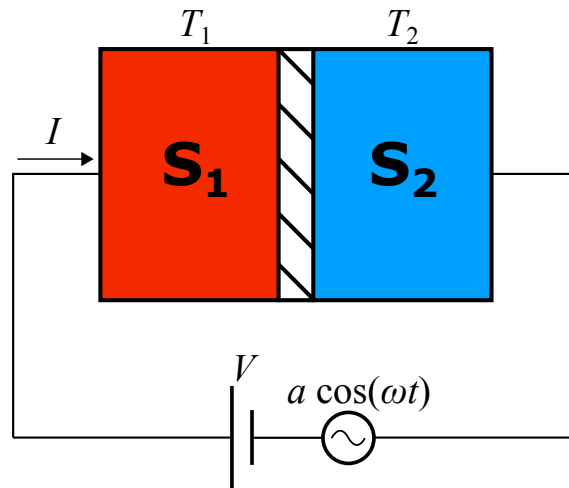


Figure 2.6: Simple circuit scheme of the photon-assisted bipolar thermoelectricity. The two superconductors have a different gap  $\Delta_1 > \Delta_2$  and are subject to a temperature difference  $T_1 > T_2$ . The S-I-S' junction is powered by a DC and an AC voltage source.

In this section, we focus on another relevant effect present in superconductors. Thermoelectricity consists on the generation of electrical power due to a temperature difference. The Seebeck effect, which describes the electromotive force developed between two points at a different temperature, was independently discovered by A. Volta in 1794 [176] and T. J. Seebeck in 1821 [177]. The charge carriers in the material have a higher kinetic energy at higher temperatures, so temperature gradients in the material cause the diffusion of the charge carriers from hot to cold regions. In most

materials, at room-temperature the generated potential difference is proportional to the temperature difference:  $V \propto \Delta T$ . This linear relation allows, for example, to easily calibrate electrical devices such as thermocouples to build temperature sensors.

In the normal state, within the linear regime, thermoelectricity scales linearly with the operating temperature, so the sensitivity of thermoelectric sensors drops drastically at low temperatures. This issue is overcome in superconducting materials, at these temperatures thermoelectricity is very strong due to the nonlinearity of the effect in superconductors. Thermoelectricity has been experimentally reported to be orders of magnitude bigger than the result expected for non-superconducting metals at the same operating temperature [178]. Thermoelectric effects in superconducting junctions have been studied both theoretically and experimentally over the past 10 years. Hybrid superconducting systems with explicit broken particle-hole symmetry show unipolar thermoelectricity [76, 102, 179–185]. The particle-hole symmetry around the Fermi surface of Bardeen-Cooper-Schrieffer (BCS) superconductors can be broken, for instance, in superconductor/ferromagnet hybrid structures. The magnetic proximity effect in a thin superconductor-ferromagnetic insulator bilayer causes an almost homogeneous spin splitting of the density of states (DoS) [186]. If the electronic transport is spin-polarized, for example via a tunnelling spin-filter [1, 187–189], the DoS contribution of one spin component becomes predominant over the other one, leading to an effective particle-hole symmetry breaking [180].

Several applications have been proposed based on the unique thermoelectric properties of S/I/S' and FI/S/I/F junctions: ultrasensitive thermoelectric radiation detectors [9] which can be used in various applications ranging from astrophysical observations [10, 190–192] to security imaging and materials characterization [193], flux controlled high-frequency oscillators fed with a thermal gradient [194], and controlled generators galvanically disconnected from external circuits [195].

Recently, it has been theoretically [194–196] and experimentally [178, 197] shown that superconducting tunnel junctions, where the Josephson coupling is properly suppressed, develop a large thermoelectric effect if the electrode with the larger gap has a higher temperature. In contrast to systems with magnetic proximity effect, in superconducting tunnel junctions the electron-hole symmetry is broken by the combination of a sufficiently strong thermal gradient and a monotonously decreasing DoS which induces spontaneous voltage polarization. The resulting thermoelectricity is *bipolar* and strongly nonlinear.

In this section, we study the thermoelectric effect in asymmetric Josephson junctions under photon-assisted tunnelling (PAT). PAT has been extensively studied in the dissipative regime [198–208]. However, the influence of PAT on the recently observed bipolar thermoelectricity is still unexplored. In addition, we study the cooling properties of the junction. By applying an external bias, for specific temperature conditions [195], it is possible to extract heat and reduce the electronic temperature of the lower gap superconductor [18, 195, 209]. Thermoelectricity and refrigeration are complementary effects. However, the second law of thermodynamics prevents a thermodynamical machine from operating as a heat engine and a cooler at the same time.

### 2.3.1 Model and methods

In this section, we consider a S-I-S' tunnel junction consisting of two bulk superconductors with different superconducting gaps  $\Delta_1 > \Delta_2$ , where the left superconductor ( $S_1$ ) is fixed at a higher temperature than the right superconductor ( $S_2$ )  $T_1 > T_2$ . The gap decreases monotonously with the temperature, so it is not possible to use identical S electrodes in the junction. There are several ways to obtain a gap asymmetry between the electrodes. The conceptually simplest option is using different superconducting materials for each electrode,  $S_2$  having a smaller gap than  $S_1$ . A more suitable option for experiments is using the same superconducting material in both electrodes and attaching a normal layer to the right superconductor. The inverse proximity effectively suppresses the gap of the right superconductor [178, 197, 210], obtaining the desired effect. The advantage

of this configuration is that a single S material is required for the implementation of the device. Moreover, the thickness of the superconducting and normal layers can be chosen so as to fine-tune the asymmetry between the junction gaps. On the negative side, the inverse proximity will also affect the sharpness of the DoS, thus negatively impacting the thermoelectric generation, as recent measurements seem to indicate [197]. The asymmetry between the two terminals is quantified by the asymmetry parameter  $r = \Delta_{0,2}/\Delta_{0,1} < 1$ , where  $\Delta_{0,\alpha}$  is the zero-temperature gap of electrode  $\alpha$ .

To simplify the calculation, we assume that the superconductors are spatially homogeneous, so they are described by the bulk BCS GF derived in Sec. 1.4.1

$$\check{g}^R(\varepsilon) = \frac{-i(\varepsilon + i\Gamma)\tau_3 + \Delta\tau_1}{\sqrt{\Delta^2 - (\varepsilon + i\Gamma)^2}}. \quad (2.39)$$

For a detailed treatment of the SN bilayer as the smaller gap electrode, one can refer to Ref. [210], where the inhomogeneity of the SN bilayer is analysed in order to optimise the thermoelectric effect. In Eq. (2.39), we write the Dynes parameter  $\Gamma$  explicitly, the inelastic scattering effects have an important effect on the broadening of the DoS peaks, so the Dynes parameter plays a crucial role in the efficiency of the thermoelectric effects. Applying the formula for the DoS (1.64), the DoS of a bulk superconductor is given by

$$N(\varepsilon) = N_0 \operatorname{Re} \left\{ \frac{-i(\varepsilon + i\Gamma)}{\sqrt{\Delta^2 - (\varepsilon + i\Gamma)^2}} \right\}. \quad (2.40)$$

Each S electrode is kept in thermal equilibrium at different temperatures  $T_\alpha$ , with  $\alpha = 1, 2$ . The superconducting gaps of each superconductor  $\Delta_\alpha$  is determined self-consistently by the gap equation [see Eq. (1.72)]

$$\Delta \ln \left( \frac{T}{T_{c0}} \right) = 2\pi T \sum_{n=0} \left( f(\omega_n) - \frac{\Delta}{\omega_n} \right), \quad (2.41)$$

where  $f(\omega_n)$  is given by the anomalous part of the GF (2.39), obtained by analytic continuation of the GF to the complex plane  $\varepsilon \rightarrow i\omega_n$ .

The tunnelling current between the two superconductors (1.84) has three contributions: the quasiparticle current, the Cooper pair current, and the interference current which gives the interference contribution associated with breaking and recombination processes of Cooper pairs in different electrodes [110, 211–213]. The latter two contributions stem from the Josephson coupling, and they depend on the phase difference between the superconductors. At finite bias, those terms oscillate between positive and negative values and might be detrimental to a stable thermoelectric effect [194]. Therefore, we assume that the Josephson coupling is sufficiently weak [19, 178, 214, 215], and neglect those terms such that we consider only the quasiparticle (qp) current which is phase-independent. The Josephson coupling between the two sides of the junction may be suppressed, for instance, by applying a suitable in-plane magnetic field to induce Fraunhofer interference, or via a small out-of-plane magnetic field in a superconducting quantum interference device (SQUID) [178, 197].

The DC tunnelling qp charge  $I_\alpha$  and heat  $\dot{Q}_\alpha$  currents flowing out from electrode  $\alpha = 1, 2$  are given by (see Eq. (1.85))

$$\begin{pmatrix} I_\alpha \\ \dot{Q}_\alpha \end{pmatrix} = \frac{G_T}{e^2} \int d\varepsilon \begin{pmatrix} -e \\ \varepsilon - \mu_\alpha \end{pmatrix} \frac{N_\alpha(\varepsilon - \mu_\alpha)}{N_{0,\alpha}} \frac{N_{\bar{\alpha}}(\varepsilon - \mu_{\bar{\alpha}})}{N_{0,\bar{\alpha}}} (f_\alpha(\varepsilon - \mu_\alpha) - f_{\bar{\alpha}}(\varepsilon - \mu_{\bar{\alpha}})), \quad (2.42)$$

with  $\bar{\alpha}$  the opposite side with respect to  $\alpha$ . Here,  $-e$  is the electron charge,  $G_T$  is the conductance of the junction, and  $f_\alpha(E) = [\exp\{(E/k_B T_\alpha)\} + 1]^{-1}$  is the  $\alpha$ -lead Fermi-Dirac distribution. The shift

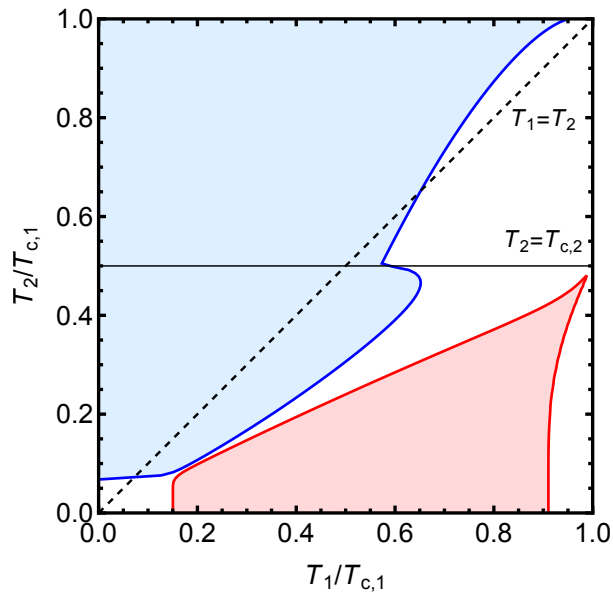


Figure 2.7: Non-linear thermoelectricity (red) and cooling (blue) regions for a superconductor with  $T_{c,1} = 2T_{c,2}$ . The dashed line delimits the equal temperature contour  $T_1 = T_2$ . The solid horizontal line shows the temperature  $T_2 = T_{c,2}$  above which  $S_2$  becomes a normal metal.

in the chemical potential of the electrodes is determined by the voltage source  $V$ :  $\mu_1 - \mu_2 = -eV$ . For non-equilibrium temperature  $T_1 > T_2$ , there is the possibility to develop the bipolar thermoelectric effect, as shown in Fig. 2.7.

The reciprocity of the S-I-S' electric device can be easily checked in Eq. (2.42) by inverting the voltage bias  $V \rightarrow -V$ . The DoS of the superconductors is electron-hole symmetric and the distribution function is odd in energy, so the quasiparticle charge current in the junction is odd in voltage  $I(-V) = -I(V)$ . We can also check the first law of thermodynamics (energy conservation relation) in Eq. (2.42)

$$\dot{Q}_1 + \dot{Q}_2 - \dot{W} = 0, \quad (2.43)$$

where  $\dot{W} = -VI$  describes the electric power generated (dissipated) for  $\dot{W} > 0$  ( $\dot{W} < 0$ ) by the junction. Here we use the active sign convention by considering the electrical work done by the junction over its surroundings as positive.

As shown in Fig. 2.8(a-b), the junction thermal equilibrium  $T_1 = T_2$  shows only a dissipative behaviour ( $IV \geq 0$ ). Panels (a) and (b) are the well-known tunnelling quasiparticle currents of an S-N and an S-S junction. In the former, at  $T = 0$  there is no tunnelling current until  $e|V| > \Delta$ , so the voltage bias provides enough energy to create an excitation in the superconductor. In the latter, a bias of  $e|V| > \Delta_1 + \Delta_2$  is needed. At higher voltages, the characteristic curve  $I(V)$  tends to the Ohmic limit  $I = G_T V$ . In a symmetric junction with a temperature difference [Fig. 2.8(c)], the characteristic curve shows a dissipative matching-peak at  $eV_p = \Delta_1 - \Delta_2$ . In asymmetric junctions, if the temperature of the electrode with the bigger gap is high enough  $T_1 \gtrsim T_2/r$ , bipolar thermoelectricity may arise in the junction [178, 196], with the current  $I$  flowing against the bias ( $IV < 0$ ), as shown in Fig. 2.8(d). The thermoelectric effect occurs at subgap voltages  $e|V| \lesssim \Delta_1 + \Delta_2$  [194–196]: the current is 0 for no voltage-difference and grows in magnitude to a maximum around the matching peak  $V_p$ . Further increasing the voltage bias decreases the magnitude of the current until the current becomes dissipative for  $e|V| \gtrsim \Delta_1 + \Delta_2$ .

If an AC source is included in addition to the DC voltage,  $V(t) = V + a \cos(\omega t)$ , as shown in Fig. 2.7, for instance, by placing the junction in a microwave field, the average current is not simply given by Eq. (2.42). The time-averaged DC tunnel (charge|heat) currents  $\bar{I}|\bar{Q} = (1/T) \int_0^T dt I|\dot{Q}(t)$

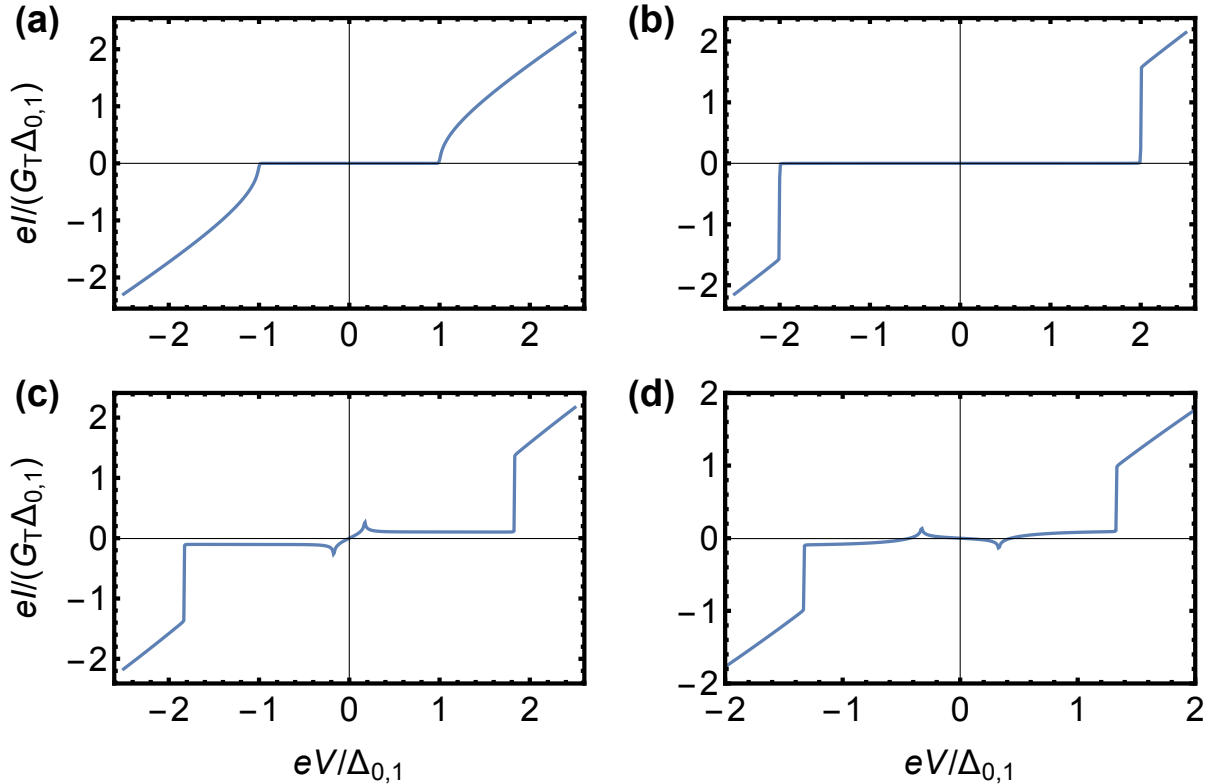


Figure 2.8: Tunnelling quasiparticle current for (a) S/N junction at  $T_1 = T_2 = 0$ , (b) S/S junction at  $T_1 = T_2 = 0$ , (c) S/S junction at  $T_1 > T_2$ , and (d) S/S' junction with  $\Delta_{0,1} > \Delta_{0,2}$  at  $T_1 > T_2$ .

take the form [198, 208, 216]

$$\begin{pmatrix} \bar{I} \\ \bar{Q} \end{pmatrix} = \sum_{n=-\infty}^{\infty} J_n^2\left(\frac{ea}{\omega}\right) \begin{pmatrix} I(V - n\omega/e) \\ \dot{Q}(V - n\omega/e) \end{pmatrix}, \quad (2.44)$$

where  $T = 2\pi/\omega$  is the period of the AC voltage. This is the standard result for photon-assisted tunnelling (PAT), where  $J_n(x)$  is the  $n$ -th Bessel function of the first kind. In Eq. (2.44), we assume that the frequency of the AC voltage is small enough so that it modulates the potential energy of the quasiparticles adiabatically [203, 217, 218]. In this approximation, the AC frequency is necessarily bounded by the plasma frequency of the two electrodes, and the driving frequency needs to be  $\omega < 2\Delta$  in order to neglect high-order processes in the current due to the direct breaking of Cooper pairs because of photon absorption. At the same time, we mainly focus on quite small amplitudes of the voltage oscillations  $ea \ll \Delta$ , as we explain in Chap. 6, since high amplitudes are detrimental for the thermoelectric effect, restoring the usual dissipative behaviour at high energies. Finally, the averaged current  $\bar{I}$  is also reciprocal  $\bar{I}(-V) = -\bar{I}(V)$  due to the reciprocity of the junction  $I(V)$ .

In the following, we explain the main results obtained for the time-averaged thermoelectric and cooling properties of the S-I-S' junction under photon-assisted tunnelling, and compare them to the DC case. Two figures of merit that quantify the thermoelectric effect are the generated electric power  $\dot{W}$ , and the thermoelectric Seebeck voltage  $V_S$ , for which  $I(\pm V_S) = 0$ . The Seebeck voltage corresponds to the voltage provided by the junction in an open circuit configuration. The cooling power is quantified by the coefficient of performance  $\text{COP} = -\dot{Q}_2/\dot{W}$ , which describes the efficiency of the extracted heat with respect to the applied work.

### 2.3.2 Summary of the results

Here we summarise the main results of Chap. 6. An S-I-S' tunnel junction shows a thermoelectric matching peak at  $V = \pm V_p = \pm(\Delta_1 - \Delta_2)/e$ . The characteristic curve of the junction is modified under the influence of photon-assisted tunnelling. The AC voltage source leads to a weighted replication of the bipolar thermoelectric DC characteristic curve displaced in voltages, as shown by Eq. (2.44). The matching peak is split into sidebands at  $V = \pm V_p + n\omega/e$ ,  $n \in \mathbb{Z}$ , as determined by Eq. (2.44). Thus, PAT redistributes power to other voltages. Generally, the PAT leads to a reduction of the net thermopower output, but as shown in Fig. 1 of Chap. 6, it enhances the thermoelectricity at the sidebands. This allows to enhance the thermoelectric power and efficiency at the working point of the device by selecting an appropriate frequency. Moreover, the PAT broadens the thermoelectric region potentially increasing even the obtainable Seebeck voltage (Fig. 2(b) of Chap. 6). Therefore, changes in the operating point of the junction will have a less dramatic effect over the thermoelectric performance.

Another advantage introduced by PAT is the appearance of additional stable working points specified by the sidebands, as shown in Fig. 2(c) of Chap. 6. Therefore, PAT can be used to design devices with an increased number of states at different voltages, potentially increasing the number of logic states of a thermoelectric volatile memory [219–221].

Finally, PAT also influences the cooling performance of the junction. Similar to the thermoelectric effect, the PAT redistributes the cooling capabilities into sidebands, allowing to increase the COP at specific voltages determined by the frequency of the AC field (Fig. 3 of Chap. 6).

In summary, we have studied the thermoelectric properties of a superconducting junction under a microwave field. A temperature difference may be used to generate electrical power, and conversely, electrical power may be supplied to a system to transport heat. Another key property that may arise in hybrid superconducting structures with SOC is spin transport, relevant for spintronic applications.

## 2.4 Dynamical Hall responses of disordered superconductors

In this section, we study the Hall and spin Hall effects in superconductors. The Hall effect was discovered by E. Hall in the 19th century [222]. The injection of an electric current into a conductor with a perpendicular magnetic field leads to the presence of a transverse charge current. In finite-sized (open) conductors, the charge carried by the transverse current is accumulated on the sides of the conductor, generating a Hall voltage. The Hall effect can directly be incorporated into the Drude model [223, 224] of electronic conduction once the Lorenz force due to the magnetic field is included. The AC Hall effect describes the transverse charge current under a varying electric field. In diffusive normal metals the Hall conductivity is proportional to the longitudinal conductivity, where the proportionality constant is  $\omega_c \tau$  [225], with  $\omega_c = eB_0/m$  the cyclotron frequency. The longitudinal and Hall currents become frequency-dependent in the superconducting state [226], featuring both in-phase and out-of-phase current contributions. Moreover, the longitudinal and Hall conductivities have different frequency-dependence, so they are no longer proportional.

The in-phase component of the longitudinal response describes electronic transitions in the superconductor and features a superconducting gap at low temperatures. The out-of-phase response arises due to the supercurrent. Despite some attempts over the years [227, 228] based on phenomenological two-fluid models and Bardeen-Cooper-Schrieffer (BCS) theory, there has been no microscopic extension of the Drude model for the dynamical Hall response in superconductors in the diffusive regime. The quasiclassical formalism allows for an easy treatment of the dynamical Hall effect in superconductors. In this section, we extend the Mattis-Bardeen theory for the dynamical response of superconductors to include the Hall response. We introduce the theory necessary to

compute the longitudinal and transverse currents in a superconductor within the quasiclassical formalism.

Additionally, we study the dynamical spin Hall effect in superconductors. In the presence of spin-orbit interaction, a charge current in a conductor generates a transverse spin current, and vice versa [229]. There are two major mechanisms for the spin Hall effect: the *intrinsic* mechanism, produced by the inversion symmetry breaking either due to the lattice (Dresselhaus spin-orbit coupling (SOC) [230]) or the sample structure (Rashba spin-orbit coupling [231]), and the *extrinsic* mechanism, resulting from the spin-dependence of the impurity scattering. Recent extensions of the quasiclassical Usadel equation [65, 70] introduced in Sec. 1.4.4 allow to describe the charge and spin Hall effects [65, 70] in a unified way. In the following, we utilize these extensions to study said dynamic responses.

### 2.4.1 Model and methods

In this subsection, we introduce the specific scenarios studied in Chap. 7. Our study encompasses a broad scope, focusing on superconductors subjected to time-dependent electromagnetic fields, alongside exchange fields and linear-in-momentum spin-orbit coupling, which can be treated as effective SU(2) potentials [62]. These systems are described by the Hamiltonian (1.73).

As introduced in Sec. 1.4.4, the electromagnetic U(1) and spin-related SU(2) potentials can jointly be described by the generalized four-potential  $\check{A}^\mu$  [66–68]<sup>1</sup>

$$\check{A}^0 = -e\varphi\tau_3 + \frac{\hbar}{2}A^{0j}\sigma_j \quad (2.45a)$$

$$\check{A}^i = -eA^i\tau_3 + \frac{\hbar}{2}A^{ij}\sigma_j. \quad (2.45b)$$

$\varphi$  and  $\mathbf{A}$  are the usual U(1) scalar and vector electromagnetic potentials, while  $A^{0j}$  and  $A^{ij}$  are SU(2) potentials describing the Zeeman or exchange field and the linear-in-momentum SOC, respectively [69].

The field strength associated with the four-potential  $\check{A}$  is

$$\check{F}^{\mu\nu} = \partial^\mu \check{A}^\nu - \partial^\nu \check{A}^\mu - \frac{i}{\hbar}[\check{A}^\mu, \check{A}^\nu]. \quad (2.46)$$

We are interested in the charge and spin currents generated by an electric field, which is given by the  $\check{E}^j \equiv \check{F}^{0j} = -eE^j\tau_3 + (\hbar/2)E^{jl}\sigma_l$  components of the field strength tensor (2.46), where the Latin indices range  $j = 1, 2, 3$ . In the linear response regime, the current and the field are related via the response tensor:

$$j^{i\mu}(\omega) = \sigma^{i\mu, j\nu}(\omega)E^{j\nu}(\omega). \quad (2.47)$$

Here,  $j^{i0}$  are the components of the charge current, whereas  $j^{ij}$  is the spin-current tensor. The usual U(1) electric field is given by  $E^j \equiv E^{j0}$ , and  $E^{jl}$  denote the components of the SU(2) electric field. The real part of  $\sigma^{i\mu, j\nu}$  describes the in-phase response, whereas the imaginary part is the out-of-phase response of the current to the field.

Our goal is to find the conductivity tensor  $\sigma^{i\mu, j\nu}(\omega)$  in diffusive superconducting systems showing different types of Hall effects. For this purpose, we use the quasiclassical approach generalized in Refs. [65, 70] to include SOC. The covariant version of the Usadel equation allows describing the Hall and intrinsic spin Hall effects. For intrinsic SOC the Usadel equation takes the form of Eq. (1.76), while for extrinsic SOC it is given by Eq. (1.78). The Usadel equation together with the

<sup>1</sup>In this section we restore the  $\hbar$  to explicitly show the dimensions of the spin current and conductivity.



normalization condition specify the value of the GF. The charge and spin currents of the system are given by the GF [see Eqs. (1.66-1.69)]

$$j^{i0}(\mathbf{r}, t) = -\frac{\pi\hbar\sigma_D}{8e} \text{Tr} \{ \tau_3 \check{J}^i(\mathbf{r}, t, t)^K \} \quad (2.48)$$

$$j^{ij}(\mathbf{r}, t) = \frac{\hbar}{2} \frac{\pi\hbar\sigma_D}{8e^2} \text{Tr} \{ \sigma_j \check{J}^i(\mathbf{r}, t, t)^K \}, \quad (2.49)$$

where the Drude conductivity is given by  $\sigma_D = \nu_F e^2 D$ ,  $\nu_F$  is the density of states at the Fermi energy, and the  $K$  superscript denotes the Keldysh block of the matrix current  $\check{J}$ , given by Eq. (1.77) for intrinsic and Eq. (1.80) for extrinsic SOC.

We assume that the electric field is small enough so that it can be treated perturbatively. We consider a single-frequency electric field along the  $x$ -direction  $\mathbf{E}(t) = E_0 e^{-i\omega t} \hat{\mathbf{u}}_x$  described via the vector potential  $\mathbf{A}(t) = -iE_0/\omega e^{-i\omega t} \hat{\mathbf{u}}_x$ . Solving the GF from the Usadel equation, we may compute the charge  $j^{i0}(t)$  and spin  $j^{ij}(t)$  currents. Dividing the current by the electric field  $E_0 e^{-i\omega t}$  we obtain the conductivity tensor  $\sigma^{i\mu, j\nu}(\omega)$ . To study the inverse Hall effect, i.e., the conversion of a spin current into a transversal charge current, we consider an SU(2) driving field  $E^{jl}(t) = \mathcal{E}_0 e^{-i\omega t}$  which generates a  $l$ -polarized spin current in the  $j$ -direction. This electric field is described via the SU(2) vector potential  $\check{A}^j(t) = -i\hbar\mathcal{E}_0/(2\omega) e^{-i\omega t} \sigma_l$ .

### Conductivity tensor and Onsager symmetries

The conductivity tensor in Eq. (2.47) can be decomposed into four blocks,

$$\sigma^{i\mu, j\nu} = \begin{pmatrix} \sigma^{i0, j0} & \sigma^{i0, jl} \\ \sigma^{ik, j0} & \sigma^{ik, jl} \end{pmatrix}. \quad (2.50)$$

The Onsager reciprocal relations relate the conductivities between different pairs of driving fields and their conjugate currents. They demonstrate the reciprocity between inverse effects, such as the Hall, the spin Hall or spin-galvanic effects and their corresponding inverse effects. The elements of the conductivity tensor (2.50) are related through the Onsager reciprocal relations  $\sigma^{j0, i0}(\mathbf{B}) = \sigma^{i0, j0}(-\mathbf{B})$ ,  $\sigma^{jl, ik}(\mathbf{B}) = \sigma^{ik, jl}(-\mathbf{B})$  and  $\sigma^{i0, jl}(\mathbf{B}) = -\sigma^{jl, i0}(-\mathbf{B})$ , where  $\mathbf{B}$  comprises all TRS breaking fields [232]. The minus sign in the last relation appears due to the spin currents having opposite T-parity to charge currents [233].

The charge block  $\sigma^{ij} \equiv \sigma^{i0, j0}$  is the usual  $3 \times 3$  conductivity tensor describing the electric effects. The diagonal elements are the longitudinal conductivities (Ohm's law), while the off-diagonal elements describe the Hall effect. The spin block  $\sigma^{ik, jl}$  is a  $9 \times 9$  matrix relating the spin currents to the spin SU(2) fields. For instance, some of the off-diagonal elements of the spin block describe the spin-swapping effect. The spin-charge blocks  $\sigma^{ik, j0}$  and  $\sigma^{i0, jl}$  describe the spin Hall and inverse spin Hall effects, respectively.

The susceptibility  $\chi = i\omega\sigma$  is the response function to the vector potentials. From the fluctuation-dissipation theorem for  $\chi$  [234], it follows that the Hermitian part of the generalized conductivity tensor  $\sigma' = \frac{1}{2}(\sigma + \sigma^\dagger)$  is the dissipative contribution, while the anti-Hermitian part  $\sigma'' = \frac{1}{2i}(\sigma - \sigma^\dagger)$  is the reactive contribution.

### Kerr and Faraday rotations

In normal metals, the Hall effect can easily be measured through the transverse Hall voltage developed between the interfaces of the material. On superconductors, the supercurrent mediated by the superconducting correlations is dissipationless, so it does not generate any voltage drop. Another way to probe the Hall effect is through the Faraday or Kerr effect measurement as shown in Fig. 2.9(a). Linearly polarized light is shone over a sample: part of the light is transmitted

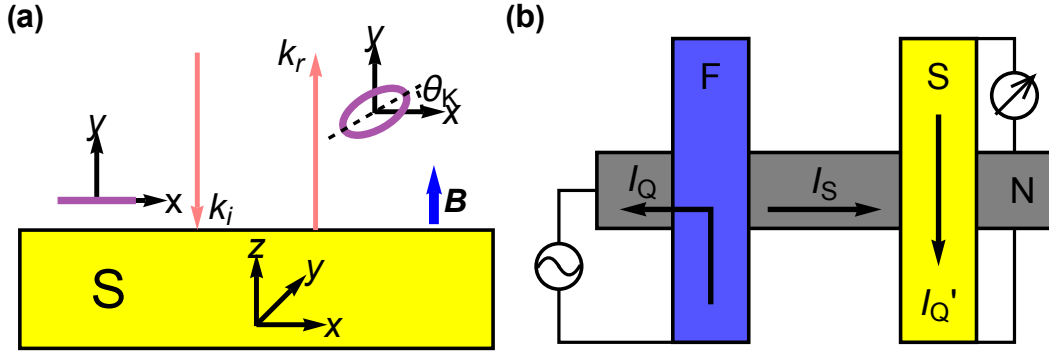


Figure 2.9: (a) Proposed setup for the measurement of the Hall effect. Materials subjected to a magnetic field show circular birefringence, *i.e.* left and right polarized light waves propagate with different velocities. The Kerr rotation angle is related to the longitudinal and transversal conductivities of the material. (b) Proposed setup for the detection of the inverse spin Hall effect in a superconductor using a lateral spin valve. Suppose a charge current  $I_Q$  is injected from the ferromagnet (F) to the normal metal (N). In that case, the non-equilibrium spin accumulation generated at the interface generates a pure spin current  $I_S$  to the right of F. The superconductor absorbs the spin current owing to its strong SOC, generating a charge current  $I_Q'$  due to the inverse spin Hall effect.

and the rest is reflected from the sample with an elliptical polarization [235, 236]. The rotation of the polarization axis and the ellipticity of the transmitted and reflected lights are determined by the boundary conditions of the electromagnetic field at the sample's boundary. The rotation angle is described by the Faraday and Kerr angles, which are in general complex quantities  $\phi_{K(F)} = \theta_{K(F)} + i\varepsilon_{K(F)}$ : the rotation angle  $\theta_{K(F)}$  specifies the rotation of the major axis of the elliptically polarized reflected light. The imaginary part  $\varepsilon_{K(F)}$  specifies the ratio of the minor to the major axes of the ellipsoid. The Faraday-Kerr rotation of the polarization state of light can experimentally be measured by passing the reflected light through a polarizer. The polarization direction is obtained by measuring the intensity of the reflected light with the polarizer oriented in parallel and perpendicular to the incident light.  $\phi_K$  and  $\phi_F$  depend on the longitudinal and transversal conductivities of the sample, so they can be straightforwardly calculated from our theory.

The applied magnetic field responsible for the Hall effect and the light shone over the sample cannot penetrate into a thick superconductor due to the Meissner effect. The penetration of the magnetic field is determined by the London penetration depth. However, the (Kerr) reflection is also a surface effect because of the finite skin depth of the electromagnetic field, and the (Faraday) transmission takes place only if the material is thinner than the corresponding skin depth. For simplicity, we assume a constant magnetic field, which is a valid approximation if the London penetration depth is larger than either the skin depth (for Kerr reflection) or the sample thickness (for Faraday transmission).

In the specific case where the linearly polarized electromagnetic wave incides normally with respect to the sample surface, the Faraday  $\phi_F$  and Kerr  $\phi_K$  angles take a simple form. Using Maxwell equations and the boundary conditions for the electromagnetic field, the angles are given by [235, 236]

$$\phi_K = i \frac{r_+ - r_-}{r_+ + r_-} \simeq \frac{\sigma^{yx}}{\sigma^{xx} \sqrt{1 + i \frac{\sigma^{xx}}{\omega \epsilon_0}}}, \quad (2.51)$$

$$\phi_F = \frac{\omega d}{c} \frac{r_+ - r_-}{(1 - r_+)(1 - r_-)} \simeq i \frac{d}{2c \epsilon_0} \frac{\sigma^{yx}}{\sqrt{1 + i \frac{\sigma^{xx}}{\omega \epsilon_0}}}, \quad (2.52)$$

where  $r_{\pm}$  are the reflection coefficients for left- and right-handed (with respect to the applied field) circularly polarized light,  $\epsilon_0$  is the vacuum permittivity, and  $d$  is the sample thickness. Note that the expression is obtained by assuming a small perturbation from the external magnetic field and only considering linear terms in the Hall conductivity ( $\sigma^{yx}$ ). This approximation is valid when the Hall conductivity is much smaller than the longitudinal conductivity, a condition often met in many materials. Noting  $\sigma_D$  as a natural scale of conductivity and defining the plasma frequency  $\omega_p = \sqrt{\sigma_D/(\epsilon_0\tau)}$ , we notice that the second term inside the square root in Eqs. (2.51) and (2.52) can also be written as  $\sigma^{xx}/(\omega\epsilon_0) = (\sigma^{xx}/\sigma_D)\omega_p^2\tau/\omega$ , providing a direct way to compare dimensionful quantities. For frequencies of interest here,  $\omega \lesssim \Delta/\hbar$ , the typical range is  $\omega \ll \omega_p, 1/\tau$ , and therefore the first term inside the square root in Eqs. (2.51) and (2.52) can typically be disregarded. The order of magnitude of the polarization rotation is hence proportional to the small factor  $\omega_c\tau\sqrt{\omega/(\omega_p^2\tau)}$ , with  $\omega_c = eB_0/m$  the cyclotron frequency.

### Lateral spin valve

The spin Hall effect can be measured in a device known as lateral spin valve. A lateral spin valve consists of a normal metal (N) bridging a ferromagnetic injector (F) and a detector, which in our case is a superconductor (S) with SOC, as shown in Fig. 2.9(b). A charge current  $I_Q$  is injected from F into the left side of N. The non-equilibrium spin accumulation generated at the interface is relaxed within the spin diffusion length, generating a pure spin current  $I_S$  to the right of F. If the distance between the F and the S is shorter than the spin diffusion length, a non-equilibrium spin accumulation is generated at S [237]. The spin current is absorbed by the superconductor owing to its strong SOC. The polarization of the spin current is tuned to lie out-of-plane by applying a normal magnetic field. A perpendicular charge current  $I'_Q$  is generated at the S due to the inverse spin Hall effect. This AC current can experimentally be measured by closing the S wire with a superconducting loop coupled to a rf-SQUID.

Alternatively, the measurement can be realized with a dynamic version of the setup as used in Ref. [238]. There, two heavy-metal (Pt) injectors are used to generate and detect a magnon current in a ferromagnetic insulator. A heavy-metal superconductor placed in the middle absorbs part of the magnon current and converts it into a charge current via the inverse spin Hall effect. Replacing the DC injection with a finite-frequency injection then allows studying the AC spin Hall response of the superconductor.

### 2.4.2 Summary of the results

Here, we summarize the main results obtained in Chap. 7. Using a recent extension of the quasiclassical Usadel equation [65, 70], we provide a unified description of charge and spin transport to study the dynamical response of dissipative superconductors to charge U(1) and spin SU(2) fields. The model recovers known results in the appropriate limits, such as the Mattis-Bardeen response (Fig. 1 of Chap. 7), the normal state Hall conductivity, and the spin Hall conductivity for normal metals with Rashba spin-orbit coupling.

We have explicitly verified that the Onsager relations between the direct and inverse Hall effects are satisfied, demonstrating the reciprocity between inverse effects. Superconductors show out-of-phase Hall (Fig. 2 of Chap. 7) and spin Hall (Fig. 4 of Chap. 7) currents, described by a finite imaginary part of the Hall conductivities. According to the fluctuation-dissipation theorem [234], these out-of-phase Hall currents are dissipative. This is supported by the gap found on the imaginary part of the Hall conductivities for  $\hbar\omega < 2\Delta_0$ : the dissipative current is mediated by quasiparticles, so at  $T = 0$  the processes that allow energy absorption are limited to the creation of electron-hole pairs, which require frequencies greater than  $2\Delta_0$  [43].

Our findings can be verified through optical spectroscopy via the Faraday-Kerr rotation of the polarization state of light in the case of the ordinary Hall effect, determined by Eqs. (2.51) and (2.52), and in a lateral spin valve in the case of the spin Hall effect, where a superconductor with SOC is used as a detector.

# Chapter 3

## Summary

*The most incomprehensible  
thing about the world  
is that it is comprehensible.*

— Albert Einstein

This Thesis presents a comprehensive study of several non-equilibrium properties of superconductors with various types of spin-dependent fields. Superconductors with spin-dependent fields may find diverse applications in spintronics, thermoelectricity, sensing, and topological quantum computing. The theoretical framework employed to investigate this system is the quasiclassical Green's function method. This formalism offers a convenient means to describe hybrid structures through appropriate boundary conditions, accounting for non-controllable disorder inherent in real devices. Furthermore, the GF method deals with a reduced set of kinetic-like equations, making it computationally efficient compared to microscopic models like tight-binding approaches.

Chapter 1 introduces the Keldysh GF formalism, utilized for studying the non-equilibrium properties of superconductors. The aim of this chapter is twofold: firstly, it serves as the theoretical basis for the systems studied in subsequent chapters. Secondly, it pretends to serve as a guide to become acquainted with the quasiclassical GF formalism. It encompasses the derivation of the Eilenberger and Usadel quasiclassical equations and delineates the boundary conditions and relevant observables necessary for studying time-dependent non-equilibrium phenomena.

In Chapter 2, we apply the theory outlined in Chapter 1 to specific systems, presenting the primary results obtained. Detailed analyses of these systems are provided in Chapters 4-7, comprising selected publications derived from the work undertaken during this doctoral research. Chapter 4 (Ref. [239]) serves as a warm-up to extract the properties of a superconducting system with spin-dependent fields. It investigates singlet and triplet superconducting correlations in the vicinity of a sharp domain wall and explains how they manifest in the local DoS. In Chap. 5 (Ref. [240]), we compute the non-equilibrium (static) properties of superconductors with spin-dependent fields. Specifically, we explore the anomalous Josephson effect in an Andreev interferometer device. Lastly, Chapters 6 and 7 introduce time-dependent electric and spin-fields. In Chap. 6 (Ref. [241]), we investigate the time-averaged thermoelectric and cooling capabilities of asymmetric superconducting tunnel junctions. In Chap. 7 (Ref. [242]), we study the dynamical charge and spin transport in diffusive superconductors.

Additional topics explored during this doctoral research, albeit not included in this Thesis, encompass the study of spectral properties and critical temperature of superconductors of arbitrary thickness (Ref. [78]), charge transport properties of mixed-parity superconductors (Ref. [243]), spin-valve effect in superconductors, superconducting fluctuations, weak localization in systems with generic spin-dependent fields (Ref. [244]), and the analysis of conductance and spin-textures in

quantum networks with spin-orbit coupling (Ref. [245])<sup>1</sup>. The peer-reviewed publications resulting from these studies are listed after Chapter 7. The quasiclassical GF formalism was employed in all the aforementioned topics except for the latter one, where the ballistic conductance was computed within the quantum network formalism [247–253]. This highlights the versatility of the quasiclassical theory.

Future research on superconducting structures could include the study of the transport properties of superconductors in the presence of exotic types of spin-dependent fields such as Weyl-type SOC [254–256] and altermagnetism [257–259]. Moreover, the quasiclassical formalism may be applied to systems with internal degrees of freedom other than spin (valleys, sublattice isospin, etc.), and systems with anisotropic disorder, or disorder that depends on the internal degrees of freedom. In this respect, it would be interesting to generalise the quasiclassical formalism to the multiband superconductors, which may provide additional transport channels which possibly also show up in Hall-like responses, such as the valley Hall effect. Finally, quasiclassics has successfully been used to study fluctuation conductivity in disordered superconducting films [260], one of the planned future research goals of the author of this Thesis is to expand upon these studies by incorporating the effects of spin-dependent fields.

In the following we include the publications comprising this Thesis.

---

<sup>1</sup>Other publications related to the topics in the Thesis are Refs. [210] and [246].

## Chapter 4

Quasiparticle density of states and triplet correlations in superconductor/ferromagnetic-insulator structures across a sharp domain wall

## Quasiparticle density of states and triplet correlations in superconductor/ferromagnetic-insulator structures across a sharp domain wall

Alberto Hijano <sup>1,2,\*</sup> Vitaly N. Golovach <sup>1,3,4,†</sup> and F. Sebastián Bergeret <sup>1,3,‡</sup>

<sup>1</sup>*Centro de Física de Materiales (CFM-MPC) Centro Mixto CSIC-UPV/EHU, E-20018 Donostia-San Sebastián, Spain*

<sup>2</sup>*Department of Condensed Matter Physics, University of the Basque Country UPV/EHU, 48080 Bilbao, Spain*

<sup>3</sup>*Donostia International Physics Center (DIPC), 20018 Donostia-San Sebastián, Spain*

<sup>4</sup>*IKERBASQUE, Basque Foundation for Science, 48011 Bilbao, Spain*



(Received 24 February 2022; revised 19 April 2022; accepted 25 April 2022; published 6 May 2022)

A ferromagnetic insulator (FI) in contact with a superconductor (S) is known to induce a spin splitting of the BCS density of states at the FI/S interface. This spin splitting causes the Cooper pairs to reduce their singlet-state correlations and acquire odd-in-frequency triplet correlations. We consider a diffusive FI/S bilayer with a sharp magnetic domain wall in the FI, and we study the local quasiparticle density of states and triplet superconducting correlations. In the case of collinear alignment of the domains, we obtain analytical results by solving the Usadel equation. For a small enough exchange field or weak superconductivity, we also find an analytical expressions for arbitrary magnetic textures, which reveals how the triplet component vector depends on the local magnetization of the FI. For an arbitrary angle between the magnetizations and the strength of the exchange field, we numerically solve the problem of a sharp domain wall. We finally propose two different setups based on FI/S/F stacks, where F is a ferromagnetic layer, to filter out singlet pairs and detect the presence of triplet correlations via tunneling differential conductance measurements.

DOI: [10.1103/PhysRevB.105.174507](https://doi.org/10.1103/PhysRevB.105.174507)

### I. INTRODUCTION

The exchange coupling at the interface between a ferromagnetic insulator (FI) and a thin superconducting layer (S) can lead to a spin-splitting of the density of states (DOS) in the S layer, as observed in numerous experiments [1–5]. Recently, there has been a renewed interest in these systems due to various proposed applications. These applications include spin valves [6,7], spin batteries [8,9], magnetometers [10,11], thermometers [12,13], caloritronic devices [14–16], thermoelectric elements [17,18], and radiation detectors [19,20]. FI/S structures have also been explored in the context of Majorana fermions in semiconducting wires [21–23].

Most of these applications require a robust superconducting gap with a sizable spin-splitting. This can be achieved, for example, in EuS/Al systems [2,4,5,7,24], where the interfacial exchange interaction leads to a sharp spin-splitting in S layers with thicknesses smaller than the coherent length. On the theoretical side, the effect of the interfacial exchange field and the induced spin-splitting on the superconducting state has been studied in numerous works [5,25–27]. Most of these works assume a homogeneous spin-splitting field. This assumption is justified, even in a multidomain situation, if the characteristic domain size of EuS is much longer than the superconducting coherence length  $\xi_0$ .

There are, however, situations in which the domain size may be of the order of the superconducting coherence length. The effect of domain walls in magnetic and insulating ferromagnets on adjacent superconductors has been studied theoretically [28–32] and experimentally [4,33], while Ref. [34] studied the influence of domain-wall dynamics on superconductivity. In particular, Ref. [4] provided experimental evidence that EuS consists of multiple domains with a size of the order of the coherence length of the Al layer attached to it. The authors of that work contrast spectroscopic measurements with a theoretical model that assumed alternating up/down domains of different sizes. In the present work, we generalize this approach and study a FI/S structure with two noncollinear magnetic domains.

Despite the amount of experimental work on FI/S systems, almost all of it focuses on studying its quasiparticle spectrum. There is, however, an interesting aspect that is not often mentioned in these works. The mere existence of an interfacial exchange field leads to conversion of singlet superconducting correlations to triplet ones [35–38]. The induced triplet component has a total zero spin projection if the FI consists of a single domain with homogeneous magnetization. However, in FI/S systems with noncollinear magnetization, triplet components with different spin-projections may coexist with the singlet one.

In this work, we study the equilibrium properties of a FI/S bilayer with a sharp domain wall separating two magnetic domains. We present an analytical solution for the Usadel equation for a FI/S bilayer consisting of two semi-infinite magnetic domains with collinear magnetization and noncollinear magnetization in the weak exchange field limit,

\*alberto.hijano@ehu.es

†vitaly.golovach@ehu.es

‡fs.bergeret@csic.es



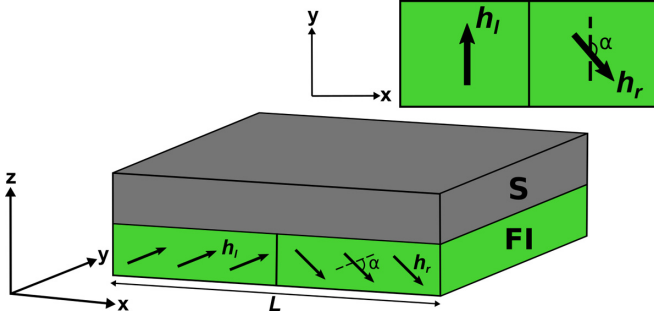


FIG. 1. Schematic view of the S/FI structure under consideration. The ferromagnetic insulator has two domains with arbitrary in-plane magnetization direction. The inset shows the top view of the FI. The magnetizations of the two domains lie on the  $xy$  plane, and they form an angle  $\alpha$ .

and we use numerical methods to solve the noncollinear case with arbitrary exchange field strength. Additionally, we study the spatial evolution of the triplet correlations near a domain wall, and we propose a method to detect them using tunneling spectroscopy of an additional ferromagnetic layer. The work is organized as follows: In Sec. II we present the main equations describing a diffusive superconductor attached to a FI layer with multiple domains and a general Lagrangian from which one can derive the Usadel equation. We identify conserved quantities within each domain. In Sec. III we use these integrals of motion to derive an analytical expression for the DOS of a FI/S system with two collinear domains of arbitrary magnitude. In Sec. IV we generalized these results to the case of noncollinear magnetization. Finally, in Sec. V we study the properties and spatial evolution of the triplet correlations, and we suggest a way to detect them. We summarize the results in Sec. VI.

## II. THE MODEL

We consider a FI/S bilayer structure; see Fig. 1. A diffusive superconducting film is placed on top of a FI film. A typical example is Eu/Al studied in several papers [2,4,5,7,24]. In these systems the EuS film is polycrystalline, and magnetic domains with sharp boundaries are very common, particularly before the first magnetization of the EuS [4].

To describe the system, we use the quasiclassical Green's function (GF) formalism extended to treat spin-dependent fields [35]. In this case, the GF  $\check{g}$  is a  $4 \times 4$  matrix in Nambu-spin space. In the diffusive limit, it does not depend on momentum and is determined by the Usadel equation [39]. The interfacial exchange field is introduced as an effective boundary condition at the FI/S interface [38,40,41]. Assuming that the thickness of the S layer is smaller than the coherence length, one can integrate the Usadel equation over the thickness to reduce the dimension of the problem. The resulting Usadel equation for the retarded GF reads

$$D\nabla \cdot (\check{g}\nabla\check{g}) + [i\varepsilon\tau_3 - i\mathbf{h} \cdot \boldsymbol{\sigma}\tau_3 - \check{\Delta}, \check{g}] = 0, \quad (1)$$

where  $\nabla = (\partial_x, \partial_y)$ ,  $D$  is the diffusion constant,  $\varepsilon$  is the energy,  $\mathbf{h}$  is the effective exchange field stemming from the interface, and  $\check{\Delta} = \Delta\tau_1$  is the order parameter. The exchange field is only finite at the FI/S interface, and we approximate it as  $|\mathbf{h}_{\text{int}}| = h_{\text{int}}a\delta(z)$ , where  $h_{\text{int}}(x, y)$  is the exchange field at the interface, and  $a$  is the thickness of an effective layer over which the exchange interaction is finite [38,42]. After integration over the  $z$  direction, the effective exchange field is given by  $h = h_{\text{int}}a/d$  [5]. It is worth noting that the critical temperature of the S layer decreases with decreasing thickness, such that at low temperatures superconductivity can be fully suppressed when  $h > \Delta/\sqrt{2}$  [43,44]. In this work, we consider values of the exchange field that are weak enough such that superconducting ordering and the exchange field coexist. The matrices  $\sigma_i$  ( $\tau_i$ ),  $i = 1, 2, 3$ , in Eq. (1) are the Pauli matrices in the spin (Nambu) space. The general structure of  $\check{g}$  is

$$\check{g} = \hat{g}\tau_3 + \hat{f}\tau_1, \quad (2)$$

where  $\hat{g}$  and  $\hat{f}$  are the normal and anomalous GF in spin-space.

The GF satisfies the normalization condition  $\check{g}^2 = 1$ , and it can be parametrized with the help of the generalized  $\theta$ -parametrization [45],

$$\check{g} = (\cos\theta V_0 - \sin\theta \mathbf{V} \cdot \boldsymbol{\sigma})\tau_3 + (\sin\theta V_0 + \cos\theta \mathbf{V} \cdot \boldsymbol{\sigma})\tau_1, \quad (3)$$

which is described by two scalars  $\theta$  and  $V_0$  and the vector  $\mathbf{V}$ .  $V_0$  and  $\mathbf{V}$  satisfy the condition

$$V_0^2 + \mathbf{V}^2 = 1. \quad (4)$$

$V_0$  and  $\mathbf{V}$  describe the singlet and triplet correlations, respectively. If  $\mathbf{h}$  is homogeneous, then  $\mathbf{V}$  is parallel to it, but in general, as we show on Sec. V,  $\mathbf{V}$  is not parallel to the local exchange field.

In the above parametrization, the Usadel equation reduces to the following set of equations:

$$D\nabla^2\theta + 2i\varepsilon\sin\theta V_0 - 2i\cos\theta\mathbf{h} \cdot \mathbf{V} + 2\Delta\cos\theta V_0 = 0, \quad (5a)$$

$$D(V_0\nabla^2\mathbf{V} - \mathbf{V}\nabla^2V_0) + 2i\varepsilon\cos\theta\mathbf{V} - 2i\sin\theta\mathbf{h}V_0 - 2\Delta\sin\theta\mathbf{V} = 0. \quad (5b)$$

It is useful for finding analytical solutions to write a Lagrangian that leads to Eqs. (5) as the Euler-Lagrange equations:

$$\mathcal{L} = \frac{D}{2} \sum_{\mu} (\nabla V_{\mu})^2 + \frac{D}{2} (\nabla\theta)^2 + 2i\varepsilon\cos\theta V_0 + 2i\sin\theta\mathbf{h} \cdot \mathbf{V} - 2\Delta\sin\theta V_0, \quad (6)$$

with  $\mu = 0, 1, 2, 3$ . This Lagrangian coincides with the form of the nonlinear  $\sigma$ -model from which the Usadel equation can also be derived [46,47].

The above equations are valid for arbitrary magnetic textures. In the following, we focus on the situation of two semi-infinite magnetic domains with constant magnetization. The domains are separated by a sharp domain wall at  $x = 0$  with a length much smaller than the superconducting coherence length. We assume that one of the domains ( $x < 0$ ) is polarized along the  $y$  axis, whereas the magnetization of the

other domain ( $x > 0$ ) forms an angle  $\alpha$  with the  $y$  axis; see Fig. 1. At distances much larger than the coherence length, the GF takes its bulk form. The system has translational symmetry along the  $y$  and  $z$  directions, so the parameters only depend on the  $x$  coordinate.

On each domain, the Lagrangian (6) does not depend explicitly on the position  $\mathbf{r}$ , so the corresponding Hamiltonian is an integral of motion in each domain. The conserved quantity is namely given by

$$\mathcal{E} = \frac{D}{2} \sum_{\mu} (\nabla V_{\mu})^2 + \frac{D}{2} (\nabla \theta)^2 - 2i\varepsilon \cos \theta V_0 - 2i \sin \theta \mathbf{h} \cdot \mathbf{V} + 2\Delta \sin \theta V_0. \quad (7)$$

The values of  $\mathcal{E}$  far away from the domain wall, where the GF is given by the bulk solution and therefore is constant in space, can be easily obtained:

$$\mathcal{E} = -2i\varepsilon \cos \bar{\theta} \bar{V}_0 - 2i \sin \bar{\theta} \mathbf{h} \cdot \bar{\mathbf{V}} + 2\Delta \sin \bar{\theta} \bar{V}_0, \quad (8)$$

where the bulk values  $\bar{\theta}$  and  $\bar{\mathbf{V}}$  of the GF are given by the inverse relations of Eq. (2),

$$\tan \theta = \frac{f_0}{g_0}, \quad (9a)$$

$$\mathbf{V} = -\frac{\mathbf{g}}{\sin \theta}, \quad (9b)$$

$$V_0 = \frac{g_0}{\cos \theta}, \quad (9c)$$

and the bulk GF is given by

$$\hat{g} = \frac{-i(\varepsilon - \mathbf{h} \cdot \boldsymbol{\sigma})}{\sqrt{\Delta^2 - (\varepsilon - \mathbf{h} \cdot \boldsymbol{\sigma})^2}}, \quad (10a)$$

$$\hat{f} = \frac{\Delta}{\sqrt{\Delta^2 - (\varepsilon - \mathbf{h} \cdot \boldsymbol{\sigma})^2}}, \quad (10b)$$

with  $\hat{g} = g_0 + \mathbf{g} \cdot \boldsymbol{\sigma}$ ,  $\hat{f} = f_0 + \mathbf{f} \cdot \boldsymbol{\sigma}$ . In the following section, we use these expressions to define integrals of motion that allow for an analytical solution when the magnetic domains are collinear.

### III. DOMAINS WITH COLLINEAR MAGNETIZATION

If the magnetization of the two domains is collinear, the problem can be greatly simplified. First, only the component of the vector  $\mathbf{V}$  parallel to the magnetization is nonzero. Without any loss of generality, we assume that the magnetizations

lie in the  $z$  axis, such that  $V_1 = V_2 = 0$ . In this case, Eq. (5) reads

$$D\theta'' + 2i\varepsilon \sin \theta \cos \theta_3 - 2ih \cos \theta \sin \theta_3 + 2\Delta \cos \theta \cos \theta_3 = 0, \quad (11a)$$

$$D\theta_3'' + 2i\varepsilon \cos \theta \sin \theta_3 - 2ih \sin \theta \cos \theta_3 - 2\Delta \sin \theta \sin \theta_3 = 0, \quad (11b)$$

where  $V_3 = \sin \theta_3$ . One can combine these equations to obtain two decoupled equations for each spin component:

$$D\theta_{\pm}'' + 2i\varepsilon \sin \theta_{\pm} \mp 2ih \sin \theta_{\pm} + 2\Delta \cos \theta_{\pm} = 0, \quad (12)$$

where  $\theta_{\pm} = \theta \pm \theta_3$ , respectively, describe the spin-up and -down components of the GF.

Since the problem is decoupled in spin space, one can derive equations in (12) from two independent Lagrangians:

$$\mathcal{L}_{\pm} = \frac{D}{2} \theta_{\pm}'^2 + 2i\varepsilon \cos \theta_{\pm} \mp 2ih \cos \theta_{\pm} - 2\Delta \sin \theta_{\pm}. \quad (13)$$

Because  $\mathcal{L}_{\pm}$  do not depend explicitly on  $x$ , the following quantities are conserved in space:

$$\mathcal{E}_{\pm} = \frac{D}{2} \theta_{\pm}'^2 - 2i\varepsilon \cos \theta_{\pm} \pm 2ih \cos \theta_{\pm} + 2\Delta \sin \theta_{\pm}. \quad (14)$$

These expressions can be evaluated at the bulk where the spatial derivative vanishes and the GF is given by the bulk solution [see Eq. (10)].  $\cos \theta_{\pm}$  and  $\sin \theta_{\pm}$  are given by the spin components  $\hat{g}$  and  $\hat{f}$ , respectively, where the  $\pm$  sign corresponds to the up/down spin index,

$$\mathcal{E}_{\pm} = 2\sqrt{\Delta^2 - (\varepsilon \mp h)^2} = \frac{2\Delta}{\sin \bar{\theta}_{\pm}}. \quad (15)$$

Here  $\bar{\theta}_{\pm}$  are the values of  $\theta_{\pm}$  at the bulk. In the following, we omit the spin subscript to simplify the notation. Substituting Eq. (14) into (15) and applying trigonometric identities, we arrive at

$$\sin \bar{\theta} \frac{D}{8\Delta} \theta'^2 = \sin^2 \frac{\theta - \bar{\theta}}{2}. \quad (16)$$

Equation (16) does not explicitly contain the independent variable  $x$ . Taking the square root on both sides of the equation, we obtain a first-order differential equation that can be integrated to obtain

$$\tan \frac{\theta - \bar{\theta}_{l/r}}{4} = \begin{cases} c_l e^{x/\lambda_l}, & x \leq 0, \\ c_r e^{-x/\lambda_r}, & x \geq 0, \end{cases} \quad (17)$$

where  $\lambda_{\pm, l/r}^2 = D/[2\sqrt{\Delta^2 - (\varepsilon \mp h_{l/r})^2}]$  is chosen such that  $\text{Re}\{\lambda_{l/r}\} > 0$ , and that the exponential functions decay away from the domain wall.  $h_{l/r}$  is the value of the exchange field in the left ( $x < 0$ ) and right ( $x > 0$ ) domains.

From Eq. (17) one can obtain the spatial dependence of  $\theta(x)$  by determining the constants  $c_{l,r}$ . For this we use the fact that the GF and its derivative are continuous at the domain wall. Applying this condition, we obtain the values of the constants in Eq. (17),

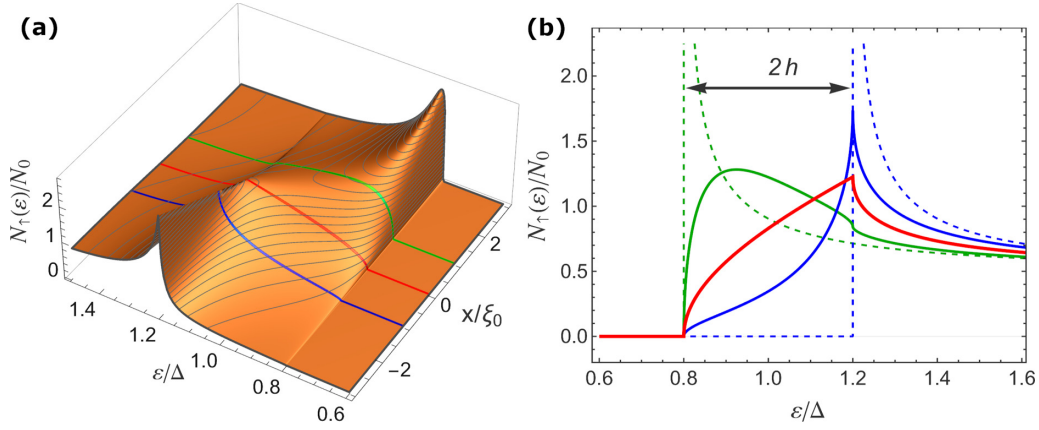


FIG. 2. Local DOS (for spin-up) of the superconductor film for domains with opposite magnetization strength and effective exchange field  $h = 0.2\Delta$ . The line traces of the right panel are taken at  $x = -\xi_0$  (blue),  $x = 0$  (red), and  $x = \xi_0$  (green). The dashed lines show the BCS spin-splitting of the DOS deep inside of the domains  $x \rightarrow -\infty$  (blue) and  $x \rightarrow \infty$  (green).

$$c_{l/r} = \mp \frac{\frac{\lambda_{l/r}}{\lambda_{r/l}} (1 - \tan^2 \frac{\Delta\theta}{4}) + 1 + \tan^2 \frac{\Delta\theta}{4} - \sqrt{\left[\frac{\lambda_{l/r}}{\lambda_{r/l}} (1 - \tan^2 \frac{\Delta\theta}{4}) + 1 + \tan^2 \frac{\Delta\theta}{4}\right]^2 + \frac{4\lambda_{l/r}^2}{\lambda_{r/l}^2} \tan^2 \frac{\Delta\theta}{4}}}{2 \frac{\lambda_{l/r}}{\lambda_{r/l}} \tan \frac{\Delta\theta}{4}}, \quad (18)$$

where  $\Delta\theta = \theta_r - \theta_l$ , and the upper and lower signs correspond to the left and right domains, respectively. The sign of the square root on Eq. (18) is chosen such that the DOS is positive and the solution is physically meaningful. Setting the order parameter to zero in the right domain and the exchange fields to zero, we recover the results by Altland *et al.* [48] for a singlet S/N junction. Golubov *et al.* [49] also followed a similar procedure to study the DOS at ferromagnetic and normal layers on S(FN) and S(FF) structures.

Equation (17) together with Eq. (18) determine the analytical solution for the two semi-infinite collinear domains. The local DOS is related to the GF through the expression

$$\begin{aligned} \frac{N(\varepsilon)}{N_0} &= \frac{1}{2} \text{Re}\{\text{Tr} \hat{g}(\varepsilon)\} \\ &= \frac{1}{2} \text{Re}\{\cos \theta_+ + \cos \theta_-\}. \end{aligned} \quad (19)$$

As a first example, we assume that the magnetizations of the two domains are opposite in direction but equal in amplitude ( $h_l = -h_r = h$ ). In this case, the DOS at the domain wall ( $x = 0$ ) has a simple form

$$\frac{N(\varepsilon)}{N_0} = \text{Re} \left\{ \frac{\sqrt{\Delta^2 - (\varepsilon - h)^2} - \sqrt{\Delta^2 - (\varepsilon + h)^2}}{2ih} \right\}, \quad (20)$$

which leads to the red curves in Fig. 2. This analytical result coincides with the numerical result obtained in Refs. [4,32] for a narrow domain wall between two collinear domains. In Fig. 2, we show the spatial dependence of the DOS for spin-up electrons in the antiparallel magnetization configuration. Far from the domain wall, the coherent peaks of the DOS are well-defined (dashed lines). The presence of the domain wall smears the peak. In Fig. 3(a) we show the spatial dependence of the full DOS. Specifically, Fig. 3(b) shows the DOS at the values of  $x$  indicated by the colored lines in panel (a).

The magnitude of the exchange field is the same on both domains so the total DOS is symmetric with respect to  $x = 0$ . For large enough distances away from the domain wall, the BCS peak is shifted by the exchange field to  $\varepsilon = \Delta \pm h$ . Near the domain wall, there is a crossover between the position of the spin-up/spin-down peaks over a length scale of the order of the superconducting coherence length  $\xi_0 = \sqrt{D/\Delta}$ . Notice that around the domain wall, the inner peak is broader and lower than the outer peak [see Fig. 3(b)], but the gap edge remains, as expected, at  $\varepsilon < \Delta - h$ .

A second interesting example is when the exchange field is only finite in one of the regions ( $x < 0$ ). This corresponds to an S layer only partly covered by the the FI layer. In Fig. 3(c), we show the local DOS in this case. The spin-split DOS at  $x \ll -\xi_0$  evolves into the usual BCS DOS at  $x \gg \xi_0$ , over the length  $\xi_0$  around the domain wall. The splitting of the DOS peaks does not decrease smoothly, as one would expect in a system in which the exchange field is suppressed gradually over a length much larger than  $\xi_0$ . Namely, the inner peak is smeared in a similar way to the antiparallel magnetization case [Fig. 3(b)], such that the DOS has the same “shark-fin” shape right at  $x = 0$  [red curve in Fig. 3(d)]. All of the above predictions could be proven by performing local tunneling spectroscopy measurements.

#### IV. NONCOLLINEAR MAGNETIZATION

In the previous section, we focused on the collinear magnetization case in which it was possible to decouple the components of the Usadel equation. In that case, we can find conserved quantities, Eq. (15), and we obtain analytically expressions for the GF. If the magnetizations are noncollinear, the system lacks enough symmetries to reduce the number of coupled equations. Nonetheless, it is possible to solve the Usadel equation (5) analytically in the weak superconducting

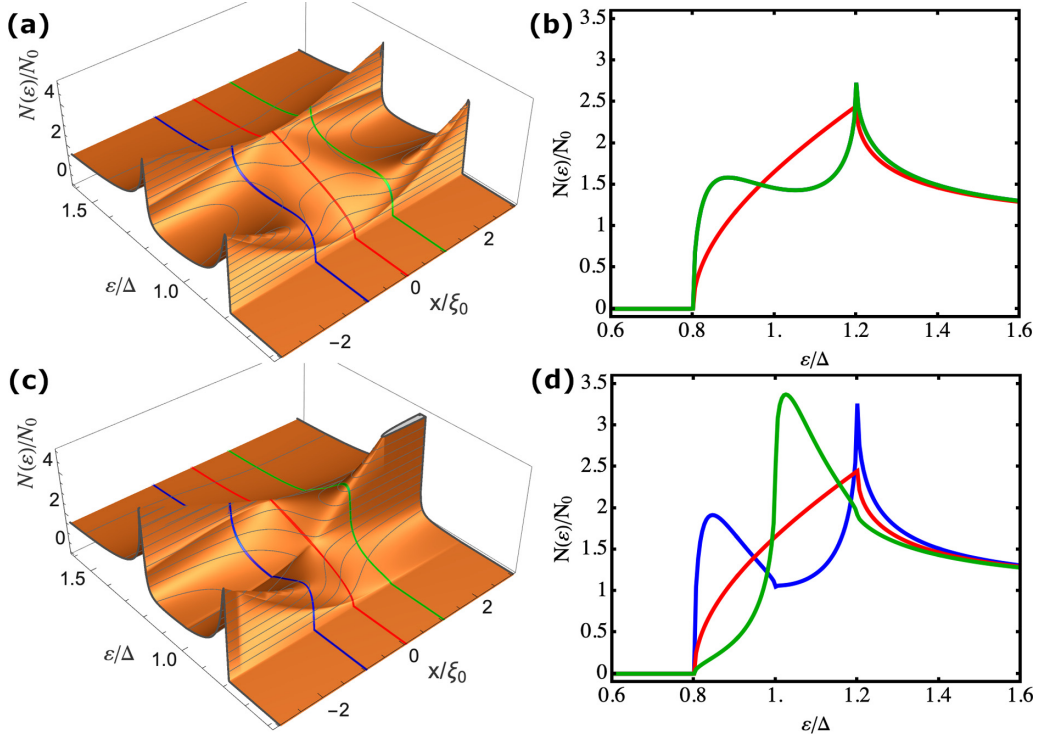


FIG. 3. Local DOS of the S layer for (a,b)  $h_l = 0.2\Delta$  and  $h_r = -0.2\Delta$ , and (c,d)  $h_l = 0.2\Delta$  and  $h_r = 0$ . The color lines in the right panels are taken at  $x = -\xi_0$  (blue),  $x = 0$  (red), and  $x = \xi_0$  (green).

or weak exchange field limits, as discussed in the next subsections. Later below, we study the two-domain situation for an arbitrarily large exchange field numerically [50].

### A. Weak superconductivity

If the superconductor is close to the critical temperature  $T_c$ , the Usadel equation (5) can be linearized for a small order parameter ( $\Delta \ll T, h$ ). This limit is very illustrative to understand the lengthscales involved in the system.

Near  $T_c$  the GF can be approximated by  $\hat{g} = \tau_3 + \hat{f}\tau_1$ . The linearized Usadel equation determines the anomalous GF  $\hat{f}$ ,

$$\frac{D}{2}f_0'' + i\varepsilon f_0 - i\mathbf{h} \cdot \mathbf{f} + \Delta = 0, \quad (21a)$$

$$\frac{D}{2}\mathbf{f}'' + i\varepsilon\mathbf{f} - i\mathbf{h}f_0 = 0, \quad (21b)$$

where the spin structure is

$$\hat{f} = f_0 + \sum_{j=1,3} f_j \sigma_j, \quad (22)$$

where  $f_0$  is the singlet, and  $f_j$ ,  $j = 1, 2, 3$ , are the triplet components. For the two semi-infinite domain structures considered in this work, the solution to Eq. (21) is given by

$$f_0 = \bar{f}_0 + c_+ e^{-q_+|x|} + c_- e^{-q_-|x|}, \quad (23a)$$

$$\mathbf{f} = \bar{\mathbf{f}} + i\mathbf{h} \sum_{j=\pm} \frac{c_j}{q_j^2 D/2 + i\varepsilon} e^{-q_j|x|} + \mathbf{d} e^{-q|x|}, \quad (23b)$$

where  $\bar{f}_0$  and  $\bar{\mathbf{f}}$  are the asymptotic values at  $x = \pm\infty$  of the singlet and triplet components, respectively, and  $q_{\pm}^2 = -2i(\varepsilon \mp h)/D$ ,  $q^2 = -2i\varepsilon/D$ . The triplet can be written as

the sum of the component parallel to the local exchange field [second term in Eq. (23b)], and the component orthogonal to it proportional to the vector  $\mathbf{d}$ , with  $\mathbf{h} \cdot \mathbf{d} = \mathbf{0}$ . The component perpendicular to the local exchange field decays away from the domain wall over the length  $\xi_\varepsilon = \text{Re}\{q\}^{-1}$ , whereas the correction to the bulk (parallel) solution is significant at distances less than  $\xi_h = \text{Re}\{q_+\}^{-1} = \text{Re}\{q_-\}^{-1}$ .

### B. Weak exchange field

Another analytical limiting case is the case of a weak exchange field ( $|\mathbf{h}| \ll \Delta$ ). In this case, one can linearize the Usadel equation (5) and solve the system for an arbitrary magnetization texture. In zeroth order in  $\mathbf{h}$ , only the singlet component of the GF is finite and it is given by Eqs. (9) and (10) setting  $\mathbf{h} = \mathbf{0}$ ,

$$\tan \theta = \frac{\Delta}{-i\varepsilon}, \quad (24a)$$

$$V_0 = 1. \quad (24b)$$

To first order in  $\mathbf{h}$ , both  $\theta$  and  $V_0$  are not corrected, whereas the triplet vector  $\mathbf{V}$  is determined by

$$\mathbf{V}'' - \lambda^{-2}\mathbf{V} = \frac{2i\Delta}{D\sqrt{\Delta^2 - \varepsilon^2}}\mathbf{h}(x'), \quad (25)$$

where  $\lambda^2 = D/(2\sqrt{\Delta^2 - \varepsilon^2})$  ( $\text{Re}\{\lambda\} > 0$ ) is the energy-dependent coherence length. The solution of this equation can be written as

$$\mathbf{V} = \int dx' G(x, x') \frac{2i\Delta}{D\sqrt{\Delta^2 - \varepsilon^2}}\mathbf{h}, \quad (26)$$

where  $G(x, x')$  is the Green's function of the differential equation (25) determined by

$$(\partial_x^2 - \lambda^{-2})G(x, x') = \delta(x - x'). \quad (27)$$

Solving Eq. (27), we arrive at

$$\mathbf{V}(x) = \frac{-i\Delta}{\sqrt{2D}(\Delta^2 - \varepsilon^2)^{3/4}} \int dx' e^{-|x-x'|/\lambda} \mathbf{h}(x'). \quad (28)$$

This result shows explicitly the spatial dependence of the triplet vector. It is determined by the exchange field averaged over the length  $\lambda$ . For example, if the spatial variation of the exchange field  $\mathbf{h}(x)$  is slower than the length  $\lambda$ , then the vector  $\mathbf{V}$  is locally parallel to the exchange field. In particular, in the case of two magnetic domains separated by a smooth (with respect to the length  $\lambda$ ) domain wall, the vector  $\mathbf{V}$  is always aligned with the local field  $\mathbf{h}$ .

In this work, we are mainly interested in sharp domain walls, i.e., domain walls with sizes much smaller than  $\lambda$ . If we model such a situation by a steplike exchange field with  $\mathbf{h} = \mathbf{h}_l\theta(-x) + \mathbf{h}_r\theta(x)$ , then the triplet vector at the left and right sides of the domain wall can be obtained from Eq. (28):

$$\mathbf{V}_{l/r} = \frac{-i\Delta}{2(\Delta^2 - \varepsilon^2)} [2\mathbf{h}_{l/r} + (\mathbf{h}_{r/l} - \mathbf{h}_{l/r})e^{-|x|/\lambda}]. \quad (29)$$

As expected, at distances much larger than  $\lambda$  from the domain wall,  $\mathbf{V}$  is parallel to the local exchange field. In contrast, the transverse component to the field is maximized at the domain wall and decays over  $\lambda$  away from it. The above analytical results are obtained for weak exchange fields. In the next section, we consider an arbitrarily strong exchange field.

### C. Arbitrary exchange field

In this section, we consider two domains with an arbitrarily large exchange field and an arbitrary angle between the domain magnetizations, and we solve numerically the Usadel equation. For this it is convenient to differentiate twice Eq. (4) and substitute the result into Eq. (5). We thus arrive at [32,51]

$$D\theta'' + 2i\varepsilon \sin\theta V_0 - 2i \cos\theta \mathbf{h} \cdot \mathbf{V} + 2\Delta \cos\theta V_0 = 0, \quad (30a)$$

$$DV'' + DV(V_0'^2 + \mathbf{V}'^2) + 2i \sin\theta((\mathbf{h} \cdot \mathbf{V})\mathbf{V} - \mathbf{h}) - 2(-i\varepsilon \cos\theta + \Delta \sin\theta)V_0\mathbf{V} = 0, \quad (30b)$$

$$DV_0'' + DV_0(V_0'^2 + \mathbf{V}'^2) + 2i \sin\theta \mathbf{h} \cdot \mathbf{V}V_0 + 2(-i\varepsilon \cos\theta + \Delta \sin\theta)(1 - V_0^2) = 0. \quad (30c)$$

We solve the above equations numerically for an S layer of finite length  $L$ . The domain wall is located at  $x = 0$ . The spectral current vanishes at the boundaries with vacuum. In the generalized  $\theta$ -parametrization, this translates into the following boundary conditions for Eq. (30):

$$\theta'|_{x=\pm L/2} = 0, \quad (31a)$$

$$\mathbf{V}'|_{x=\pm L/2} = 0, \quad (31b)$$

$$V_0'|_{x=\pm L/2} = 0. \quad (31c)$$

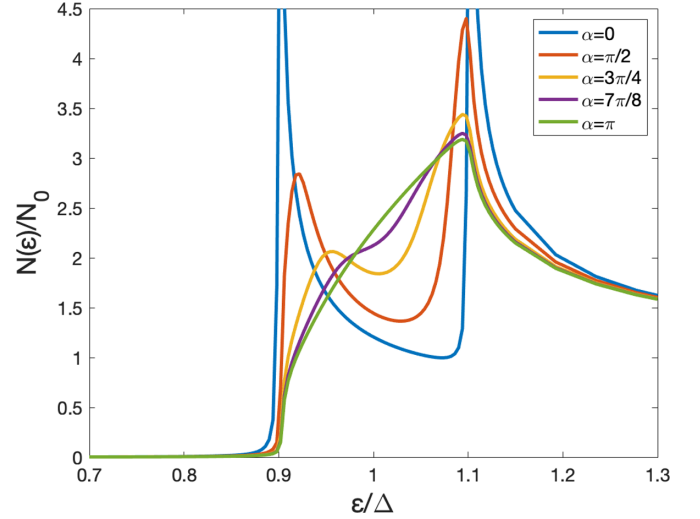


FIG. 4. Density of states at the domain wall for different values of the angle  $\alpha$  between the domains' magnetizations.

In Fig. 4 we show the computed total DOS at the domain wall for domains with the same exchange field magnitude  $h = 0.1\Delta$  and different orientations (see Fig. 1). In the  $\alpha = 0$  case, the exchange field is uniform along the sample, so the DOS is the homogeneous spin-split BCS. Both peaks are broadened and lowered by increasing  $\alpha$ , and the DOS exhibits the “shark-fin” when the magnetizations are antiparallel. The spin-splitting is still visible up to values of  $\alpha \approx 7\pi/8$ .

### V. TRIPLET PAIR CORRELATIONS IN FI/S STRUCTURES AND THEIR DETECTION

In the previous sections, we analyzed the quasiparticle spectrum. Here we focus on another aspect of the FI/S structures: the superconducting triplet pair-correlations. These appear due to the finite interfacial exchange field that converts a conventional singlet into triplet pairs [35,52].

Within our model, pair correlations are described by the anomalous component  $\hat{f}$  introduced in Eq. (2), which in the spin-space has the general structure given by Eq. (22). Because we consider the strict diffusive limit, all components of  $\hat{f}$  are isotropic in momentum ( $s$ -wave symmetry). From the Fermi statistics for fermion pairs, it follows that  $f_0$  is an even function of frequency whereas  $f_j$  are odd [35,53–55]. The following association between the different components of the condensate and the spin state of electron pairs can be made [56]:

$$(\uparrow\downarrow - \downarrow\uparrow) \leftrightarrow 2f_0, \quad (32)$$

$$-(\uparrow\uparrow - \downarrow\downarrow) \leftrightarrow 2f_1, \quad (33)$$

$$(\uparrow\uparrow + \downarrow\downarrow) \leftrightarrow 2if_2, \quad (34)$$

$$(\uparrow\downarrow + \downarrow\uparrow) \leftrightarrow 2f_3. \quad (35)$$

In other words, each triplet component of the condensate is associated with maximally entangled states. In a conventional BCS superconductor, only the singlet component  $f_0$  is finite. Triplet components are finite in the presence of an exchange

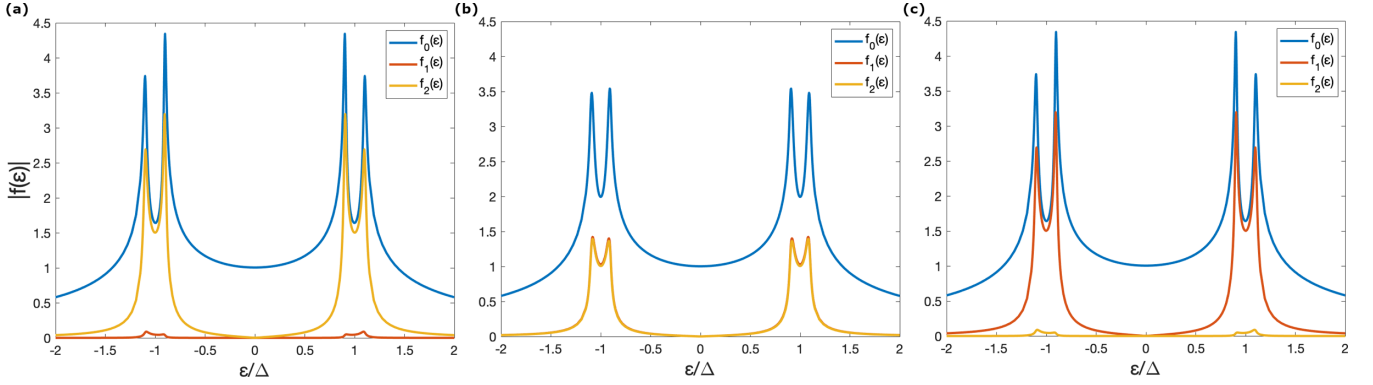


FIG. 5. The spectral weight of the singlet and triplet components of  $\hat{f}$  at different points in the superconductor: (a)  $x = -5\xi_0$ , (b)  $x = 0$ , and (c)  $x = 5\xi_0$ . We have chosen  $\alpha = \pi/2$ ,  $L = 10\xi_0$ , and  $h_{l/r} = 0.1\Delta$ .

field. In a homogeneous case, we choose the spin quantization axis along the magnetization direction, e.g., the  $z$  axis. The only finite components of the condensates are, in this case,  $f_0$  and  $f_3$ . All triplet components may appear in a multidomain situation with arbitrary magnetization directions.

Here we study the singlet and triplet correlations in a FI/S bilayer with two noncollinear domains; see Fig. 1. We assume that  $\alpha = \pi/2$  such that two components  $f_1, f_2$  are finite. The length of S is  $L = 10\xi_0$ . In Fig. 5 we show the spatial dependence of the singlet and triplet components of  $\hat{f}$  for all energies, calculated numerically. All condensate components show peaks at  $|\varepsilon| = \Delta \pm h$  and decay to zero at energies much larger than the gap. Inside the gap, the amplitude of the singlet is of the order of 1. In contrast, at  $\varepsilon = 0$  the triplet components are of the order of  $\Gamma/\Delta$ , where  $\Gamma$  is the Dynes parameter [57] describing inelastic scattering. They increase linearly at small energies and become comparable to the singlet component within the range  $|\varepsilon| \in [\Delta - h, \Delta + h]$ . Far away from the domain wall, only the triplet component parallel to the local exchange field is finite. Both components,  $f_1$  and  $f_2$ ,

have the same magnitude at the domain wall, as anticipated from our analytical result, Eq. (28). In Fig. 6(a), we show the spatial dependence of the triplet correlations at  $\varepsilon = \Delta - h$ . The length over which the triplet components change is of the order of the coherence length.

A natural question is how to detect the triplet components in this type of system. This can be achieved, for example, through spin-polarized spectroscopy [58]. Another way to detect the triplet components is to place a ferromagnetic layer (F) on top of a superconductor. The DOS of the F layer is modified by the superconducting correlations induced via the proximity effect. Such a modification can be measured by a normal tunneling probe. In the case of a weak proximity effect, we can linearize the Usadel equation in the F region. The DOS in the ferromagnet is then given by (see the Appendix for details)

$$\frac{N(\varepsilon, x, z)}{N_0} = 1 - \frac{1}{4} \text{Re}\{\text{Tr} \hat{f}^2(\varepsilon, x, z)\}. \quad (36)$$

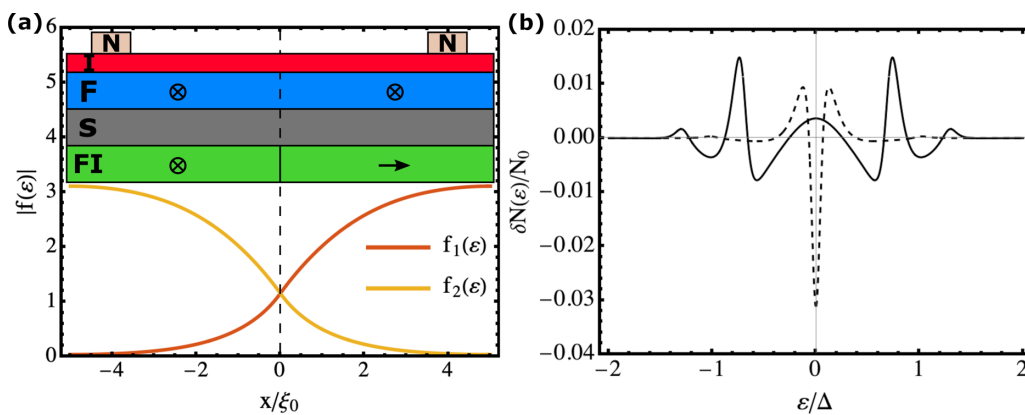


FIG. 6. (a) Spatial dependence of triplet correlations for energy  $\varepsilon = \Delta - h$ . We show the proposed geometry to detect the triplet correlations in the inset. An F layer is placed on top of an S layer; if the F layer is thick enough, only the triplet correlations perpendicular to the magnetization of the F layer will propagate along the ferromagnet. The long-range triplet correlations manifest as a zero-energy peak on the local DOS, measured through tunnel differential conductance measurements with a normal metal probe (N). (b) The correction to the DOS of the ferromagnet at the F/I interface, see panel (a), far to the right of the domain wall (solid line). The deviation from the normal DOS is due to the penetration of the long-range component of the triplet condensate. For comparison, we show the DOS of an N layer in contact with a conventional singlet superconductor (dashed line). At zero energy, the singlet (triplet) component induced in the N (F) layer is real (purely imaginary), resulting in a negative (positive) correction to the DOS. The parameters used in the plot are  $h = 0.3\Delta$ ,  $\gamma = 5\xi_0$ , and  $t = 3\xi_0$ . The DOS of the F case is normalized by  $(\Delta/\Gamma)^2$  for comparison.

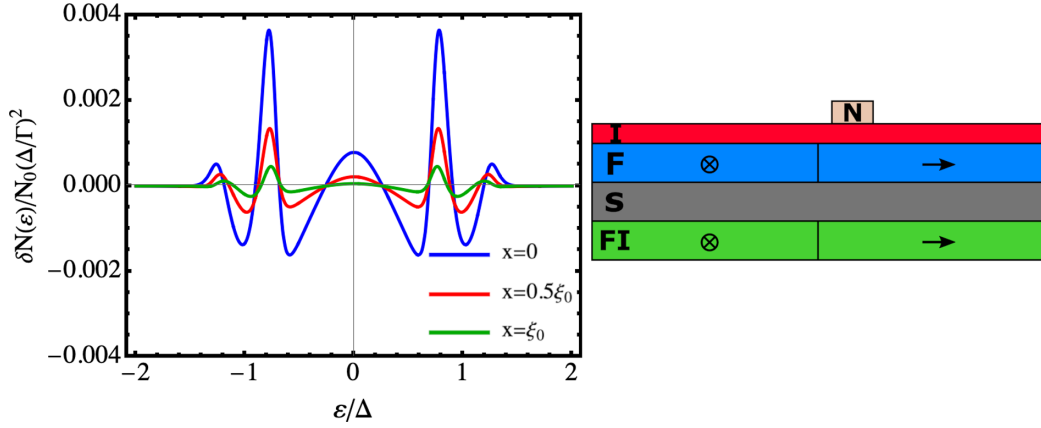


FIG. 7. Correction to the DOS of the ferromagnet at the F/I interface at different distances from the domain wall. In this setup, the ferromagnet magnetization is aligned with respect to the magnetization of the FI. The parameters used are  $h = 0.3\Delta$ ,  $\gamma = 5\xi_0$ , and  $t = 3\xi_0$ .

The second term is the correction to the DOS due to the proximity effect. Because of the trace over spin, this term has two contributions: one proportional to the square of the singlet component, and one to the sum of the squares of the triplet components. The singlet component is real at low energies, so its correction to the DOS is negative. This explains that if S is a singlet superconductor and F is a normal layer (no exchange and hence no triplet), the DOS is suppressed at  $\epsilon = 0$ ; see the dashed line in Fig. 6(b). On the other hand, in the presence of an exchange field, the triplet component at  $\epsilon = 0$  is purely imaginary [see Eq. (A3)] and hence its contribution to the DOS, according to Eq. (36), is positive. Thus, the sign of the correction of the DOS at  $\epsilon = 0$  is determined by the competition between singlet and triplet amplitudes [59].

To separate the triplet from the singlet component, we propose a setup like the one sketched in Fig. 6. Due to the presence of the FI, triplet pairs are induced in the superconductor, as described above. To filter out the singlet correlations, an F layer with a magnetization noncollinear to the FI is placed; see the inset of Fig. 6(a). The singlet component and triplet parallel to the F magnetization (short-range triplet) decay over the magnetic length  $\sim \kappa_F^{-1}$ . In contrast, the triplet component orthogonal to the magnetization of F (long-range triplet) decays over the length  $\sim \kappa_\epsilon^{-1}$  (see Appendix). Thus, by choosing the thickness  $t$  of the F layer such that  $\kappa_F^{-1} \ll t \ll \kappa_\epsilon^{-1}$ , the DOS of F at the tunneling barrier will only be corrected by the long-range triplet component. This situation can be realized by using F layers with a strong exchange field, such as Co or Fe.

In Appendix, we compute the correction to the density of states in the ferromagnet. In the two-domain situation studied above, when the F layer is placed above the right domain far from the domain wall [see Fig. 6(a)], the triplet component in F at zero energy is purely imaginary [Eq. (A3)], so according to Eq. (A4) there is a positive correction to the DOS,

$$\frac{N(0, \infty, t)}{N_0} = 1 + \frac{\varepsilon_b^2 h^2 \Delta^2}{2(\Delta^2 - h^2)^3}, \quad (37)$$

where  $\varepsilon_b = D/(2\gamma t)$  is an energy scale related to the interface transparency, and  $\gamma$  is a parameter describing the interface resistance. The solid line in Fig. 6(b) shows the DOS of the F layer at the tunneling barrier computed for all energies.

One sees a local maximum at  $\epsilon = 0$ , and also maxima at  $|\epsilon| = \Delta \pm h$  related to the triplet peaks shown in Fig. 5. In this way, the existence of triplets generated in the spin-split superconductor can be demonstrated by performing tunneling spectroscopy, with the normal electrode probe; see Fig. 6(a).

Finally, we consider an F layer consisting of two domains that are collinear to the adjacent FI domains (see Fig. 7). This situation may correspond to the case in which the magnetic coupling of the F and FI leads to local collinear magnetizations. According to our previous analysis, triplet correlations of both kinds are present in the S near the domain wall. In other words, long-range triplet correlations will be present in certain positions of the F/I interface and affect the local DOS. In Fig. 7, we show the correction to the DOS at different points of the F/I interface. The zero-energy peak appears at regions close to the domain wall. The peak vanishes when moving away from the domain wall. Such measurements could be done with the help of the STM technique and may reveal the magnetic texture of the system. Another possible setup to isolate the odd-frequency correlations at zero energy are S/N bilayers with a spin-active interface [60,61].

## VI. CONCLUSION

In this work, we have studied the spectral properties of superconductor-ferromagnetic insulator bilayers in the presence of a domain wall separating two magnetic domains. In the first part, we focus on the quasiparticle spectrum, and we analyze how the density of states of the superconductor is affected by the magnetic configuration. In the case of two semi-infinite domains with collinear magnetization and a sharp domain wall between them, it is possible to find two integrals of motion that allow for an analytical solution of the Usadel equation. With the help of this solution, we determine the local DOS of the superconductor for different magnitudes of the exchange field. At the domain wall, the DOS exhibits a “shark-fin” shape. This feature appears when the domain magnetizations are antiparallel or when one of the domains has a negligible small exchange field. We have also studied FI layers with noncollinear magnetization direction. We show that near the domain wall, the spin-splitting is quite robust with respect to the relative angle  $\alpha$  between the magnetiza-

tions, but the heights of the coherent peaks are significantly affected by it. All these predictions can be verified by local tunnel spectroscopy experiments, which will reveal information about the local magnetic configuration of the FI.

In the second part, we have analyzed the spectral properties of the singlet and triplet components of the superconducting condensate in the S layer. We have found an analytical expression for the quasiclassical Green's function in the presence of an arbitrary magnetic texture in the FI in the case of a weak exchange field. Our expression reveals how the local exchange field spatially determines the triplet components induced in the superconductor. For arbitrary strength of the exchange interaction, we have determined the singlet and triplet components numerically in the presence of a sharp domain wall. We propose different ways of detecting the triplet correlations using a FI/S/F junction, where F is a ferromagnetic metal and a tunneling probe at the outer F interface. The presence of the triplet component manifests itself as a zero bias maximum in the tunneling differential conductance. The proposed setup can then be used as a source of spin-triplet pairs, whose entanglement can be proven in experiments using quantum dots as pair splitters [62].

#### ACKNOWLEDGMENTS

We thank S. Ilić for useful discussions. This work was partially funded by the Spanish Ministerio de Ciencia, Innovación y Universidades (MICINN) through Project No. PID2020-114252GB-I00 (SPIRIT), and EU's Horizon 2020 research and innovation program under Grant Agreement No. 800923 (SUPERTED). A.H. acknowledges funding by the University of the Basque Country (Project No. PIF20/05).

#### APPENDIX: CORRECTION TO THE TUNNELING DIFFERENTIAL CONDUCTANCE IN THE FERROMAGNET

In this Appendix, we show how the tunneling differential conductance measured on top of the F layer [see Fig. 6(a)] is affected by the leakage of the superconducting condensate into the ferromagnet.

The GF on a diffusive ferromagnet satisfies the Usadel equation (1) with  $\Delta = 0$ . If the transmission coefficient of the S/F interface is very low, the proximity effect in the F layer is weak and the Usadel equation can be linearized as

$$\partial_{zz}^2 f_0 + i\kappa_\varepsilon^2 f_0 - i\kappa_F^2 f_2 = 0, \quad (\text{A1a})$$

$$\partial_{zz}^2 \mathbf{f} + i\kappa_\varepsilon^2 \mathbf{f} - i\kappa_F^2 f_0 \hat{\mathbf{y}} = 0, \quad (\text{A1b})$$

where  $\kappa_\varepsilon^2 = 2\varepsilon/D$ ,  $\kappa_F^2 = 2h_F/D$ , and  $h_F$  is the field of the ferromagnet. Here we have assumed that the magnetization direction of the F layer lies on the  $y$  axis.

The S/F interface is described by the linearized Kuprianov-Lukichev condition [63],

$$\gamma \partial_z f_0|_{z=0} = -f_{S,0}, \quad (\text{A2a})$$

$$\gamma \partial_z \mathbf{f}|_{z=0} = -\mathbf{f}_S. \quad (\text{A2b})$$

Here,  $\gamma = \sigma_F R_b$  is the parameter describing the barrier strength, where  $R_b$  is the normal-state tunneling resistance per unit area, and  $\sigma_F$  is the conductivity of the ferromagnet. The anomalous GF on the S layer is given by  $\hat{f}_S = f_{S,0} + \mathbf{f}_S \cdot \boldsymbol{\sigma}$ .

We assume that the thickness  $t$  of the F layer is much longer than the coherence length in the ferromagnetic layer  $\kappa_F t \gg 1$ . In the long-junction regime, the condensate function is mediated primarily by the long-range triplet superconducting correlations [35,64,65], whereas the singlet and short-range triplet correlations decay over the length  $\kappa_F^{-1}$ . At the outer interface of the F layer, the condensate function is given by the only long-range component  $f_1$ . Solving the Usadel equation (A1b), we obtain

$$f_1(\varepsilon, x, t) = \frac{f_{S,1}(\varepsilon, x)}{\frac{1-i}{\sqrt{2}} \kappa_\varepsilon \gamma \sinh\left(\frac{1-i}{\sqrt{2}} \kappa_\varepsilon t\right)}. \quad (\text{A3})$$

In the case of the weak proximity effect, the DOS of the ferromagnet is given by Eq. (36). Using Eq. (A3), we arrive at

$$\frac{N(\varepsilon, x, t)}{N_0} = 1 - \frac{1}{2} \text{Re} \left\{ \frac{i f_{S,1}(\varepsilon, x)^2}{\gamma^2 \kappa_\varepsilon^2 \sinh^2\left(\frac{1-i}{\sqrt{2}} \kappa_\varepsilon t\right)} \right\}, \quad (\text{A4})$$

where the anomalous GF of the superconductor  $f_{S,1}(\varepsilon, x)$  is obtained by solving Eqs. (30) and (31). If the S layer is a homogeneous superconductor with an exchange field along the  $x$  direction, the DOS is given by Eq. (37).

- 
- [1] J. S. Moodera, X. Hao, G. A. Gibson, and R. Meservey, *Phys. Rev. Lett.* **61**, 637 (1988).
- [2] X. Hao, J. S. Moodera, and R. Meservey, *Phys. Rev. B* **42**, 8235 (1990).
- [3] R. Meservey and P. Tedrow, *Phys. Rep.* **238**, 173 (1994).
- [4] E. Strambini, V. N. Golovach, G. De Simoni, J. S. Moodera, F. S. Bergeret, and F. Giazotto, *Phys. Rev. Materials* **1**, 054402 (2017).
- [5] A. Hijano, S. Ilić, M. Rouco, C. González-Orellana, M. Ilyn, C. Rogero, P. Virtanen, T. T. Heikkilä, S. Khorshidian, M. Spies, N. Ligato, F. Giazotto, E. Strambini, and F. S. Bergeret, *Phys. Rev. Research* **3**, 023131 (2021).
- [6] G.-X. Miao, J. Chang, B. A. Assaf, D. Heiman, and J. S. Moodera, *Nat. Commun.* **5**, 3682 (2014).
- [7] G. De Simoni, E. Strambini, J. S. Moodera, F. S. Bergeret, and F. Giazotto, *Nano Lett.* **18**, 6369 (2018).
- [8] K.-R. Jeon, J.-C. Jeon, X. Zhou, A. Migliorini, J. Yoon, and S. S. P. Parkin, *ACS Nano* **14**, 15874 (2020).
- [9] R. Ojajärvi, T. T. Heikkilä, P. Virtanen, and M. A. Silaev, *Phys. Rev. B* **103**, 224524 (2021).
- [10] M. Alidoust, K. Halterman, and J. Linder, *Phys. Rev. B* **88**, 075435 (2013).
- [11] E. Strambini, F. Bergeret, and F. Giazotto, *Europhys. Lett.* **112**, 17013 (2015).
- [12] F. Giazotto, T. T. Heikkilä, A. Luukanen, A. M. Savin, and J. P. Pekola, *Rev. Mod. Phys.* **78**, 217 (2006).
- [13] F. Giazotto, P. Solinas, A. Braggio, and F. S. Bergeret, *Phys. Rev. Applied* **4**, 044016 (2015).





- [14] F. Giazotto and F. Bergeret, *Appl. Phys. Lett.* **102**, 132603 (2013).
- [15] F. Giazotto, T. T. Heikkilä, and F. S. Bergeret, *Phys. Rev. Lett.* **114**, 067001 (2015).
- [16] F. Giazotto and F. Bergeret, *Appl. Phys. Lett.* **116**, 192601 (2020).
- [17] P. Machon, M. Eschrig, and W. Belzig, *Phys. Rev. Lett.* **110**, 047002 (2013).
- [18] A. Ozaeta, P. Virtanen, F. S. Bergeret, and T. T. Heikkilä, *Phys. Rev. Lett.* **112**, 057001 (2014).
- [19] T. T. Heikkilä, R. Ojajarvi, I. J. Maasilta, E. Strambini, F. Giazotto, and F. S. Bergeret, *Phys. Rev. Applied* **10**, 034053 (2018).
- [20] Z. Geng, A. P. Helenius, T. T. Heikkilä, and I. J. Maasilta, *J. Low Temp. Phys.* **199**, 585 (2020).
- [21] Y. Oreg, G. Refael, and F. von Oppen, *Phys. Rev. Lett.* **105**, 177002 (2010).
- [22] R. M. Lutchyn, J. D. Sau, and S. Das Sarma, *Phys. Rev. Lett.* **105**, 077001 (2010).
- [23] X.-F. Dai, X.-Q. Wang, T. Gong, L.-L. Zhang, and W. Gong, *J. Phys. E* **128**, 114585 (2021).
- [24] J. S. Moodera, T. S. Santos, and T. Nagahama, *J. Phys.: Condens. Matter* **19**, 165202 (2007).
- [25] T. Tokuyasu, J. A. Sauls, and D. Rainer, *Phys. Rev. B* **38**, 8823 (1988).
- [26] P. Virtanen, A. Vargunin, and M. Silaev, *Phys. Rev. B* **101**, 094507 (2020).
- [27] M. Rouco, S. Chakraborty, F. Aikebaier, V. N. Golovach, E. Strambini, J. S. Moodera, F. Giazotto, T. T. Heikkilä, and F. S. Bergeret, *Phys. Rev. B* **100**, 184501 (2019).
- [28] A. Y. Aladyshkin, A. I. Buzdin, A. A. Fraerman, A. S. Mel'nikov, D. A. Ryzhov, and A. V. Sokolov, *Phys. Rev. B* **68**, 184508 (2003).
- [29] M. Houzet and A. I. Buzdin, *Phys. Rev. B* **74**, 214507 (2006).
- [30] I. V. Bobkova and A. M. Bobkov, *JETP Lett.* **109**, 57 (2019).
- [31] D. S. Rabinovich, I. V. Bobkova, A. M. Bobkov, and M. A. Silaev, *Phys. Rev. B* **99**, 214501 (2019).
- [32] F. Aikebaier, P. Virtanen, and T. Heikkilä, *Phys. Rev. B* **99**, 104504 (2019).
- [33] Z. Yang, M. Lange, A. Volodin, R. Szymczak, and V. V. Moshchalkov, *Nat. Mater.* **3**, 793 (2004).
- [34] J. Linder and K. Halterman, *Phys. Rev. B* **90**, 104502 (2014).
- [35] F. S. Bergeret, A. F. Volkov, and K. B. Efetov, *Rev. Mod. Phys.* **77**, 1321 (2005).
- [36] A. Cottet, *Phys. Rev. Lett.* **107**, 177001 (2011).
- [37] F. S. Bergeret, M. Silaev, P. Virtanen, and T. T. Heikkilä, *Rev. Mod. Phys.* **90**, 041001 (2018).
- [38] T. T. Heikkilä, M. Silaev, P. Virtanen, and F. S. Bergeret, *Prog. Surf. Sci.* **94**, 100540 (2019).
- [39] K. D. Usadel, *Phys. Rev. Lett.* **25**, 507 (1970).
- [40] F. S. Bergeret, A. Verso, and A. F. Volkov, *Phys. Rev. B* **86**, 214516 (2012).
- [41] M. Eschrig, A. Cottet, W. Belzig, and J. Linder, *New J. Phys.* **17**, 083037 (2015).
- [42] X.-P. Zhang, F. S. Bergeret, and V. N. Golovach, *Nano Lett.* **19**, 6330 (2019).
- [43] B. S. Chandrasekhar, *Appl. Phys. Lett.* **1**, 7 (1962).
- [44] A. M. Clogston, *Phys. Rev. Lett.* **9**, 266 (1962).
- [45] D. A. Ivanov and Y. V. Fominov, *Phys. Rev. B* **73**, 214524 (2006).
- [46] A. Kamenev, *Field Theory of Non-Equilibrium Systems* (Cambridge University Press, Cambridge, 2011), Chap. 14.
- [47] A. Altland and B. Simons, *Condensed Matter Field Theory*, 2nd ed. (Cambridge University Press, Cambridge, 2010), Chap. 1.
- [48] A. Altland, B. D. Simons, and D. T. Semchuk, *Adv. Phys.* **49**, 321 (2000).
- [49] A. A. Golubov, M. Y. Kupriyanov, and M. Siegel, *J. Exp. Theor. Phys.* **81**, 180 (2005).
- [50] Domain walls with noncollinear magnetization may induce stray fields that could affect superconductivity. In this work, we neglect the orbital effects of stray fields and assume that the superconducting gap is homogeneous in the S layer. The stray fields depend on the geometry and size of the magnetic layer, so we assume that the FI geometry is such that it minimizes the magnetostatic energy and, therefore, the stray fields. For any angle  $\alpha$ , the stray field can be minimized if the orientation of the domains is chosen to be  $\pm\alpha/2$  with respect to the  $x$  axis.
- [51] T. E. Baker, A. Richie-Halford, and A. Bill, *Phys. Rev. B* **94**, 104518 (2016).
- [52] F. S. Bergeret, A. F. Volkov, and K. B. Efetov, *Phys. Rev. Lett.* **86**, 4096 (2001).
- [53] V. L. Berezinskii, *Sov. J. Exp. Theor. Phys. Lett.* **20**, 628 (1974).
- [54] Y. Tanaka, M. Sato, and N. Nagaosa, *J. Phys. Soc. Jpn.* **81**, 011013 (2012).
- [55] J. Linder and A. V. Balatsky, *Rev. Mod. Phys.* **91**, 045005 (2019).
- [56] M. Eschrig, *Phys. Today* **64**(1), 43 (2011).
- [57] R. C. Dynes, V. Narayanamurti, and J. P. Garno, *Phys. Rev. Lett.* **41**, 1509 (1978).
- [58] I. V. Bobkova, A. M. Bobkov, and W. Belzig, *New J. Phys.* **21**, 043001 (2019).
- [59] T. Yokoyama, Y. Tanaka, and A. A. Golubov, *Phys. Rev. B* **75**, 134510 (2007).
- [60] J. Linder, T. Yokoyama, A. Sudbø, and M. Eschrig, *Phys. Rev. Lett.* **102**, 107008 (2009).
- [61] J. Linder, A. Sudbø, T. Yokoyama, R. Grein, and M. Eschrig, *Phys. Rev. B* **81**, 214504 (2010).
- [62] L. Hofstetter, S. Csonka, J. Nygård, and C. Schönenberger, *Nature (London)* **461**, 960 (2009).
- [63] M. Y. Kupriyanov and V. F. Lukichev, *Zh. Eksp. Teor. Fiz.* **94**, 139 (1988) [*Sov. Phys. JETP* **67**, 1163 (1988)].
- [64] A. I. Buzdin, A. S. Mel'nikov, and N. G. Pugach, *Phys. Rev. B* **83**, 144515 (2011).
- [65] A. V. Samokhvalov, J. W. A. Robinson, and A. I. Buzdin, *Phys. Rev. B* **100**, 014509 (2019).



## Chapter 5

**Anomalous Andreev interferometer: Study of an anomalous Josephson junction coupled to a normal wire**


## Anomalous Andreev interferometer: Study of an anomalous Josephson junction coupled to a normal wire

Alberto Hijano <sup>1,2,\*</sup>, Stefan Ilić,<sup>1,†</sup> and F. Sebastián Bergeret <sup>1,3,‡</sup>

<sup>1</sup>Centro de Física de Materiales (CFM-MPC) Centro Mixto CSIC-UPV/EHU, E-20018 Donostia-San Sebastián, Spain

<sup>2</sup>Department of Condensed Matter Physics, University of the Basque Country UPV/EHU, 48080 Bilbao, Spain

<sup>3</sup>Donostia International Physics Center (DIPC), 20018 Donostia-San Sebastián, Spain

 (Received 26 June 2021; revised 27 August 2021; accepted 17 December 2021; published 30 December 2021)

Josephson junctions (JJs), where both time-reversal and inversion symmetry are broken, exhibit a phase shift  $\varphi_0$  in their current-phase relation. This allows for an anomalous supercurrent to flow in the junction even in the absence of a phase bias between the superconductors. We show that a finite phase shift also manifests in the so-called Andreev interferometers—a device that consists of a mesoscopic conductor coupled to the  $\varphi_0$  junction. Due to the proximity effect, the resistance of this conductor is phase sensitive—it oscillates by varying the phase of the JJ. As a result, the quasiparticle current  $I_{qp}$  flowing through the conductor has an anomalous component, which exists only at finite  $\varphi_0$ . Thus, the Andreev interferometry could be used to probe the  $\varphi_0$  effect. We consider two realizations of the  $\varphi_0$  junction and calculate  $I_{qp}$  in the interferometer: a superconducting structure with spin-orbit coupling and a system of spin-split superconductors with spin-polarized tunneling barriers.

DOI: [10.1103/PhysRevB.104.214515](https://doi.org/10.1103/PhysRevB.104.214515)

### I. INTRODUCTION

The dc Josephson effect establishes that the current flowing between two superconductors with a phase difference  $\varphi$ , obtained for instance by applying a magnetic flux to the closed circuit, is given as  $I_J = I_c \sin \varphi$ . Here  $I_c$  is the critical current of the junction. In such junctions the phase difference of the ground state is  $\varphi = 0$ . In a system where (only) time-reversal symmetry is broken, such as superconductor/ferromagnet/superconductor (S/F/S) structures, it was shown that the current-phase relation can acquire a phase shift of  $\pi$ , and therefore such junctions are called  $\pi$  junctions [1–4].

In junctions where both time-reversal and inversion symmetries are broken the current-phase relation takes a more general form [5]

$$I_S = I_c \sin(\varphi + \varphi_0) = I_0^S \sin \varphi + I_{an}^S \cos \varphi. \quad (1)$$

Such JJs are known as  $\varphi_0$  junctions by analogy. This effect is referred to as the anomalous Josephson effect (AJE). In general, the current-phase relation of a JJ given by Eq. (1) can be decomposed into the usual current  $I_0^S$  and anomalous current  $I_{an}^S$ .  $I_{an}^S$  is nonzero only if the appropriate symmetries are broken, leading to a finite supercurrent even at zero phase difference between the superconductors.

AJE reflects the interplay between spin-dependent fields and superconductivity. This interaction is the basis of several effects and applications that are attracting the interest of a large community, such as topological [6–8] and unconventional [9,10] superconductivity, superconducting spintronics

[11], and novel superconducting electronic elements [12]. The most well-known proposals for AJE involve superconducting structures with spin-orbit interaction [5,13–20], some of which have been successfully tested in experiment [21–24]. Other theoretical studies have proposed numerous alternative realizations of AJE: in S/F/S junctions with a nonhomogeneous magnetization texture [25–32], junctions of unconventional superconductors [33–36], and between topologically nontrivial superconducting leads [37]. An anomalous current-phase relation can also be obtained under non-equilibrium situation in multiterminal structures [38–40].  $\varphi_0$  junctions could prove to be a key component for quantum electronics, as they can provide a stable phase bias to quantum circuits, and could therefore be particularly useful in phase-coherent superconducting electronics and spintronics [11,23].

In this paper, we consider a  $\varphi_0$  junction coupled to a mesoscopic conductor, in a device known as Andreev interferometer [41–44]. The basic physical idea behind such devices is the following: Superconducting correlations are induced in the conductor by the proximity effect, and as a consequence, its resistance becomes sensitive to the phase of the Josephson junction. This means that a simple resistance measurement performed on the conductor can reveal details about the phase dynamics of the adjacent superconducting structure. In the 90s this topic was particularly active, and several types of Andreev interferometers were theoretically proposed [45–48] and experimentally realized [49,50]. Andreev interferometers have been used to study the magnetoresistance oscillations [51], electric transport [43,52–57], and thermopower and thermal transport [58–61] in S/N structures.

Our goal is to establish how the anomalous phase shift  $\varphi_0$  manifests on the quasi-particle transport through the Andreev interferometer shown in Fig. 1(a). An important advantage of this geometry is that it allows for a decoupling of the superconducting loop with the  $\varphi_0$  junction, and the

\*alberto.hijano@ehu.es

†stefan.ilic@csic.es

‡fs.bergeret@csic.es

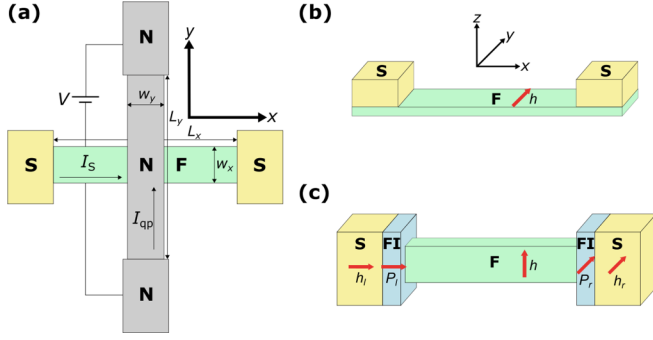


FIG. 1. (a) Schematic structure of the Andreev interferometer. (b) S/F/S structure. Here, F is a wire with Rashba spin-orbit coupling, and a spin-splitting field  $\mathbf{h}$ . (c) S/FI/F/FI/S structure. FI layers act as spin-filtering barriers with polarizations  $\mathbf{P}_{r/l}$ , and they induce spin-splitting fields  $\mathbf{h}_{r/l}$  in adjacent S layers. F is a ferromagnet with an exchange field  $\mathbf{h}$ .

normal wire where the conductance measurement is done, such that the noise associated with the measurement process does not perturb the  $\varphi_0$  junction. Our main result is that the phase-dependent contribution to the dissipative (quasiparticle) current through the vertical arm of the interferometer can be written as

$$\delta I_{qp}(\varphi) = I_c^{qp} \cos(\varphi + \varphi_0^{qp}) = I_0^{qp} \cos \varphi + I_{an}^{qp} \sin \varphi. \quad (2)$$

Therefore, this current also exhibits an anomalous phase shift  $\varphi_0^{qp}$ . Here  $I_0^{qp}$  is the usual component, which exists in Andreev interferometers with conventional junctions.  $I_{an}^{qp}$  is the anomalous component, which can only exist in the presence of a  $\varphi_0$  junction. Note that the phase shift in the Josephson current  $\varphi_0$  and in the quasiparticle current  $\varphi_0^{qp}$  are in general not equal, but they have similar magnitude and can be directly related to each other (see the Fig. 2). Our result suggests a way to experimentally obtain the value of  $\varphi_0$  from  $\varphi_0^{qp}$  by performing conductance measurements.

We study the two main realizations of  $\varphi_0$  junctions. Namely, Josephson junctions with Rashba spin-orbit coupling

(SOC) and multilayer ferromagnetic structures [Figs. 1(b) and 1(c)]. In both cases the anomalous phase is related to the existence of a Lifshitz invariant in the free energy [62–64]. In the first example such invariant stems from an interplay between a Zeeman field and the SOC, whereas in the second example it stems from non-coplanar magnetizations of magnetic layers.

## II. THE SETUP

We consider the geometry shown in Fig. 1(a). The  $\varphi_0$  junction lies along the  $x$  direction, and consists of a ferromagnetic wire placed between two superconducting reservoirs. These superconductors are connected in a loop (not shown), so that when a magnetic field is applied through the loop, the resulting flux creates a phase difference between them and leads to a Josephson current flowing along the  $x$  wire. An additional normal wire (N) is placed perpendicularly to the F wire (on the  $y$  direction). N is connected to two normal reservoirs. We assume that the F and N wires intersect at their midpoints. A voltage difference between the normal electrodes leads to a quasiparticle current  $I_{qp}$  in the  $y$  wire, which can be decomposed in two contributions:  $I_{qp} = I_{\Omega} + \delta I_{qp}(\varphi)$ , where  $I_{\Omega}$  is the usual Ohmic contribution, whereas  $\delta I_{qp}(\varphi)$  is the phase-dependent part given in Eq. (2). The latter is affected by the proximity effect with the  $x$  wire.

In the rest of this paper we determine the usual and anomalous components of  $\delta I_{qp}(\varphi)$  for two different realizations of a  $\varphi_0$  junction: a S/F/S junction with Rashba SOC [Fig. 1(b), Sec. III] and a S/FI/F/FI/S junction, where FI stands for a ferromagnetic insulator [Fig. 1(c), Sec. IV]. In the first example, a magnetic field and a spin-orbit coupling provide time-reversal and inversion symmetry breaking, respectively, which leads to the anomalous phase shift [5,17]. Here the anomalous Josephson current is  $I_{an}^S \propto h\kappa_{\alpha}$ , with  $\kappa_{\alpha}$  being a parameter associated with singlet-triplet conversion due to the SOC, and  $h$  is a weak exchange or Zeeman field [see Eq. (3)]. In the second example, the  $\varphi_0$  effect occurs if the FI tunneling barriers are spin-polarized, so that the barrier polarizations  $\mathbf{P}_{r/l}$  and the magnetization direction in the F layer  $\mathbf{h}$  are

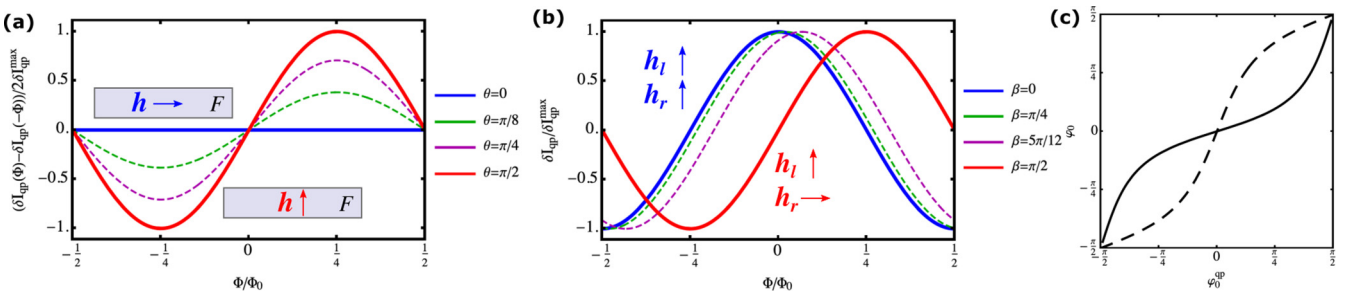


FIG. 2. (a) Component of the quasiparticle current odd in flux, which corresponds to  $I_{an}^{qp}$ , for the configuration shown in Fig 1(b).  $\theta$  is an angle between the in-plane exchange field in the F layer and the  $x$  axis. The Josephson phase is given by  $\varphi = 2\pi\Phi/\Phi_0$ , where  $\Phi$  is the applied flux and  $\Phi_0$  is the flux quantum. (b) Quasiparticle current along the  $y$  wire for different magnetization directions for the configuration shown in Fig 1(c). The exchange fields on the S electrodes  $\mathbf{h}_{r/l}$  are taken to be perpendicular to the exchange field on the F wire in order to maximize the current, while they form an angle  $\beta$ . (c) Relation between the anomalous phase shifts in the Josephson current  $\varphi_0$  and in the quasiparticle current  $\varphi_0^{qp}$  for the junction with Rashba SOC (solid) and S/FI/F/FI/S junction (dashed), calculated from the expressions provided in Appendices A and B, respectively. In the first case, the value of the exchange field is  $h = 0.1\Delta$  and the Rashba coupling constant ranges from  $\kappa_{\alpha}\xi_0 \in [-0.5, 0.5]$ . In the second case, the exchange field is  $h = 0.1\Delta$  and the splitting of the superconducting electrodes are  $h_{r/l} = 0.1\Delta$ , where they form an angle  $\beta \in [-\pi/2, \pi/2]$ . The temperature is  $T = 0.01T_{c0}$  in both cases.

noncoplanar, and therefore the magnetization inversion symmetry is broken [25–32]. The anomalous Josephson current is  $I_{\text{an}}^S \propto \chi$ , where  $\chi = \mathbf{n}_h \cdot (\mathbf{n}_l \times \mathbf{n}_r)$  is the so-called chirality of the junction (see Fig. 1). Here,  $\mathbf{n}_h$  and  $\mathbf{n}_{r/l}$  are the unit vectors along the exchange field and polarization directions. We will show that in both examples, the interferometer quasiparticle anomalous current  $I_{\text{an}}^{\text{qp}}$  has the same dependence on the spin-dependent fields as the anomalous Josephson current  $I_{\text{an}}^S$ ; namely,  $I_{\text{an}}^{\text{qp}} \propto h\kappa_\alpha$  in the first example, and  $I_{\text{an}}^{\text{qp}} \propto \chi$  in the second example.

### III. JOSEPHSON JUNCTION WITH RASHBA SOC

We first study a S/F/S structure, shown in Fig. 1(b). Here, F is a wire with Rashba spin-orbit coupling (SOC), and an exchange field  $\mathbf{h}$ , which comes either from intrinsic magnetization (F is a ferromagnet) or from an externally applied magnetic field. For this configuration, the anomalous Josephson current is only affected by the component of the exchange field perpendicular to the current direction  $x$ , so we consider a field oriented along the  $y$  direction  $\mathbf{h} = h\mathbf{y}$  in order to maximize the  $\varphi_0$  effect [17].

We describe the system using the quasiclassical Green's function (GF) formalism [65]. In the diffusive limit, GFs are obtained as a solution of the Usadel equation [66]. SOC can be included as a background SU(2) field [67–69]. Superconducting correlations are described by the condensate GF,  $\hat{f}$ , which is a  $2 \times 2$  matrix in spin space that consists of a singlet component,  $f_0$  and, in general, three triplet components,  $f_j \sigma_j$ , where  $j = 1, 2, 3$  and  $\sigma_j$  are the three Pauli matrices. We assume that the proximity effect in the F wire is weak due, for example, to low S/F transmission coefficient. In this case, the Usadel equation can be linearized [17]. For the situation under consideration, transport in  $x$  direction and  $h$  field in  $y$  direction, only the condensate components  $f_0$  and  $f_2$  are finite and satisfy:

$$\pm \partial_{xx}^2 f_0^{R/A} + i\kappa_\varepsilon^2 f_0^{R/A} - i\kappa_F^2 f_2^{R/A} - \kappa_\alpha \partial_x f_2^{R/A} = 0 \quad (3a)$$

$$\pm \partial_{xx}^2 f_2^{R/A} + i\kappa_\varepsilon^2 f_2^{R/A} - i\kappa_F^2 f_0^{R/A} - \kappa_\alpha \partial_x f_0^{R/A} = 0 \quad (3b)$$

where  $\kappa_\varepsilon^2 = 2\varepsilon/D$ ,  $\kappa_F^2 = 2h/D$  and  $\kappa_\alpha = 4\alpha^3 \tau/m$ . Here,  $\varepsilon$  is the energy,  $D$  is the diffusion constant,  $h$  is the exchange field, and  $\alpha$  is the Rashba coupling constant. The upper and lower sign correspond to the retarded and advanced condensate GFs  $\hat{f}^{R/A}$  respectively. In the following we omit the superscript to simplify the notation. Moreover, to simplify the calculation, in Eq. (3) we have neglected the renormalization of the exchange field by the SOC, and the relaxation of the triplet component due to SOC [23].

The Usadel equation (3) is supplemented by boundary conditions describing the interfaces between different materials. The S/F junctions are described by the generalized Kuprianov-Lukichev conditions [70]

$$\pm \partial_n f_{0,r/l} + \eta_{r/l} \kappa_\alpha f_{2,r/l} = \mp \frac{1}{\gamma} \mathcal{F}_0 e^{i\eta_{r/l} \varphi/2} \quad (4a)$$

$$\partial_n f_{2,r/l} = 0. \quad (4b)$$

Here,  $\mathcal{F}_0 = \Delta/\sqrt{\Delta^2 - \varepsilon^2}$  is the anomalous GF of the superconducting electrode,  $\partial_n$  is the normal derivative at the surface and  $\gamma = \sigma_F R_b$  is the parameter describing the barrier

strength, where  $R_b$  is the normal-state tunneling resistance per unit area and  $\sigma_F$  is the conductivity of the ferromagnet.  $\eta_{r/l} = \pm 1$  for the right ( $x = L_x/2$ ) and left boundaries ( $x = -L_x/2$ ).

The condensate function in the  $y$  wire  $\hat{f}_y$  is induced by the proximity effect with the  $x$  wire. To find  $\hat{f}_y$ , we start from the Kuprianov-Lukichev condition describing the interface between the two wires, and the Usadel equation in the  $y$  wire. Provided that the widths of the wires  $w_{x,y}$  are much smaller than the superconducting coherence length, we can integrate the Usadel equation over the cross-section of the wire. If the interface resistance is much larger than the resistance of the wires,  $R_B \gg L_{x,y}/\sigma_{F,N}$ , we find the equation determining  $\hat{f}_y$ :

$$\pm \partial_{yy}^2 \hat{f}_y + i\kappa_\varepsilon'^2 \hat{f}_y = -\frac{w_x}{\gamma_0^2} \hat{f}(0) \delta(y). \quad (5)$$

Here,  $\gamma_0^2 = R_B \sigma_N w_y$  and  $\kappa_\varepsilon'^2 = 2\varepsilon/D_y$ , with  $R_B$  being the resistance per unit area of the interface of the  $x$  and  $y$  wires and  $\sigma_N$  is the normal-state conductance of the  $y$  wire. The Dirac delta term describes the proximity effect, and is a source term. The contact of the  $y$  wire with the normal reservoirs is assumed to be ideal so that the condensate functions vanish at the ends of the wire is  $\hat{f}_y(\pm L_y/2) = 0$ .

A voltage bias  $V$  is applied between the normal electrodes. Due to our assumption of large  $R_B$  we can neglect the inverse proximity effect. Thus, in leading order the phase-dependent correction to the quasiparticle current is given by [71–73]

$$\delta I_{\text{qp}} = \frac{-\sigma_N}{16eL_y} \int d\varepsilon F_T(\varepsilon, V/2) \langle \text{Tr}(\check{f}_y^{\check{R}} - \check{f}_y^{\check{A}})^2 \rangle. \quad (6)$$

Here  $\langle \dots \rangle = 1/L_y \int_{-L_y/2}^{L_y/2} dy (\dots)$  denotes average over the length,  $\check{f}^{R/A}$  is the  $4 \times 4$  matrix GF in Nambu-spin space [see Eq. (A1) in the Appendix] and  $F_T$  is defined as  $F_T(\varepsilon, V) = \frac{1}{2} [\tanh \frac{\varepsilon + eV}{2T} - \tanh \frac{\varepsilon - eV}{2T}]$ . Solving the boundary value problem, Eqs. (3) and (4), we first calculate the  $\hat{f}$  for the  $x$ -wire, and then  $\hat{f}_y$  for the  $y$ -wire from Eq. (5). Using Eq. (6) we then obtain the usual and anomalous quasiparticle currents entering Eq. (2).

Up to the leading order terms in exchange field and Rashba SOC, the quasiparticle current takes the following form:

$$I_0^{\text{qp}} = c_1, \quad (7)$$

$$I_{\text{an}}^{\text{qp}} = c_2 h \kappa_\alpha. \quad (8)$$

The factors  $c_1$  and  $c_2$  depend on  $T$  and  $L_{x,y}$ , and their exact form is given by Eqs. (A14) and (A15) in the Appendix. Both components of the quasiparticle current depend on the spin-dependent fields in the same way as the components of Josephson current [17]:  $I_0^S$  and  $I_0^{\text{qp}}$  are independent of these fields, whereas  $I_{\text{an}}^S, I_{\text{an}}^{\text{qp}} \sim h\kappa_\alpha$ . Note that the result for the anomalous current, Eq. (8), also holds in the case when exchange field in the F layer is not fully aligned with the  $y$ -direction, by taking  $h = h_{\text{tot}} \sin \theta$ . Here  $h_{\text{tot}}$  is an arbitrarily oriented in-plane field, and  $\theta$  is an angle between the field and the  $x$  direction. To illustrate this, in Fig. 2(a) we plot the odd component of the anomalous quasiparticle current,  $I_{\text{an}}^{\text{qp}} \sin \varphi = \frac{1}{2} [I_{\text{qp}}(\varphi) - I_{\text{qp}}(-\varphi)]$ , for different values of  $\theta$ . The current is normalized with respect to its maximum value for clarity. For  $\theta = 0$ , the exchange field is parallel to the wire,

so there is no anomalous phase shift and  $I_{\text{an}}^{\text{qp}}$  vanishes. The  $\varphi_0$  effect is maximized for  $\theta = \pi/2$ , where the exchange field is perpendicular to the wire. In Fig. 2(c) we plot the relation between the  $\varphi_0$  phase-shift in the Josephson current, and the phase-shift measured in the quasiparticle current  $\varphi_0^{\text{qp}}$ . All expressions presented in this paper are valid for arbitrary temperature. For the numerical computations however, we only focus on low temperatures,  $T = 0.01T_{c0}$ , where the magnitude of the quasiparticle current is maximized.

#### IV. S/FI/F/FI/S JUNCTION

Another configuration to obtain a  $\varphi_0$  junction is a S/FI/F/FI/S junction with noncoplanar magnetizations [Fig. 1(c)]. This configuration has not yet been realized in experiment, but has been theoretically predicted to show AJE [25–32]. In these structures, the role of the FI layers is twofold: firstly, they induce an exchange field  $\mathbf{h}_{r/l}$  in the adjacent S layer, and secondly, they act as spin-polarized tunneling barriers with a polarization  $\mathbf{P}_{r/l}$ . The linearized Usadel equation in the F layer reads

$$\pm \partial_{xx}^2 \hat{f} + i\kappa_\varepsilon^2 \hat{f} - i \frac{\kappa_F^2}{2} \{\sigma_3, \hat{f}\} = 0, \quad (9)$$

where  $\{.,.\}$  is an anticommutator. We have assumed, without loss of generality, that the exchange field in the F-wire points on the  $z$  direction.

The S/F junctions with spin-filtering barriers are described by the generalized Kuprianov-Lukichev boundary condition [74,75]. The exchange fields  $\mathbf{h}_{r/l}$  induced via the magnetic proximity effect in the S electrodes point in the same direction as the polarization vectors  $\mathbf{P}_{r/l}$ . The linearized boundary conditions read

$$\begin{aligned} \pm \gamma \partial_n \hat{f}_{r/l} &= \frac{1}{2} [\hat{\mathcal{G}}_{r/l} \mathbf{P}_{r/l} \cdot \boldsymbol{\sigma}, \hat{f}_{r/l}] \\ &+ \frac{1}{2} \{\hat{\mathcal{G}}_{r/l}, \hat{f}_{r/l}\} \mp \sqrt{1 - P_{r/l}^2} \hat{\mathcal{F}}_{r/l} e^{in_{r/l}\varphi/2}. \end{aligned} \quad (10)$$

Here,  $\hat{\mathcal{G}}_{r/l}$  and  $\hat{\mathcal{F}}_{r/l}$  are the normal and anomalous GFs of the spin-split superconducting electrode, respectively. In the weak exchange field limit, they are given by

$$\hat{\mathcal{G}}_{r/l} = \mathcal{G}_0 - \mathbf{h}_{r/l} \cdot \boldsymbol{\sigma} \frac{d\mathcal{G}_0}{d\varepsilon} \quad (11a)$$

$$\hat{\mathcal{F}}_{r/l} = \mathcal{F}_0 - \mathbf{h}_{r/l} \cdot \boldsymbol{\sigma} \frac{d\mathcal{F}_0}{d\varepsilon} \quad (11b)$$

with  $\mathcal{G}_0 = -i\varepsilon/\sqrt{\Delta^2 - \varepsilon^2}$ .

Generally, the coherence length in the ferromagnetic layer is much shorter than in a normal metal  $\kappa_F^{-1} \ll \kappa_N^{-1}$ , where  $\kappa_N = \sqrt{2T/D}$ . We assume the long-junction regime, so that  $\kappa_F^{-1} \ll L_x \ll \kappa_N^{-1}$ . In this regime the length of the  $x$  wire  $L_x$  is much longer than the penetration length of the Cooper pairs  $\kappa_F^{-1}$  in the F layer, so that the condensate functions  $\hat{f}$  and  $\hat{f}_y$  are mediated primarily by the long-range triplet superconducting correlations [9,76,77], whereas the singlet and short-range triplet correlations decay over the length  $\kappa_F^{-1}$ .

To calculate the interferometer current, we proceed similarly as in the previous example. First, from Eqs. (9) and (10), we find  $\hat{f}$  in the  $x$  wire, and then calculate the current

in the  $y$  wire from Eqs. (5) and (6). The usual and anomalous quasiparticle currents are given by [32]

$$I_0^{\text{qp}} = c_3 \sqrt{1 - P_r^2} \sqrt{1 - P_l^2} \gamma^{-2} \mathbf{h}_{l\perp} \cdot \mathbf{h}_{r\perp} \quad (12)$$

$$I_{\text{an}}^{\text{qp}} = c_4 \sqrt{1 - P_r^2} \sqrt{1 - P_l^2} \gamma^{-3} (P_l h_r + P_r h_l) \mathbf{z} \cdot (\mathbf{n}_l \times \mathbf{n}_r), \quad (13)$$

where  $\mathbf{h}_{r/l\perp} = \mathbf{h}_{r/l} - (\mathbf{h}_{r/l} \cdot \mathbf{h})\mathbf{h}/h^2$  are the components of  $\mathbf{h}_{r/l}$  perpendicular to  $\mathbf{h}$  [see Eqs. (B12) and (B13) in the Appendix for the exact form of the coefficients  $c_3$  and  $c_4$ ].

From Eq. (13), we see that the anomalous quasiparticle current is proportional to the scalar triple product of the magnetizations  $I_{\text{an}}^{\text{qp}} \propto \chi = \mathbf{z} \cdot (\mathbf{n}_l \times \mathbf{n}_r)$  [32]. Here,  $\chi$  is the junction chirality, and it is nonzero only if the barrier polarizations and the magnetization direction are noncoplanar. As in the previous example, the quasiparticle current and the Josephson current have the same dependence on the spin-dependent fields: for the usual components  $I_0^S, I_0^{\text{qp}} \propto \mathbf{h}_{l\perp} \cdot \mathbf{h}_{r\perp}$ , and for the anomalous components  $I_{\text{an}}^S, I_{\text{an}}^{\text{qp}} \propto \chi$ .

Usually,  $I_0^{\text{qp}}$  is the dominant contribution to the interferometer current, as it is of the lower order in the small barrier parameter  $\gamma^{-1}$ , namely  $I_{\text{an}}^{\text{qp}}/I_0^{\text{qp}}, I_{\text{an}}^S/I_0^S \sim \gamma^{-1} \ll 1$ . However, if  $\mathbf{h}_{l\perp} \cdot \mathbf{h}_{r\perp} = 0$  the usual component vanishes and only the anomalous current contributes. In other words, the measured quasiparticle current is directly linked to the  $\varphi_0$  effect. To illustrate this point further, in Fig. 2(b) we use the analytical formulas (B12) and (B13) to plot the normalized quasiparticle current for different magnetic configurations. Here,  $\beta$  is the angle formed by the exchange fields on the S electrodes  $\mathbf{h}_{r/l}$ , which are taken to be perpendicular to  $\mathbf{h}$ . Unlike in panel (a), here we plot the total anomalous quasiparticle current  $I_{\text{an}}^{\text{qp}}$  to stress the shift from an even-in-phase to odd-in-phase behavior when the angle between the electrode magnetizations increases. For  $\beta = 0$ , there is no  $\varphi_0$  effect, so the current is even in the phase.  $I_0^{\text{qp}}$  decreases with increasing  $\beta$  and vanishes for  $\beta = \pi/2$ . In this case, the oscillation of  $\delta I_{\text{qp}}$  are given by the anomalous quasiparticle current, so that  $\delta I_{\text{qp}}$  becomes odd in  $\varphi$ . In Fig. 2(c) we plot the relation between the  $\varphi_0$  and  $\varphi_0^{\text{qp}}$ .

It is worth mentioning, that to simplify equations and obtain analytical solutions, we have assumed a low barrier transmission at the S/F interfaces and between the  $x$  and  $y$  wires. Consequently, the obtained quasiparticle current, being proportional to powers of a small interface parameter, is also small. However, the findings of our work should still hold qualitatively in setups with smaller interface resistances, where the quasiparticle currents should be significantly larger. In other words, our results give a lower bound of the current amplitude. Moreover, the expressions for the quasiparticle current, Eqs. (7), (8), (12), and (13) are valid for all temperatures. Indeed, the temperature dependence enters the coefficients  $c_i$ , ( $i = 1, 2, 3, 4$ ), given in Eqs. (A14), (A15), (B12), and (B13). From these expressions one can show that the quasiparticle current amplitudes are maximized at low temperatures, and they decrease monotonically towards zero at the superconducting critical temperature. This behavior of  $\delta I^{\text{qp}}$  is in contrast with the temperature behavior of the critical Josephson current, whose sign may be reversed by changing the temperature [2] (i.e., when a  $0-\pi$  transition occurs).

## V. CONCLUSION

In summary, we have studied the current-phase relation of an Andreev interferometer with an anomalous Josephson junction. We have shown how the quasiparticle current through the normal arm of the interferometer is affected by the appearance of an anomalous phase  $\varphi_0$ . Specifically, we have studied the AJE in S/F/S structures with spin-splitting field and Rashba SOC or spin-filtering barriers. Our results show that there is also an anomalous contribution to the phase-dependent part of the quasiparticle current proportional to  $\sin \varphi$  when  $\varphi_0$  is different from 0 and  $\pi$ . Moreover, the usual and anomalous quasiparticle currents have the same dependence on the spin-dependent fields as the anomalous Josephson current. Suitable materials for the realization of the anomalous Andreev interferometer are InSb [21], Bi wires [78], Bi<sub>2</sub>Se<sub>3</sub> [22], and InAs [24,79] due to the large spin-orbit coupling, in combination with conventional superconductors and normal metals. In particular, in systems with InAs a large

phase shift  $\varphi_0 \approx \pi/2$  was experimentally observed [23] in the Josephson current, and based on our findings, we expect equally strong effect in the Andreev interferometer geometry. For the ferromagnetic interferometers we propose EuS/Al structures to engineer a  $\varphi_0$  junction in a S/FI/F/FI/S junction due to the well-defined splitting and strong barrier polarization [80], while the F layer can consist of a Co wire [81,82].

## ACKNOWLEDGMENTS

This work was partially funded by the Spanish Ministerio de Ciencia, Innovación y Universidades (MICINN) through Projects No. FIS2017-82804-P and No. PID2020-114252GB-I00 (SPIRIT), and EU's Horizon 2020 research and innovation program under Grant Agreement No. 800923 (SUPERTED). A.H. acknowledges funding by the University of the Basque Country (Project No. PIF20/05).

## APPENDIX A: JOSEPHSON JUNCTION WITH RASHBA SOC

In this Appendix we present a detailed derivation of the expressions used in the main text for the currents in the presence of Rashba SOC. In Sec. A 1 we first present the derivation of the Josephson current in the  $x$  wire, followed by the derivation of the quasiparticle current in the  $y$  wire in Sec. A 2.

### 1. Current along the $x$ wire

We start by solving the linearized Usadel equation, Eq. (3), with the appropriate boundary conditions—Eq. (4). First, let us note that the retarded and advanced anomalous Green's functions (GFs) in Nambu-spin space have the following structure

$$\check{f} = \begin{pmatrix} 0 & \hat{f}(\varepsilon) \\ \hat{f}(-\varepsilon) & 0 \end{pmatrix}, \quad (\text{A1})$$

where  $\hat{X} = \mathcal{T}\hat{X}\mathcal{T}^{-1}$ , and  $\mathcal{T} = i\sigma_2\mathcal{K}$  is the time-reversal transformation, with  $\mathcal{K}$  being the complex conjugate operation. Moreover, we can relate  $\check{f}^A$  to  $\check{f}^R$  as

$$\check{f}^A(\varepsilon, \mathbf{h}, \alpha) = \check{f}^R(-\varepsilon, -\mathbf{h}, -\alpha). \quad (\text{A2})$$

In the following we only write the retarded GF and omit the superscript to simplify the notation.

We find the condensate function  $\hat{f}$  perturbatively in  $\kappa_\alpha$ , keeping terms up to the first order in this parameter. The solution is

$$\begin{aligned} f_0 = & \left[ \left( \left( 1 + \frac{\kappa_\alpha x}{2} \right) A_{1,+} + B_{1,+} \right) e^{i\varphi/2} + \left( \left( 1 + \frac{\kappa_\alpha x}{2} \right) A_{2,+} + B_{2,+} \right) e^{-i\varphi/2} \right] e^{\kappa_+ x} \\ & + \left[ \left( \left( 1 + \frac{\kappa_\alpha x}{2} \right) A_{2,+} - B_{2,+} \right) e^{i\varphi/2} + \left( \left( 1 + \frac{\kappa_\alpha x}{2} \right) A_{1,+} - B_{1,+} \right) e^{-i\varphi/2} \right] e^{-\kappa_+ x} \\ & + \left[ \left( \left( 1 - \frac{\kappa_\alpha x}{2} \right) A_{1,-} - B_{1,-} \right) e^{i\varphi/2} + \left( \left( 1 - \frac{\kappa_\alpha x}{2} \right) A_{2,-} - B_{2,-} \right) e^{-i\varphi/2} \right] e^{\kappa_- x} \\ & + \left[ \left( \left( 1 - \frac{\kappa_\alpha x}{2} \right) A_{2,-} + B_{2,-} \right) e^{i\varphi/2} + \left( \left( 1 - \frac{\kappa_\alpha x}{2} \right) A_{1,-} + B_{1,-} \right) e^{-i\varphi/2} \right] e^{-\kappa_- x}, \end{aligned} \quad (\text{A3})$$

$$\begin{aligned} f_2 = & \left[ \left( \left( 1 + \frac{\kappa_\alpha x}{2} \right) A_{1,+} + B_{1,+} \right) e^{i\varphi/2} + \left( \left( 1 + \frac{\kappa_\alpha x}{2} \right) A_{2,+} + B_{2,+} \right) e^{-i\varphi/2} \right] e^{\kappa_+ x} \\ & + \left[ \left( \left( 1 + \frac{\kappa_\alpha x}{2} \right) A_{2,+} - B_{2,+} \right) e^{i\varphi/2} + \left( \left( 1 + \frac{\kappa_\alpha x}{2} \right) A_{1,+} - B_{1,+} \right) e^{-i\varphi/2} \right] e^{-\kappa_+ x} \\ & - \left[ \left( \left( 1 - \frac{\kappa_\alpha x}{2} \right) A_{1,-} - B_{1,-} \right) e^{i\varphi/2} + \left( \left( 1 - \frac{\kappa_\alpha x}{2} \right) A_{2,-} - B_{2,-} \right) e^{-i\varphi/2} \right] e^{\kappa_- x} \\ & - \left[ \left( \left( 1 - \frac{\kappa_\alpha x}{2} \right) A_{2,-} + B_{2,-} \right) e^{i\varphi/2} + \left( \left( 1 - \frac{\kappa_\alpha x}{2} \right) A_{1,-} + B_{1,-} \right) e^{-i\varphi/2} \right] e^{-\kappa_- x}, \end{aligned} \quad (\text{A4})$$

where  $\kappa_\pm = \sqrt{-i\kappa_\varepsilon^2 \pm i\kappa_F^2}$ , and the coefficients are given by

$$A_{1,\pm} = \frac{\mathcal{F}_0}{4\gamma\kappa_\pm} \frac{e^{\kappa_\pm L_x/2}}{\sinh \kappa_\pm L_x}, \quad (\text{A5a})$$



$$A_{2,\pm} = \frac{\mathcal{F}_0}{4\gamma\kappa_{\pm}} \frac{e^{-\kappa_{\pm}L_x/2}}{\sinh \kappa_{\pm}L_x}, \quad (\text{A5b})$$

$$B_{1,\pm} = \frac{\kappa_{\alpha}\mathcal{F}_0}{8\gamma\kappa_{\pm}} \frac{1}{\sinh \kappa_{\pm}L_x} \left( \frac{1}{\kappa_{\mp} \sinh \kappa_{\mp}L_x} (e^{-\kappa_{\pm}L_x/2} - e^{\kappa_{\pm}L_x/2} \cosh \kappa_{\mp}L_x) - \frac{L_x}{2} e^{\kappa_{\pm}L_x/2} \right), \quad (\text{A5c})$$

$$B_{2,\pm} = \frac{\kappa_{\alpha}\mathcal{F}_0}{8\gamma\kappa_{\pm}} \frac{1}{\sinh \kappa_{\pm}L_x} \left( \frac{1}{\kappa_{\mp} \sinh \kappa_{\mp}L_x} (-e^{-\kappa_{\pm}L_x/2} + e^{-\kappa_{\pm}L_x/2} \cosh \kappa_{\mp}L_x) + \frac{L_x}{2} e^{-\kappa_{\pm}L_x/2} \right). \quad (\text{A5d})$$

Having found the condensate function, we proceed to calculate the Josephson current in the F wire, which is given as

$$I_S = \frac{\pi\sigma_F T}{e} \sum_{\omega} \text{Im}(f_0^*(\partial_x f_0 - \kappa_{\alpha} f_2) - f_2^* \partial_x f_0). \quad (\text{A6})$$

Note that in Eq. (A6) we introduce the Matsubara frequencies  $\omega = 2\pi(n + 1/2)T$ . The Matsubara GF is obtained by analytic continuation of  $\check{f}$  to the complex plane  $\varepsilon \rightarrow i\omega$ . We can use the boundary conditions (4) to simplify the previous equation:

$$I_S = \frac{2\pi T}{eR_b} \sum_{\omega>0} \text{Im} f_0^*(L_x/2) \mathcal{F}_0 e^{i\varphi/2}. \quad (\text{A7})$$

After substitution the Eqs. (A3) and (A4) in Eq. (A7), we find the Josephson current:

$$I_S = \frac{2\pi\sigma_S T}{e\gamma^2} \sum_{\omega>0} \mathcal{F}_0^2 \left[ \text{Re} \frac{1}{\kappa_+ \sinh(\kappa_+ L_x)} \sin \varphi + \kappa_{\alpha} \text{Im} \left( \frac{-L_x/2}{\kappa_+ \sinh(\kappa_+ L_x)} + \frac{\cosh(\kappa_+ L_x)}{|\kappa_+|^2 |\sinh(\kappa_+ L_x)|^2} \right) \cos \varphi \right]. \quad (\text{A8})$$

Here we identify the usual  $I_0$  and anomalous  $I_{\text{an}}$  components of the Josephson current as the terms proportional to  $\sin \varphi$  and  $\cos \varphi$ , respectively. The usual component is independent of the SOC strength, while the anomalous current is proportional to  $\kappa_{\alpha}$  and is nonvanishing if the exchange field  $h$  is finite.

## 2. Current along the y wire

Starting from Eq. (5), and imposing  $\check{f}_y(\pm L_y/2) = 0$ , we find the condensate function in the y wire

$$\check{f}_y = \frac{w_x}{2\gamma_0^2 \sqrt{-i\kappa'_\varepsilon} \cosh(\sqrt{-i\kappa'_\varepsilon} L_y/2)} \check{f}(0) \sinh(\sqrt{-i\kappa'_\varepsilon} (L_y/2 - |y|)), \quad (\text{A9})$$

where  $\check{f}(0)$  is the condensate function for the x wire (found in Sec. A1), evaluated at the intersection of x and y wires. Next, we use  $\check{f}_y$  to calculate the quasiparticle current  $\delta I_{\text{qp}}$  from Eq. (6). We decompose this current as  $\delta I_{\text{qp}} = \delta I_1 + \delta I_2$ , where

$$\delta I_1 = -\frac{\sigma_N}{eL_y} \int d\varepsilon F_T(\varepsilon, V/2) \frac{1}{16} \langle \text{Tr}((\check{f}^R)^2 + (\check{f}^A)^2) \rangle = \frac{\pi T \sigma_N}{2eL_y} \text{Im} \sum_{\omega>0} \langle \text{Tr} \check{f}(\omega + ieV/2)^2 \rangle, \quad (\text{A10})$$

$$\delta I_2 = \frac{4\sigma_N}{eL_y} \int_0^\infty d\varepsilon F_T(\varepsilon, V/2) \frac{1}{16} \langle \text{Tr}(\check{f}^R \check{f}^A) \rangle. \quad (\text{A11})$$

Using solution (A9), the summands in Eq. (A10) can be written as

$$\langle \text{Tr} \check{f}(\omega + ieV/2)^2 \rangle = \frac{w_x^2}{\gamma_0^4 \kappa'_\omega{}^2 \cosh^2(\kappa'_\omega L_y/2)} \left( \frac{\sinh(\kappa'_\omega L_y)}{2\kappa'_\omega L_y} - \frac{1}{2} \right) (|f_0(0)|^2 - |f(0)|^2) \Big|_{\omega=2\pi(n+1/2)T+ieV/2}, \quad (\text{A12})$$

where  $f_0(0)$  and  $f(0)$  are the singlet and triplet component of the GF of the x wire at the crossing point. Similarly, the integrand in Eq. (A11) can be written as

$$\begin{aligned} \langle \text{Tr}(\check{f}^R \check{f}^A) \rangle &= \frac{w_x^2 \left( \frac{\sinh(\sqrt{2}\kappa'_\varepsilon L_y/2)}{\sqrt{2}\kappa'_\varepsilon L_y} - \frac{\sinh(\sqrt{2}i\kappa'_\varepsilon L_y/2)}{\sqrt{2}i\kappa'_\varepsilon L_y} \right)}{2\gamma_0^4 |\kappa'_\varepsilon|^2 |\cosh(\sqrt{-i\kappa'_\varepsilon} L_y/2)|^2} (f_0(\varepsilon, \mathbf{h}, \alpha) f_0(\varepsilon, -\mathbf{h}, -\alpha)^* \\ &\quad + f_0(-\varepsilon, \mathbf{h}, \alpha)^* f_0(-\varepsilon, -\mathbf{h}, -\alpha) - f(\varepsilon, \mathbf{h}, \alpha) \cdot f(\varepsilon, -\mathbf{h}, -\alpha)^* - f(-\varepsilon, \mathbf{h}, \alpha)^* \cdot f(-\varepsilon, -\mathbf{h}, -\alpha)). \end{aligned} \quad (\text{A13})$$

Finally, the usual ( $I_0^{\text{qp}}$ ) and anomalous ( $I_{\text{an}}^{\text{qp}}$ ) quasiparticle currents are

$$\begin{aligned} I_0^{\text{qp}} &= \frac{\pi\sigma_N T}{2eL_y} \text{Im} \sum_{n \geq 0} \frac{w_x^2 \left( \frac{\sinh(\kappa'_\omega L_y)}{2\kappa'_\omega L_y} - \frac{1}{2} \right)}{\gamma_0^4 \kappa'_\omega{}^2 \cosh^2(\kappa'_\omega L_y/2)} \frac{\mathcal{F}_0^2}{4\gamma^2} \left( \frac{1}{\kappa_+^2 \sinh^2(\kappa_+ L_x/2)} + \frac{1}{\kappa_-^2 \sinh^2(\kappa_- L_x/2)} \right) \Big|_{\omega=2\pi(n+1/2)T+ieV/2} \\ &\quad + \frac{\sigma_N}{4eL_y} \int_0^\infty d\varepsilon F_T(\varepsilon, V/2) \frac{w_x^2 \left( \frac{\sinh(\sqrt{2}\kappa'_\varepsilon L_y/2)}{\sqrt{2}\kappa'_\varepsilon L_y} - \frac{\sinh(\sqrt{2}i\kappa'_\varepsilon L_y/2)}{\sqrt{2}i\kappa'_\varepsilon L_y} \right)}{\gamma_0^4 |\kappa'_\varepsilon|^2 |\cosh(\sqrt{-i\kappa'_\varepsilon} L_y/2)|^2} \frac{|\mathcal{F}_0|^2}{4\gamma^2} \end{aligned}$$

$$\times \left( \frac{1}{|\kappa_+|^2 |\sinh(\kappa_+ L_x/2)|^2} + \frac{1}{|\kappa_-|^2 |\sinh(\kappa_- L_x/2)|^2} \right), \quad (\text{A14})$$

$$I_{\text{an}}^{\text{qp}} = \kappa_\alpha \frac{\pi \sigma_N T}{2eL_y} \text{Im} \sum_{n \geq 0} \frac{w_x^2 \left( \frac{\sinh(\kappa'_\omega L_y)}{2\kappa'_\omega L_y} - \frac{1}{2} \right)}{\gamma_0^4 \kappa'_\omega{}^2 \cosh^2(\kappa'_\omega L_y/2)} \frac{\mathcal{F}_0^2}{4\gamma^2} \left( \frac{L_x}{2\kappa_+^2 \sinh^2(\kappa_+ L_x/2)} - \frac{L_x}{2\kappa_-^2 \sinh^2(\kappa_- L_x/2)} \right. \\ \left. + \frac{\tanh(\kappa_- L_x/2)}{\kappa_+^2 \kappa_- \sinh^2(\kappa_+ L_x/2)} - \frac{\tanh(\kappa_+ L_x/2)}{\kappa_-^2 \kappa_+ \sinh^2(\kappa_- L_x/2)} \right) \Big|_{\omega=2\pi(n+1/2)T+ieV/2} \\ + \kappa_\alpha \frac{\sigma_N}{4eL_y} \int_0^\infty d\varepsilon F_T(\varepsilon, V/2) \frac{w_x^2 \left( \frac{\sinh(\sqrt{2}\kappa'_\varepsilon L_y/2)}{\sqrt{2}\kappa'_\varepsilon L_y} - \frac{\sinh(\sqrt{2}i\kappa'_\varepsilon L_y/2)}{\sqrt{2}i\kappa'_\varepsilon L_y} \right)}{\gamma_0^4 |\kappa'_\varepsilon|^2 |\cosh(\sqrt{-i}\kappa'_\varepsilon L_y/2)|^2} \frac{|\mathcal{F}_0|^2}{4\gamma^2} \\ \times \text{Im} \left\{ \frac{\tanh(\kappa_- L_x/2)}{|\kappa_+|^2 \kappa_- |\sinh(\kappa_+ L_x/2)|^2} - \frac{\tanh(\kappa_+ L_x/2)}{|\kappa_-|^2 \kappa_+ |\sinh(\kappa_- L_x/2)|^2} \right\}. \quad (\text{A15})$$

The factors  $c_1$  and  $c_2$  defined in Eqs. (7) and (8) of the main text can be extracted from Eqs. (A14) and (A15) by assuming the limit of weak exchange field  $h$ .

## APPENDIX B: S/FI/F/FI/S JUNCTION

In this Appendix we present a detailed derivation of the expressions used in the main text for the currents in the S/FI/F/FI/S geometry. In Sec. B 1 we first present the derivation of the Josephson current in the  $x$  wire, followed by the derivation of the quasiparticle current in the  $y$ -wire in Sec. B 2.

### 1. Current along the $x$ wire

The general solution of Eq. (9) for the condensate function in the  $x$  wire reads

$$\hat{f} = (A + A\sigma_3)e^{\kappa_+ x} + (B + B\sigma_3)e^{-\kappa_+ x} + (C - C\sigma_3)e^{\kappa_- x} + (D - D\sigma_3)e^{-\kappa_- x} + E\sigma_1 e^{i\kappa_\varepsilon x} + F\sigma_1 e^{-i\kappa_\varepsilon x} + G\sigma_2 e^{i\kappa_\varepsilon x} + H\sigma_2 e^{-i\kappa_\varepsilon x}. \quad (\text{B1})$$

Coefficients in Eq. (B1) can be found by applying the boundary conditions [Eq. (10)]. In the ferromagnetic wire, the supercurrent is given as

$$I_S = \pi \sigma_F \frac{T}{e} \sum_\omega \text{Im} \{ f_0^* \partial_x f_0 - f^* \cdot \partial_x f \}, \quad (\text{B2})$$

where  $\hat{f}_\omega = f_0 + \mathbf{f} \cdot \boldsymbol{\sigma}$  is decomposed into the scalar singlet amplitude  $f_0$  and the vector of triplet states  $\mathbf{f}$ . Assuming  $\kappa_F^{-1} \ll L_x \ll \kappa_\omega^{-1}$ , we can substitute the long range components  $f_1$  and  $f_2$  by their average values, given by

$$\langle f_{1/2} \rangle = \frac{\partial_x f_{1/2}|_{x=-L_x/2} - \partial_x f_{1/2}|_{x=L_x/2}}{\kappa_\omega^2 L_x}. \quad (\text{B3})$$

Then, using the boundary conditions [Eq. (10)], the long range triplet components are given by

$$\langle f_{1/2} \rangle = \frac{1}{\kappa_\omega^2 L_x \gamma} (i\mathcal{G}_{1,0}(P_{1,2/3} f_{3/1}(-L_x/2) - P_{1,3/1} f_{2/3}(-L_x/2)) - \sqrt{1 - P_l^2} \mathcal{F}_{l,1/2} e^{-i\varphi/2} \\ + i\mathcal{G}_{r,0}(P_{r,2/3} f_{3/1}(L_x/2) - P_{r,3/1} f_{2/3}(L_x/2)) - \sqrt{1 - P_r^2} \mathcal{F}_{r,1/2} e^{i\varphi/2}), \quad (\text{B4})$$

where  $\hat{\mathcal{G}}_{r/l}$  and  $\hat{\mathcal{F}}_{r/l}$  are given by Eq. (11). Using solution (B1), we can calculate the  $f_0$  and  $f_3$  near each boundary independently without overlapping. To first order in  $\gamma^{-1}$ , we obtain:

$$f_{0,r/l}^{(1)} = \frac{\sqrt{1 - P_{r/l}^2}}{2\gamma} \left( \frac{\mathcal{F}_{r/l,0} + \mathcal{F}_{r/l,3}}{\kappa_+} e^{-\kappa_+(L_x/2 \mp x)} + \frac{\mathcal{F}_{r/l,0} - \mathcal{F}_{r/l,3}}{\kappa_-} e^{-\kappa_-(L_x/2 \mp x)} \right) e^{i\eta_{r/l}\varphi/2} \quad (\text{B5})$$

$$f_{3,r/l}^{(1)} = \frac{\sqrt{1 - P_{r/l}^2}}{2\gamma} \left( \frac{\mathcal{F}_{r/l,0} + \mathcal{F}_{r/l,3}}{\kappa_+} e^{-\kappa_+(L_x/2 \mp x)} - \frac{\mathcal{F}_{r/l,0} - \mathcal{F}_{r/l,3}}{\kappa_-} e^{-\kappa_-(L_x/2 \mp x)} \right) e^{i\eta_{r/l}\varphi/2}. \quad (\text{B6})$$

The second-order terms in  $\gamma^{-1}$  are also important to obtain the anomalous Josephson effect:

$$f_{0,r/l}^{(2)} = \frac{-i\mathcal{G}_{r/l,0}}{2\gamma} (P_{r/l,1} \langle f_2 \rangle - P_{r/l,2} \langle f_1 \rangle) \left( \frac{e^{-\kappa_+(L_x/2 \mp x)}}{\kappa_+} - \frac{e^{-\kappa_-(L_x/2 \mp x)}}{\kappa_-} \right) \quad (\text{B7})$$

$$f_{3,r/l}^{(2)} = \frac{-i\mathcal{G}_{r/l,0}}{2\gamma} (P_{r/l,1}\langle f_2 \rangle - P_{r/l,2}\langle f_1 \rangle) \left( \frac{e^{-\kappa_+(L_x/2 \mp x)}}{\kappa_+} + \frac{e^{-\kappa_-(L_x/2 \mp x)}}{\kappa_-} \right). \quad (\text{B8})$$

To lowest order in  $\gamma^{-1}$ , the current (B2) can be written as

$$I_S = \frac{\pi\sigma_F T}{e\gamma} \sum_{\omega} \text{Im} \pm \sqrt{1 - P_r^2} (f_0^* \mathcal{F}_{r/l,0} - f^* \cdot \mathcal{F}_{r/l}) e^{in_{r/l}\varphi/2} \Big|_{x=\pm L_x/2}. \quad (\text{B9})$$

Finally, we find the usual and anomalous Josephson currents:

$$I_0^S = -\frac{2\pi}{eR_b} (\mathbf{h}_{l\perp} \cdot \mathbf{h}_{r\perp}) \frac{\sqrt{1 - P_r^2} \sqrt{1 - P_l^2}}{\sqrt{2}L_x\gamma^2} \sum_{\omega>0} \frac{T\mathcal{F}_0^2}{\kappa_N^2} \quad (\text{B10})$$

$$I_{\text{an}}^S = -\frac{2\pi}{eR_b} (\chi_l - \chi_r) \frac{\sqrt{1 - P_r^2} \sqrt{1 - P_l^2}}{\kappa_F h L_x \gamma^3} \sum_{\omega>0} \frac{T\mathcal{G}_0 \mathcal{F}_0 \mathcal{F}'_0}{\kappa_{\omega}^2}. \quad (\text{B11})$$

For simplicity we have assumed the same amplitude of the order parameter in the two electrodes. The chiralities are defined as  $\chi_{r/l} = \mathbf{h} \cdot (\mathbf{P}_{r/l} \times \mathbf{h}_{l/r})$ , and  $\mathbf{h}_{r/l\perp} = \mathbf{h}_{r/l} - (\mathbf{h}_{r/l} \cdot \mathbf{h})\mathbf{h}/h^2$  are the components of  $\mathbf{h}_{r/l}$  perpendicular to  $\mathbf{h}$ .

## 2. Current along the y wire

We obtain the quasiparticle current in the y-wire by following the same procedure as in Sec. A 2. The coefficients  $c_3$  and  $c_4$  in Eqs. (12) and (13) are

$$c_3 = -\frac{\pi T \sigma_N}{2eL_y} \text{Im} \sum_{n \geq 0} \frac{w_x^2 \left( \frac{\sinh(\kappa'_\omega L_y)}{2\kappa'_\omega L_y} - \frac{1}{2} \right)}{\gamma_0^4 \kappa'_\omega{}^2 \cosh^2(\kappa'_\omega L_y/2)} \frac{2(\mathcal{F}'_0)^2}{\kappa_\omega^4 L_x^2} \Big|_{\omega=2\pi(n+1/2)T+ieV/2} \\ + \frac{\sigma_N}{4eL_y} \int_0^\infty d\varepsilon F_T(\varepsilon, V/2) \frac{w_x^2 \left( \frac{\sinh(\sqrt{2}\kappa'_\varepsilon L_y/2)}{\sqrt{2}\kappa'_\varepsilon L_y} - \frac{\sinh(\sqrt{2}i\kappa'_\varepsilon L_y/2)}{\sqrt{2}i\kappa'_\varepsilon L_y} \right)}{\gamma_0^4 |\kappa'_\varepsilon|^2 |\cosh(\sqrt{-i}\kappa'_\varepsilon L_y/2)|^2} \frac{2|\mathcal{F}'_0|^2}{|\kappa_\varepsilon|^4 L_x^2}, \quad (\text{B12})$$

$$c_4 = \frac{\pi T \sigma_N}{2eL_y} \text{Im} \sum_{n \geq 0} \frac{w_x^2 \left( \frac{\sinh(\kappa'_\omega L_y)}{2\kappa'_\omega L_y} - \frac{1}{2} \right)}{\gamma_0^4 \kappa'_\omega{}^2 \cosh^2(\kappa'_\omega L_y/2)} \frac{\sqrt{2}\mathcal{G}_0 \mathcal{F}_0 \mathcal{F}'_0}{\kappa_F \kappa_\omega^4 L_x^2} \Big|_{\omega=2\pi(n+1/2)T+ieV/2} \\ + \frac{\sigma_N}{4eL_y} \int_0^\infty d\varepsilon F_T(\varepsilon, V/2) \frac{w_x^2 \left( \frac{\sinh(\sqrt{2}\kappa'_\varepsilon L_y/2)}{\sqrt{2}\kappa'_\varepsilon L_y} - \frac{\sinh(\sqrt{2}i\kappa'_\varepsilon L_y/2)}{\sqrt{2}i\kappa'_\varepsilon L_y} \right)}{\gamma_0^4 |\kappa'_\varepsilon|^2 |\cosh(\sqrt{-i}\kappa'_\varepsilon L_y/2)|^2} \frac{-\sqrt{2}\text{Re}\{\mathcal{G}_0^* \mathcal{F}_0^* \mathcal{F}'_0\}}{\kappa_F |\kappa_\varepsilon|^4 L_x^2}. \quad (\text{B13})$$

- 
- [1] A. I. Buzdin, L. N. Bulaevskii, and S. V. Panjukov, *JETP Lett.* **35**, 178 (1982).  
[2] V. V. Ryazanov, V. A. Oboznov, A. Y. Rusanov, A. V. Veretennikov, A. A. Golubov, and J. Aarts, *Phys. Rev. Lett.* **86**, 2427 (2001).  
[3] A. I. Buzdin, *Rev. Mod. Phys.* **77**, 935 (2005).  
[4] V. A. Oboznov, V. V. Bol'ginov, A. K. Feofanov, V. V. Ryazanov, and A. I. Buzdin, *Phys. Rev. Lett.* **96**, 197003 (2006).  
[5] A. Buzdin, *Phys. Rev. Lett.* **101**, 107005 (2008).  
[6] S. Frolov, M. Manfra, and J. Sau, *Nat. Phys.* **16**, 718 (2020).  
[7] M. Sato and Y. Ando, *Rep. Prog. Phys.* **80**, 076501 (2017).  
[8] M. Leijnse and K. Flensberg, *Semicond. Sci. Technol.* **27**, 124003 (2012).  
[9] F. S. Bergeret, A. F. Volkov, and K. B. Efetov, *Rev. Mod. Phys.* **77**, 1321 (2005).  
[10] J. Linder and A. V. Balatsky, *Rev. Mod. Phys.* **91**, 045005 (2019).  
[11] J. Linder and J. W. Robinson, *Nat. Phys.* **11**, 307 (2015).  
[12] F. Ando, Y. Miyasaka, T. Li, J. Ishizuka, T. Arakawa, Y. Shiota, T. Moriyama, Y. Yanase, and T. Ono, *Nature (London)* **584**, 373 (2020).  
[13] A. A. Reynoso, G. Usaj, C. A. Balseiro, D. Feinberg, and M. Avignon, *Phys. Rev. Lett.* **101**, 107001 (2008).  
[14] A. Zazunov, R. Egger, T. Jonckheere, and T. Martin, *Phys. Rev. Lett.* **103**, 147004 (2009).  
[15] A. Brunetti, A. Zazunov, A. Kundu, and R. Egger, *Phys. Rev. B* **88**, 144515 (2013).  
[16] T. Yokoyama, M. Eto, and Y. V. Nazarov, *Phys. Rev. B* **89**, 195407 (2014).  
[17] F. S. Bergeret and I. V. Tokatly, *Europhys. Lett.* **110**, 57005 (2015).  
[18] F. Konschelle, I. V. Tokatly, and F. S. Bergeret, *Phys. Rev. B* **92**, 125443 (2015).  
[19] K. N. Nesterov, M. Houzet, and J. S. Meyer, *Phys. Rev. B* **93**, 174502 (2016).  
[20] I. V. Bobkova, A. M. Bobkov, A. A. Zyuzin, and M. Alidoust, *Phys. Rev. B* **94**, 134506 (2016).

- [21] D. B. Szombati, S. Nadj-Perge, D. Car, S. R. Plissard, E. P. A. M. Bakkers, and L. P. Kouwenhoven, *Nat. Phys.* **12**, 568 (2016).
- [22] A. Assouline, C. Feuillet-Palma, N. Bergeal, T. Zhang, A. Mottaghizadeh, A. Zimmers, E. Lhuillier, M. Eddrie, P. Atkinson, M. Aprili, and H. Aubin, *Nat. Commun.* **10**, 126 (2019).
- [23] E. Strambini, A. Iorio, O. Durante, R. Citro, C. Sanz-Fernández, C. Guarcello, I. V. Tokatly, A. Braggio, M. Rocci, N. Ligato *et al.*, *Nat. Nanotechnol.* **15**, 656 (2020).
- [24] W. Mayer, M. C. Dartiailh, J. Yuan, K. S. Wickramasinghe, E. Rossi, and J. Shabani, *Nat. Commun.* **11**, 212 (2020).
- [25] V. Braude and Y. V. Nazarov, *Phys. Rev. Lett.* **98**, 077003 (2007).
- [26] R. Grein, M. Eschrig, G. Metalidis, and G. Schön, *Phys. Rev. Lett.* **102**, 227005 (2009).
- [27] I. Margaritis, V. Paltoglou, and N. Flytzanis, *J. Phys.: Condens. Matter* **22**, 445701 (2010).
- [28] J.-F. Liu and K. S. Chan, *Phys. Rev. B* **82**, 184533 (2010).
- [29] I. Kulagina and J. Linder, *Phys. Rev. B* **90**, 054504 (2014).
- [30] A. Moor, A. F. Volkov, and K. B. Efetov, *Phys. Rev. B* **92**, 180506(R) (2015).
- [31] S. Mironov and A. Buzdin, *Phys. Rev. B* **92**, 184506 (2015).
- [32] M. A. Silaev, I. V. Tokatly, and F. S. Bergeret, *Phys. Rev. B* **95**, 184508 (2017).
- [33] S. Yip, *Phys. Rev. B* **52**, 3087 (1995).
- [34] M. Sigrist, *Prog. Theor. Phys.* **99**, 899 (1998).
- [35] S. Kashiwaya and Y. Tanaka, *Rep. Prog. Phys.* **63**, 1641 (2000).
- [36] P. M. R. Brydon, B. Kastening, D. K. Morr, and D. Manske, *Phys. Rev. B* **77**, 104504 (2008).
- [37] C. Schrade, S. Hoffman, and D. Loss, *Phys. Rev. B* **95**, 195421 (2017).
- [38] P. E. Dolgirev, M. S. Kalenkov, and A. D. Zaikin, *Phys. Rev. B* **97**, 054521 (2018).
- [39] P. E. Dolgirev, M. S. Kalenkov, A. E. Tarkhov, and A. D. Zaikin, *Phys. Rev. B* **100**, 054511 (2019).
- [40] D. Margineda, J. Claydon, F. Qeivanaj, and C. Checkley, *arXiv:2105.13968*.
- [41] A. G. Mal'shukov, *Phys. Rev. B* **97**, 064515 (2018).
- [42] P. E. Dolgirev, M. S. Kalenkov, and A. D. Zaikin, *Phys. Status Solidi RRL* **13**, 1800252 (2019).
- [43] A. F. Volkov, *Phys. Rev. B* **102**, 094517 (2020).
- [44] G. Blasi, F. Taddei, L. Arrachea, M. Carrega, and A. Braggio, *Phys. Rev. B* **102**, 241302(R) (2020).
- [45] A. Zaitsev, *Phys. B: Condens. Matter* **203**, 274 (1994).
- [46] T. H. Stoof and Y. V. Nazarov, *Phys. Rev. B* **53**, 14496 (1996).
- [47] Y. V. Nazarov and T. H. Stoof, *Phys. Rev. Lett.* **76**, 823 (1996).
- [48] A. A. Golubov, F. K. Wilhelm, and A. D. Zaikin, *Phys. Rev. B* **55**, 1123 (1997).
- [49] V. T. Petrashov, V. N. Antonov, P. Delsing, and R. Claeson, *Phys. Rev. Lett.* **70**, 347 (1993).
- [50] V. T. Petrashov, V. N. Antonov, P. Delsing, and T. Claeson, *Phys. Rev. Lett.* **74**, 5268 (1995).
- [51] V. Antonov, V. Petrashov, and P. Delsing, *Physica C: Superconductivity* **352**, 173 (2001).
- [52] V. T. Petrashov, K. G. Chua, K. M. Marshall, R. S. Shaikhaidarov, and J. T. Nicholls, *Phys. Rev. Lett.* **95**, 147001 (2005).
- [53] N. L. Plaszkó, P. Rakyta, J. Cserti, A. Kormányos, and C. J. Lambert, *Nanomaterials* **10**, 1033 (2020).
- [54] C. Checkley, A. Iagallo, R. Shaikhaidarov, J. T. Nicholls, and V. T. Petrashov, *J. Phys.: Condens. Matter* **23**, 135301 (2011).
- [55] F. Deon, S. Šopić, and A. F. Morpurgo, *Phys. Rev. Lett.* **112**, 126803 (2014).
- [56] A. V. Galaktionov, A. D. Zaikin, and L. S. Kuzmin, *Phys. Rev. B* **85**, 224523 (2012).
- [57] A. V. Galaktionov and A. D. Zaikin, *Phys. Rev. B* **88**, 104513 (2013).
- [58] J. Eom, C.-J. Chien, and V. Chandrasekhar, *Phys. Rev. Lett.* **81**, 437 (1998).
- [59] A. Parsons, I. A. Sosnin, and V. T. Petrashov, *Phys. Rev. B* **67**, 140502(R) (2003).
- [60] V. Chandrasekhar, *Supercond. Sci. Technol.* **22**, 083001 (2009).
- [61] A. F. Volkov and V. V. Pavlovskii, *Phys. Rev. B* **72**, 014529 (2005).
- [62] V. M. Edelstein, *J. Phys.: Condens. Matter* **8**, 339 (1996).
- [63] V. P. Mineev and K. V. Samokhin, *Phys. Rev. B* **78**, 144503 (2008).
- [64] E. Bauer and M. Sigrist, eds., *Non-Centrosymmetric Superconductors: Introduction and Overview*, Lecture Notes in Physics No. 847 (Springer Verlag, Heidelberg, 2012).
- [65] W. Belzig, F. K. Wilhelm, C. Bruder, G. Schön, and A. D. Zaikin, *Superlattices Microstruct.* **25**, 1251 (1999).
- [66] K. D. Usadel, *Phys. Rev. Lett.* **25**, 507 (1970).
- [67] F. S. Bergeret and I. V. Tokatly, *Phys. Rev. Lett.* **110**, 117003 (2013).
- [68] F. S. Bergeret and I. V. Tokatly, *Phys. Rev. B* **89**, 134517 (2014).
- [69] I. V. Tokatly, *Phys. Rev. B* **96**, 060502(R) (2017).
- [70] M. Y. Kuprianov and V. F. Lukichev, *Zh. Eksp. Teor. Fiz.* **94**, 139 (1988) [*Sov. Phys. JETP* **67**, 1163 (1988)].
- [71] A. F. Volkov and H. Takayanagi, *Phys. Rev. Lett.* **76**, 4026 (1996).
- [72] A. F. Volkov and V. V. Pavlovskii, *AIP Conf. Proc.* **427**, 343 (1998).
- [73] A. Volkov and V. Pavlovskii, *Phys. Usp.* **41**, 191 (1998).
- [74] F. S. Bergeret, A. Verso, and A. F. Volkov, *Phys. Rev. B* **86**, 214516 (2012).
- [75] M. Eschrig, A. Cottet, W. Belzig, and J. Linder, *New J. Phys.* **17**, 083037 (2015).
- [76] A. I. Buzdin, A. S. Mel'nikov, and N. G. Pugach, *Phys. Rev. B* **83**, 144515 (2011).
- [77] A. V. Samokhvalov, J. W. A. Robinson, and A. I. Buzdin, *Phys. Rev. B* **100**, 014509 (2019).
- [78] A. Murani, A. Kasumov, S. Sengupta, Y. A. Kasumov, V. Volkov, I. Khodos, F. Brisset, R. Delagrè, A. Chepelienskii, R. Deblock *et al.*, *Nat. Commun.* **8**, 15941 (2017).
- [79] C. Baumgartner, L. Fuchs, L. Frés, S. Reinhardt, S. Gronin, G. C. Gardner, M. J. Manfra, N. Paradiso, and C. Strunk, *Phys. Rev. Lett.* **126**, 037001 (2021).
- [80] M. Rouco, S. Chakraborty, F. Aikebaier, V. N. Golovach, E. Strambini, J. S. Moodera, F. Giazotto, T. T. Heikkilä, and F. S. Bergeret, *Phys. Rev. B* **100**, 184501 (2019).
- [81] J. Wang, M. Singh, M. Tian, N. Kumar, B. Liu, C. Shi, J. Jain, N. Samarth, T. Mallouk, and M. Chan, *Nat. Phys.* **6**, 389 (2010).
- [82] T. S. Khaire, M. A. Khasawneh, W. P. Pratt, and N. O. Birge, *Phys. Rev. Lett.* **104**, 137002 (2010).

## Chapter 6

# Microwave-Assisted Thermoelectricity in S-I-S' Tunnel Junctions

## Microwave-Assisted Thermoelectricity in $S$ - $I$ - $S'$ Tunnel Junctions


A. Hijano<sup>1,2,\*</sup>, F.S. Bergeret<sup>1,3,†</sup>, F. Giazotto<sup>4,‡</sup> and A. Braggio<sup>4,§</sup>

<sup>1</sup>Centro de Física de Materiales (CFM-MPC), Centro Mixto CSIC-UPV/EHU, Donostia-San Sebastián 20018, Spain

<sup>2</sup>Department of Condensed Matter Physics, University of the Basque Country UPV/EHU, Bilbao 48080, Spain

<sup>3</sup>Donostia International Physics Center (DIPC), Donostia-San Sebastián 20018, Spain

<sup>4</sup>NEST Istituto Nanoscienze-CNR and Scuola Normale Superiore, Pisa 56127, Italy

 (Received 8 November 2022; revised 31 January 2023; accepted 15 March 2023; published 7 April 2023)

Asymmetric superconducting tunnel junctions with gaps  $\Delta_1 > \Delta_2$  have been proven to show a peculiar nonlinear bipolar thermoelectric effect. This arises due to the spontaneous breaking of electron-hole symmetry in the system, and it is maximized at the matching-peak bias  $|V| = V_p = (\Delta_1 - \Delta_2)/e$ . In this paper, we investigate the interplay of photon-assisted tunneling (PAT) and bipolar thermoelectric generation. In particular, we show how thermoelectricity, at the matching peak, is supported by photon absorption and emission processes at the frequency-shifted sidebands  $V = \pm V_p + n\hbar\omega$ ,  $n \in \mathbb{Z}$ . This represents a sort of *microwave-assisted thermoelectricity*. We show the existence of multiple stable solutions, being associated with different photon sidebands, when a load is connected to the junction. Finally, we discuss how the nonlinear cooling effects are modified by the PAT. The proposed device can detect millimeter-wavelength signals by converting a temperature gradient into a thermoelectric current or voltage.

DOI: [10.1103/PhysRevApplied.19.044024](https://doi.org/10.1103/PhysRevApplied.19.044024)

### I. INTRODUCTION

Hybrid superconducting systems with explicit broken particle-hole symmetry show unipolar thermoelectricity [1–9]. The particle-hole symmetry around the Fermi surface of Bardeen-Cooper-Schrieffer (BCS) superconductors can be broken, for instance, in superconductor/ferromagnet hybrid structures. The magnetic proximity effect in a thin superconductor-ferromagnetic insulator bilayer causes an almost homogeneous spin splitting of the density of states (DOS) [10]. If the electronic transport is spin-polarized, for example via a tunneling spin filter [11–14], the DOS contribution of one spin component becomes predominant over the other one, leading to an effective particle-hole symmetry breaking [4].

It has recently been theoretically [15–17] and experimentally [18,19] shown that superconducting tunnel junctions, where the Josephson coupling is properly suppressed, develop a large thermoelectric effect if the electrode with the larger gap has a higher temperature. In contrast to systems with magnetic proximity effect, in superconducting tunnel junctions the electron-hole symmetry is broken by the combination of a sufficiently

strong thermal gradient and a monotonically decreasing DOS, which induces spontaneous voltage polarization. The resulting thermoelectricity is *bipolar* and strongly nonlinear.

We focus here on photon-assisted tunneling (PAT), which has been extensively studied in the dissipative regime [20–30]. However, the influence of PAT on the recently observed bipolar thermoelectricity is still unexplored. In this work, we address microwave-assisted thermoelectricity by investigating the interplay between PAT and bipolar thermoelectricity in a superconductor-insulator-superconductor ( $S$ - $I$ - $S'$ ) tunnel junction. This kind of tunnel junction normally works at very low temperatures in order to preserve the superconductivity. It is worth noting that thermoelectricity at these temperatures is very strong [18] due to the nonlinearity of the effect. The obtained results show intriguing perspectives for application as millimeter-wavelength signal detectors [7], flux-controlled high-frequency oscillators [17], controlled generators [16], superconducting qubits [31–35], quantum sensors [36,37], and, more broadly, in the emergent field of superconducting quantum technologies.

This paper is organized as follows: In Sec. II we present the basic equations describing the dc and ac tunneling charge and heat currents through a tunnel junction. In Sec. III we numerically obtain the  $I(V)$  characteristic curves and study the thermoelectric power output. Finally,

\*alberto.hijano@ehu.eus

†fs.bergeret@csic.es

‡francesco.giazotto@sns.it

§alessandro.braggio@nano.cnr.it

we study the impact of the ac voltage source on the cooling power of the junction. We summarize the results in Sec. IV.

## II. THE MODEL

We consider an  $S$ - $I$ - $S'$  tunnel junction where each superconducting electrode is kept in thermal equilibrium; see Fig. 1(a). The gap of the left superconductor ( $S_1$ ) is considered to be higher than that of the right superconductor ( $S_2$ ),  $\Delta_1 > \Delta_2$ . This can be done by using different superconducting materials for each electrode or by taking advantage of the inverse proximity effect by attaching a normal layer to the right superconductor, which effectively suppresses the gap [18]. The asymmetry parameter  $r = \Delta_{0,2}/\Delta_{0,1} < 1$  quantifies the asymmetry between the two terminals, where  $\Delta_{0,\alpha}$  is the zero-temperature gap of electrode  $\alpha$ . If the electrodes are powered by a constant voltage source  $V$ , the chemical potential of the electrodes are shifted by  $\mu_1 - \mu_2 = -eV$ .

The tunneling current between the two superconductors has three contributions: the quasiparticle current, the Cooper-pair current, and the interference current, which gives the interference contribution associated with breaking and recombination processes of Cooper pairs in different electrodes [38–41]. The latter two contributions stem from the Josephson coupling, and they depend on the phase difference between the superconductors. At finite bias, those terms oscillate between positive and negative values, and might be detrimental to a stable thermoelectric effect [17]. Therefore, we assume that the Josephson coupling is sufficiently weak [18,42–44], and neglect those terms, such that we consider only the quasiparticle current, which is phase-independent. The Josephson current can also be suppressed by applying a suitable in-plane magnetic field or by applying a small out-of-plane magnetic field in a superconducting quantum interference device (SQUID) as in [18,19].

The dc tunneling quasiparticle charge  $I_\alpha$  and heat  $\dot{Q}_\alpha$  currents flowing out from electrode  $\alpha = 1, 2$  are

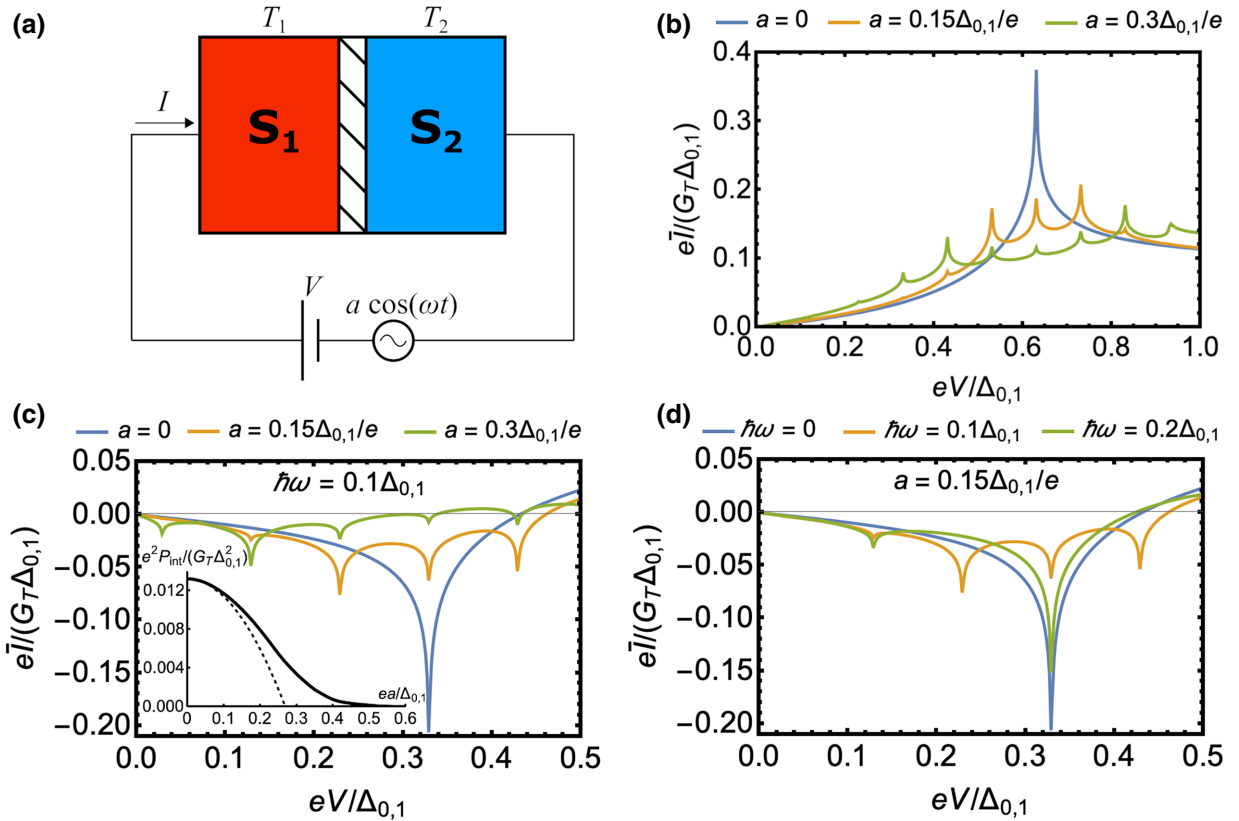


FIG. 1. (a) Simple circuit scheme of the photon-assisted bipolar thermoelectricity. The two superconductors have a different gap  $\Delta_1 > \Delta_2$  and are subject to a temperature difference  $T_1 > T_2$ . The  $S$ - $I$ - $S'$  junction is powered by a dc and an ac voltage source. (b) Equilibrium  $\bar{I}(V)$  curves for a finite ac voltage with  $\hbar\omega = 0.1\Delta_{0,1}$  and different amplitudes  $a$ . (c,d) Time-averaged quasiparticle current  $\bar{I}(V)$  dependence on the amplitude (c) and angular frequency (d) of the ac field. The inset in panel (c) shows the integrated thermoelectric power as a function of  $a$  (solid line) and the behavior predicted in the small-signal limit (dashed line). The temperatures are  $T_1 = T_2 = 0.4T_{c,1}$  in panel (b), and  $T_1 = 0.7T_{c,1}$  and  $T_2 = 0$  for panels (c) and (d).

given by

$$\begin{pmatrix} I_\alpha \\ \dot{Q}_\alpha \end{pmatrix} = \frac{G_T}{e^2} \int dE \begin{pmatrix} -e \\ E - \mu_\alpha \end{pmatrix} N_\alpha(E - \mu_\alpha) N_{\bar{\alpha}}(E - \mu_{\bar{\alpha}}) \\ \times (f_\alpha(E - \mu_\alpha) - f_{\bar{\alpha}}(E - \mu_{\bar{\alpha}})), \quad (1)$$

with  $\bar{\alpha}$  the opposite side with respect to  $\alpha$ . Here,  $-e$  is the electron charge,  $G_T$  is the conductance of the junction, and  $f_\alpha(E) = [\exp(E/k_B T_\alpha) + 1]^{-1}$  is the  $\alpha$ -lead Fermi-Dirac distribution. The BCS DOS is given by  $N_\alpha(E) = \text{Re}\{-i(E + i\Gamma_\alpha)/\sqrt{\Delta_\alpha^2 - (E + i\Gamma_\alpha)^2}\}$ , where  $\Gamma_\alpha$  is the Dynes parameter [45], describing inelastic processes. The Dynes parameter accounts for the broadening of the BCS coherent peaks at  $E = \pm\Delta$  in the DOS. In the calculations below, we set  $\Gamma_1 = \Gamma_2 = 10^{-4}\Delta_{0,1}$ , which is a reasonable value typically found in experiments with high-quality tunnel junctions [46–49].

From Eq. (1), one can easily check that the  $S$ - $I$ - $S'$  is a reciprocal electric device. Indeed, the DOS of the superconducting electrodes is electron-hole symmetric, so that the quasiparticle charge current in the junction is odd in voltage  $I(-V) = -I(V)$ , where we focus here on the current flowing out of the left electrode,  $I \equiv I_1$ . Moreover, due to energy conservation,  $\dot{Q}_1 + \dot{Q}_2 - \dot{W} = 0$ , where  $\dot{W} = -VI$  describes the electric power generated (dissipated) for  $\dot{W} > 0$  ( $\dot{W} < 0$ ) by the junction. Here we use the active sign convention by considering the electrical work done by the junction over its surroundings as positive. At the equilibrium  $T_1 = T_2$ , the junction is dissipative ( $IV > 0$ ). When the temperature of the left electrode, with a bigger gap, is higher than that on the right electrode,  $T_1 \gtrsim T_2/r$ , it is possible to generate bipolar thermoelectricity [15,18] with the current  $I$  flowing against the bias ( $IV < 0$ ). This occurs at subgap voltages  $e|V| \lesssim \Delta_1 + \Delta_2$  [15–17]. Furthermore, from the negative differential conductance at  $V \approx 0$ , the thermocurrent grows to a maximum around the matching peak  $eV_p = \Delta_1 - \Delta_2$ , and for  $e|V| \gtrsim \Delta_1 + \Delta_2$  it again becomes dissipative. In an open-circuit configuration, a thermoelectric Seebeck voltage  $\pm V_S$  is induced, for which  $I(\pm V_S) = 0$ . The double sign of the Seebeck voltage reflects the *bipolarity* of the thermoelectric effect, which is a consequence of the reciprocity of the device.

If an ac source is included in addition to the dc voltage,  $V(t) = V + a \cos(\omega t)$ , for instance by placing the junction in a microwave field, the average current is no longer simply given by Eq. (1). The time-averaged dc tunnel (charge and heat) currents  $\bar{I} = (1/T) \int_0^T dt I(t)$  and  $\bar{Q} = (1/T) \int_0^T dt \dot{Q}(t)$  take the form [20,30,50]

$$\begin{pmatrix} \bar{I} \\ \bar{Q} \end{pmatrix} = \sum_{n=-\infty}^{\infty} J_n^2\left(\frac{ea}{\hbar\omega}\right) \begin{pmatrix} I(V - n\hbar\omega/e) \\ \dot{Q}(V - n\hbar\omega/e) \end{pmatrix}, \quad (2)$$

where  $T = 2\pi/\omega$  is the period of the ac voltage. This is the standard result for PAT, where  $J_n(x)$  is the  $n$ th

Bessel function of the first kind. In Eq. (2) we assume that the frequency of the ac voltage is small enough so that it modulates the potential energy of the quasiparticles adiabatically [25,51,52]. In this approximation, the ac frequency is necessarily bounded by the plasma frequency of the two electrodes and the driving frequency needs to be  $\hbar\omega < 2\Delta$ , in order to neglect high-order processes in the current due to the direct breaking of Cooper pairs due to photon absorption. At the same time, we will mainly focus on quite small amplitudes of the voltage oscillations,  $ea \ll \Delta$ , as we will explain in Sec. III, since high amplitudes are detrimental for the thermoelectric effect restoring the usual dissipative behavior at high energies. Finally, the averaged current  $\bar{I}$  is also reciprocal,  $\bar{I}(-V) = -\bar{I}(V)$ , due to the reciprocity of the junction  $I(V)$ . For this reason, in the following, we show only results for positive biases.

### III. RESULTS

In Fig. 1(b) we show the  $\bar{I}(V)$  characteristic curve for the equilibrium case  $T_1 = T_2 = 0.4T_{c,1}$  in the presence of PAT with  $\hbar\omega = 0.1\Delta_{0,1}$  for different amplitudes. As expected for equilibrium temperatures, the junction has only a dissipative behavior and the PAT introduces different sidebands near the matching peak  $V_p$ . Indeed, if the frequency  $\hbar\omega/e$  of the ac voltage is larger than the width of the matching peak and the amplitude  $a$  is not too high (see later), we expect to see a weighted replication of the dc characteristics displaced in voltage in the sidebands. According to Eq. (2), one easily finds the position of the matching peak sidebands at  $eV = eV_p + n\hbar\omega$ ,  $n \in \mathbb{Z}$ .

In Figs. 1(c) and 1(d) we show the  $\bar{I}(V)$  characteristics when the junction is subject to a temperature difference  $T_1 = 0.7T_{c,1}$  and  $T_2 = 0$ , with  $T_{c,\alpha}$  the critical temperatures of the electrodes. The temperature difference of the electrodes has been chosen in order to maximize the thermoelectric effect, as previously stated [15]. Figures 1(c) and 1(d) show the effect of  $a$  and  $\omega$  on  $\bar{I}(V)$ , respectively. For  $a = 0$  or  $\omega = 0$  (blue line), the voltage source has no ac component, so the electric current displays the conventional behavior for a single thermoelectric peak centered at  $eV_p = \Delta_1 - \Delta_2$ . The sharpness of the thermoelectric peak depends on the phenomenological Dynes parameter, with lower  $\Gamma$  favoring sharper peaks.

As expected from Eq. (2), for a finite ac voltage source, the quasiparticle current presents multiple thermoelectric peaks which are separated periodically in voltage. As the value of  $a$  increases, the height of the main thermoelectric peak decreases in absolute value while the sidebands increase in size. Clearly, at fixed  $\omega$ , by changing the amplitude  $a$ , the weights given by the Bessel functions change such that the height of the sideband peaks change correspondingly. Physically, for  $V > 0$ , the sideband thermoelectric peaks in the averaged current correspond to



processes where photons are absorbed (emitted), respectively, for  $n < 0$  ( $n > 0$ ) to support thermoelectricity at the sideband voltages. Note that the signature of the thermoelectric peak corresponding to the sidebands can also be found in the dissipative regime as a dip of the  $\bar{I}(V)$  characteristics [see the dip at  $eV/\Delta_{0,1} \approx 0.45$  of the green line in Fig. 1(c)]. All sidebands do not necessarily become thermoelectric, being weighted by a different Bessel function and mixing different channels in the thermoelectric and dissipative regimes. In general, the  $I(V)$  characteristic at sufficiently high voltages remains in the dissipative regime.

In other words, the ac source seems to redistribute the thermoelectric power to different sidebands. This can be better quantified by looking at the integrated thermoelectric power, defined as

$$P_{\text{int}} = - \int_0^{V_S} dV \bar{I}(V), \quad (3)$$

which decreases with increasing  $a$  [see inset of Fig. 1(c)], and remains almost constant under variations of  $\omega$  (not shown). The dashed line in the inset corresponds to the power given in the small-signal limit. Indeed, when  $x = (ea/\hbar\omega) \ll 1$ , the variation of the averaged current may be obtained by expanding the Bessel functions to the lowest order  $J_0(x) \approx 1 - x^2/4$  and  $J_{\pm n}(x) \approx (\pm x/2)^n/n!$  in Eq. (2), and retaining only  $x^2$  terms; one finds the current variation  $\Delta\bar{I} = (ea/(2\hbar\omega))^2 [I(V + \hbar\omega/e) - 2I(V) + I(V - \hbar\omega/e)]$ . This is physically equivalent to retaining only the contribution of the first two sidebands with  $n = \pm 1$  [25]. This simple approximation already shows that  $P_{\text{int}}$  is indeed reduced by increasing the amplitude  $a$ . Furthermore, when the amplitude becomes comparable to the matching peak voltage  $V_p$ , the ac signal starts to explore points of the  $I(V)$  characteristic curve with positive current ( $I > 0$ ) and the averaged thermocurrent needs to be correspondingly suppressed.

The previous discussion shows that the PAT in general just redistributes the thermoelectric power but does not increase, on average, the intrinsic thermoelectric capabilities of the junction. This is not unexpected, since also for the cooling properties of normal-metal–insulator–superconductor tunnel junctions a similar result is observed for the cooling capabilities in the presence of PAT [53–56]. However, the redistribution due to PAT determines new values of voltages (sidebands) where the system is strongly thermoelectric for biases where the thermoelectric performance was originally smaller. For such particular values of the bias, one observes a microwave *enhanced* bipolar thermoelectricity. Furthermore, in the absence of an ac source, the thermoelectric peaks can be very narrow in voltage range, so a change in the operating point (dc voltage) could result in a drastic reduction of the thermoelectric power. This may happen,

for example, with a change in the load resistance when the junction operates as a thermoelectric generator. The ac source widening the  $\bar{I}(V)$  characteristic thermoelectric curve reduces the issue of a precise biasing. At the same time, it allows one to tune the voltages where the thermoelectric effect is maximized by varying  $\omega$ , and in this way it increases the tunability of the device. In other words, there are regimes in the biases where the thermoelectricity is literally microwave-assisted, showing a unique interplay between thermoelectricity and coherent absorption and emission of photons. This increased tunability and better performance at specific biases may be relevant for some specific applications. Furthermore, we expect that the photon detection in  $S$ - $I$ - $S'$  junctions can be quantum-limited [36,37], analogously to what has been reported for tunnel junctions in the equilibrium (dissipative) case [24,25].

In Fig. 2 we analyze the power generated by the thermoelectric effect. Figure 2(a) shows the maximum power for a given  $a$  and  $\omega$ , i.e., the point of the  $\bar{I}$  characteristic curve which maximizes the thermoelectric power  $P = \max_V(-\bar{I}(V)V)$ . For low values of  $a$ , the maximum power still coincides with the central peak. But increasing the amplitude of the ac source decreases the depth of the central peak, reducing the maximum power accordingly. Above a certain amplitude, roughly delimited by the lower dashed line in Fig. 2(a), the maximum power shows an oscillatory behavior. This dashed line represents the points where the weight of the first terms in the series given by Eq. (2) becomes greater than the zeroth term with increasing amplitude, i.e.,  $J_1(ea/\hbar\omega) = J_0(ea/\hbar\omega)$  for  $ea/\hbar\omega = 1.43$ . Therefore, above this line, the maximum power can also be found in one of the sidebands. In the presence of PAT, the power of the sidebands varies significantly with  $\omega$ , generating this complex oscillatory behavior presented in Fig. 2(a). The middle ( $ea/\hbar\omega = 2.63$ ) and upper ( $ea/\hbar\omega = 3.77$ ) dashed lines correspond to the boundaries where the second ( $|n| = 2$ ) and third ( $|n| = 3$ ) terms, respectively, become predominant in Eq. (2). As shown in Fig. 2(a), there is a shift of the oscillating pattern delimited by the middle dashed line, and the oscillating behavior almost vanishes above the upper line.

In Fig. 2(b) we show the Seebeck voltage  $V_S$  dependence on the amplitude  $a$  taken at different frequencies  $\omega$ . It can be seen that  $V_S$  increases in steps by increasing the amplitude. As discussed above, the influence of  $a$  on the thermoelectric effect is to redistribute the power to other voltages by increasing the number of thermoelectric sideband peaks. Each step is associated with the contribution of additional sidebands which, once they cross the  $\bar{I} = 0$  line, shift the Seebeck voltage sharply. However, beyond a certain value of  $a$ , as discussed above, the suppression of the thermoelectric effect leads to a drop of the Seebeck voltage, as shown by the  $\hbar\omega = 0.06\Delta_{0,1}$  (blue) line.

The  $S$ - $I$ - $S'$  junction can be used as a thermoelectric power source by replacing the external dc voltage source

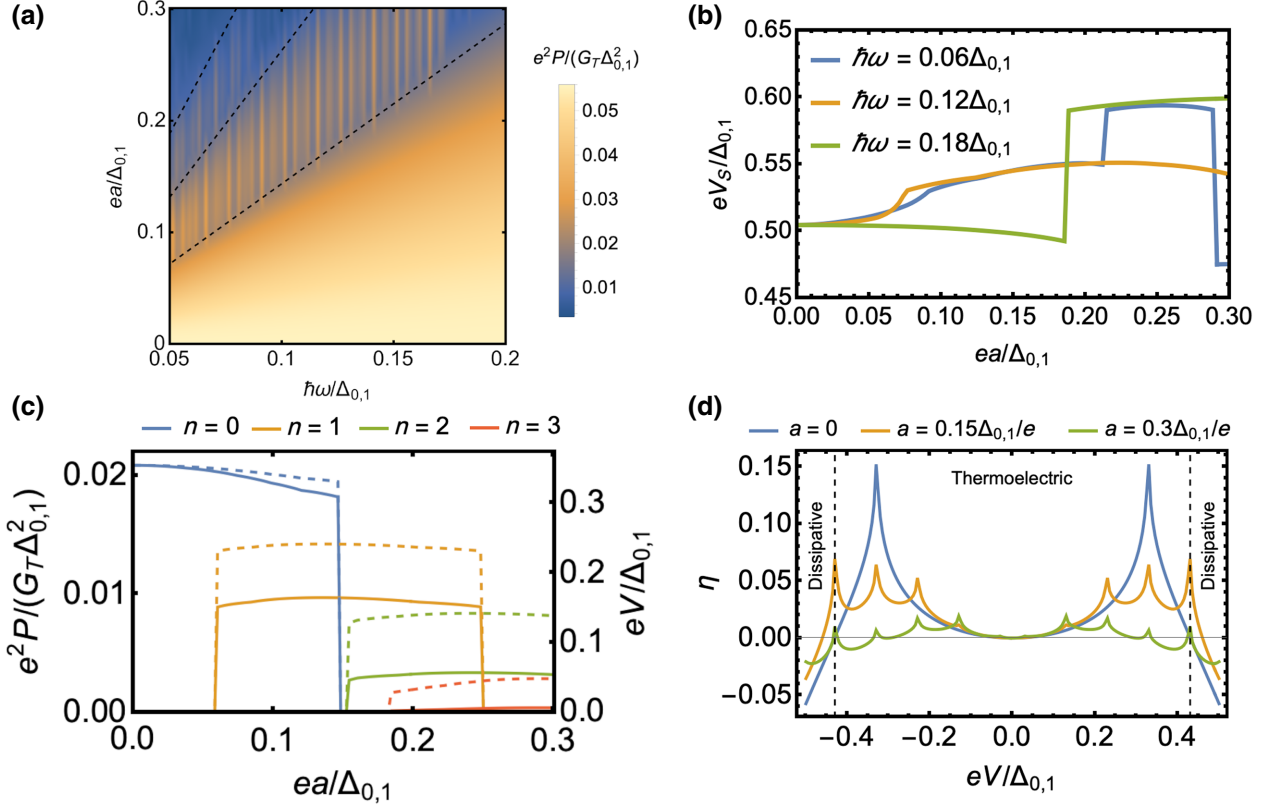


FIG. 2. (a) Maximum power and (b) Seebeck voltage as functions of the amplitude and angular frequency of the ac field. (c) Power (solid) and voltage (dashed) of the stable points of the  $\bar{I}(V)$  characteristic curve for a fixed load  $R = 6G_T^{-1}$ . (d) Efficiency  $\eta$  of the thermoelectric effect. In panels (c) and (d), the frequency is set to  $\hbar\omega = 0.1\Delta_{0,1}$ . The temperatures of the superconducting electrodes are  $T_1 = 0.7T_{c,1}$  and  $T_2 = 0$  for panels (a), (c), and (d), and  $T_1 = 0.6T_{c,1}$  and  $T_2 = 0$  for panel (b).

with a resistive load  $R$ . Ohm's law constrains the values that the current and the voltage can take, so that the current can only flow when the junction operates as a thermoelectric generator. The operating points are determined by the intersection of the  $\bar{I}(V)$  characteristic curve with a line of slope  $-1/R$ . Similarly to the purely dc case, only the solutions with a *positive*  $d\bar{I}/dV$  are stable in the presence of PAT [15,16,18]. As shown in Fig. 2(c), the inclusion of an ac voltage source allows also for multiple stable working points which appear at different voltages (dashed lines) and consequently different powers (solid lines). In the example, we consider a load value of  $R = 6G_T^{-1}$ . For certain ac amplitudes we get multiple stable points labeled with different  $n$ . The  $n = 0$  (blue) line corresponds to the solution associated with the matching peak, while the  $n = 1, 2, 3$  lines correspond to sidebands with a lower voltage. It is possible to find stable points with a higher voltage by choosing a higher load resistance (not shown). For  $0.06 < ea/\Delta_{0,1} < 0.15$ , one can find two stable working points for  $n = 0$  (blue), due to the main peak, and  $n = 1$  (yellow), corresponding to the first sideband. The system can be driven to the stable working points by applying current pulses similarly to what has been realized

in Ref. [18] in the absence of any ac signal. Therefore, PAT can be used to design devices with an increased number of states occurring at different voltages. This, for example, would increase the number of logic states of the proposed thermoelectric volatile memory [57–59].

Figure 2(d) shows the thermal efficiency  $\eta = \dot{W}/\dot{Q}_1$ , which describes the ratio of the net work output to the heat input, for different values of  $a$ . As in the case of the power, the inclusion of an ac source does not offer a way to increase globally the maximum efficiency. However, the widening of the curves is beneficial to avoid efficiency drops stemming from changes in the voltage operating point. The dashed vertical lines in Fig. 2(d) show the area where the system is thermoelectric  $V < V_S$ , and where it is dissipative in the absence of the ac signal. We see that PAT *widens* the voltage values where the system is thermoelectric. The ac signal leads to a moderate efficiency reduction at the matching peak, but it increases its efficiency for certain values of  $V$ .

Finally, in Fig. 3 we investigate the cooling power of the  $S$ - $I$ - $S'$  junction. By applying an external bias, for specific temperature conditions [16], it is possible to extract heat and reduce the electronic temperature of the lower-gap

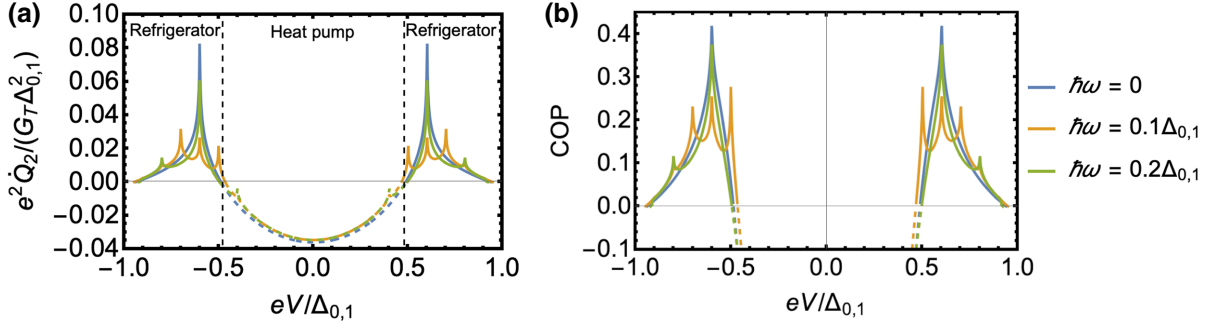


FIG. 3. (a) Heat current (cooling power) extracted from the right (cold) superconducting electrode in the cooling regime and (b) coefficient of performance (COP) for different frequencies. The amplitude of the ac voltage is set to  $ea = 0.15\Delta_{0,1}$ . The temperatures of the superconducting electrodes are  $T_1 = 0.5T_{c,1}$  and  $T_2 = 0.4T_{c,1}$ .

superconductor [16,43,54]. In Fig. 3(a) we show the heat extracted from the lower-gap superconductor for temperatures  $T_1 = 0.5T_{c,1}$  and  $T_2 = 0.4T_{c,1}$ . The voltage range where there is no cooling is represented by dashed lines. If the applied voltage is small, the system does not reach the cooling regime and the heat flows from the hot to the cold terminal. The cooling shares some similarities with the thermoelectric effect; it requires the hot superconductor to possess a larger gap than the cold superconductor and the cooling power is maximized at voltage bias  $eV = \Delta_1 - \Delta_2$ . With PAT, the ac voltage source creates additional sidebands to the cooler, *widening* the window where the cooling is possible [53]. Figure 3(b) shows the coefficient of performance  $\text{COP} = -\dot{Q}_2/\dot{W}$ , which describes the efficiency of the extracted heat with respect to the applied work. Similarly to the thermoelectric efficiency, the maximum COP is slightly suppressed by the presence of PAT since also in this case the PAT will not increase globally the efficiency of the system but will redistribute the cooling capabilities over different cooling sidebands. Analogously to the thermoelectricity, there are specific values of the bias where the cooling is microwave-enhanced.

#### IV. CONCLUSIONS

In this work, we have discussed the influence of photon-assisted tunneling on the bipolar thermoelectric effect occurring in an  $S$ - $I$ - $S'$  tunnel junction. The ac voltage source leads to a weighted replication of the bipolar thermoelectric dc characteristic curve displaced in voltages. This leads to the appearance of sidebands whose position is determined by the frequency of the ac field. The redistribution of the power to other voltages leads globally to a reduction of the net thermopower output of the matching peak, but it broadens the thermoelectric region, potentially increasing even the obtainable Seebeck voltage. Therefore, changes in the operating point of the junction will have a less dramatic effect over the thermoelectric performance. We have specifically investigated how this redistribution mechanism of the bipolar thermoelectricity

is influenced by the ac signal amplitude. The photon emission and absorption sidebands for the bipolar thermoelectricity constitute, in a certain sense, *microwave-assisted thermoelectricity*. The thermoelectric power and the efficiency for some specific values of the voltages is even enhanced.

Furthermore, the system can be driven to the additional stable working points selected by the sidebands, so PAT can be used to design devices with an increased number of states at different voltages, potentially increasing the number of logic states of a thermoelectric volatile memory [57–59].

Finally, we have studied the influence of PAT on the cooling performance of the junction. Similar to the thermoelectric effect, the cooling power is also influenced by the presence of PAT, and the redistribution of the cooling capabilities into sidebands also allows one to increase the COP at specific voltages.

From the fundamental point of view, this application shows the intriguing interplay between thermoelectricity and coherent photon absorption and emission in an experimentally accessible setup. We think that the obtained results could be relevant for quantum-limited microwave detection [18,19], quantum sensing, and microwave-superconducting technologies.

#### ACKNOWLEDGMENTS

A.H. acknowledges funding from the University of the Basque Country (Project PIF20/05). F.S.B. acknowledges financial support from Spanish AEI through projects PID2020-114252GB-I00 (SPIRIT) and TED2021-130292B-C42, the Basque Government through Grant No. IT-1591-22, and the A. v. Humboldt Foundation. F.S.B. and F.G. acknowledge the EU Horizon 2020 Research and Innovation Framework Programme under Grant No. 800923 (SUPERTED). F.G. and A.B. acknowledge the EU Horizon 2020 Research and Innovation Framework Programme under Grants No. 964398 (SUPERGATE) and No. 101057977 (SPECTRUM). A.B.

acknowledges the Royal Society through the International Exchanges between the UK and Italy (Grants No. IEC R2 192166 and No. IEC R2 212041).




- 
- [1] F. S. Bergeret, M. Silaev, P. Virtanen, and T. T. Heikkilä, Colloquium: Nonequilibrium effects in superconductors with a spin-splitting field, *Rev. Mod. Phys.* **90**, 041001 (2018).
- [2] T. T. Heikkilä, M. Silaev, P. Virtanen, and F. S. Bergeret, Thermal, electric and spin transport in superconductor/ferromagnetic-insulator structures, *Prog. Surf. Sci.* **94**, 100540 (2019).
- [3] P. Machon, M. Eschrig, and W. Belzig, Nonlocal Thermoelectric Effects and Nonlocal Onsager Relations in a Three-Terminal Proximity-Coupled Superconductor-Ferromagnet Device, *Phys. Rev. Lett.* **110**, 047002 (2013).
- [4] A. Ozaeta, P. Virtanen, F. Bergeret, and T. Heikkilä, Predicted Very Large Thermoelectric Effect in Ferromagnet-Superconductor Junctions in the Presence of a Spin-Splitting Magnetic Field, *Phys. Rev. Lett.* **112**, 057001 (2014).
- [5] S. Kolenda, M. J. Wolf, and D. Beckmann, Observation of Thermoelectric Currents in High-Field Superconductor-Ferromagnet Tunnel Junctions, *Phys. Rev. Lett.* **116**, 097001 (2016).
- [6] T. T. Heikkilä, R. Ojajarvi, I. J. Maasilta, E. Strambini, F. Giazotto, and F. S. Bergeret, Thermoelectric Radiation Detector based on Superconductor-Ferromagnet Systems, *Phys. Rev. Appl.* **10**, 034053 (2018).
- [7] S. Chakraborty and T. T. Heikkilä, Thermoelectric radiation detector based on a superconductor-ferromagnet junction: Calorimetric regime, *J. Appl. Phys.* **124**, 123902 (2018).
- [8] E. Strambini, M. Spies, N. Ligato, S. Ilić, M. Rouco, C. González-Orellana, M. Ilyn, C. Rogero, F. Bergeret, J. Moodera, *et al.*, Superconducting spintronic tunnel diode, *Nat. Commun.* **13**, 1 (2022).
- [9] Z. Geng and I. J. Maasilta, Analytical models for the pulse shape of a superconductor-ferromagnet tunnel junction thermoelectric microcalorimeter, *J. Low Temp. Phys.* **209**, 419 (2022).
- [10] R. Meservey and P. Tedrow, Spin-polarized electron tunneling, *Phys. Rep.* **238**, 173 (1994).
- [11] J. S. Moodera, T. S. Santos, and T. Nagahama, The phenomena of spin-filter tunnelling, *J. Phys.: Condens. Matter* **19**, 165202 (2007).
- [12] G.-X. Miao, J. Chang, B. A. Assaf, D. Heiman, and J. S. Moodera, Spin regulation in composite spin-filter barrier devices, *Nat. Commun.* **5**, 3682 (2014).
- [13] G. De Simoni, E. Strambini, J. S. Moodera, F. S. Bergeret, and F. Giazotto, Toward the absolute spin-valve effect in superconducting tunnel junctions, *Nano Lett.* **18**, 6369 (2018).
- [14] J. P. Morten, A. Brataas, and W. Belzig, Spin transport and magnetoresistance in ferromagnet/superconductor/ferromagnet spin valves, *Phys. Rev. B* **72**, 014510 (2005).
- [15] G. Marchegiani, A. Braggio, and F. Giazotto, Nonlinear Thermoelectricity with Electron-Hole Symmetric Systems, *Phys. Rev. Lett.* **124**, 106801 (2020).
- [16] G. Marchegiani, A. Braggio, and F. Giazotto, Superconducting nonlinear thermoelectric heat engine, *Phys. Rev. B* **101**, 214509 (2020).
- [17] G. Marchegiani, A. Braggio, and F. Giazotto, Phase-tunable thermoelectricity in a Josephson junction, *Phys. Rev. Res.* **2**, 043091 (2020).
- [18] G. Germanese, F. Paolucci, G. Marchegiani, A. Braggio, and F. Giazotto, Bipolar thermoelectric Josephson engine, *Nat. Nanotechnol.* **17**, 1084 (2022).
- [19] G. Germanese, F. Paolucci, G. Marchegiani, A. Braggio, and F. Giazotto, Phase Control of Bipolar Thermoelectricity in Josephson Tunnel Junctions, *Phys. Rev. Appl.* **19**, 014074 (2023).
- [20] P. K. Tien and J. P. Gordon, Multiphoton process observed in the interaction of microwave fields with the tunneling between superconductor films, *Phys. Rev.* **129**, 647 (1963).
- [21] J. N. Sweet and G. I. Rochlin, Microwave-photon-assisted tunneling in Sn-I-Sn superconducting tunnel junctions, *Phys. Rev. B* **2**, 656 (1970).
- [22] C. A. Hamilton and S. Shapiro, rf-induced effects in superconducting tunnel junctions, *Phys. Rev. B* **2**, 4494 (1970).
- [23] B. Kofoed, U. K. Poulsen, and K. Saermark, Microwave-assisted tunnelling effects in small-area thin-film superconducting tunnel junctions, *Phys. Status Solidi A* **23**, 87 (1974).
- [24] J. Tucker, Quantum limited detection in tunnel junction mixers, *IEEE J. Quantum Electron.* **15**, 1234 (1979).
- [25] J. R. Tucker and M. J. Feldman, Quantum detection at millimeter wavelengths, *Rev. Mod. Phys.* **57**, 1055 (1985).
- [26] K. Hamasaki, K. Yoshida, F. Irie, and K. Enpuku, Capacitance measurement of Josephson tunnel junctions with microwave-induced dc quasiparticle tunneling currents, *J. Appl. Phys.* **53**, 3713 (1982).
- [27] S. P. Kashinje and P. Wyder, Photon-assisted tunnelling in a magnetic field, *J. Phys. C: Solid State Phys.* **19**, 3193 (1986).
- [28] Q.-f. Sun, J. Wang, and T.-h. Lin, Photon-assisted Andreev tunneling through a mesoscopic hybrid system, *Phys. Rev. B* **59**, 13126 (1999).
- [29] B. Leone, J. Gao, T. Klapwijk, B. Jackson, W. Laauwen, and G. de Lange, Hot electron effect in terahertz hybrid devices, *IEEE Trans. Appl. Supercond.* **11**, 649 (2001).
- [30] P. Kot, R. Drost, M. Uhl, J. Ankerhold, J. C. Cuevas, and C. R. Ast, Microwave-assisted tunneling and interference effects in superconducting junctions under fast driving signals, *Phys. Rev. B* **101**, 134507 (2020).
- [31] M. Houzet, K. Serniak, G. Catelani, M. H. Devoret, and L. I. Glazman, Photon-Assisted Charge-Parity Jumps in a Superconducting Qubit, *Phys. Rev. Lett.* **123**, 107704 (2019).
- [32] X. Pan, Y. Zhou, H. Yuan, L. Nie, W. Wei, L. Zhang, J. Li, S. Liu, Z. H. Jiang, G. Catelani, L. Hu, F. Yan, and D. Yu, Engineering superconducting qubits to reduce quasiparticles and charge noise, *Nat. Commun.* **13**, 7196 (2022).

- [33] C.-H. Liu, D. C. Harrison, S. Patel, C. D. Wilen, O. Rafferty, A. Shearow, A. Ballard, V. Iaia, J. Ku, B. L. T. Plourde, and R. McDermott, Quasiparticle poisoning of superconducting qubits from resonant absorption of pair-breaking photons, [ArXiv:2203.06577](#) (2022)
- [34] S. Diamond, V. Fatemi, M. Hays, H. Nho, P. D. Kurilovich, T. Connolly, V. R. Joshi, K. Serniak, L. Frunzio, L. I. Glazman, and M. H. Devoret, Distinguishing Parity-Switching Mechanisms in a Superconducting Qubit, [PRX Quantum](#) **3**, 040304 (2022).
- [35] G. Marchegiani, L. Amico, and G. Catelani, Quasiparticles in Superconducting Qubits with Asymmetric Junctions, [PRX Quantum](#) **3**, 040338 (2022).
- [36] F. Paolucci, G. Germanese, A. Braggio, and F. Giazotto, A highly-sensitive broadband superconducting thermoelectric single-photon detector, [ArXiv:2302.02933](#) (2023)
- [37] G. Germanese, F. Paolucci, A. Braggio, and F. Giazotto, Broadband passive superconducting thermoelectric single-photon detector, Patent (06/02/2023), Filing number: 102023000001854.
- [38] A. Barone and G. Paternò, *Physics and Applications of the Josephson Effect* (Wiley, New York, 1982), p. 35. (Chapter 2)
- [39] B. Josephson, Possible new effects in superconductive tunnelling, [Phys. Lett.](#) **1**, 251 (1962).
- [40] R. E. Harris, Cosine and other terms in the Josephson tunneling current, [Phys. Rev. B](#) **10**, 84 (1974).
- [41] D. R. Gulevich, V. P. Koshelets, and F. V. Kusmartsev, Josephson flux-flow oscillator: The microscopic tunneling approach, [Phys. Rev. B](#) **96**, 024515 (2017).
- [42] A. Barone, G. Paternò, M. Russo, and R. Vaglio, Light-induced transition from “small” to “large” Josephson junctions, [Phys. Lett. A](#) **53**, 393 (1975).
- [43] F. Giazotto, T. T. Heikkilä, A. Luukanen, A. M. Savin, and J. P. Pekola, Opportunities for mesoscopics in thermometry and refrigeration: Physics and applications, [Rev. Mod. Phys.](#) **78**, 217 (2006).
- [44] A. Fornieri and F. Giazotto, Towards phase-coherent caloritronics in superconducting circuits, [Nat. Nanotechnol.](#) **12**, 944 (2017).
- [45] R. C. Dynes, V. Narayanamurti, and J. P. Garno, Direct Measurement of Quasiparticle-Lifetime Broadening in a Strong-Coupled Superconductor, [Phys. Rev. Lett.](#) **41**, 1509 (1978).
- [46] F. Giazotto, T. T. Heikkilä, F. Taddei, R. Fazio, J. P. Pekola, and F. Beltram, Tailoring Josephson Coupling through Superconductivity-Induced Nonequilibrium, [Phys. Rev. Lett.](#) **92**, 137001 (2004).
- [47] A. V. Timofeev, C. P. García, N. B. Kopnin, A. M. Savin, M. Meschke, F. Giazotto, and J. P. Pekola, Recombination-Limited Energy Relaxation in a Bardeen-Cooper-Schrieffer Superconductor, [Phys. Rev. Lett.](#) **102**, 017003 (2009).
- [48] M. J. Martínez-Pérez, A. Fornieri, and F. Giazotto, Rectification of electronic heat current by a hybrid thermal diode, [Nat. Nanotechnol.](#) **10**, 303 (2015).
- [49] J. K. Julin, S. Chaudhuri, M. Laitinen, T. Sajavaara, and I. J. Maasilta, Stability, sub-gap current,  $1/f$ -noise, and elemental depth profiling of annealed Al:Mn-AlO<sub>x</sub>-Al normal metal-insulator-superconducting tunnel junctions, [AIP Adv.](#) **6**, 125026 (2016).
- [50] G. Falci, V. Bubanja, and G. Schön, Quasiparticle and Cooper pair tunneling in small capacitance Josephson junctions, [Z. Phys. B Condens. Matter](#) **85**, 451 (1991).
- [51] N. S. Wingreen, A.-P. Jauho, and Y. Meir, Time-dependent transport through a mesoscopic structure, [Phys. Rev. B](#) **48**, 8487 (1993).
- [52] A.-P. Jauho, N. S. Wingreen, and Y. Meir, Time-dependent transport in interacting and noninteracting resonant-tunneling systems, [Phys. Rev. B](#) **50**, 5528 (1994).
- [53] N. B. Kopnin, F. Taddei, J. P. Pekola, and F. Giazotto, Influence of photon-assisted tunneling on heat flow in a normal metal-superconductor tunnel junction, [Phys. Rev. B](#) **77**, 104517 (2008).
- [54] J. T. Muhonen, M. Meschke, and J. P. Pekola, Micrometre-scale refrigerators, [Rep. Prog. Phys.](#) **75**, 046501 (2012).
- [55] K. Y. Tan, M. Partanen, R. E. Lake, J. Govenius, S. Masuda, and M. Möttönen, Quantum-circuit refrigerator, [Nat. Commun.](#) **8**, 15189 (2017).
- [56] M. Silveri, H. Grabert, S. Masuda, K. Y. Tan, and M. Möttönen, Theory of quantum-circuit refrigeration by photon-assisted electron tunneling, [Phys. Rev. B](#) **96**, 094524 (2017).
- [57] F. Giazotto, F. Paolucci, A. Braggio, G. Marchegiani, and G. Germanese, Superconducting bipolar thermoelectric memory and method for writing a superconducting bipolar thermoelectric memory, Patent (21/12/2021), Filing number: 102021000032042.
- [58] G. Marchegiani, A. Braggio, and F. Giazotto, Noise effects in the nonlinear thermoelectricity of a Josephson junction, [Appl. Phys. Lett.](#) **117**, 212601 (2020).
- [59] C. Guarcello, P. Solinas, A. Braggio, M. Di Ventra, and F. Giazotto, Josephson Thermal Memory, [Phys. Rev. Appl.](#) **9**, 014021 (2018).



## Chapter 7

# Dynamical Hall responses of disordered superconductors

**Dynamical Hall responses of disordered superconductors**Alberto Hijano <sup>1,2,\*</sup> Sakineh Vosoughi-nia <sup>3,4,5,†</sup> F. Sebastián Bergeret,<sup>1,6</sup> Pauli Virtanen,<sup>3</sup> and Tero T. Heikkilä <sup>3,‡</sup><sup>1</sup>*Centro de Física de Materiales Centro Mixto CSIC-UPV/EHU, E-20018 Donostia–San Sebastián, Spain*<sup>2</sup>*Department of Condensed Matter Physics, University of the Basque Country UPV/EHU, 48080 Bilbao, Spain*<sup>3</sup>*Department of Physics and Nanoscience Center, University of Jyväskylä, P.O. Box 35 (YFL), FI-40014 Jyväskylä, Finland*<sup>4</sup>*AGH University of Krakow, Academic Centre for Materials and Nanotechnology, al. A. Mickiewicza 30, 30-059 Krakow, Poland*<sup>5</sup>*Institute of Physics, Marie Curie-Skłodowska University, 20-031 Lublin, Poland*<sup>6</sup>*Donostia International Physics Center, 20018 Donostia–San Sebastián, Spain*

(Received 30 June 2023; accepted 7 September 2023; published 19 September 2023)

We extend the Mattis-Bardeen theory for the dynamical response of superconductors to include different types of Hall responses. This is possible thanks to a recent modification of the quasiclassical Usadel equation, which allows for analyzing Hall effects in disordered superconductors and including the precise frequency dependence of such effects. Our results form a basis for analyzing dynamical experiments especially on novel thin-film superconductors, where ordinary Hall and spin Hall effects can both show up.

DOI: [10.1103/PhysRevB.108.104506](https://doi.org/10.1103/PhysRevB.108.104506)**I. INTRODUCTION**

Simultaneous application of electric and magnetic fields on a conductor leads to the presence of a charge current with a transverse component perpendicular to both fields, in addition to the ordinary longitudinal current in the direction of the electric field. This ordinary Hall effect has been known since the 19th century [1] and it can be directly incorporated into the Drude model [2,3] of electronic conduction once the Lorentz force due to the magnetic field is included. Varying the electric field in time leads to similarly varying longitudinal and transverse charge currents [4]. This dynamical Hall effect can be observed for example in optical spectroscopy via the Faraday-Kerr rotation of the polarization state of light [5,6]. For frequencies low compared to the scattering rate and for materials in their normal state, both longitudinal and Hall currents are in phase with the electric field. This is in contrast with the superconducting state [7], featuring both in-phase and out-of-phase contributions. For the longitudinal response, the former describes electronic transitions and features a superconducting gap at low temperatures, whereas the latter results from the supercurrent. Despite some attempts over the years [8,9] based on phenomenological two-fluid models and Bardeen-Cooper-Schrieffer (BCS) theory, to our knowledge the microscopic extension of the Drude model for the dynamical Hall response in superconductors in the dirty limit has not been presented before. We fill this gap by deriving the frequency dependent linear conductivity of dirty superconductors in the presence of the Hall effect and discuss how the in- and out-of-phase parts of the transverse response show up

in the amplitude and phase of the frequency dependent Kerr response of such materials.

In type II superconductors, motion of vortices and the flux they carry gives additional contributions to the Hall effect [10–13]. By now, especially in the steady state, these effects are well studied. Here we consider situations below the critical field in which no vortices are present, concentrating on the time-dependent response in the uniform gapped state.

In the presence of spin-orbit interaction, another type of Hall effect called the spin Hall effect occurs [14]. It involves the generation of a transverse spin current in response to a charge current. There are two major mechanisms for this spin Hall effect: in the *intrinsic* mechanism, it is produced by the inversion symmetry breaking either due to the lattice (Dresselhaus spin-orbit coupling (SOC) [15]) or the sample structure (Rashba spin-orbit coupling [16]), and in the *extrinsic* mechanism it results from the spin dependence of the scattering.

In superconductors, the spin Hall effect couples (equilibrium) supercurrents and spin [17–21]. In addition, superconductors show also a quasiparticle spin Hall effect, which behaves otherwise similar to the normal-state version but depends strongly on temperature. Vortex motion can also generate it [22]. In this paper, we examine the dynamical spin Hall response in superconductors and show how it also contains in- and out-of-phase contributions similar to the longitudinal current response. In the normal state, our frequency dependent results are consistent with the literature predictions [23,24], where the intrinsic spin Hall current is maximal at frequencies comparable with the spin-relaxation rate, whereas the extrinsic mechanism produces spin Hall response also at low frequencies. Superconductivity actually provides a tool for probing these different mechanisms as in the intrinsic case it leads to strongly temperature dependent spin Hall responses. Hence, whereas the frequency dependence may be difficult to probe on a wide scale of the order of the spin-relaxation rate,

\*alberto.hijano@ehu.es

†sakineh.vosoughi@gmail.com

‡tero.t.heikkila@jyu.fi



in the superconducting case one may fix the frequency and rather vary the temperature. Such studies may then provide information about the nature of the relevant mechanisms for the spin Hall effect.

Our paper is based on the recent extensions of the quasi-classical Usadel equation to govern ordinary and spin Hall effects [25,26], both in the extrinsic and intrinsic cases. We utilize these extensions here to study those dynamic responses. The dynamical Hall effect can be studied on conventional spin singlet superconductors in the presence of the time-independent magnetic field. Because of Meissner screening, it shows up as a surface effect, but the same is true for the normal state because of the finite skin depth. On the other hand, the spin Hall effects require strong spin-orbit interaction and are especially interesting in thin-film systems involving either heavy-metal superconductors or the presence of a nearby heavy metal in which case the spin-orbit coupling would enter as a proximity effect. On the other hand, our paper provides a baseline to compare the results of dynamical experiments on frequency dependent electromagnetic susceptibility of two-dimensional superconductors where possible spin ordering or orbital degrees of freedom may complicate the dynamic response.

Our paper is organized as follows. In Sec. II we outline the theory for describing the various Hall effects in superconductors by introducing ordinary and SU(2) vector potentials and the accompanying field strength tensor terms into the Usadel equation. In Sec. III we analyze the symmetry properties of the resulting dynamical response matrix. This section uses dynamical SU(2) fields as a formal tool for uncovering those symmetries. Section IV shows how the ordinary Mattis-Bardeen response [7] naturally comes from our formalism. Then Sec. V discusses the dynamical Hall response, and Secs. VI and VII discuss the dynamical spin Hall and inverse spin Hall responses in superconductors. Finally, Sec. VIII discusses the results and possible extensions of the theory to new materials.

## II. THEORY OF HALL EFFECTS IN DISORDERED SUPERCONDUCTORS

In this section, we introduce the specific scenarios and main equations used in this paper. Our paper encompasses a broad scope, focusing on superconductors subjected to electromagnetic fields, alongside exchange fields and linear-in-momentum spin-orbit coupling, which can be treated as effective SU(2) potentials [27]. These can be described by the following Hamiltonian:

$$\mathcal{H} = \frac{(\mathbf{p} - \check{\mathbf{A}})^2}{2m} - \mu_{\text{ch}} + V_{\text{imp}} + \tau_3 \check{A}^0 - i\check{\Delta}, \quad (1)$$

where  $\mathbf{p}$  is the momentum,  $m$  is the electron mass,  $\mu_{\text{ch}}$  is the chemical potential,  $\check{\Delta} = \Delta\tau_1$  is the superconducting order parameter for  $s$ -wave superconductors, and  $\sigma_j$  and  $\tau_j$  are the Pauli matrices in spin and Nambu spaces, respectively.  $V_{\text{imp}}$  is a random impurity potential that consists of the usual elastic scattering and the spin-orbit interaction [25,28,29].  $\check{A}^\mu$  is the generalized four-potential containing both U(1) and SU(2)

components [30–32] given by

$$\check{A}^0 = -e\phi\tau_3 + \frac{\hbar}{2}A^{0j}\sigma_j, \quad (2a)$$

$$\check{A}^i = -eA^i\tau_3 + \frac{\hbar}{2}A^{ij}\sigma_j. \quad (2b)$$

$\phi$  and  $\mathbf{A}$  are the usual U(1) scalar and vector electromagnetic potentials, while  $A^{0j}$  and  $A^{ij}$  are SU(2) potentials describing the Zeeman or exchange field and the linear-in-momentum SOC, respectively [24]. Here and below a sum over repeated indices is assumed.

As in conventional electrodynamics we can define the field strength associated with  $\check{A}$ :

$$\check{F}^{\mu\nu} = \partial^\mu \check{A}^\nu - \partial^\nu \check{A}^\mu - \frac{i}{\hbar}[\check{A}^\mu, \check{A}^\nu]. \quad (3)$$

The last commutator appears because of the fact that the SU(2) components are non-Abelian. Here and below Greek indices range  $\mu = 0, 1, 2, 3$ .

In what follows, we are interested in the currents (charge and spin) generated by the electric field, which is given by the  $\check{E}^j \equiv \check{F}^{0j} = -eE^j\tau_3 + (\hbar/2)E^{jl}\sigma_l$  components of the field strength tensor (3), where the Latin indices range  $j = 1, 2, 3$ . In the linear response regime the current and the field are related via the response tensor:

$$j^{i\mu}(\omega) = \sigma^{i\mu, j\nu}(\omega)E^{j\nu}(\omega). \quad (4)$$

Here  $j^{i0}$  are the components of the charge current whereas  $j^{ij}$  is the spin-current tensor. The usual U(1) electric field is given by  $E^j \equiv E^{j0}$ , and  $E^{jl}$  denote the components of the SU(2) electric field. The real part of  $\sigma^{i\mu, j\nu}$  describes the in-phase response, and the imaginary part is the out-of-phase response of the current to the field.

Our goal is to find the conductivity tensor  $\sigma^{i\mu, j\nu}(\omega)$  in diffusive superconducting systems showing different types of Hall effects. For this we use the quasiclassical approach generalized in Refs. [25,26] to include SOC.

To describe the transport properties of the system we use the gauge covariant quasiclassical Green's function (GF) formalism. The GF  $\check{g}(t, t')$  is an  $8 \times 8$  matrix in Keldysh-Nambu-spin space [33–35],  $\check{g} = \begin{pmatrix} \check{g}^R & \check{g}^K \\ 0 & \check{g}^A \end{pmatrix}$ , where the Keldysh GF  $\check{g}^K = \check{g}^R \cdot \check{h} - \check{h} \cdot \check{g}^A$  describes the nonequilibrium properties of the system. Here,  $\check{h}$  is the distribution function and the center dot is used to denote a convolution in time, i.e., integration in the intermediate time variable. The caron symbol, e.g., in  $\check{g}$ , denotes matrices in Keldysh  $\otimes$  Nambu  $\otimes$  spin or Nambu  $\otimes$  spin space. The quasiclassical GF satisfies the normalization condition  $\check{g} \cdot \check{g} = \delta(t - t')$ .

In systems with time translational symmetry, the Green's function can be Fourier transformed in the  $\tau = t - t'$  variable into the energy domain as

$$\check{g}(\varepsilon) = \int d\tau e^{i\varepsilon\tau/\hbar} \check{g}(\tau). \quad (5)$$

For a bulk superconductor the retarded and advanced GFs in the energy domain are given by

$$\check{g}_0^{R/A}(\varepsilon) = g_0(\varepsilon)\tau_3 + f_0(\varepsilon)\tau_1, \quad (6)$$

where  $g_0$  and  $f_0$  are the normal and anomalous parts of the bulk GF,

$$g_0(\varepsilon) = \frac{-i(\varepsilon \pm i\Gamma)}{\sqrt{\Delta^2 - (\varepsilon \pm i\Gamma)^2}}, \quad (7a)$$

$$f_0(\varepsilon) = \frac{\Delta}{\sqrt{\Delta^2 - (\varepsilon \pm i\Gamma)^2}}, \quad (7b)$$

and the equilibrium distribution function is given by  $\check{h}(\varepsilon) = \tanh \frac{\varepsilon}{2k_B T}$ . The upper and lower signs correspond to the retarded and advanced GFs respectively. The convergence factor  $\Gamma \rightarrow 0^+$  guarantees that the retarded (advanced) GF is zero for negative (positive) time  $t - t'$ . Nonetheless, a finite  $\Gamma$  may also describe inelastic scattering effects present in real materials [36]. Such inelastic processes are responsible for the smoothing of the density of states peaks at the superconducting gap. The order parameter  $\Delta(T)$  needs to be computed self-consistently [12] with the gap equation

$$\Delta \ln \left( \frac{T}{T_{c0}} \right) = 2\pi k_B T \sum_{n=0} \left( f_0(\omega_n) - \frac{\Delta}{\omega_n} \right), \quad (8)$$

where  $\omega_n = 2\pi k_B T(n + 1/2)$ , with  $n \in \mathbb{Z}$ , are the Matsubara frequencies,  $T_{c0}$  is the zero-field critical temperature, and  $f_0(\omega_n)$  is the Matsubara anomalous GF (7b), obtained by analytic continuation of the GF to the complex plane  $\varepsilon + i\Gamma \rightarrow i\omega_n$ .

In diffusive systems where the scattering rate  $\tau^{-1}$  is much higher than the other energy scales in the system, excluding the Fermi energy, the GF is determined from the well-known Usadel equation [37]. The covariant version of the Usadel equation [25,26] allows describing the Hall and intrinsic spin Hall effects. For intrinsic SOC the Usadel equation reads [30–32]

$$\hbar D \tilde{\nabla}_i \check{J}^i - \{\tau_3 \hbar \partial_t, \check{g}\} - [i\check{A}^0 \tau_3 + \check{\Delta}, \check{g}] = 0, \quad (9)$$

and for extrinsic SOC [25]

$$\hbar D (\tilde{\nabla}_i \check{J}^i + \check{T}) - \{\tau_3 \hbar \partial_t, \check{g}\} - \left[ i\check{A}^0 \tau_3 + \check{\Delta} + \frac{\sigma_i \check{g} \sigma_i}{8\tau_{SO}}, \check{g} \right] = 0, \quad (10)$$

where  $D$  is the diffusion coefficient,  $\tau_{SO} = 9\tau / (8\lambda^4 p_F^4)$  is the spin-orbit relaxation time,  $\lambda$  describes the SOC strength,  $p_F$  is the Fermi momentum,  $\tilde{\nabla}_i \check{X} = \partial_i \check{X} - i/\hbar [\check{A}^i, \check{X}]$  is the covariant derivative,  $\check{T}$  is an extrinsic SOC correction due to an effective torque originating from the spin Hall and the spin swapping effects [28,29]

$$\check{T} = i\epsilon_{ijk} \frac{\varkappa}{4} [\tilde{\nabla}_i \check{g} \cdot \tilde{\nabla}_j \check{g}, \sigma_k] + \epsilon_{ijk} \frac{\theta}{4} [\sigma_k, \check{g} \cdot \tilde{\nabla}_i \check{g} \cdot \tilde{\nabla}_j \check{g}], \quad (11)$$

and  $\check{J}^i$  is the matrix current given by

$$\check{J}^i = \check{g} \cdot \tilde{\nabla}_i \check{g} + \frac{\tau}{4m} (\{\check{F}^{ij} + \check{g} \cdot \check{F}^{ij} \cdot \check{g}, \tilde{\nabla}_j \check{g}\} - i\hbar \tilde{\nabla}_j \check{g} \cdot [\tilde{\nabla}_i \check{g}, \tilde{\nabla}_j \check{g}]) \quad (12)$$

for intrinsic SOC [26] and

$$\check{J}^i = \check{g} \cdot \tilde{\nabla}_i \check{g} - i\epsilon_{ijk} \frac{\varkappa}{4} [\check{g} \cdot \tilde{\nabla}_j \check{g}, \sigma_k + \check{g} \cdot \sigma_k \check{g}] - \epsilon_{ijk} \frac{\theta}{4} \{\tilde{\nabla}_j \check{g}, \sigma_k + \check{g} \cdot \sigma_k \check{g}\} \quad (13)$$

for extrinsic SOC [25]. Here  $\varkappa = 2p_F^2 \lambda^2 / 3$  and  $\theta = 2\hbar p_F \lambda^2 / \ell$  are spin-swapping and spin Hall coefficients [38], respectively, with  $\epsilon_{ijk}$  the Levi-Civita symbol and  $\ell$  the mean-free path. The first term in Eqs. (12) and (13) is the standard diffusive current, while the second term is the leading contribution from spin-charge coupling describing the Hall effect.

The Usadel equation together with the normalization condition specifies the value of the GF. The observable quantities of the system are given by the GF, for example, the charge and spin currents are given by

$$j^{i0}(\mathbf{r}, t) = -\frac{\pi \hbar \sigma_D}{8e} \text{Tr} \{ \tau_3 \check{J}^i(\mathbf{r}, t, t)^K \}, \quad (14)$$

$$j^{ij}(\mathbf{r}, t) = \frac{\hbar \pi \hbar \sigma_D}{2 \cdot 8e^2} \text{Tr} \{ \sigma_j \check{J}^i(\mathbf{r}, t, t)^K \}, \quad (15)$$

where the Drude conductivity is given by  $\sigma_D = v_F e^2 D$ ,  $v_F$  is the density of states at the Fermi energy, and the  $K$  superscript denotes the Keldysh block of the matrix current.

### III. ONSAGER SYMMETRIES

The Onsager reciprocal relations relate the conductivities between different pairs of driving fields and their conjugate currents. They demonstrate the reciprocity between inverse effects, such as the Hall, the spin Hall, or spin-galvanic effects and their corresponding inverse effects.

The conductivity tensor in Eq. (4) can be decomposed into four blocks:

$$\sigma^{i\mu, j\nu} = \begin{pmatrix} \sigma^{i0, j0} & \sigma^{i0, jl} \\ \sigma^{ik, j0} & \sigma^{ik, jl} \end{pmatrix}. \quad (16)$$

The elements of the conductivity tensor are related through the Onsager reciprocal relations  $\sigma^{j0, i0}(\mathbf{B}) = \sigma^{i0, j0}(-\mathbf{B})$ ,  $\sigma^{jl, ik}(\mathbf{B}) = \sigma^{ik, jl}(-\mathbf{B})$ , and  $\sigma^{i0, jl}(\mathbf{B}) = -\sigma^{jl, i0}(-\mathbf{B})$ , where  $\mathbf{B}$  denotes all time-reversal symmetry (TRS) breaking fields [39]. The minus sign in the last relation appears due to the spin currents having opposite  $T$  parity to charge currents [40]. The charge block  $\sigma^{ij} \equiv \sigma^{i0, j0}$  is the usual  $3 \times 3$  conductivity tensor describing the electric effects. The diagonal elements are the longitudinal conductivities (Ohm's law), while the off-diagonal elements describe the Hall effect. For instance, the system considered in Sec. V consists of a superconductor pierced by a magnetic field in the  $z$  direction. The magnetic field breaks the TRS, allowing for nonzero transverse conductivities in the  $xy$  plane. Due to rotational invariance around the  $z$  axis, the transverse (Hall) conductivities are related through the relation  $\sigma^{xy} = -\sigma^{yx}$ .

The spin block  $\sigma^{ik, jl}$  is a  $9 \times 9$  matrix relating the spin currents to the spin SU(2) fields. For instance, some of the off-diagonal elements of the spin block describe the spin-swapping effect. The spin-charge blocks  $\sigma^{ik, j0}$  and  $\sigma^{i0, jl}$  describe the spin Hall and inverse spin Hall effects, respectively. In Sec. VI we study the spin Hall effect in a superconductor due to intrinsic and extrinsic SOC. In the intrinsic case the SOC is of the Rashba type, while in the extrinsic case the SOC is introduced by impurities. Since there are no TRS breaking fields, the spin Hall conductivities satisfy  $\sigma^{i0, jl} = -\sigma^{jl, i0}$ . In the intrinsic case, inversion symmetry in

the  $z$  direction is broken by the Rashba SOC, so the spin Hall effect is restricted to the  $xy$  plane. In the extrinsic case, the isotropy of the impurities results in spin currents in the plane perpendicular to the charge current direction  $i$ , so that the spin Hall conductivities are related through  $\sigma^{lj,i0} = -\sigma^{jl,i0}$ .

The susceptibility  $\chi = i\omega\sigma$  is the response function to the vector potentials. From the fluctuation-dissipation theorem for  $\chi$  [41], it follows that the Hermitian part of the generalized conductivity tensor  $\sigma' = \frac{1}{2}(\sigma + \sigma^\dagger)$  is the dissipative contribution, while the anti-Hermitian part  $\sigma'' = \frac{1}{2i}(\sigma - \sigma^\dagger)$  is the reactive contribution.

#### IV. MATTIS-BARDEEN THEORY WITHIN QUASICLASSICS

In this section we apply the quasiclassical GF formalism introduced in Sec. II to the linear response theory to compute the longitudinal (charge) conductivity of a diffusive superconductor subjected to a time-dependent electric field  $\mathbf{E}(t)$ . In particular, we consider a superconductor in a microwave field which has extensively been experimentally realized [42–46].

In diffusive normal metals the Drude model predicts a purely dissipative response [4], that is to say, the current is in phase with the electric field. Superconductors however show a reactive current which is most relevant at small frequencies compared to the superconducting gap. The frequency dependent microwave response of an  $s$ -wave superconductor is described within the Mattis-Bardeen theory [7]. These results can be rederived in the present approach as follows.

We assume that the electric field is small enough so that it can be treated perturbatively. The bulk GF (6) is corrected by the driving field, but the leading current contribution is given by the bulk GF. We start from a single-frequency electric field along the  $x$  direction  $\mathbf{E}(t) = E_0 e^{-i\omega t} \hat{\mathbf{u}}_x$  described via the vector potential  $\mathbf{A}(t) = -iE_0/\omega e^{-i\omega t} \hat{\mathbf{u}}_x$ . Therefore, the only nonzero term of the potential (2) is  $\dot{A}^x = -eA^x \tau_3$ . Using Eq. (14) we compute the longitudinal current  $j^x(t)$ , and dividing by the electric field  $E_0 e^{-i\omega t}$  we obtain the longitudinal conductivity  $\sigma^{xx}(\omega)$ . The convolutions in Eq. (12) can conveniently be computed after a Fourier transformation into the energy domain. From (14), we get (see Supplemental Material [47])

$$\begin{aligned} \sigma^{xx}(\omega) = \frac{\sigma_D}{2\hbar\omega} \int d\varepsilon [\text{Re}g_0(\varepsilon_+) \text{Re}g_0(\varepsilon) + \text{Im}f_0(\varepsilon_+) \text{Im}f_0(\varepsilon)] [h(\varepsilon_+) - h(\varepsilon)] + i\{2[\text{Re}g_0(\varepsilon) \text{Im}g_0(\varepsilon) + \text{Re}f_0(\varepsilon) \text{Im}f_0(\varepsilon)] h(\varepsilon) \\ + [-\text{Re}g_0(\varepsilon_+) \text{Im}g_0(\varepsilon) + \text{Im}f_0(\varepsilon_+) \text{Re}f_0(\varepsilon)] h(\varepsilon_+) + [-\text{Im}g_0(\varepsilon_+) \text{Re}g_0(\varepsilon) + \text{Re}f_0(\varepsilon_+) \text{Im}f_0(\varepsilon)] h(\varepsilon)\}, \end{aligned} \quad (17)$$

where  $\varepsilon_+ = \varepsilon + \hbar\omega$ . The expression is lengthy, but we can identify the different parts. The first term on the first line is the dissipative contribution. It yields the normal-state result  $\sigma^{xx} = \sigma_D$  when  $f_0(\varepsilon) = 0$  and  $g_0(\varepsilon) = 1$ . The rest of the terms are out of phase and describe the supercurrent effects. The prefactors of the distribution function terms are nonzero only when  $\varepsilon$  is of the order of  $\Delta$  and decay at large energies, ensuring the convergence of the integrals. In general, the integral needs to be evaluated numerically.

In Fig. 1 we show the frequency dependence of the longitudinal conductivity  $\sigma^{xx}(\omega)$  for different temperatures [47]. The conductivity is in agreement with the BCS theory and the experimental measurements [42,43]. At  $T = 0$  the real part of

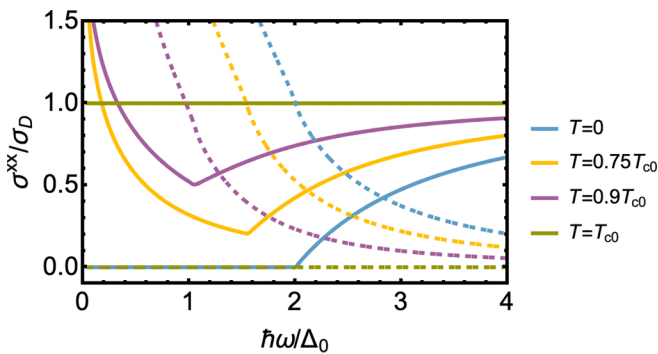


FIG. 1. Mattis-Bardeen response of a superconductor for different temperatures. The solid and dashed lines correspond to the real and imaginary parts of the conductivity, respectively.

the conductivity is zero for  $\hbar\omega < 2\Delta_0$ , where  $\Delta_0 = 1.76k_B T_{c0}$  is the zero-temperature gap, and it increases monotonously with a finite slope for  $\hbar\omega > 2\Delta_0$  so that it approaches the Drude conductivity in the  $\omega \rightarrow \infty$  limit. At  $T = 0$  there are no thermally excited quasiparticles, so the processes that allow energy absorption are limited to the creation of electron-hole pairs, which require frequencies greater than  $2\Delta_0$  [48]. The effect of temperature in the conductivity is twofold; on the one hand, the superconducting gap  $\Delta(T)$  is reduced with increasing temperature, so the the absorption edge is reduced to lower frequencies. On the other hand, at finite temperatures quasiparticles are thermally excited, allowing energy absorption processes at lower frequencies.

Regarding the imaginary part of the conductivity, at  $T = 0$  it diverges as  $1/\omega$  for  $\hbar\omega \ll 2\Delta_0$ . In superconductors where the electromagnetic field varies slowly in space on the scale of the coherence length the charge current is determined by the London equation [49]. For diffusive superconductors at  $T = 0$ , the London equation is given by  $\mathbf{j} = -(\pi \Delta_0 \sigma_D / \hbar) \mathbf{A}$ , where the vector potential is given in the London gauge [48]. The London equation describes the free-acceleration aspect of the supercurrent response. For the plane wave vector potential considered here [see above Eq. (17)] the electric current is given by  $\mathbf{j} = i\pi \Delta_0 \sigma_D / (\hbar\omega) \mathbf{E}$ , so at low frequencies the conductivity is purely imaginary and proportional to  $1/\omega$ .

At the critical temperature the gap is completely suppressed  $\Delta(T_{c0}) = 0$  and the metal transitions into the normal state, so the conductivity is given by the AC Drude model [4]. In diffusive normal metals the Drude conductivity is

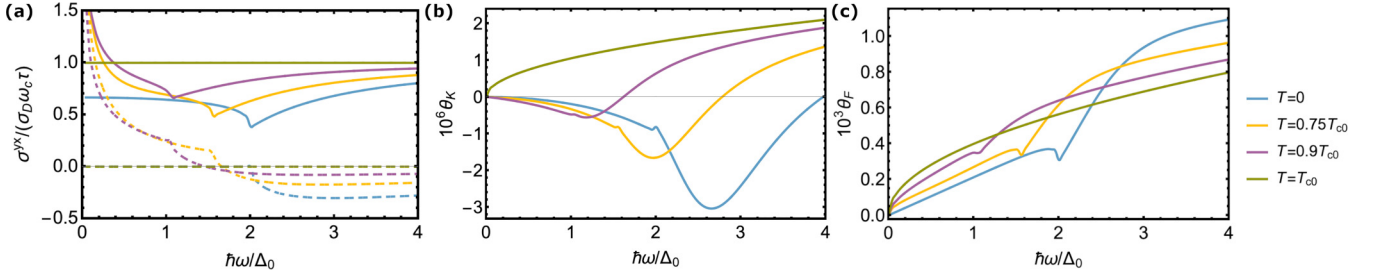


FIG. 2. (a) Hall response of a superconductor for different temperatures. The solid and dashed lines correspond to the real and imaginary parts of the conductivity, respectively. (b) Kerr and (c) Faraday rotation angles of linearly polarized incident light for different temperatures. The parameters used in panels (b) and (c) are  $\tau = 5 \times 10^{-2} \hbar/\Delta_0$ ,  $\omega_c = 0.2\Delta_0/\hbar$ ,  $\omega_p = 3 \times 10^4 \Delta_0/\hbar$ , and  $d = 0.2\lambda$ , where  $\lambda$  is the London penetration length.

frequency independent at frequencies much smaller than the elastic scattering rate and equal to the DC Drude conductivity  $\sigma_D$ .

## V. ORDINARY HALL EFFECT AND KERR ROTATION

In this section we study the Hall response of a superconductor in a microwave field subjected to a constant magnetic field  $\mathbf{B} = B_0 \hat{u}_z$ . In the Landau gauge, the vector potential is given by  $\mathbf{A}^x = -e(-iE_0/\omega e^{-i\omega t} - B_0 y)\tau_3$ . The

only nonzero elements of the field strength tensor (3) are  $\check{F}^{xy} = -\check{F}^{yx} = -eB_0\tau_3$ . We assume that both the electric and magnetic fields are small and compute the electric currents to leading order in both fields. In addition to the longitudinal conductivity given by the Mattis-Bardeen response (17), the system shows a transverse conductivity  $\sigma^{yx}$  due to the interaction between the magnetic field and the electric current. The leading term of the Hall current is proportional to  $E_0 B_0$  and it is given by the second current term in Eq. (12). The Hall conductivity is given by the y component of Eq. (14) [47]:

$$\begin{aligned} \sigma^{yx}(\omega) = & \frac{3\sigma_D \omega_c \tau}{4} + \frac{\sigma_D \omega_c \tau}{16\hbar\omega} \int d\varepsilon \{g_0(\varepsilon_+)K(\varepsilon)^* + g_0(\varepsilon)^*K(\varepsilon_+) + 2f_0(\varepsilon)^*f_0(\varepsilon_+)[g_0(\varepsilon_+) + g_0(\varepsilon)^*]\}[h(\varepsilon_+) - h(\varepsilon)] \\ & + \{g_0(\varepsilon_+)K(\varepsilon) - g_0(\varepsilon)K(\varepsilon_+) + 2f_0(\varepsilon)f_0(\varepsilon_+)[g_0(\varepsilon_+) - g_0(\varepsilon)]\}h(\varepsilon) \\ & + \{g_0(\varepsilon_+)^*K(\varepsilon)^* - g_0(\varepsilon)^*K(\varepsilon_+)^* + 2f_0(\varepsilon)^*f_0(\varepsilon_+)^*[g_0(\varepsilon_+)^* - g_0(\varepsilon)^*]\}h(\varepsilon_+), \end{aligned} \quad (18)$$

where  $\omega_c = eB_0/m$  is the cyclotron frequency and  $K(\varepsilon) = g_0(\varepsilon)^2 - f_0(\varepsilon)^2$ . In the normal state  $g_0(\varepsilon) = 1$  and  $f_0(\varepsilon) = 0$ , the first line in the integrand tends to  $2[h(\varepsilon_+) - h(\varepsilon)]$  and integrates to  $4\omega$ , whereas the two other lines tend to zero. Together, these terms provide the normal-state Hall conductivity  $\sigma^{yx} = \sigma_D \omega_c \tau$ , valid to the first order in  $\omega_c$ .

In Fig. 2(a) we show the Hall conductivity as a function of frequency at different temperatures. At  $T = 0$  the real part of the conductivity shows a sharp minimum at  $\hbar\omega = 2\Delta_0$  and asymptotically approaches the normal-state Hall conductivity  $\sigma^{yx} = \sigma_D \omega_c \tau$  at high frequencies. The real part of the conductivity is finite at  $T = 0$ , while the imaginary part remains equal to zero until a threshold frequency is achieved. This is consistent with the experimental measurements of the Hall conductivity in superconducting  $\text{YBa}_2\text{Cu}_3\text{O}_{7-\delta}$  samples by Spielman *et al.* [9]. As argued in Sec. III, the dissipative contribution to the current is described by the Hermitian part of the conductivity tensor Eq. (16). Due to the  $\sigma^{xy} = -\sigma^{yx}$  symmetry relation, the dissipative part of the Hall current is given by the imaginary part of  $\sigma^{yx}$ , i.e., the out-of-phase component, while the reactive part is given by  $\text{Re}\sigma^{yx}$ . This is the reason why at  $T = 0$  the imaginary part of the conductivity is nonzero only for  $\hbar\omega > 2\Delta_0$ , so that the signal may be absorbed to create the electron-hole pairs. The temperature

dependence of the Hall conductivity is very similar to that of the longitudinal conductivity discussed in Sec. IV. The superconducting gap decreases with increasing temperature, so the absorption edge and the minimum of  $\text{Re}\sigma^{yx}$  are shifted to lower frequencies. For  $T = T_{c0}$ , we recover the normal-state Hall conductivity. The normal-state Hall response is nondissipative, in the leading order in  $\omega_c \tau$ , whereas in the superconducting state the response has a dissipative quasiparticle component.

Note that although the off-diagonal elements of  $\sigma$  remain nonzero in the static limit  $\omega \rightarrow 0$  in the superconducting state, all elements of the resistivity tensor  $\rho = \sigma^{-1}$  vanish for  $\omega \rightarrow 0$ . Hence, the relation  $\mathbf{j} = \sigma \mathbf{E}$ , or  $\mathbf{E} = \rho \mathbf{j}$ , does not imply here that uniform static supercurrent generates electric fields or a Hall effect. Such equilibrium electric fields are expected to exist when the superflow is nonuniform, [50] but such configuration is not considered in the model here.

### A. Kerr and Faraday rotations

The Hall conductivity can be probed optically through the Faraday or Kerr effect measurement as shown in Fig. 3(a), where linearly polarized light transmitting or reflecting from the sample becomes elliptically polarized [5,6]. The

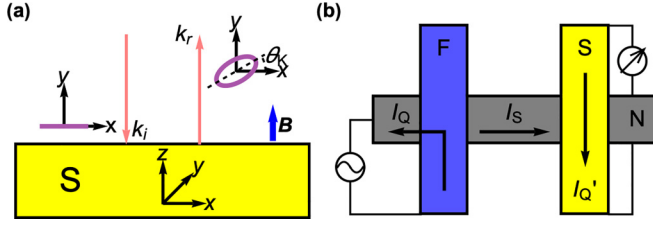


FIG. 3. (a) Proposed setup for the measurement of the Hall effect. Materials subjected to a magnetic field show circular birefringence, i.e., left and right polarized light waves propagate with different velocities. The Kerr rotation angle is related to the longitudinal and transversal conductivities of the material. (b) Proposed setup for the detection of the inverse spin Hall effect in a superconductor using a lateral spin valve. If a charge current  $I_Q$  is injected from the ferromagnet (F) to the normal metal (N), the nonequilibrium spin accumulation generated at the interface generates a pure spin current  $I_S$  to the right of F. The superconductor absorbs the spin current owing to its strong SOC, generating a charge current  $I_Q'$  due to the inverse spin Hall effect.

polarization rotation is described by the Faraday and Kerr angles which are in general complex quantities: their real part describes the amplitude of polarization rotation, and their imaginary part describes the ellipticity of the reflected polarization. These angles can be straightforwardly calculated from our theory. However, for simplicity the theory assumes a constant magnetic field, a situation that cannot be realized in the case of thick superconductors because of the Meissner effect expelling the field from inside the superconductor. However, the (Kerr) reflection is also a surface effect because of the finite skin depth of the electromagnetic field, and the transmission takes place only if the material is thinner than the corresponding skin depth. In other words, our estimates are accurate in the case where the London penetration depth is larger than either the skin depth (for Kerr reflection) or the sample thickness (for Faraday transmission).

The skin depth can be obtained by solving the Maxwell equations inside the material. Disregarding the small correction from the Hall effect, it is obtained from

$$\ell_{\text{skin}} = \frac{c}{\omega \text{Im} \sqrt{1 + i\sigma^{xx}/(\omega\epsilon_0)}}. \quad (19)$$

On the other hand, the London penetration depth  $\lambda$  is the zero-frequency limit of this skin depth. At  $T = 0$ ,  $\sigma^{xx} \approx i\chi_0/\omega$ , where  $\chi_0 = \pi\Delta_0\sigma_D/\hbar$ , and hence  $\lambda \approx c/\sqrt{\chi_0/\epsilon_0}$ .

For the simplest geometry, i.e., normal incidence of a linearly polarized electromagnetic wave onto the sample, using Maxwell equations and the boundary conditions, one can obtain the Kerr  $\phi_K$  and Faraday  $\phi_F$  angles as [5,6]

$$\phi_K = i \frac{r_+ - r_-}{r_+ + r_-} \simeq \frac{\sigma^{yx}}{\sigma^{xx} \sqrt{1 + i\frac{\sigma^{xx}}{\omega\epsilon_0}}}, \quad (20)$$

$$\phi_F = \frac{\omega d}{c} \frac{r_+ - r_-}{(1 - r_+)(1 - r_-)} \simeq i \frac{d}{2c\epsilon_0} \frac{\sigma^{yx}}{\sqrt{1 + i\frac{\sigma^{xx}}{\omega\epsilon_0}}}, \quad (21)$$

where  $r_{\pm}$  are the reflection coefficients for left- and right-handed (with respect to the applied field) circularly polarized light,  $\epsilon_0$  is the vacuum permittivity, and  $d$  is the sample thickness. Note that the expression is obtained by assuming

a small perturbation from the external magnetic field and only considering linear terms in the Hall conductivity ( $\sigma^{yx}$ ). This approximation is valid when the Hall conductivity is much smaller than the longitudinal conductivity, a condition often met in many materials. Noting  $\sigma_D$  as a natural scale of conductivity and defining the plasma frequency  $\omega_p = \sqrt{\sigma_D/(\epsilon_0\tau)}$ , we notice that the latter term inside the square root can also be written as  $\sigma^{xx}/(\omega\epsilon_0) = (\sigma^{xx}/\sigma_D)\omega_p^2\tau/\omega$ , providing a direct way to compare dimensionful quantities. For frequencies of interest here,  $\omega \lesssim \Delta/\hbar$ , the typical range is  $\omega \ll \omega_p, 1/\tau$ , and therefore the first term inside the square root in Eq. (20) can typically be disregarded. The order of magnitude of the polarization rotation is hence proportional to the small factor  $\omega_c\tau\sqrt{\omega/(\omega_p^2\tau)}$ .

The Faraday-Kerr rotation of the polarization state of light can experimentally be measured by passing the reflected light through a polarizer. The polarization direction is obtained by measuring the intensity of the reflected light with the polarizer oriented in parallel and perpendicular to the incident light. The Kerr (Faraday) rotation angle  $\theta_{K(F)}$  specifies the rotation of the major axis of the elliptically polarized reflected light. It is given by the real part of  $\phi_{K(F)} = \theta_{K(F)} + i\epsilon_{K(F)}$ , plotted in Figs. 2(b) and 2(c). The imaginary part  $\epsilon_{K(F)}$  specifies the ratio of the minor to the major axes of the ellipsoid.

In Fig. 2(b) we show the Kerr rotation angle (20) for normal incident light. The parameters used are  $\tau = 5 \times 10^{-2}\hbar/\Delta_0$ ,  $\omega_c = 0.2\Delta_0/\hbar$ , and  $\omega_p = 3 \times 10^4\Delta_0/\hbar$ ; these values are accessible in experiments.  $\sigma^{xx}$  and  $\sigma^{yx}$  are computed evaluating Eqs. (17) and (18). The Kerr rotation angle is of the order of  $\mu\text{rad}$ , which is an experimentally measurable rotation [51]. In the normal state  $\sigma^{xx}$  and  $\sigma^{yx}$  are positive numbers, so  $\theta_K$  is always positive. In the superconducting state both conductivities acquire an imaginary part, allowing for positive and negative values of  $\theta_K$ . In Fig. 2(c) we show the Faraday rotation angle (21).  $\theta_F$  has a weaker dependence on temperature, but it is three orders of magnitude greater than  $\theta_K$ , so it is easier to measure than  $\theta_K$ .

Besides coupling to free-space light, the dynamical Hall effect can be accessed by studying the scattering parameters of microwaves in a multiterminal geometry. In particular, the matrix  $S$  of scattering parameters depends on the admittance matrix  $Y(\omega)$  of the studied sample [52]:

$$S(\omega) = \frac{1 - \mathcal{Z}^{1/2}Y(\omega)\mathcal{Z}^{1/2}}{1 + \mathcal{Z}^{1/2}Y(\omega)\mathcal{Z}^{1/2}}, \quad (22)$$

where  $\mathcal{Z} = \text{diag}(Z_1, \dots, Z_N)$  is a diagonal matrix containing the characteristic impedances of transmission lines connected to each terminal  $i$ . This way, in case the bulk superconductor response gives the dominating contribution to the admittance matrix—in other words, interface effects can be disregarded—the Hall response can be related with the off-diagonal components of  $S$ .

## VI. DYNAMICAL SPIN HALL RESPONSE AND ITS DETECTION WITH MAGNETIC RESONANCE

In this section we study the spin Hall effect in a superconductor with SOC subjected to a microwave field. Several methods have been proposed and realized to measure the spin Hall and its inverse effects including electrical measurements

[53–56] and Kerr rotation microscopy [51]. In Fig. 3(b) we propose a measurement setup based on a lateral spin valve. A lateral spin valve consists of a normal metal (N) bridging a ferromagnetic injector (F) and a detector, which in our case is a superconductor (S) with SOC. A charge current  $I_Q$  is injected from F into the left side of N. The nonequilibrium spin accumulation generated at the interface is relaxed within the spin diffusion length, generating a pure spin current  $I_S$  to the right of F. If the distance between the F and the S is shorter than the spin diffusion length, a nonequilibrium spin accumulation is generated at S [55]. The spin current is absorbed by the superconductor owing to its strong SOC. The polarization of the spin current is tuned to lie out of plane by applying a normal magnetic field. A perpendicular charge current  $I_Q$  is generated at the S due to the inverse spin Hall effect. This AC current can experimentally be measured by closing the S wire with a superconducting loop coupled to a rf superconducting quantum interference device.

Alternatively, the measurement can be realized with a dynamic version of the setup used in Ref. [57]. There, two heavy-metal (Pt) injectors are used to generate and detect a magnon current in a ferromagnetic insulator. A heavy-metal superconductor placed in the middle absorbs part of the magnon current and converts it into a charge current via the inverse spin Hall effect. Replacing the DC injection by a finite-frequency injection then allows studying the AC spin Hall response of the superconductor. It also becomes interesting to separate the in- and out-of-phase oscillating parts of the detected signal, in comparison with the injected current.

### A. Intrinsic spin Hall response

First, we study the spin Hall effect in a superconductor with Rashba SOC subjected to a microwave field. The Rashba SOC interaction is linear in momentum

$$\mathcal{H}_R = \alpha(\mathbf{p} \times \hat{\mathbf{u}}_z) \cdot \boldsymbol{\sigma} \quad (23)$$

so it can be described through the SU(2) four-potential  $\check{A}^x = m\alpha\sigma_y$ ,  $\check{A}^y = -m\alpha\sigma_x$ . The term  $-eA^x\tau_3$  should be added to  $\check{A}^x$  to account for the time-dependent electric field. For Rashba SOC the nonzero elements of the field strength tensor are  $\check{F}^{xy} = -\check{F}^{yx} = 2m^2\alpha^2\sigma_z/\hbar$ .

The terms contributing to the spin Hall current in Eq. (12) depend on the first-order correction of the GF due to the time-dependent electric field. We expand the GF to the first order in the electric field  $\check{g} = \check{g}_0 + \delta\check{g} + O(E_0^2)$ , where  $\delta\check{g}$  is the correction to the bulk GF. The Rashba SOC does not modify the bulk GF of a superconductor  $\check{g}_0$ , so it is given by Eqs. (6) and (7). Unlike the bulk GF,  $\check{g}_0(t, t') = \check{g}_0(t - t')$ , the first-order correction is not time-translation invariant due to the time-dependent electric field. Based on the time dependence of the electric field, we use the ansatz  $\delta\check{g}(t, t') = e^{-i\omega t} \delta\check{g}(t - t')$  for the correction of the GF. The normalization condition for  $\delta\check{g}$  reads  $\check{g}_0(\varepsilon_+) \delta\check{g}(\varepsilon) + \delta\check{g}(\varepsilon) \check{g}_0(\varepsilon) = 0$ , and the Usadel equation (9) to first order in  $E_0$  is given by

$$\begin{aligned} & -\varepsilon_\alpha([\sigma_y, \check{g}_0(\varepsilon_+)[\sigma_y, \delta\check{g}(\varepsilon)] + [\sigma_x, \check{g}_0(\varepsilon_+)[\sigma_x, \delta\check{g}(\varepsilon)]) \\ & + i\hbar\omega\tau_3\delta\check{g}(\varepsilon) + [i\varepsilon\tau_3 - \check{\Delta}, \delta\check{g}(\varepsilon)] \\ & = i\varepsilon_E[\sigma_x, \{\sigma_z, \tau_3\check{g}_0(\varepsilon) - \check{g}_0(\varepsilon_+)\tau_3\}], \end{aligned} \quad (24)$$

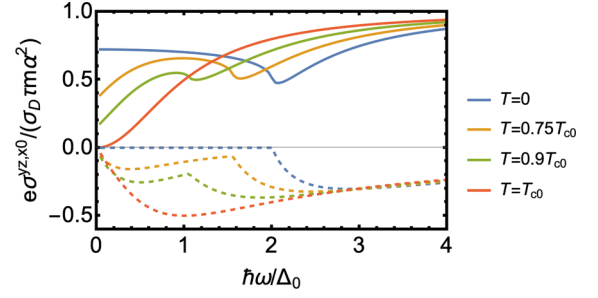


FIG. 4. Spin Hall response of a superconductor for different temperatures. The solid and dashed lines correspond to the real and imaginary parts of the conductivity, respectively. The value of the Dyakonov-Perel energy used is  $\varepsilon_\alpha = 0.25\Delta_0$ .

where  $\delta\check{g}(\varepsilon)$  is the Fourier transform (5) of  $\delta\check{g}(t - t')$ ,  $\varepsilon_\alpha = Dm^2\alpha^2/\hbar$  is the Dyakonov-Perel energy (scattering rate), and  $\varepsilon_E = D\tau m^2\alpha^3 eE_0/(\hbar^2\omega)$ . The spin structure of  $\delta\check{g}(\varepsilon)$  can be inferred from the Rashba Hamiltonian (23). As shown in Sec. IV, the microwave field generates a longitudinal current along the  $x$  direction. The Rashba SOC gives rise to intrinsic zero-field spin splitting [58]. The motion of an electron in a two-dimensional electron gas through a perpendicular electric field results in a magnetic field in the rest frame of the electron that couples to the spin as given by Eq. (23), where the momentum-dependent magnetic field is  $\mu_B \mathbf{B}_{\text{eff}} = \alpha(\mathbf{p} \times \hat{\mathbf{u}}_z)$ . Therefore, a vector potential in the  $x$  direction spin splits the GF in the spin- $y$  direction as  $\delta\check{g} = \delta g_y \sigma_y \tau_3 + \delta f_y \sigma_y \tau_1$ . In Appendix A we solve Eq. (24) analytically and obtain closed form solutions for the retarded/advanced GFs  $\delta\check{g}^{R/A}$  and the distribution function  $\delta\check{h}$ , where  $\delta\check{g}^K(\varepsilon) = \delta\check{g}^R(\varepsilon)h(\varepsilon) - h(\varepsilon_+)\delta\check{g}^A(\varepsilon) + \check{g}_0^R(\varepsilon_+)\delta\check{h}(\varepsilon) - \delta\check{h}(\varepsilon)\check{g}_0^A(\varepsilon)$ .

Plugging the solution into Eq. (15) we obtain the spin Hall conductivity [47]:

$$\begin{aligned} \sigma^{yz,x0}(\omega) &= \frac{\sigma_D \tau m \alpha^2}{e} - \frac{\sigma_D m \alpha}{4e^2 E_0} \int d\varepsilon g_0(\varepsilon_+) \delta g_y^K(\varepsilon) \\ &+ f_0(\varepsilon_+) \delta f_y^K(\varepsilon) + 2[\text{Re} g_0(\varepsilon_+) \delta g_y^A(\varepsilon) \\ &+ i \text{Im} f_0(\varepsilon_+) \delta f_y^A(\varepsilon)] h(\varepsilon_+). \end{aligned} \quad (25)$$

In Fig. 4 we show the spin Hall conductivity for a superconductor with intrinsic SOC. The value of the Dyakonov-Perel energy used is  $\varepsilon_\alpha = 0.25\Delta_0$ . In Appendix B we obtain a closed form expression for the spin Hall conductivity in the normal state, which agrees with literature predictions [23,24]. The spin conductivity depends on two characteristic frequency scales related to  $\varepsilon_\alpha$  and  $\Delta(T)$ . In homogeneous metals, the DC spin current is covariantly conserved unless extrinsic sources of spin relaxation such as magnetic impurities are included [59], or nonlinear in  $\mathbf{p}$  SOC is considered, such as cubic Dresselhaus interaction [60]. This shows up as a vanishing spin Hall conductivity at  $\omega = 0$ . The real part of the conductivity increases monotonically with an increasing frequency, reaching the asymptotic value  $\sigma^{yz,x0} = \sigma_D \tau m \alpha^2 / e$  for  $\hbar\omega \gg \varepsilon_\alpha$ , while the imaginary part reaches an extremum at  $\hbar\omega = 4\varepsilon_\alpha$  and decays to zero at high frequencies.

In the superconducting state, the temperature dependence of the spin Hall conductivity is most relevant at frequencies

lower than  $2\Delta$ . The absolute values of the real and imaginary parts of the spin Hall conductivity have a minimum at  $\hbar\omega = 2\Delta$ . Due to the  $\sigma^{i0,jl} = -\sigma^{jl,i0}$  Onsager relation, the dissipative component of the spin Hall conductivity is given by the imaginary part of  $\sigma^{yz,x0}$ . Similar to the ordinary Hall response, at  $T = 0$  the out-of-phase spin current vanishes below the absorption edge  $2\Delta_0$ .

### B. Extrinsic spin Hall response

We consider the response of the system with SOC due to extrinsic impurity scattering. In this case, the matrix current takes the form (13). Due to the isotropy of the impurity scattering, we have spin Hall currents in both  $y$  and  $z$  directions. In this case the spin currents (15) can be computed analytically. The conductivities are given by

$$\sigma^{zy,x0} = -\sigma^{yz,x0} = \frac{\hbar\sigma_D\theta}{2e}, \quad (26)$$

which do not depend on the frequency or temperature. This is a consequence of the diffusive regime considered in this paper. For extrinsic SOC, the spin Hall conductivity is real, i.e., it is nondissipative. In the following section we study the inverse Hall effect in systems with intrinsic and extrinsic SOC and explicitly show that the Onsager relations are satisfied.

## VII. INVERSE SPIN HALL RESPONSE

In this section we compute the charge current generated in systems with intrinsic and extrinsic SOC due to the inverse Hall effect. The charge current and the U(1) electric field are conjugate variables, in the same way the spin current has a conjugate force field  $E^{jl}$  which generates  $l$ -polarized spin currents along the  $j$  direction. This force field can be generated by the gradient of a Zeeman field, a time-dependent SOC, or a spin dependent chemical potential [61,62].

### A. Intrinsic SOC

We consider an SU(2) driving field  $E^{yz}(t) = \mathcal{E}_0 e^{-i\omega t}$  which generates a  $z$ -polarized spin current in the  $y$  direction. This electric field is described via the SU(2) vector potential  $\check{A}^y(t) = -i\hbar\mathcal{E}_0/(2\omega)e^{-i\omega t}\sigma_z$ . Taking the Rashba SOC into account, the vector potentials are given by  $\check{A}^x = m\alpha\sigma_y$ ,  $\check{A}^y = -m\alpha\sigma_x - i\hbar\mathcal{E}_0/(2\omega)e^{-i\omega t}\sigma_z$ , so that the nonzero elements of the field strength tensor are  $\check{F}^{xy} = -\check{F}^{yx} = 2m^2\alpha^2\sigma_z/\hbar - i(m\alpha\mathcal{E}_0/\omega)e^{-i\omega t}\sigma_x$ . Following a similar procedure to the one used in Sec. VI A, we obtain the correction to the bulk GF due to the driving field (see Appendix A) and compute the charge current along the  $x$  direction using Eq. (14). The inverse spin Hall conductivity is

$$\sigma^{x0,yz}(\omega) = -\frac{\sigma_D\tau m\alpha^2}{e} + \frac{\sigma_D\tau m^2\alpha^3}{e\hbar^2\mathcal{E}_0} \int d\varepsilon \delta g_y^K(\varepsilon). \quad (27)$$

Evaluating Eqs. (25) and (27) numerically we have checked that the spin Hall and inverse spin Hall conductivities satisfy the Onsager relation introduced in Sec. III  $\sigma^{x0,yz} = -\sigma^{yz,x0}$ .

### B. Extrinsic SOC

As it has been argued in Sec. VIB, systems with extrinsic SOC subjected to an electric field generate spin currents in both directions perpendicular to the electric field. For this reason, we consider two driving fields  $E^{yz}(t) = \mathcal{E}_0 e^{-i\omega t}$  and  $E^{zy}(t) = \mathcal{E}_0 e^{-i\omega t}$  and compute the charge current generated in the  $x$  direction in each case. Following an equivalent procedure to Sec. VIB, it is possible to obtain the inverse spin Hall conductivities analytically. They are

$$\sigma^{x0,zy} = -\sigma^{x0,yz} = -\frac{\hbar\sigma_D\theta}{2e}. \quad (28)$$

In this case we may evaluate the Onsager symmetry analytically by comparing Eqs. (26) and (28) to obtain  $\sigma^{i0,jl} = -\sigma^{jl,i0}$ . The proportionality between the conductivities shows that the spin Hall and inverse spin Hall effects are reciprocal effects.

## VIII. CONCLUSIONS

In this paper, we have used a unified description of charge and spin transport to study the dynamical response of dissipative superconductors to U(1) and SU(2) electric fields. We have used the gauge covariant quasiclassical GF formalism to obtain the charge and spin conductivities of superconductors in the presence of magnetic fields and spin-orbit interaction. Our model recovers known results in the appropriate limits, such as the normal-state Hall conductivity and the spin Hall conductivity for normal metals with Rashba spin-orbit coupling. While diffusive normal metals show a purely dissipative response, superconductors show a reactive current that decays in frequency as  $\omega^{-1}$ , as described by the Mattis-Bardeen theory. We have analyzed the Onsager reciprocal relations between the direct and inverse Hall effects and have explicitly shown that they are satisfied.

Our findings show that both the ordinary and spin Hall conductivities show a dissipative component related to the out-of-phase current. In the case of the ordinary Hall effect, the dissipative current contribution only arises in the superconducting state. For intrinsic spin Hall effect, the imaginary (dissipative) part of the Hall conductivity is always weaker in the superconducting state than in the normal state. At low frequencies, the spin Hall conductivity of a superconductor with Rashba SOC is dominated by the in-phase component, while in the normal state it is of the same order as the out-of-phase component. For extrinsic SOC, the spin Hall response is frequency and temperature independent and proportional to the spin Hall angle. In other words, there is no correction from superconductivity on the extrinsic spin Hall conductivity.

The dynamical Hall effect can be observed in optical spectroscopy via the Faraday-Kerr rotation of the polarization state of light in conventional superconductors. Suitable materials for the measurement of the spin Hall effect due to intrinsic SOC are Bi<sub>2</sub>Se<sub>3</sub>/monolayer NbSe<sub>2</sub> heterostructures [63], or LaAlO<sub>3</sub>/SrTiO<sub>3</sub> interfaces [64,65], where the Rashba SOC can be tuned by applying a gate voltage. For the extrinsic spin Hall effect we propose Nb [66], NbN [56], and V [67], as they are superconductors with sizable impurity-induced SOC. For the detection of the spin Hall effect we propose a lateral spin

valve, where a superconductor with SOC is used as a detector [see Fig. 3(b)].

Our paper focuses on investigating the dynamic charge and spin responses in conventional singlet single-band superconductors. It is worth noting that spin ordering, as for example on iron based superconductors [68,69], would be interesting to study. Our results can be readily generalized to include the effects of such spin ordering for example via the presence of an exchange field. Moreover, orbital degrees of freedom in multiband superconductors may provide additional dynamical channels, which possibly also show up in dynamic Hall-like responses, such as the valley Hall effect. Such effects may become visible in the dynamic responses of superconducting twisted multilayer graphene or field-biased bilayer graphene. Describing such effects would require generalizing our quasi-classical approach to the multiband case.

### ACKNOWLEDGMENTS

We thank Y. Lu for useful discussion. A.H. acknowledges funding from the University of the Basque Country (Project No. PIF20/05). S.V. acknowledges JYU Visiting Fellow Programme Grant 2023 (Registry No. 1643/13.00.05.00/2022) from the University of Jyväskylä, and support from National Science Center Grant No. UMO-2020/38/E/ST3/00418 and Project No. 2018/29/B/ST3/00937. This work was supported by the Academy of Finland (Contracts No. 317118 and No. 321982). F.S.B. and A.H. acknowledge financial support from Spanish MCIN/AEI Grant 10.13039/501100011033 through Projects No. PID2020-114252GB-I00 (SPIRIT) and No. TED2021-130292B-C42, and from the Basque Government through Grant No. IT-1591-22.

### APPENDIX A: CLOSED FORM SOLUTION FOR THE CORRECTED GF

Unlike for extrinsic SOC, the spin conductivity for intrinsic SOC depends on the correction of the GF due to the electric field  $\delta\check{g}$ . In this Appendix we solve Eq. (24) analytically and provide a closed form solution for  $\delta\check{g}$ . As argued in Sec. VIA,  $\delta\check{g}$  has the following spin structure:  $\delta\check{g} = \delta\check{g}_y\sigma_y$ . The retarded and advanced parts of the Usadel equation (24) are simplified to

$$\begin{aligned} & -4\varepsilon_\alpha\check{g}_0(\varepsilon_+)\delta\check{g}_y(\varepsilon) + i\hbar\omega\tau_3\delta\check{g}_y(\varepsilon) + [i\varepsilon\tau_3 - \check{\Delta}, \delta\check{g}_y(\varepsilon)] \\ & = 4\varepsilon_E[\tau_3\check{g}_0(\varepsilon) - \check{g}_0(\varepsilon_+)\tau_3]. \end{aligned} \quad (\text{A1})$$

The left-hand side of the commutator in Eq. (A1) is proportional to the bulk GF  $\check{g}_0(\varepsilon)$  [see Eqs. (6) and (7)]. Using the normalization condition  $\check{g}_0(\varepsilon_+)\delta\check{g}_y(\varepsilon) + \delta\check{g}_y(\varepsilon)\check{g}_0(\varepsilon) = 0$ , Eq. (A1) becomes a matrix equation of the form  $\check{A}\delta\check{g}_y = \check{B}$ , such that  $\delta\check{g}_y$  is given by

$$\begin{aligned} \delta\check{g}_y(\varepsilon) & = 4\varepsilon_E[-4\varepsilon_\alpha\check{g}_0(\varepsilon_+) + i\hbar\omega\tau_3 + i\varepsilon\tau_3 - \check{\Delta} \\ & \quad - \sqrt{\Delta^2 - \varepsilon^2}\check{g}_0(\varepsilon_+)]^{-1}[\tau_3\check{g}_0(\varepsilon) - \check{g}_0(\varepsilon_+)\tau_3]. \end{aligned} \quad (\text{A2})$$

The Keldysh equation for the distribution function  $\delta\check{h} = \delta h_y\sigma_y$  reads

$$\begin{aligned} & [-4\varepsilon_\alpha\check{g}_0^R(\varepsilon_+) + i\hbar\omega\tau_3][\check{g}_0^R(\varepsilon_+) - \check{g}_0^A(\varepsilon)]\delta h_y(\varepsilon) \\ & \quad + [i\varepsilon\tau_3 - \check{\Delta}, \check{g}_0^R(\varepsilon_+) - \check{g}_0^A(\varepsilon)]\delta h_y(\varepsilon) \\ & = 4\varepsilon_E[\check{g}_0^R(\varepsilon_+)\tau_3 - \tau_3\check{g}_0^A(\varepsilon)][h(\varepsilon) - h(\varepsilon_+)], \end{aligned} \quad (\text{A3})$$

so  $\delta h_y$  is given by

$$\begin{aligned} \delta h_y(\varepsilon) & = 4\varepsilon_E\{[-4\varepsilon_\alpha\check{g}_0^R(\varepsilon_+) + i\hbar\omega\tau_3][\check{g}_0^R(\varepsilon_+) - \check{g}_0^A(\varepsilon)] \\ & \quad + [i\varepsilon\tau_3 - \check{\Delta}, \check{g}_0^R(\varepsilon_+) - \check{g}_0^A(\varepsilon)]\}^{-1}[\check{g}_0^R(\varepsilon_+)\tau_3 \\ & \quad - \tau_3\check{g}_0^A(\varepsilon)][h(\varepsilon) - h(\varepsilon_+)]. \end{aligned} \quad (\text{A4})$$

Following a similar procedure for the inverse spin Hall effect, the correction of the retarded and advanced GFs due to the SU(2) electric field considered in Sec. VII A is given by

$$\begin{aligned} \delta\check{g}_y(\varepsilon) & = \varepsilon_E[-4\varepsilon_\alpha\check{g}_0(\varepsilon_+) + i\hbar\omega\tau_3 + i\varepsilon\tau_3 - \check{\Delta} \\ & \quad - \sqrt{\Delta^2 - \varepsilon^2}\check{g}_0(\varepsilon_+)]^{-1}[\check{g}_0(\varepsilon_+)\check{g}_0(\varepsilon) - 1], \end{aligned} \quad (\text{A5})$$

where  $\varepsilon_E = Dm\alpha\mathcal{E}_0/\omega$  and the correction to the distribution function is

$$\begin{aligned} \delta h_y(\varepsilon) & = \varepsilon_E\{[-4\varepsilon_\alpha\check{g}_0^R(\varepsilon_+) + i\hbar\omega\tau_3][\check{g}_0^R(\varepsilon_+) - \check{g}_0^A(\varepsilon)] \\ & \quad + [i\varepsilon\tau_3 - \check{\Delta}, \check{g}_0^R(\varepsilon_+) - \check{g}_0^A(\varepsilon)]\}^{-1}[\check{g}_0^R(\varepsilon_+)\check{g}_0^A(\varepsilon) - 1] \\ & \quad \times [h(\varepsilon_+) - h(\varepsilon)]. \end{aligned} \quad (\text{A6})$$

### APPENDIX B: SPIN HALL CONDUCTIVITY IN THE NORMAL STATE

In the normal state ( $T \geq T_{c0}$ ) the bulk GF is given by

$$\check{g}_0^R(\varepsilon) = \tau_3, \quad \check{g}_0^A(\varepsilon) = -\tau_3, \quad \check{g}_0^K(\varepsilon) = 2\tau_3h(\varepsilon). \quad (\text{B1})$$

The right-hand sides of the retarded and advanced parts of Eq. (24) vanish, so the solution to the homogeneous equations is  $\delta\check{g}^R = \delta\check{g}^A = 0$ , i.e.,  $\check{g}^{R/A}$  are not corrected by the electric field. Solving the Keldysh part of Eq. (24), we obtain the correction to the distribution function:

$$\delta\check{h} = \frac{4\varepsilon_E}{i\hbar\omega - 4\varepsilon_\alpha}[h(\varepsilon) - h(\varepsilon_+)]\sigma_y. \quad (\text{B2})$$

Finally, we perform the integral in Eq. (25) analytically and obtain the spin Hall conductivity in the normal state:

$$\sigma^{yz,x0}(\omega) = \frac{\sigma_D\tau m\alpha^2\hbar\omega}{e(\hbar\omega + 4i\varepsilon_\alpha)}. \quad (\text{B3})$$

Following the same procedure for the inverse spin Hall effect, the correction to the GF is  $\delta\check{g}^R = \delta\check{g}^A = 0$  and

$$\delta\check{h} = \frac{\varepsilon_E}{i\hbar\omega - 4\varepsilon_\alpha}[h(\varepsilon) - h(\varepsilon_+)]\sigma_y. \quad (\text{B4})$$

The inverse spin Hall conductance Eq. (27) in the normal state is simplified to

$$\sigma^{x0,yz}(\omega) = -\frac{\sigma_D\tau m\alpha^2\hbar\omega}{e(\hbar\omega + 4i\varepsilon_\alpha)}, \quad (\text{B5})$$

satisfying the Onsager relation  $\sigma^{x0,yz} = -\sigma^{yz,x0}$ .



- [1] E. H. Hall, On a new action of the magnet on electric currents, *Am. J. Math.* **2**, 287 (1879).
- [2] P. Drude, Zur elektronentheorie der metalle, *Ann. Phys. (Leipzig)* **306**, 566 (1900).
- [3] P. Drude, Zur elektronentheorie der metalle; II. Teil. Galvanomagnetische und thermomagnetische effecte, *Ann. Phys. (Leipzig)* **308**, 369 (1900).
- [4] N. W. Ashcroft and N. D. Mermin, *Solid State Physics* (Saunders, New York, 1976), Chap. 1.
- [5] K. Shinagawa, Faraday and Kerr effects in ferromagnets, in *Magneto-Optics*, edited by S. Sugano and N. Kojima (Springer, New York, 2000), pp. 137–177.
- [6] H. Ebert, Magneto-optical effects in transition metal systems, *Rep. Prog. Phys.* **59**, 1665 (1996).
- [7] D. C. Mattis and J. Bardeen, Theory of the anomalous skin effect in normal and superconducting metals, *Phys. Rev.* **111**, 412 (1958).
- [8] P. B. Miller, Frequency-dependent Hall effect in normal and superconducting metals, *Phys. Rev.* **121**, 435 (1961).
- [9] S. Spielman, B. Parks, J. Orenstein, D. T. Nemeth, F. Ludwig, J. Clarke, P. Merchant, and D. J. Lew, Observation of the Quasiparticle Hall Effect in Superconducting  $\text{YBa}_2\text{Cu}_3\text{O}_{7-\delta}$ , *Phys. Rev. Lett.* **73**, 1537 (1994).
- [10] J. Bardeen and M. J. Stephen, Theory of the motion of vortices in superconductors, *Phys. Rev.* **140**, A1197 (1965).
- [11] G. Blatter, M. V. Feigel'man, V. B. Geshkenbein, A. I. Larkin, and V. M. Vinokur, Vortices in high-temperature superconductors, *Rev. Mod. Phys.* **66**, 1125 (1994).
- [12] N. B. Kopnin, *Theory of Nonequilibrium Superconductivity* (Oxford, New York, 2001).
- [13] N. B. Kopnin, Vortex dynamics and mutual friction in superconductors and Fermi superfluids, *Rep. Prog. Phys.* **65**, 1633 (2002).
- [14] J. Sinova, S. O. Valenzuela, J. Wunderlich, C. H. Back, and T. Jungwirth, Spin Hall effects, *Rev. Mod. Phys.* **87**, 1213 (2015).
- [15] G. Dresselhaus, Spin-orbit coupling effects in zinc blende structures, *Phys. Rev.* **100**, 580 (1955).
- [16] Y. A. Bychkov and E. I. Rashba, Properties of a 2D electron gas with lifted spectral degeneracy, *JETP Lett.* **39**, 78 (1984).
- [17] V. M. Edelstein, Magnetolectric Effect in Polar Superconductors, *Phys. Rev. Lett.* **75**, 2004 (1995).
- [18] S. K. Yip, Two-dimensional superconductivity with strong spin-orbit interaction, *Phys. Rev. B* **65**, 144508 (2002).
- [19] O. Dimitrova and M. V. Feigel'man, Theory of a two-dimensional superconductor with broken inversion symmetry, *Phys. Rev. B* **76**, 014522 (2007).
- [20] D. F. Agterberg, Magnetolectric effects, helical phases, and FFLO phases, in *Non-Centrosymmetric Superconductors*, Lecture Notes in Physics Vol. 847 (Springer, New York, 2012), pp. 155–170.
- [21] F. Konschelle, I. V. Tokatly, and F. S. Bergeret, Theory of the spin-galvanic effect and the anomalous phase shift  $\varphi_0$  in superconductors and Josephson junctions with intrinsic spin-orbit coupling, *Phys. Rev. B* **92**, 125443 (2015).
- [22] A. Vargunin and M. Silaev, Flux flow spin Hall effect in type-II superconductors with spin-splitting field, *Sci. Rep.* **9**, 5914 (2019).
- [23] E. G. Mishchenko, A. V. Shytov, and B. I. Halperin, Spin Current and Polarization in Impure Two-Dimensional Electron Systems with Spin-Orbit Coupling, *Phys. Rev. Lett.* **93**, 226602 (2004).
- [24] C. Gorini, R. Raimondi, and P. Schwab, Onsager Relations in a Two-Dimensional Electron Gas with Spin-Orbit Coupling, *Phys. Rev. Lett.* **109**, 246604 (2012).
- [25] P. Virtanen, F. S. Bergeret, and I. V. Tokatly, Magnetolectric effects in superconductors due to spin-orbit scattering: Nonlinear  $\sigma$ -model description, *Phys. Rev. B* **104**, 064515 (2021).
- [26] P. Virtanen, F. S. Bergeret, and I. V. Tokatly, Nonlinear  $\sigma$  model for disordered systems with intrinsic spin-orbit coupling, *Phys. Rev. B* **105**, 224517 (2022).
- [27] F. S. Bergeret and I. V. Tokatly, Singlet-Triplet Conversion and the Long-Range Proximity Effect in Superconductor-Ferromagnet Structures with Generic Spin Dependent Fields, *Phys. Rev. Lett.* **110**, 117003 (2013).
- [28] F. S. Bergeret and I. V. Tokatly, Manifestation of extrinsic spin Hall effect in superconducting structures: Nondissipative magnetolectric effects, *Phys. Rev. B* **94**, 180502(R) (2016).
- [29] C. Huang, I. V. Tokatly, and F. S. Bergeret, Extrinsic spin-charge coupling in diffusive superconducting systems, *Phys. Rev. B* **98**, 144515 (2018).
- [30] F. S. Bergeret and I. V. Tokatly, Spin-orbit coupling as a source of long-range triplet proximity effect in superconductor-ferromagnet hybrid structures, *Phys. Rev. B* **89**, 134517 (2014).
- [31] F. S. Bergeret and I. V. Tokatly, Theory of diffusive  $\varphi_0$  Josephson junctions in the presence of spin-orbit coupling, *Europhys. Lett.* **110**, 57005 (2015).
- [32] I. V. Tokatly, Usadel equation in the presence of intrinsic spin-orbit coupling: A unified theory of magnetolectric effects in normal and superconducting systems, *Phys. Rev. B* **96**, 060502(R) (2017).
- [33] W. Belzig, F. K. Wilhelm, C. Bruder, G. Schön, and A. D. Zaikin, Quasiclassical Green's function approach to mesoscopic superconductivity, *Superlattices Microstruct.* **25**, 1251 (1999).
- [34] M. V. Feigel'man, A. I. Larkin, and M. A. Skvortsov, Keldysh action for disordered superconductors, *Phys. Rev. B* **61**, 12361 (2000).
- [35] A. Kamenev and A. Levchenko, Keldysh technique and nonlinear  $\sigma$ -model: Basic principles and applications, *Adv. Phys.* **58**, 197 (2009).
- [36] R. C. Dynes, V. Narayanamurti, and J. P. Garno, Direct Measurement of Quasiparticle-Lifetime Broadening in a Strong-Coupled Superconductor, *Phys. Rev. Lett.* **41**, 1509 (1978).
- [37] K. D. Usadel, Generalized Diffusion Equation for Superconducting Alloys, *Phys. Rev. Lett.* **25**, 507 (1970).
- [38] M. B. Lifshits and M. I. Dyakonov, Swapping Spin Currents: Interchanging Spin and Flow Directions, *Phys. Rev. Lett.* **103**, 186601 (2009).
- [39] P. Jacquod, R. S. Whitney, J. Meair, and M. Büttiker, Onsager relations in coupled electric, thermoelectric, and spin transport: The tenfold way, *Phys. Rev. B* **86**, 155118 (2012).
- [40] J. Shi, P. Zhang, D. Xiao, and Q. Niu, Proper Definition of Spin Current in Spin-Orbit Coupled Systems, *Phys. Rev. Lett.* **96**, 076604 (2006).
- [41] L. D. Landau and E. M. Lifshitz, *Course of Theoretical Physics* (Pergamon, New York, 1969), Vol. 5.
- [42] R. E. Glover and M. Tinkham, Transmission of superconducting films at millimeter-microwave and far infrared frequencies, *Phys. Rev.* **104**, 844 (1956).

- [43] R. E. Glover and M. Tinkham, Conductivity of superconducting films for photon energies between 0.3 and  $40kT_c$ , *Phys. Rev.* **108**, 243 (1957).
- [44] S. Sridhar, Microwave response of thin-film superconductors, *J. Appl. Phys.* **63**, 159 (1988).
- [45] C. Song, T. W. Heitmann, M. P. DeFeo, K. Yu, R. McDermott, M. Neeley, J. M. Martinis, and B. L. T. Plourde, Microwave response of vortices in superconducting thin films of Re and Al, *Phys. Rev. B* **79**, 174512 (2009).
- [46] G. Catto, W. Liu, S. Kundu, V. Lahtinen, V. Vesterinen, and M. Möttönen, Microwave response of a metallic superconductor subject to a high-voltage gate electrode, *Sci. Rep.* **12**, 6822 (2022).
- [47] See Supplemental Material at <http://link.aps.org/supplemental/10.1103/PhysRevB.108.104506> for the full derivation of the calculation provided in the MATHEMATICA file. The full code to generate the plots in the paper is also included in the MATHEMATICA file.
- [48] M. Tinkham, *Introduction to Superconductivity*, 2nd ed. (McGraw-Hill, New York, 1996), Chap. 3.
- [49] P. G. de Gennes, *Superconductivity of Metals and Alloys* (CRC, Boca Raton, FL, 2018), Chap. 2.
- [50] J. Bok and J. Klein, "Electric Fields" in Superconductors, *Phys. Rev. Lett.* **20**, 660 (1968).
- [51] Y. K. Kato, R. C. Myers, A. C. Gossard, and D. D. Awschalom, Observation of the spin Hall effect in semiconductors, *Science* **306**, 1910 (2004).
- [52] R. E. Collin, *Foundations for Microwave Engineering* (Wiley, New York, 2001).
- [53] S. O. Valenzuela and M. Tinkham, Direct electronic measurement of the spin Hall effect, *Nature (London)* **442**, 176 (2006).
- [54] S. Takahashi and S. Maekawa, Spin Hall effect in superconductors, *Jpn. J. Appl. Phys.* **51**, 010110 (2012).
- [55] Y. Niimi, H. Suzuki, Y. Kawanishi, Y. Omori, T. Valet, A. Fert, and Y. Otani, Extrinsic spin Hall effects measured with lateral spin valve structures, *Phys. Rev. B* **89**, 054401 (2014).
- [56] T. Wakamura, H. Akaike, Y. Omori, Y. Niimi, S. Takahashi, A. Fujimaki, S. Maekawa, and Y. Otani, Quasiparticle-mediated spin Hall effect in a superconductor, *Nat. Mater.* **14**, 675 (2015).
- [57] K.-R. Jeon, J.-C. Jeon, X. Zhou, A. Migliorini, J. Yoon, and S. S. P. Parkin, Giant transition-state quasiparticle spin-Hall effect in an exchange-spin-split superconductor detected by nonlocal magnon spin transport, *ACS Nano* **14**, 15874 (2020).
- [58] G. Bihlmayer, Y. Koroteev, P. Echenique, E. Chulkov, and S. Blügel, The Rashba-effect at metallic surfaces, *Surf. Sci.* **600**, 3888 (2006).
- [59] C. Sanz-Fernández, J. Borge, I. V. Tokatly, and F. S. Bergeret, Nonlocal magnetoelectric effects in diffusive conductors with spatially inhomogeneous spin-orbit coupling, *Phys. Rev. B* **100**, 195406 (2019).
- [60] A. G. Mal'shukov and K. A. Chao, Spin hall conductivity of a disordered two-dimensional electron gas with Dresselhaus spin-orbit interaction, *Phys. Rev. B* **71**, 121308(R) (2005).
- [61] I. Žutić, J. Fabian, and S. Das Sarma, Spin-Polarized Transport in Inhomogeneous Magnetic Semiconductors: Theory of Magnetic/Nonmagnetic  $p$ - $n$  Junctions, *Phys. Rev. Lett.* **88**, 066603 (2002).
- [62] J. Fabian, I. Žutić, and S. Das Sarma, Theory of spin-polarized bipolar transport in magnetic  $p$ - $n$  junctions, *Phys. Rev. B* **66**, 165301 (2002).
- [63] H. Yi, L.-H. Hu, Y. Wang, R. Xiao, J. Cai, D. R. Hickey, C. Dong, Y.-F. Zhao, L.-J. Zhou, R. Zhang, A. R. Richardella, N. Alem, J. A. Robinson, M. H. W. Chan, X. Xu, N. Samarth, C.-X. Liu, and C.-Z. Chang, Crossover from Ising- to Rashba-type superconductivity in epitaxial  $\text{Bi}_2\text{Se}_3/\text{monolayer NbSe}_2$  heterostructures, *Nat. Mater.* **21**, 1366 (2022).
- [64] A. D. Caviglia, M. Gabay, S. Gariglio, N. Reyren, C. Cancellieri, and J.-M. Triscone, Tunable Rashba Spin-Orbit Interaction at Oxide Interfaces, *Phys. Rev. Lett.* **104**, 126803 (2010).
- [65] M. Ben Shalom, M. Sachs, D. Rakhmilevitch, A. Palevski, and Y. Dagan, Tuning Spin-Orbit Coupling and Superconductivity at the  $\text{SrTiO}_3/\text{LaAlO}_3$  Interface: A Magnetotransport Study, *Phys. Rev. Lett.* **104**, 126802 (2010).
- [66] K.-R. Jeon, C. Ciccarelli, H. Kurebayashi, J. Wunderlich, L. F. Cohen, S. Komori, J. W. A. Robinson, and M. G. Blamire, Spin-Pumping-Induced Inverse Spin Hall Effect in  $\text{Nb}/\text{Ni}_{80}\text{Fe}_{20}$  Bilayers and Its Strong Decay Across the Superconducting Transition Temperature, *Phys. Rev. Appl.* **10**, 014029 (2018).
- [67] T. Wang, W. Wang, Y. Xie, M. A. Warsi, J. Wu, Y. Chen, V. O. Lorenz, X. Fan, and J. Q. Xiao, Large spin Hall angle in vanadium film, *Sci. Rep.* **7**, 1306 (2017).
- [68] Y. Kamihara, H. Hiramatsu, M. Hirano, R. Kawamura, H. Yanagi, T. Kamiya, and H. Hosono, Iron-based layered superconductor:  $\text{LaOFeP}$ , *J. Am. Chem. Soc.* **128**, 10012 (2006).
- [69] Y. Kamihara, T. Watanabe, M. Hirano, and H. Hosono, Iron-based layered superconductor  $\text{La}[\text{O}_{1-x}\text{F}_x]\text{FeAs}$  ( $x = 0.05\text{--}0.12$ ) with  $T_c = 26$  K, *J. Am. Chem. Soc.* **130**, 3296 (2008).

# Full list of publications

*Experience is the teacher of all things.*

— Julius Caesar, *Commentarii de Bello Civili*

This Thesis has resulted in the following peer-reviewed publications and preprints. Below we list them in chronological order:

1. A. Hijano, S. Ilić, M. Rouco, C. González-Orellana, M. Ilyn, C. Rogero, P. Virtanen, T. T. Heikkilä, S. Khorshidian, M. Spies, N. Ligato, F. Giazotto, E. Strambini, and F. S. Bergeret, Coexistence of superconductivity and spin-splitting fields in superconductor/ferromagnetic insulator bilayers of arbitrary thickness, [[arXiv:2012.15549](#)] *Phys. Rev. Research* **3**, 023131 (2021)
2. A. Hijano, S. Ilić, and F. S. Bergeret, Anomalous Andreev interferometer: Study of an anomalous Josephson junction coupled to a normal wire, [[arXiv:2106.14021](#)] *Phys. Rev. B* **104**, 214515 (2021)
3. A. Hijano, V. N. Golovach, and F. S. Bergeret, Quasiparticle density of states and triplet correlations in superconductor/ferromagnetic-insulator structures across a sharp domain wall, [[arXiv:2202.09098](#)] *Phys. Rev. B* **105**, 174507 (2022)
4. T. Kokkeler, A. Hijano, and F. S. Bergeret, Anisotropic differential conductance of a mixed-parity superconductor/ferromagnet structure, [[arXiv:2212.00346](#)] *Phys. Rev. B* **107**, 104506 (2023)
5. A. Hijano, F. S. Bergeret, F. Giazotto, and A. Braggio, Microwave-Assisted Thermoelectricity in S-I-S' Tunnel Junctions, [[arXiv:2211.04288](#)] *Phys. Rev. Applied* **19**, 044024 (2023)
6. A. Hijano, F. S. Bergeret, F. Giazotto, and A. Braggio, Bipolar thermoelectricity in S/I/NS and S/I/SN superconducting tunnel junctions, [[arXiv:2303.18212](#)] *Appl. Phys. Lett.* **122**, 242603 (2023)
7. A. Hijano, E. J. Rodríguez, D. Bercioux, and D. Frustaglia, Spin-texture topology in curved circuits driven by spin-orbit interactions, [[arXiv:2209.11653](#)] *Comm. Phys.* **6**, 186 (2023)
8. A. Hijano, S. Vosoughi-nia, F. S. Bergeret, P. Virtanen, and T. T. Heikkilä, Dynamical Hall responses of disordered superconductors, [[arXiv:2306.17785](#)] *Phys. Rev. B* **108**, 104506 (2023)
9. Z. Geng, A. Hijano, S. Ilić, M. Ilyn, I. Maasilta, A. Monfardini, M. Spies, E. Strambini, P. Virtanen, M. Calvo, C. González-Orellana, A. P. Helenius, S. Khorshidian, C. I. Levartoski de Araujo, F. Levy-Bertrand, C. Rogero, F. Giazotto, F. S. Bergeret and T. T. Heikkilä, Superconductor-ferromagnet hybrids for non-reciprocal electronics and detectors, [[arXiv:2302.12732](#)] *Supercond. Sci. Technol.* **36**, 123001 (2023)

10. A. Hijano, S. Ilić and F. S. Bergeret, Weak localization at arbitrary disorder in systems with generic spin-dependent fields, [[arXiv:2311.01148](#)]
11. H. Matsuki, A. Hijano, F. S. Bergeret, J. W. A. Robinson, Absolute superconducting spin switch with spin-orbit coupling, in preparation

# References

*If I have seen further,  
it is by standing on the  
shoulders of giants.*

— Isaac Newton

- [1] G. D. Simoni, E. Strambini, J. S. Moodera, F. S. Bergeret, and F. Giazotto, “Toward the absolute spin-valve effect in superconducting tunnel junctions”, *Nano Lett.* **18**, 6369 (2018).
- [2] P. Machon, M. Eschrig, and W. Belzig, “Nonlocal thermoelectric effects and nonlocal onsager relations in a three-terminal proximity-coupled superconductor-ferromagnet device”, *Phys. Rev. Lett.* **110**, 047002 (2013).
- [3] F. Giazotto, T. T. Heikkilä, and F. S. Bergeret, “Very large thermophase in ferromagnetic josephson junctions”, *Phys. Rev. Lett.* **114**, 067001 (2015).
- [4] F. Hübner, M. J. Wolf, D. Beckmann, and H. v. Löhneysen, “Long-range spin-polarized quasiparticle transport in mesoscopic al superconductors with a zeeman splitting”, *Phys. Rev. Lett.* **109**, 207001 (2012).
- [5] A. Ozaeta, P. Virtanen, F. S. Bergeret, and T. T. Heikkilä, “Predicted very large thermoelectric effect in ferromagnet-superconductor junctions in the presence of a spin-splitting magnetic field”, *Phys. Rev. Lett.* **112**, 057001 (2014).
- [6] S. Kolenda, M. J. Wolf, and D. Beckmann, “Observation of thermoelectric currents in high-field superconductor-ferromagnet tunnel junctions”, *Phys. Rev. Lett.* **116**, 097001 (2016).
- [7] S. Kolenda, P. Machon, D. Beckmann, and W. Belzig, “Nonlinear thermoelectric effects in high-field superconductor-ferromagnet tunnel junctions”, *Beilstein Journal of Nanotechnology* **7**, 1579–1585 (2016).
- [8] F. Giazotto, J. W. A. Robinson, J. S. Moodera, and F. S. Bergeret, “Proposal for a phase-coherent thermoelectric transistor”, *Appl. Phys. Lett.* **105**, 062602 (2014).
- [9] T. T. Heikkilä, R. Ojajärvi, I. J. Maasilta, E. Strambini, F. Giazotto, and F. S. Bergeret, “Thermoelectric radiation detector based on superconductor-ferromagnet systems”, *Phys. Rev. Appl.* **10**, 034053 (2018).
- [10] D. Hanson, S. Hoover, A. Crites, P. A. R. Ade, K. A. Aird, J. E. Ausermann, J. A. Beall, A. N. Bender, B. A. Benson, L. E. Bleem, J. J. Bock, J. E. Carlstrom, C. L. Chang, H. C. Chiang, H.-M. Cho, A. Conley, T. M. Crawford, T. de Haan, M. A. Dobbs, W. Everett, J. Gallicchio, J. Gao, E. M. George, N. W. Halverson, N. Harrington, J. W. Henning, G. C. Hilton, G. P. Holder, W. L. Holzappel, J. D. Hrubes, N. Huang, J. Hubmayr, K. D. Irwin, R. Keisler, L. Knox, A. T. Lee, E. Leitch, D. Li, C. Liang, D. Luong-Van, G. Marsden, J. J. McMahon, J. Mehl, S. S. Meyer, L. Mocanu, T. E. Montroy, T. Natoli, J. P. Nibarger, V. Novosad, S. Padin, C. Pryke, C. L. Reichardt, J. E. Ruhl, B. R. Saliwanchik, J. T. Sayre, K. K. Schaffer,

- B. Schulz, G. Smecher, A. A. Stark, K. T. Story, C. Tucker, K. Vanderlinde, J. D. Vieira, M. P. Viero, G. Wang, V. Yefremenko, O. Zahn, and M. Zemcov (SPTpol Collaboration), “Detection of  $B$ -mode polarization in the cosmic microwave background with data from the south pole telescope”, *Phys. Rev. Lett.* **111**, 141301 (2013).
- [11] A. Luukanen, R. Appleby, M. Kemp, and N. Salmon, *Terahertz Spectroscopy and Imaging* (Springer, 2013) Chap. 19.
- [12] F. Giazotto, P. Solinas, A. Braggio, and F. S. Bergeret, “Ferromagnetic-insulator-based superconducting junctions as sensitive electron thermometers”, *Phys. Rev. Appl.* **4**, 044016 (2015).
- [13] I. V. Bobkova and A. M. Bobkov, “Thermospin effects in superconducting heterostructures”, *Phys. Rev. B* **96**, 104515 (2017).
- [14] J. Linder and M. E. Bathen, “Spin caloritronics with superconductors: enhanced thermoelectric effects, generalized onsager response-matrix, and thermal spin currents”, *Phys. Rev. B* **93**, 224509 (2016).
- [15] D. Huertas-Hernando, Y. V. Nazarov, and W. Belzig, “Absolute spin-valve effect with superconducting proximity structures”, *Phys. Rev. Lett.* **88**, 047003 (2002).
- [16] F. Giazotto and F. S. Bergeret, “Quantum interference hybrid spin-current injector”, *Appl. Phys. Lett.* **102**, 162406 (2013).
- [17] F. Giazotto and F. S. Bergeret, “Phase-tunable colossal magnetothermal resistance in ferromagnetic Josephson valves”, *Appl. Phys. Lett.* **102**, 132603 (2013).
- [18] F. Giazotto, F. Taddei, R. Fazio, and F. Beltram, “Huge nonequilibrium magnetoresistance in hybrid superconducting spin valves”, *Appl. Phys. Lett.* **89**, 022505 (2006).
- [19] F. Giazotto, T. T. Heikkilä, A. Luukanen, A. M. Savin, and J. P. Pekola, “Opportunities for mesoscopics in thermometry and refrigeration: physics and applications”, *Rev. Mod. Phys.* **78**, 217–274 (2006).
- [20] S. Kawabata, A. Ozaeta, A. S. Vasenko, F. W. J. Hekking, and F. S. Bergeret, “Efficient electron refrigeration using superconductor/spin-filter devices”, *Appl. Phys. Lett.* **103**, 032602 (2013).
- [21] E. Strambini, A. Iorio, O. Durante, R. Citro, C. Sanz-Fernández, C. Guarcello, I. V. Tokatly, A. Braggio, M. Rocci, N. Ligato, V. Zannier, L. Sorba, F. S. Bergeret, and F. Giazotto, “A Josephson phase battery”, *Nature Nanotechnology* **15**, 656–660 (2020).
- [22] E. Strambini, M. Spies, N. Ligato, S. Ilić, M. Rouco, C. González-Orellana, M. Ilyn, C. Rogero, F. S. Bergeret, J. S. Moodera, P. Virtanen, T. T. Heikkilä, and F. Giazotto, “Superconducting spintronic tunnel diode”, *Nature Communications* **13**, 2431 (2022).
- [23] V. M. Edelstein, “Magnetoelectric effect in polar superconductors”, *Phys. Rev. Lett.* **75**, 2004 (1995).
- [24] S. K. Yip, “Two-dimensional superconductivity with strong spin-orbit interaction”, *Phys. Rev. B* **65**, 144508 (2002).
- [25] O. Dimitrova and M. V. Feigel’man, “Theory of a two-dimensional superconductor with broken inversion symmetry”, *Phys. Rev. B* **76**, 014522 (2007).
- [26] D. F. Agterberg, “Magnetoelectric effects, helical phases, and FFLO phases”, in *Non-centrosymmetric superconductors*, Vol. 847, Lecture notes in physics (Springer, 2012), pp. 155–170.

- [27] F. Konschelle, I. V. Tokatly, and F. S. Bergeret, “Theory of the spin-galvanic effect and the anomalous phase shift  $\phi_0$  in superconductors and Josephson junctions with intrinsic spin-orbit coupling”, *Phys. Rev. B* **92**, 125443 (2015).
- [28] S. M. Frolov, M. J. Manfra, and J. D. Sau, “Topological superconductivity in hybrid devices”, *Nature Physics* **16**, 718–724 (2020).
- [29] T. Karzig, C. Knapp, R. M. Lutchyn, P. Bonderson, M. B. Hastings, C. Nayak, J. Alicea, K. Flensberg, S. Plugge, Y. Oreg, C. M. Marcus, and M. H. Freedman, “Scalable designs for quasiparticle-poisoning-protected topological quantum computation with Majorana zero modes”, *Phys. Rev. B* **95**, 235305 (2017).
- [30] H. Kamerlingh Onnes, “Further experiments with liquid helium. C. On the change of electric resistance of pure metals at very low temperatures etc. IV. The resistance of pure mercury at helium temperatures”, *Proceedings* **13**, 1274–1276 (1911).
- [31] J. G. Bednorz and K. A. Müller, “Possible high  $T_c$  superconductivity in the Ba-La-Cu-O system”, *Zeitschrift für Physik B Condensed Matter* **64**, 189–193 (1986).
- [32] W. Meissner and R. Ochsenfeld, “Ein neuer effekt bei eintritt der supraleitfähigkeit”, *Naturwissenschaften* **21**, 787–788 (1933).
- [33] J. Bardeen, L. N. Cooper, and J. R. Schrieffer, “Microscopic theory of superconductivity”, *Phys. Rev.* **106**, 162–164 (1957).
- [34] L. N. Cooper, “Bound electron pairs in a degenerate fermi gas”, *Phys. Rev.* **104**, 1189–1190 (1956).
- [35] H. Fröhlich, “Theory of the Superconducting State. I. The Ground State at the Absolute Zero of Temperature”, *Phys. Rev.* **79**, 845–856 (1950).
- [36] E. Maxwell, “Isotope effect in the superconductivity of mercury”, *Phys. Rev.* **78**, 477–477 (1950).
- [37] C. A. Reynolds, B. Serin, W. H. Wright, and L. B. Nesbitt, “Superconductivity of isotopes of mercury”, *Phys. Rev.* **78**, 487–487 (1950).
- [38] P. Coleman, *Introduction to Many-Body Physics* (Cambridge University Press, 2015) Chap. 14.
- [39] N. N. Bogoliubov, “A New Method in the Theory of Superconductivity. I”, *J. Exptl. Theoret. Phys.* **34**, 41 (1958).
- [40] V. V. Tolmachev and S. V. Tiablikov, “A New Method in the Theory of Superconductivity. II”, *J. Exptl. Theoret. Phys.* **34**, 46 (1958).
- [41] N. N. Bogoliubov, “A New Method in the Theory of Superconductivity. III”, *J. Exptl. Theoret. Phys.* **34**, 51 (1958).
- [42] J. Bardeen, L. N. Cooper, and J. R. Schrieffer, “Theory of superconductivity”, *Phys. Rev.* **108**, 1175–1204 (1957).
- [43] M. Tinkham, *Introduction to Superconductivity*, 2nd ed. (Dover publications, 2004) Chap. 3.
- [44] L. P. Gor’kov, *Zhur. Exptl. i. Teoret. Fiz.* **34**, 735 (1958).
- [45] A. Migdal, “Superfluidity and the moments of inertia of nuclei”, *Nuclear Physics* **13**, 655–674 (1959).
- [46] L. V. Keldysh, “Diagram technique for nonequilibrium processes”, *J. Exptl. Theoret. Phys* **20**, 1018 (1964).

- [47] N. Kopnin, *Theory of Nonequilibrium Superconductivity* (Oxford University Press, 2001) Chap. 8.
- [48] Y. Nambu, “Quasi-particles and gauge invariance in the theory of superconductivity”, *Phys. Rev.* **117**, 648–663 (1960).
- [49] A. A. Abrikosov, L. P. Gorkov, and I. E. Dzyaloshinski, *Methods of Quantum Field Theory in Statistical Physics* (Prentice-Hall, Inc., 1963) Chap. 11.
- [50] A. A. Abrikosov, L. P. Gorkov, and I. E. Dzyaloshinski, *Methods of Quantum Field Theory in Statistical Physics* (Prentice-Hall, Inc., 1963) Chap. 7.
- [51] T. Matsubara, “A New Approach to Quantum-Statistical Mechanics”, *Progress of Theoretical Physics* **14**, 351–378 (1955).
- [52] J. E. Moyal, “Quantum mechanics as a statistical theory”, *Mathematical Proceedings of the Cambridge Philosophical Society* **45**, 99–124 (1949).
- [53] D. Langenberg and A. Larkin, *Nonequilibrium superconductivity*, Modern problems in condensed matter sciences (North-Holland, 1986) Chap. 11.
- [54] W. Belzig, F. K. Wilhelm, C. Bruder, G. Schön, and A. D. Zaikin, “Quasiclassical Green’s function approach to mesoscopic superconductivity”, *Superlattices and Microstructures* **25**, 1251–1288 (1999).
- [55] A. Schmid, *Nonequilibrium Superconductivity, Phonons, and Kapitza Boundaries* (Plenum Press, 1981) Chap. 14.
- [56] G. Eilenberger, “Transformation of Gorkov’s equation for type II superconductors into transport-like equations”, *Zeitschrift für Physik A Hadrons and nuclei* **214**, 195–213 (1968).
- [57] U. Eckern and A. Schmid, “Quasiclassical green’s function in the bcs pairing theory”, *Journal of Low Temperature Physics* **45**, 137–166 (1981).
- [58] R. C. Dynes, V. Narayanamurti, and J. P. Garno, “Direct measurement of quasiparticle-lifetime broadening in a strong-coupled superconductor”, *Phys. Rev. Lett.* **41**, 1509–1512 (1978).
- [59] D. A. Ivanov and Y. V. Fominov, “Minigap in superconductor-ferromagnet junctions with inhomogeneous magnetization”, *Phys. Rev. B* **73**, 214524 (2006).
- [60] N. Schopohl and K. Maki, “Quasiparticle spectrum around a vortex line in a d-wave superconductor”, *Phys. Rev. B* **52**, 490 (1995).
- [61] K. D. Usadel, “Generalized diffusion equation for superconducting alloys”, *Phys. Rev. Lett.* **25**, 507–509 (1970).
- [62] F. S. Bergeret and I. V. Tokatly, “Singlet-triplet conversion and the long-range proximity effect in superconductor-ferromagnet structures with generic spin dependent fields”, *Phys. Rev. Lett.* **110**, 117003 (2013).
- [63] F. S. Bergeret and I. V. Tokatly, “Manifestation of extrinsic spin Hall effect in superconducting structures: nondissipative magnetoelectric effects”, *Phys. Rev. B* **94**, 180502 (2016).
- [64] C. Huang, I. V. Tokatly, and F. S. Bergeret, “Extrinsic spin-charge coupling in diffusive superconducting systems”, *Phys. Rev. B* **98**, 144515 (2018).
- [65] P. Virtanen, F. S. Bergeret, and I. V. Tokatly, “Magnetoelectric effects in superconductors due to spin-orbit scattering: nonlinear  $\sigma$ -model description”, *Phys. Rev. B* **104**, 064515 (2021).



- [66] F. S. Bergeret and I. V. Tokatly, “Spin-orbit coupling as a source of long-range triplet proximity effect in superconductor-ferromagnet hybrid structures”, *Phys. Rev. B* **89**, 134517 (2014).
- [67] F. S. Bergeret and I. V. Tokatly, “Theory of diffusive  $\phi_0$  Josephson junctions in the presence of spin-orbit coupling”, *EPL* **110**, 57005 (2015).
- [68] I. V. Tokatly, “Usadel equation in the presence of intrinsic spin-orbit coupling: a unified theory of magnetoelectric effects in normal and superconducting systems”, *Phys. Rev. B* **96**, 060502 (2017).
- [69] C. Gorini, R. Raimondi, and P. Schwab, “Onsager relations in a two-dimensional electron gas with spin-orbit coupling”, *Phys. Rev. Lett.* **109**, 246604 (2012).
- [70] P. Virtanen, F. S. Bergeret, and I. V. Tokatly, “Nonlinear  $\sigma$  model for disordered systems with intrinsic spin-orbit coupling”, *Phys. Rev. B* **105**, 224517 (2022).
- [71] M. B. Lifshits and M. I. Dyakonov, “Swapping spin currents: interchanging spin and flow directions”, *Phys. Rev. Lett.* **103**, 186601 (2009).
- [72] A. Cottet, D. Huertas-Hernando, W. Belzig, and Y. V. Nazarov, “Spin-dependent boundary conditions for isotropic superconducting Green’s functions”, *Phys. Rev. B* **80**, 184511 (2009).
- [73] J. Linder, T. Yokoyama, A. Sudbø, and M. Eschrig, “Pairing symmetry conversion by spin-active interfaces in magnetic normal-metal–superconductor junctions”, *Phys. Rev. Lett.* **102**, 107008 (2009).
- [74] F. S. Bergeret, A. Verso, and A. F. Volkov, “Electronic transport through ferromagnetic and superconducting junctions with spin-filter tunneling barriers”, *Phys. Rev. B* **86**, 214516 (2012).
- [75] M. Eschrig, A. Cottet, W. Belzig, and J. Linder, “General boundary conditions for quasiclassical theory of superconductivity in the diffusive limit: application to strongly spin-polarized systems”, *New Journal of Physics* **17**, 083037 (2015).
- [76] T. T. Heikkilä, M. Silaev, P. Virtanen, and F. S. Bergeret, “Thermal, electric and spin transport in superconductor/ferromagnetic-insulator structures”, *Progress in Surface Science* **94**, 100540 (2019).
- [77] A. Hijano, *Proximity effects in superconductor-ferromagnetic insulator bilayers of arbitrary thickness*, Master’s thesis, University of the Basque Country, 2020.
- [78] A. Hijano, S. Ilić, M. Rouco, C. González-Orellana, M. Ilyn, C. Rogero, P. Virtanen, T. T. Heikkilä, S. Khorshidian, M. Spies, N. Ligato, F. Giazotto, E. Strambini, and F. S. Bergeret, “Coexistence of superconductivity and spin-splitting fields in superconductor/ferromagnetic insulator bilayers of arbitrary thickness”, *Phys. Rev. Res.* **3**, 023131 (2021).
- [79] M. Y. Kupriyanov and V. F. Lukichev, *Zh. Eksp. Teor. Fiz.* **94**, 139, [*Sov. Phys. JETP* **67**, 1163 (1988)], 1988.
- [80] M. Eschrig, A. Cottet, W. Belzig, and J. Linder, “General boundary conditions for quasiclassical theory of superconductivity in the diffusive limit: application to strongly spin-polarized systems”, *New Journal of Physics* **17**, 083037 (2015).
- [81] Y. V. Nazarov, “Novel circuit theory of Andreev reflection”, *Superlattices and microstructures* **25**, 1221–1231 (1999).
- [82] Y. Tanaka, Y. Nazarov, and S. Kashiwaya, “Circuit theory of unconventional superconductor junctions”, *Phys. Rev. Lett.* **90**, 167003 (2003).

- [83] Y. Tanaka, Y. V. Nazarov, A. Golubov, and S. Kashiwaya, “Theory of charge transport in diffusive normal metal/unconventional singlet superconductor contacts”, *Phys. Rev. B* **69**, 144519 (2004).
- [84] Y. Tanaka, T. Kokkeler, and A. Golubov, “Theory of proximity effect in  $s + p$ -wave superconductor junctions”, *Phys. Rev. B* **105**, 214512 (2022).
- [85] G. Blonder, M. Tinkham, and T. Klapwijk, “Transition from metallic to tunneling regimes in superconducting microconstrictions: excess current, charge imbalance, and supercurrent conversion”, *Phys. Rev. B* **25**, 4515 (1982).
- [86] J. S. Moodera, X. Hao, G. A. Gibson, and R. Meservey, “Electron-Spin Polarization in Tunnel Junctions in Zero Applied Field with Ferromagnetic EuS Barriers”, *Phys. Rev. Lett.* **61**, 637–640 (1988).
- [87] X. Hao, J. S. Moodera, and R. Meservey, “Spin-filter effect of ferromagnetic europium sulfide tunnel barriers”, *Phys. Rev. B* **42**, 8235–8243 (1990).
- [88] R. Meservey and P. Tedrow, “Spin-polarized electron tunneling”, *Phys. Rep.* **238**, 173–243 (1994).
- [89] E. Strambini, V. N. Golovach, G. De Simoni, J. S. Moodera, F. S. Bergeret, and F. Giazotto, “Revealing the magnetic proximity effect in EuS/Al bilayers through superconducting tunneling spectroscopy”, *Phys. Rev. Materials* **1**, 054402 (2017).
- [90] T. Tokuyasu, J. A. Sauls, and D. Rainer, “Proximity effect of a ferromagnetic insulator in contact with a superconductor”, *Phys. Rev. B* **38**, 8823–8833 (1988).
- [91] P. Virtanen, A. Vargunin, and M. Silaev, “Quasiclassical free energy of superconductors: disorder-driven first-order phase transition in superconductor/ferromagnetic-insulator bilayers”, *Phys. Rev. B* **101**, 094507 (2020).
- [92] M. Rouco, S. Chakraborty, F. Aikebaier, V. N. Golovach, E. Strambini, J. S. Moodera, F. Giazotto, T. T. Heikkilä, and F. S. Bergeret, “Charge transport through spin-polarized tunnel junction between two spin-split superconductors”, *Phys. Rev. B* **100**, 184501 (2019).
- [93] A. Y. Aladyshev, A. I. Buzdin, A. A. Fraerman, A. S. Mel’nikov, D. A. Ryzhov, and A. V. Sokolov, “Domain-wall superconductivity in hybrid superconductor-ferromagnet structures”, *Phys. Rev. B* **68**, 184508 (2003).
- [94] M. Houzet and A. I. Buzdin, “Theory of domain-wall superconductivity in superconductor/ferromagnet bilayers”, *Phys. Rev. B* **74**, 214507 (2006).
- [95] I. V. Bobkova and A. M. Bobkov, “Reconstruction of the Density of States at the End of an S/F Bilayer”, *JETP Lett.* **109**, 57 (2019).
- [96] D. S. Rabinovich, I. V. Bobkova, A. M. Bobkov, and M. A. Silaev, “Magnetoelectric effects in superconductor/ferromagnet bilayers”, *Phys. Rev. B* **99**, 214501 (2019).
- [97] F. Aikebaier, P. Virtanen, and T. Heikkilä, “Superconductivity near a magnetic domain wall”, *Phys. Rev. B* **99**, 104504 (2019).
- [98] Z. Yang, M. Lange, A. Volodin, R. Szymczak, and V. V. Moshchalkov, “Domain-wall superconductivity in superconductor–ferromagnet hybrids”, *Nat. Mater.* **3**, 793–798 (2004).
- [99] J. Linder and K. Halterman, “Superconducting spintronics with magnetic domain walls”, *Phys. Rev. B* **90**, 104502 (2014).
- [100] F. S. Bergeret, A. F. Volkov, and K. B. Efetov, “Odd triplet superconductivity and related phenomena in superconductor-ferromagnet structures”, *Rev. Mod. Phys.* **77**, 1321–1373 (2005).

- [101] A. Cottet, “Inducing odd-frequency triplet superconducting correlations in a normal metal”, *Phys. Rev. Lett.* **107**, 177001 (2011).
- [102] F. S. Bergeret, M. Silaev, P. Virtanen, and T. T. Heikkilä, “Colloquium: nonequilibrium effects in superconductors with a spin-splitting field”, *Reviews of Modern Physics* **90**, 041001 (2018).
- [103] V. L. Berezinskii, “New model of the anisotropic phase of superfluid He<sup>3</sup>”, *Sov. J. Exp. Theor. Phys. Lett.* **20**, 628 (1974).
- [104] Y. Tanaka, M. Sato, and N. Nagaosa, “Symmetry and topology in superconductors –odd-frequency pairing and edge states–”, *Journal of the Physical Society of Japan* **81**, 011013 (2012).
- [105] J. Linder and A. V. Balatsky, “Odd-frequency superconductivity”, *Reviews of Modern Physics* **91**, 045005 (2019).
- [106] M. Eschrig, “Spin-polarized supercurrents for spintronics”, *Phys. Today* **64**, 43 (2011).
- [107] A. Kamenev, *Field theory of non-equilibrium systems* (Cambridge University Press, 2011) Chap. 14.
- [108] A. Altland and B. Simons, *Condensed matter field theory*, 2nd ed. (Cambridge University Press, 2010) Chap. 1.
- [109] L. Hofstetter, S. Csonka, J. Nygård, and C. Schönenberger, “Cooper pair splitter realized in a two-quantum-dot Y-junction”, *Nature* **461**, 960–963 (2009).
- [110] B. Josephson, “Possible new effects in superconductive tunnelling”, *Physics Letters* **1**, 251–253 (1962).
- [111] B. D. Josephson, “The discovery of tunnelling supercurrents”, *Rev. Mod. Phys.* **46**, 251–254 (1974).
- [112] L. N. Bulaevskii, V. V. Kuzii, and A. A. Sobyanin, “Superconducting system with weak coupling to the current to the ground state”, *JETP Lett.* **25**, 290 (1977).
- [113] A. I. Buzdin, L. N. Bulaevskii, and S. V. Panjukov, *JETP Lett.* **35**, 178 (1982).
- [114] V. V. Ryazanov, V. A. Oboznov, A. Y. Rusanov, A. V. Veretennikov, A. A. Golubov, and J. Aarts, “Coupling of two superconductors through a ferromagnet: evidence for a  $\pi$  junction”, *Phys. Rev. Lett.* **86**, 2427–2430 (2001).
- [115] A. I. Buzdin, “Proximity effects in superconductor-ferromagnet heterostructures”, *Rev. Mod. Phys.* **77**, 935–976 (2005).
- [116] V. A. Oboznov, V. V. Bol’ginov, A. K. Feofanov, V. V. Ryazanov, and A. I. Buzdin, “Thickness Dependence of the Josephson Ground States of Superconductor-Ferromagnet-Superconductor Junctions”, *Phys. Rev. Lett.* **96**, 197003 (2006).
- [117] A. Buzdin, “Direct Coupling Between Magnetism and Superconducting Current in the Josephson  $\phi_0$  Junction”, *Phys. Rev. Lett.* **101**, 107005 (2008).
- [118] V. M. Edelstein, “The Ginzburg - Landau equation for superconductors of polar symmetry”, *Journal of Physics: Condensed Matter* **8**, 339–349 (1996).
- [119] V. Mineev and K. Samokhin, “Nonuniform states in noncentrosymmetric superconductors: Derivation of Lifshitz invariants from microscopic theory”, *Phys. Rev. B* **78**, 144503 (2008).
- [120] E. Bauer and M. Sigrist, eds., *Non-centrosymmetric superconductors: introduction and overview*, Lecture notes in physics 847 (Springer Verlag, Heidelberg ; New York, 2012).

- [121] V. Braude and Y. V. Nazarov, “Fully developed triplet proximity effect”, *Phys. Rev. Lett.* **98**, 077003 (2007).
- [122] R. Grein, M. Eschrig, G. Metalidis, and G. Schön, “Spin-dependent cooper pair phase and pure spin supercurrents in strongly polarized ferromagnets”, *Phys. Rev. Lett.* **102**, 227005 (2009).
- [123] I. Margaritis, V. Paltoglou, and N. Flytzanis, “Zero phase difference supercurrent in ferromagnetic Josephson junctions”, *Journal of Physics: Condensed Matter* **22**, 445701 (2010).
- [124] J.-F. Liu and K. S. Chan, “Anomalous Josephson current through a ferromagnetic trilayer junction”, *Phys. Rev. B* **82**, 184533 (2010).
- [125] I. Kulagina and J. Linder, “Spin supercurrent, magnetization dynamics, and  $\phi$ -state in spin-textured Josephson junctions”, *Phys. Rev. B* **90**, 054504 (2014).
- [126] A. Moor, A. F. Volkov, and K. B. Efetov, “Nematic versus ferromagnetic spin filtering of triplet cooper pairs in superconducting spintronics”, *Phys. Rev. B* **92**, 180506 (2015).
- [127] S. Mironov and A. Buzdin, “Triplet proximity effect in superconducting heterostructures with a half-metallic layer”, *Phys. Rev. B* **92**, 184506 (2015).
- [128] M. A. Silaev, I. V. Tokatly, and F. S. Bergeret, “Anomalous current in diffusive ferromagnetic Josephson junctions”, *Phys. Rev. B* **95**, 184508 (2017).
- [129] S. Frolov, M. Manfra, and J. Sau, “Topological superconductivity in hybrid devices”, *Nature Physics* **16**, 718–724 (2020).
- [130] M. Sato and Y. Ando, “Topological superconductors: a review”, *Reports on Progress in Physics* **80**, 076501 (2017).
- [131] M. Leijnse and K. Flensberg, “Introduction to topological superconductivity and Majorana fermions”, *Semiconductor Science and Technology* **27**, 124003 (2012).
- [132] J. Linder and J. W. Robinson, “Superconducting spintronics”, *Nature Physics* **11**, 307–315 (2015).
- [133] F. Ando, Y. Miyasaka, T. Li, J. Ishizuka, T. Arakawa, Y. Shiota, T. Moriyama, Y. Yanase, and T. Ono, “Observation of superconducting diode effect”, *Nature* **584**, 373–376 (2020).
- [134] A. A. Reynoso, G. Usaj, C. A. Balseiro, D. Feinberg, and M. Avignon, “Anomalous Josephson Current in Junctions with Spin Polarizing Quantum Point Contacts”, *Phys. Rev. Lett.* **101**, 107001 (2008).
- [135] A. Zazunov, R. Egger, T. Jonckheere, and T. Martin, “Anomalous Josephson Current through a Spin-Orbit Coupled Quantum Dot”, *Phys. Rev. Lett.* **103**, 147004 (2009).
- [136] A. Brunetti, A. Zazunov, A. Kundu, and R. Egger, “Anomalous Josephson current, incipient time-reversal symmetry breaking, and Majorana bound states in interacting multilevel dots”, *Phys. Rev. B* **88**, 144515 (2013).
- [137] T. Yokoyama, M. Eto, and Y. V. Nazarov, “Anomalous Josephson effect induced by spin-orbit interaction and Zeeman effect in semiconductor nanowires”, *Phys. Rev. B* **89**, 195407 (2014).
- [138] F. Konschelle, I. V. Tokatly, and F. S. Bergeret, “Theory of the spin-galvanic effect and the anomalous phase shift  $\phi_0$  in superconductors and Josephson junctions with intrinsic spin-orbit coupling”, *Phys. Rev. B* **92**, 125443 (2015).
- [139] K. N. Nesterov, M. Houzet, and J. S. Meyer, “Anomalous Josephson effect in semiconducting nanowires as a signature of the topologically nontrivial phase”, *Phys. Rev. B* **93**, 174502 (2016).

- [140] I. V. Bobkova, A. M. Bobkov, A. A. Zyuzin, and M. Alidoust, “Magnetolectrics in disordered topological insulator Josephson junctions”, *Phys. Rev. B* **94**, 134506 (2016).
- [141] D. B. Szombati, S. Nadj-Perge, D. Car, S. R. Plissard, E. P. A. M. Bakkers, and L. P. Kouwenhoven, “Josephson  $\varphi_0$ -junction in nanowire quantum dots”, *Nature Physics* **12**, 568–572 (2016).
- [142] A. Assouline, C. Feuillet-Palma, N. Bergeal, T. Zhang, A. Mottaghizadeh, A. Zimmers, E. Lhuillier, M. Eddrie, P. Atkinson, M. Aprili, and H. Aubin, “Spin-Orbit induced phase-shift in Bi<sub>2</sub>Se<sub>3</sub> Josephson junctions”, *Nature Communications* **10**, 126 (2019).
- [143] W. Mayer, M. C. Dartiailh, J. Yuan, K. S. Wickramasinghe, E. Rossi, and J. Shabani, “Gate controlled anomalous phase shift in Al/InAs Josephson junctions”, *Nature Communications* **11**, 212 (2020).
- [144] S. Yip, “Josephson current-phase relationships with unconventional superconductors”, *Phys. Rev. B* **52**, 3087–3090 (1995).
- [145] M. Sigrist, “Time-Reversal Symmetry Breaking States in High-Temperature Superconductors”, *Progress of Theoretical Physics* **99**, 899–929 (1998).
- [146] S. Kashiwaya and Y. Tanaka, “Tunnelling effects on surface bound states in unconventional superconductors”, *Reports on Progress in Physics* **63**, 1641–1724 (2000).
- [147] P. M. R. Brydon, B. Kastening, D. K. Morr, and D. Manske, “Interplay of ferromagnetism and triplet superconductivity in a Josephson junction”, *Phys. Rev. B* **77**, 104504 (2008).
- [148] C. Schrade, S. Hoffman, and D. Loss, “Detecting topological superconductivity with  $\phi_0$  Josephson junctions”, *Phys. Rev. B* **95**, 195421 (2017).
- [149] P. E. Dolgirev, M. S. Kalenkov, and A. D. Zaikin, “Current-phase relation and flux-dependent thermoelectricity in Andreev interferometers”, *Phys. Rev. B* **97**, 054521 (2018).
- [150] P. E. Dolgirev, M. S. Kalenkov, A. E. Tarkhov, and A. D. Zaikin, “Phase-coherent electron transport in asymmetric crosslike Andreev interferometers”, *Phys. Rev. B* **100**, 054511 (2019).
- [151] D. Margineda, J. Claydon, F. Qejvanaj, and C. Checkley, “Anomalous Josephson Effect in Non-magnetic Andreev Interferometers”, arXiv preprint arXiv:2105.13968 (2021).
- [152] A. G. Mal’shukov, “Long-range effect of a Zeeman field on the electric current through the helical metal-superconductor interface in an Andreev interferometer”, *Phys. Rev. B* **97**, 064515 (2018).
- [153] P. E. Dolgirev, M. S. Kalenkov, and A. D. Zaikin, “Topology-Controlled Thermopower Oscillations in Multiterminal Andreev Interferometers”, *Phys. Status Solidi RRL* **13**, 1800252 (2019).
- [154] A. F. Volkov, “Signatures of a long-range spin-triplet component in an Andreev interferometer”, *Phys. Rev. B* **102**, 094517 (2020).
- [155] G. Blasi, F. Taddei, L. Arrachea, M. Carrega, and A. Braggio, “Nonlocal thermoelectricity in a topological Andreev interferometer”, *Phys. Rev. B* **102**, 241302 (2020).
- [156] A. Zaitsev, “Phase-coherent conductance of mesoscopic superconductor-normal-metal coupled systems”, *Physica B: Condensed Matter* **203**, 274–279 (1994).
- [157] T. H. Stoof and Y. V. Nazarov, “Kinetic-equation approach to diffusive superconducting hybrid devices”, *Phys. Rev. B* **53**, 14496–14505 (1996).
- [158] Y. V. Nazarov and T. H. Stoof, “Diffusive Conductors as Andreev Interferometers”, *Phys. Rev. Lett.* **76**, 823–826 (1996).

- [159] A. A. Golubov, F. K. Wilhelm, and A. D. Zaikin, “Coherent charge transport in metallic proximity structures”, *Phys. Rev. B* **55**, 1123–1137 (1997).
- [160] V. T. Petrashov, V. N. Antonov, P. Delsing, and R. Claeson, “Phase memory effects in mesoscopic rings with superconducting “mirrors””, *Phys. Rev. Lett.* **70**, 347–350 (1993).
- [161] V. T. Petrashov, V. N. Antonov, P. Delsing, and T. Claeson, “Phase controlled conductance of mesoscopic structures with superconducting “mirrors””, *Phys. Rev. Lett.* **74**, 5268–5271 (1995).
- [162] V. Antonov, V. Petrashov, and P. Delsing, “Phase sensitive phenomena in Andreev interferometer”, *Physica C: Superconductivity* **352**, 173–176 (2001).
- [163] V. T. Petrashov, K. G. Chua, K. M. Marshall, R. S. Shaikhaidarov, and J. T. Nicholls, “Andreev Probe of Persistent Current States in Superconducting Quantum Circuits”, *Phys. Rev. Lett.* **95**, 147001 (2005).
- [164] N. L. Plaszkó, P. Rakyta, J. Cserti, A. Kormányos, and C. J. Lambert, “Quantum Interference and Nonequilibrium Josephson Currents in Molecular Andreev Interferometers”, *Nanomaterials* **10**, 10.3390/nano10061033 (2020).
- [165] C. Checkley, A. Iagallo, R. Shaikhaidarov, J. T. Nicholls, and V. T. Petrashov, “Andreev interferometers in a strong radio-frequency field”, *Journal of Physics: Condensed Matter* **23**, 135301 (2011).
- [166] F. Deon, S. Šopić, and A. F. Morpurgo, “Tuning the influence of microscopic decoherence on the superconducting proximity effect in a graphene Andreev interferometer”, *Phys. Rev. Lett.* **112**, 126803 (2014).
- [167] A. V. Galaktionov, A. D. Zaikin, and L. S. Kuzmin, “Andreev interferometer with three superconducting electrodes”, *Phys. Rev. B* **85**, 224523 (2012).
- [168] A. V. Galaktionov and A. D. Zaikin, “Current-biased Andreev interferometer”, *Phys. Rev. B* **88**, 104513 (2013).
- [169] J. Eom, C.-J. Chien, and V. Chandrasekhar, “Phase Dependent Thermopower in Andreev Interferometers”, *Phys. Rev. Lett.* **81**, 437–440 (1998).
- [170] A. Parsons, I. A. Sosnin, and V. T. Petrashov, “Reversal of thermopower oscillations in the mesoscopic Andreev interferometer”, *Phys. Rev. B* **67**, 140502 (2003).
- [171] V. Chandrasekhar, “Thermal transport in superconductor/normal-metal structures”, *Superconductor Science and Technology* **22**, 083001 (2009).
- [172] A. Volkov and V. Pavlovskii, “Long-range thermoelectric effects in mesoscopic superconductor–normal metal structures”, *Phys. Rev. B* **72**, 014529 (2005).
- [173] A. F. Volkov and H. Takayanagi, “ac Long-Range Phase-Coherent Effects in Mesoscopic Superconductor–Normal Metal Structures”, *Phys. Rev. Lett.* **76**, 4026–4029 (1996).
- [174] A. F. Volkov and V. V. Pavlovskii, “Methods of quasiclassical Green’s functions in the theory of transport phenomena in superconducting mesoscopic structures”, *AIP Conf. Proc.* **427**, 343 (1998).
- [175] A. Volkov and V. Pavlovskii, “Phase-coherent phenomena in SNS structures”, *Physics-Uspekhi* **41**, 191–195 (1998).
- [176] C. Goupil, *Continuum Theory and Modeling of Thermoelectric Elements* (Wiley-VCH, 2016) Chap. 1.
- [177] T. J. Seebeck, “Magnetische polarisation der metalle und erze durch temperatur-differenz”, *Abhandlungen der Königlich Akademie der Wissenschaften zu Berlin*, 265 (1822).

- [178] G. Germanese, F. Paolucci, G. Marchegiani, A. Braggio, and F. Giazotto, “Bipolar thermoelectric Josephson engine”, *Nat. Nanotechnol.* **17**, 1084 (2022).
- [179] P. Machon, M. Eschrig, and W. Belzig, “Nonlocal thermoelectric effects and nonlocal onsager relations in a three-terminal proximity-coupled superconductor-ferromagnet device”, *Phys. Rev. Lett.* **110**, 047002 (2013).
- [180] A. Ozaeta, P. Virtanen, F. Bergeret, and T. Heikkilä, “Predicted very large thermoelectric effect in ferromagnet-superconductor junctions in the presence of a spin-splitting magnetic field”, *Phys. Rev. Lett.* **112**, 057001 (2014).
- [181] S. Kolenda, M. J. Wolf, and D. Beckmann, “Observation of thermoelectric currents in high-field superconductor-ferromagnet tunnel junctions”, *Phys. Rev. Lett.* **116**, 097001 (2016).
- [182] T. T. Heikkilä, R. Ojajärvi, I. J. Maasilta, E. Strambini, F. Giazotto, and F. S. Bergeret, “Thermoelectric radiation detector based on superconductor-ferromagnet systems”, *Phys. Rev. Applied* **10**, 034053 (2018).
- [183] S. Chakraborty and T. T. Heikkilä, “Thermoelectric radiation detector based on a superconductor-ferromagnet junction: calorimetric regime”, *J. Appl. Phys.* **124**, 123902 (2018).
- [184] E. Strambini, M. Spies, N. Ligato, S. Ilić, M. Rouco, C. González-Orellana, M. Ilyn, C. Rogero, F. Bergeret, J. Moodera, et al., “Superconducting spintronic tunnel diode”, *Nature communications* **13**, 1–7 (2022).
- [185] Z. Geng and I. J. Maasilta, “Analytical models for the pulse shape of a superconductor-ferromagnet tunnel junction thermoelectric microcalorimeter”, *J. Low Temp. Phys.*, 10.1007/s10909-022-02768-y (2022).
- [186] R. Meservey and P. Tedrow, “Spin-polarized electron tunneling”, *Phys. Rep.* **238**, 173–243 (1994).
- [187] J. S. Moodera, T. S. Santos, and T. Nagahama, “The phenomena of spin-filter tunnelling”, *J. Phys. Condens. Matter* **19**, 165202 (2007).
- [188] G.-X. Miao, J. Chang, B. A. Assaf, D. Heiman, and J. S. Moodera, “Spin regulation in composite spin-filter barrier devices”, *Nat. Commun.* **5**, 3682 (2014).
- [189] J. P. Morten, A. Brataas, and W. Belzig, “Spin transport and magnetoresistance in ferromagnet/superconductor/ferromagnet spin valves”, *Phys. Rev. B* **72**, 014510 (2005).
- [190] F. Paolucci and F. Giazotto, “Ghz superconducting single-photon detectors for dark matter search”, *Instruments* **5**, 14 (2021).
- [191] T. P. C. P. A. R. Ade, Y. Akiba, A. E. Anthony, K. Arnold, M. Atlas, D. Barron, D. Boettger, J. Borrill, S. Chapman, Y. Chinone, M. Dobbs, T. Elleflot, J. Errard, G. Fabbian, C. Feng, D. Flanigan, A. Gilbert, W. Grainger, N. W. Halverson, M. Hasegawa, K. Hattori, M. Hazumi, W. L. Holzapfel, Y. Hori, J. Howard, P. Hyland, Y. Inoue, G. C. Jaehnig, A. H. Jaffe, B. Keating, Z. Kermish, R. Kesitalo, T. Kisner, M. L. Jeune, A. T. Lee, E. M. Leitch, E. Linder, M. Lungu, F. Matsuda, T. Matsumura, X. Meng, N. J. Miller, H. Morii, S. Moyerman, M. J. Myers, M. Navaroli, H. Nishino, A. Orlando, H. Paar, J. Peloton, D. Poletti, E. Quealy, G. Rebeiz, C. L. Reichardt, P. L. Richards, C. Ross, I. Schanning, D. E. Schenck, B. D. Sherwin, A. Shimizu, C. Shimmin, M. Shimon, P. Siritanasak, G. Smecher, H. Spieler, N. Stebor, B. Steinbach, R. Stompor, A. Suzuki, S. Takakura, T. Tomaru, B. Wilson, A. Yadav, and O. Zahn, “A measurement of the cosmic microwave background B-mode polarization power spectrum at sub-degree scales with polarbear”, *The Astrophysical Journal* **794**, 171 (2014).

- [192] M. Madhavacheril, N. Sehgal, R. Allison, N. Battaglia, J. R. Bond, E. Calabrese, J. Caligiuri, K. Coughlin, D. Crichton, R. Datta, M. J. Devlin, J. Dunkley, R. Dünner, K. Fogarty, E. Grace, A. Hajian, M. Hasselfield, J. C. Hill, M. Hilton, A. D. Hincks, R. Hlozek, J. P. Hughes, A. Kosowsky, T. Louis, M. Lungu, J. McMahon, K. Moodley, C. Munson, S. Naess, F. Nati, L. Newburgh, M. D. Niemack, L. A. Page, B. Partridge, B. Schmitt, B. D. Sherwin, J. Sievers, D. N. Spergel, S. T. Staggs, R. Thornton, A. Van Engelen, J. T. Ward, and E. J. Wollack (Atacama Cosmology Telescope Collaboration), “Evidence of lensing of the cosmic microwave background by dark matter halos”, *Phys. Rev. Lett.* **114**, 151302 (2015).
- [193] J. N. Ullom and D. A. Bennett, “Review of superconducting transition-edge sensors for x-ray and gamma-ray spectroscopy”, *Superconductor Science and Technology* **28**, 084003 (2015).
- [194] G. Marchegiani, A. Braggio, and F. Giazotto, “Phase-tunable thermoelectricity in a Josephson junction”, *Phys. Rev. Research* **2**, 043091 (2020).
- [195] G. Marchegiani, A. Braggio, and F. Giazotto, “Superconducting nonlinear thermoelectric heat engine”, *Phys. Rev. B* **101**, 214509 (2020).
- [196] G. Marchegiani, A. Braggio, and F. Giazotto, “Nonlinear thermoelectricity with electron-hole symmetric systems”, *Phys. Rev. Lett.* **124**, 106801 (2020).
- [197] G. Germanese, F. Paolucci, G. Marchegiani, A. Braggio, and F. Giazotto, “Phase Control of Bipolar Thermoelectricity in Josephson Tunnel Junctions”, *Phys. Rev. Appl.* **19**, 014074 (2023).
- [198] P. K. Tien and J. P. Gordon, “Multiphoton process observed in the interaction of microwave fields with the tunneling between superconductor films”, *Phys. Rev.* **129**, 647–651 (1963).
- [199] J. N. Sweet and G. I. Rochlin, “Microwave-Photon-Assisted Tunneling in Sn-I-Sn Superconducting Tunnel Junctions”, *Phys. Rev. B* **2**, 656–664 (1970).
- [200] C. A. Hamilton and S. Shapiro, “Rf-induced effects in superconducting tunnel junctions”, *Phys. Rev. B* **2**, 4494–4503 (1970).
- [201] B. Kofoed, U. K. Poulsen, and K. Saermark, “Microwave-assisted tunnelling effects in small-area thin-film superconducting tunnel junctions”, *Phys. Status Solidi A* **23**, 87 (1974).
- [202] J. Tucker, “Quantum limited detection in tunnel junction mixers”, *IEEE J. Quantum Electron.* **15**, 1234–1258 (1979).
- [203] J. R. Tucker and M. J. Feldman, “Quantum detection at millimeter wavelengths”, *Rev. Mod. Phys.* **57**, 1055–1113 (1985).
- [204] K. Hamasaki, K. Yoshida, F. Irie, and K. Enpuku, “Capacitance measurement of Josephson tunnel junctions with microwave-induced dc quasiparticle tunneling currents”, *J. Appl. Phys.* **53**, 3713 (1982).
- [205] S. P. Kashinje and P. Wyder, “Photon-assisted tunnelling in a magnetic field”, *J. Phys. C: Solid State Phys.* **19**, 3193–3202 (1986).
- [206] Q.-f. Sun, J. Wang, and T.-h. Lin, “Photon-assisted Andreev tunneling through a mesoscopic hybrid system”, *Phys. Rev. B* **59**, 13126–13138 (1999).
- [207] B. Leone, J. Gao, T. Klapwijk, B. Jackson, W. Laauwen, and G. de Lange, “Hot electron effect in terahertz hybrid devices”, *IEEE Trans. Appl. Supercond.* **11**, 649–652 (2001).
- [208] P. Kot, R. Drost, M. Uhl, J. Ankerhold, J. C. Cuevas, and C. R. Ast, “Microwave-assisted tunneling and interference effects in superconducting junctions under fast driving signals”, *Phys. Rev. B* **101**, 134507 (2020).



- [209] J. T. Muhonen, M. Meschke, and J. P. Pekola, “Micrometre-scale refrigerators”, *Rep. Prog. Phys.* **75**, 046501 (2012).
- [210] A. Hijano, F. S. Bergeret, F. Giazotto, and A. Braggio, “Bipolar thermoelectricity in S/I/NS and S/I/SN superconducting tunnel junctions”, *Appl. Phys. Lett.* **122**, 242603 (2023).
- [211] A. Barone and G. Paternò, *Physics and Applications of the Josephson effect* (Wiley, 1982) Chap. 2, p. 35.
- [212] R. E. Harris, “Cosine and other terms in the Josephson tunneling current”, *Phys. Rev. B* **10**, 84–94 (1974).
- [213] D. R. Gulevich, V. P. Koshelets, and F. V. Kusmartsev, “Josephson flux-flow oscillator: The microscopic tunneling approach”, *Phys. Rev. B* **96**, 024515 (2017).
- [214] A. Barone, G. Paternò, M. Russo, and R. Vaglio, “Light-induced transition from “small” to “large” Josephson junctions”, *Phys. Lett. A* **53**, 393–394 (1975).
- [215] A. Fornieri and F. Giazotto, “Towards phase-coherent caloritronics in superconducting circuits”, *Nat. Nanotechnol.* **12**, 944–952 (2017).
- [216] G. Falci, V. Bubanja, and G. Schön, “Quasiparticle and Cooper pair tunneling in small capacitance Josephson junctions”, *Z. Phys. B Condens. Matter* **85**, 451 (1991).
- [217] N. S. Wingreen, A.-P. Jauho, and Y. Meir, “Time-dependent transport through a mesoscopic structure”, *Phys. Rev. B* **48**, 8487–8490 (1993).
- [218] A.-P. Jauho, N. S. Wingreen, and Y. Meir, “Time-dependent transport in interacting and noninteracting resonant-tunneling systems”, *Phys. Rev. B* **50**, 5528–5544 (1994).
- [219] F. Giazotto, F. Paolucci, A. Braggio, G. Marchegiani, and G. Germanese, *Superconducting bipolar thermoelectric memory and method for writing a superconducting bipolar thermoelectric memory*, *Patent*, filing number: 102021000032042, 2021.
- [220] G. Marchegiani, A. Braggio, and F. Giazotto, “Noise effects in the nonlinear thermoelectricity of a Josephson junction”, *Appl. Phys. Lett.* **117**, 212601 (2020).
- [221] C. Guarcello, P. Solinas, A. Braggio, M. Di Ventura, and F. Giazotto, “Josephson Thermal Memory”, *Phys. Rev. Applied* **9**, 014021 (2018).
- [222] E. H. Hall, “On a new action of the magnet on electric currents”, *Am. J. Math.* **2**, 287–292 (1879).
- [223] P. Drude, “Zur Elektronentheorie der Metalle”, *Ann. Phys.* **306**, 566–613 (1900).
- [224] P. Drude, “Zur Elektronentheorie der Metalle; II. Teil. Galvanomagnetische und thermomagnetische Effecte”, *Ann. Phys.* **308**, 369–402 (1900).
- [225] N. W. Ashcroft and N. D. Mermin, *Solid state physics* (Saunders College Publishing, New York, 1976) Chap. 1.
- [226] D. C. Mattis and J. Bardeen, “Theory of the anomalous skin effect in normal and superconducting metals”, *Phys. Rev.* **111**, 412 (1958).
- [227] P. B. Miller, “Frequency-dependent Hall effect in normal and superconducting metals”, *Phys. Rev.* **121**, 435 (1961).
- [228] S. Spielman, B. Parks, J. Orenstein, D. T. Nemeth, F. Ludwig, J. Clarke, P. Merchant, and D. J. Lew, “Observation of the quasiparticle Hall effect in superconducting  $\text{YBa}_2\text{Cu}_3\text{O}_{7-\delta}$ ”, *Phys. Rev. Lett.* **73**, 1537–1540 (1994).
- [229] J. Sinova, S. O. Valenzuela, J. Wunderlich, C. Back, and T. Jungwirth, “Spin Hall effects”, *Rev. Mod. Phys.* **87**, 1213 (2015).

- [230] G. Dresselhaus, “Spin-orbit coupling effects in zinc blende structures”, *Phys. Rev.* **100**, 580–586 (1955).
- [231] Y. A. Bychkov and E. I. Rashba, “Properties of a 2D electron gas with lifted spectral degeneracy”, *JETP Lett.* **39**, 78 (1984).
- [232] P. Jacquod, R. S. Whitney, J. Meair, and M. Büttiker, “Onsager relations in coupled electric, thermoelectric, and spin transport: the tenfold way”, *Phys. Rev. B* **86**, 155118 (2012).
- [233] J. Shi, P. Zhang, D. Xiao, and Q. Niu, “Proper definition of spin current in spin-orbit coupled systems”, *Phys. Rev. Lett.* **96**, 076604 (2006).
- [234] L. D. Landau and E. M. Lifshitz, *Course of theoretical physics*, Vol. 5 (Pergamon Press, 1969).
- [235] K. Shinagawa, “Faraday and Kerr effects in ferromagnets”, in *Magneto-optics*, edited by S. Sugano and N. Kojima (Springer, 2000), pp. 137–177.
- [236] H. Ebert, “Magneto-optical effects in transition metal systems”, *Rep. Progr. Phys.* **59**, 1665 (1996).
- [237] Y. Niimi, H. Suzuki, Y. Kawanishi, Y. Omori, T. Valet, A. Fert, and Y. Otani, “Extrinsic spin Hall effects measured with lateral spin valve structures”, *Phys. Rev. B* **89**, 054401 (2014).
- [238] K.-R. Jeon, J.-C. Jeon, X. Zhou, A. Migliorini, J. Yoon, and S. S. P. Parkin, “Giant transition-state quasiparticle spin-Hall effect in an exchange-spin-split superconductor detected by nonlocal magnon spin transport”, *ACS Nano* **14**, 15874–15883 (2020).
- [239] A. Hijano, V. N. Golovach, and F. S. Bergeret, “Quasiparticle density of states and triplet correlations in superconductor/ferromagnetic-insulator structures across a sharp domain wall”, *Phys. Rev. B* **105**, 174507 (2022).
- [240] A. Hijano, S. Ilić, and F. S. Bergeret, “Anomalous Andreev interferometer: Study of an anomalous Josephson junction coupled to a normal wire”, *Phys. Rev. B* **104**, 214515 (2021).
- [241] A. Hijano, F. Bergeret, F. Giazotto, and A. Braggio, “Microwave-assisted thermoelectricity in  $S$ - $I$ - $S'$  tunnel junctions”, *Phys. Rev. Appl.* **19**, 044024 (2023).
- [242] A. Hijano, S. Vosoughi-nia, F. S. Bergeret, P. Virtanen, and T. T. Heikkilä, “Dynamical Hall responses of disordered superconductors”, *Phys. Rev. B* **108**, 104506 (2023).
- [243] T. Kokkeler, A. Hijano, and F. S. Bergeret, “Anisotropic differential conductance of a mixed-parity superconductor/ferromagnet structure”, *Phys. Rev. B* **107**, 104506 (2023).
- [244] A. Hijano, S. Ilić, and F. S. Bergeret, “Weak localization at arbitrary disorder in systems with generic spin-dependent fields”, arXiv preprint arXiv:2311.01148 (2023).
- [245] A. Hijano, E. J. Rodríguez, D. Bercioux, and D. Frustaglia, “Spin-texture topology in curved circuits driven by spin-orbit interactions”, *Communications Physics* **6**, 186 (2023).
- [246] Z. Geng, A. Hijano, S. Ilić, M. Ilyn, I. Maasilta, A. Monfardini, M. Spies, E. Strambini, P. Virtanen, M. Calvo, C. González-Orellána, A. P. Helenius, S. Khorshidian, C. I. L. de Araujo, F. Levy-Bertrand, C. Rogero, F. Giazotto, F. S. Bergeret, and T. T. Heikkilä, “Superconductor-ferromagnet hybrids for non-reciprocal electronics and detectors”, *Superconductor Science and Technology* **36**, 123001 (2023).
- [247] T. Kottos and U. Smilansky, “Periodic orbit theory and spectral statistics for quantum graphs”, *Ann. Phys. (N. Y.)* **274**, 76–124 (1999).
- [248] S. Gnutzmann and U. Smilansky, “Quantum graphs: Applications to quantum chaos and universal spectral statistics”, *Adv. Phys.* **55**, 527–625 (2006).

- [249] J. Vidal, G. Montambaux, and B. Douçot, “Transmission through quantum networks”, *Phys. Rev. B* **62**, R16294–R16297 (2000).
- [250] D. Bercioux, M. Governale, V. Cataudella, and V. M. Ramaglia, “Rashba-Effect-Induced Localization in Quantum Networks”, *Phys. Rev. Lett.* **93**, 056802 (2004).
- [251] D. Bercioux, M. Governale, V. Cataudella, and V. M. Ramaglia, “Rashba effect in quantum networks”, *Phys. Rev. B* **72**, 075305 (2005).
- [252] D. Bercioux, D. Frustaglia, and M. Governale, “Signatures of spin-related phases in transport through regular polygons”, *Phys. Rev. B* **72**, 113310 (2005).
- [253] V. M. Ramaglia, V. Cataudella, G. De Filippis, and C. A. Perroni, “Ballistic transport in one-dimensional loops with Rashba and Dresselhaus spin-orbit coupling”, *Phys. Rev. B* **73**, 155328 (2006).
- [254] G. Chang, B. J. Wieder, F. Schindler, D. S. Sanchez, I. Belopolski, S.-M. Huang, B. Singh, D. Wu, T.-R. Chang, T. Neupert, S.-Y. Xu, H. Lin, and M. Z. Hasan, “Topological quantum properties of chiral crystals”, *Nature Materials* **17**, 978–985 (2018).
- [255] M. Lin, I. Robredo, N. B. M. Schröter, C. Felser, M. G. Vergniory, and B. Bradlyn, “Spin-momentum locking from topological quantum chemistry: applications to multifold fermions”, *Phys. Rev. B* **106**, 245101 (2022).
- [256] J. A. Krieger, S. Stolz, I. Robredo, K. Manna, E. C. McFarlane, M. Date, E. B. Guedes, J. H. Dil, C. Shekhar, H. Borrmann, Q. Yang, M. Lin, V. N. Strocov, M. Caputo, B. Pal, M. D. Watson, T. K. Kim, C. Cacho, F. Mazzola, J. Fujii, I. Vobornik, S. S. Parkin, B. Bradlyn, C. Felser, M. G. Vergniory, and N. B. M. Schröter, “Parallel spin-momentum locking in a chiral topological semimetal”, arXiv preprint arXiv:2210.08221 (2022).
- [257] K.-H. Ahn, A. Hariki, K.-W. Lee, and J. Kuneš, “Antiferromagnetism in RuO<sub>2</sub> as *d*-wave pommeranchuk instability”, *Phys. Rev. B* **99**, 184432 (2019).
- [258] L. Šmejkal, R. González-Hernández, T. Jungwirth, and J. Sinova, “Crystal time-reversal symmetry breaking and spontaneous Hall effect in collinear antiferromagnets”, *Sci. Adv.* **6**, eaaz8809 (2020).
- [259] L.-D. Yuan, Z. Wang, J.-W. Luo, E. I. Rashba, and A. Zunger, “Giant momentum-dependent spin splitting in centrosymmetric low-*Z* antiferromagnets”, *Phys. Rev. B* **102**, 014422 (2020).
- [260] K. S. Tikhonov, G. Schwiete, and A. M. Finkel’stein, “Fluctuation conductivity in disordered superconducting films”, *Phys. Rev. B* **85**, 174527 (2012).



*Farewell, dear city.  
Farewell, my country, where my children lived.  
There below, the Greek ships wait.*  
— Euripides, *The Trojan Women*